TESIS DE LA UNIVERSIDAD DE ZARAGOZA

2014

81

Clara Valero Lázaro

Mechanochemical modeling of wound healing: Multiphysics finite element simulations

Departamento
Ingeniería Mecánica

Director/es
Gómez Benito, María José
Javierre Pérez, Etelvina

ISSN 2254-7606

Prensas de la Universidad
Universidad Zaragoza

Universidad Zaragoza
1542

Tesis Doctoral

MECHANOCHEMICAL MODELING OF WOUND HEALING: MULTIPHYSICS FINITE ELEMENT SIMULATIONS

Autor

Clara Valero Lázaro

Director/es

Gómez Benito, María José
Javierre Pérez, Etelvina

UNIVERSIDAD DE ZARAGOZA

Ingeniería Mecánica

2014

Mechanochemical modeling of wound healing: multiphysics finite element simulations.

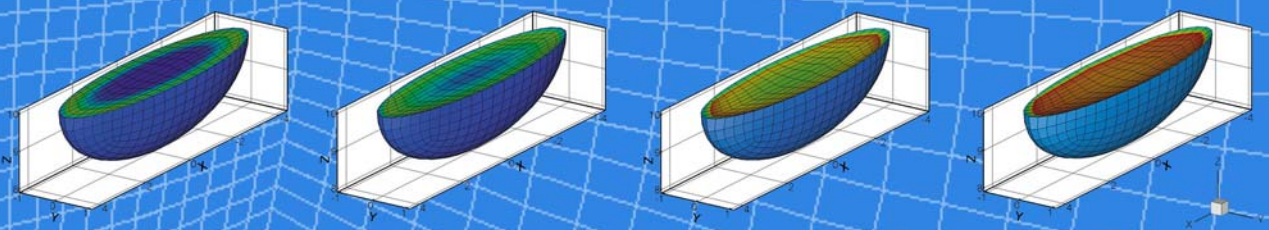

Doctoral Degree in Computational Mechanics

AUTHOR: Clara Valero Lázaro
FACULTY ADVISORS: Mª José Gómez Benito
Etelvina Javierre Pérez
2014

Universidad Zaragoza
1542

Escuela de
Ingeniería y Arquitectura
Universidad Zaragoza

Departamento de
Ingeniería Mecánica
Universidad Zaragoza

Programa Oficial de Posgrado en Mecánica Computacional

Mechanochemical modeling of wound healing: multiphysics finite element simulations.

Clara Valero Lázaro

Doctoral degree in *Computational Mechanics*

Faculty Advisors: Dra. Mª José Gómez Benito and Dra. Etelvina Javierre Pérez

Departamento de Ingeniería Mecánica
Escuela de Ingeniería y Arquitectura
Universidad de Zaragoza. Abril de 2014

Departamento de
Ingeniería Mecánica
Universidad Zaragoza

Doña María José Gómez Benito, Profesora Titular de Universidad del Departamento de Ingeniería Mecánica de la Escuela de Ingeniería y Arquitectura, de la Universidad de Zaragoza, y Doña Etelvina Javierre Pérez, Profesora del Centro Universitario de la Defensa, centro Adscrito a la Universidad de Zaragoza,

CERTIFICAN

Que la memoria de Tesis Doctoral presentada por doña Clara Valero Lázaro con el título ”Mechanochemical modeling of wound healing: multiphysics finite element simulations” ha sido realizada bajo nuestra dirección en el Departamento de Ingeniería Mecánica, de la Escuela de Ingeniería y Arquitectura, de la Universidad de Zaragoza, y se corresponde con el Proyecto de Tesis aprobado por la Comisión de Doctorado en Febrero de 2014, por lo que autorizamos su presentación en la modalidad de compendio de publicaciones y con la Mención de ”Doctor Internacional” cumpliendo por lo tanto las condiciones requeridas para que su autora pueda optar al grado de Doctora de la Universidad de Zaragoza.

Firmado, en Zaragoza, a 28 de Abril de 2014.

Fdo: María José Gómez Benito

Fdo: Etelvina Javierre Pérez

Esta tesis se presenta como un compendio de artículos publicados para optar al título de Doctor en la Universidad de Zaragoza, siguiendo el acuerdo de 20 de diciembre de 2013 del Consejo de Gobierno de la Universidad por el que se aprueba el Reglamento sobre Tesis Doctorales.

Los trabajos que forman parte de la tesis son:

1. C. Valero, E. Javierre, J. M. García-Aznar, M. J. Gómez-Benito. Nonlinear finite element simulations of injuries with free boundaries: Application to surgical wounds. *International Journal for Numerical Methods in Biomedical Engineering*(2014). Published online in Wiley Online Library (wileyonlinelibrary.com). DOI: 10.1002/cnm.2621. (Factor de impacto de la revista: 1,310).

2. C. Valero, E. Javierre, J. M. García-Aznar, M. J. Gómez-Benito. Numerical modelling of the angiogenesis process in wound contraction. *Biomechanics and Modeling in Mechanobiology 12 (2) (2013) 349–360*. DOI 10.1007/s10237-012-0403-x . (Factor de impacto de la revista:3,331).

3. C. Valero, E. Javierre, J. M. García-Aznar, M. J. Gómez-Benito. Stress evaluation during angiogenesis in skin wound healing. *The Proceedings of the 10th International Symposium on Computer Methods in Biomechanics and Biomedical Engineering*, Berlin, Alemania, 7-11 Abril, 2012. Publicado por ARUP; ISBN: 978-0-9562121-5-3.

4. C. Valero, E. Javierre, J. M. García-Aznar, M. J. Gómez-Benito. A cell-regulatory mechanism involving feedback between contraction and tissue formation guides wound healing progression.
PLOS ONE. DOI:10.1371/journal.pone.0092774. (Factor de impacto de la revista: 3,730).

Además de los artículos enumerados ya publicados, otro artículo que forma parte de esta tesis se encuentra en proceso de revisión:

5. C. Valero, E. Javierre, J. M. García-Aznar, M. J. Gómez-Benito, A. Menzel. Modeling anisotropic wound healing: effect of the relative position of wounds with respect to collagen fibers orientation. *Journal of the Mechanics and Physics of Solids*. En revisión. (Factor de impacto de la revista: 3,406).

Finalmente, otro artículo ha sido publicado como resultado del trabajo realizado durante una estancia de investigación en los EE.UU., aunque la contribución principal corresponde al grupo de Física Computacional de la Universidad de Michigan (EE.UU.):

6. M. Maraldi, C. Valero, K. Garikipati. A computational study of stress fiber-focal adhesion dynamics governing cell contractility. *Biophysical Journal*. (Factor de impacto de la revista: 3,668).

This thesis is presented as a compendium of articles published to obtain the title of Doctor at the University of Zaragoza, following the agreement of the 20th of December 2013 of the Governing Council of the University that approves the Regulations on Doctoral Thesis.

The works that are part of the thesis are:

1. C. Valero, E. Javierre, J. M. García-Aznar, M. J. Gómez-Benito. Nonlinear finite element simulations of injuries with free boundaries: Application to surgical wounds. *International Journal for Numerical Methods in Biomedical Engineering*(2014). Published online in Wiley Online Library (wileyonlinelibrary.com). DOI: 10.1002/cnm.2621. (Journal Impact factor: 1.310).

2. C. Valero, E. Javierre, J. M. García-Aznar, M. J. Gómez-Benito. Numerical modelling of the angiogenesis process in wound contraction. *Biomechanics and Modeling in Mechanobiology 12 (2) (2013) 349–360*. DOI 10.1007/s10237-012-0403-x . (Journal Impact factor:3.331).

3. C. Valero, E. Javierre, J. M. García-Aznar, M. J. Gómez-Benito. Stress evaluation during angiogenesis in skin wound healing. *The Proceedings of the 10th International Symposium on Computer Methods in Biomechanics and Biomedical Engineering*, Berlin, Germany, April 7th-11th, 2012. Published by ARUP; ISBN: 978-0-9562121-5-3.

4. C. Valero, E. Javierre, J. M. García-Aznar, M. J. Gómez-Benito. A cell-regulatory mechanism involving feedback between contraction and tissue formation guides wound healing progression.
PLOS ONE. DOI:10.1371/journal.pone.0092774. (Journal Impact factor: 3.730).

In addition to the articles previously listed and already published, another article that is under review is part of this thesis:

5. C. Valero, E. Javierre, J. M. García-Aznar, M. J. Gómez-Benito, A. Menzel. Modeling anisotropic wound healing: effect of the relative position of wounds with respect to collagen fibers orientation. *Journal of the Mechanics and Physics of Solids*. Submitted. (Journal Impact factor: 3.406).

Finally, another published article is included and, although it has been part of the work developed in the thesis, the main contributions correspond to the Computational Physics Group at the University of Michigan (USA):

6. M. Maraldi, C. Valero, K. Garikipati. A computational study of stress fiber-focal adhesion dynamics governing cell contractility. *Biophysical Journal*. (Journal Impact factor: 3.668).

Resumen

La cicatrización de heridas es una importante cuestión de salud que afecta a millones de pacientes y genera altos costes al sistema sanitario y la sociedad. Las heridas aparecen en la piel como consecuencia de daños en accidentes traumáticos y también como resultado de incisiones quirúrgicas, que a veces no son fáciles de curar.

La cicatrización de heridas suele dividirse en tres etapas superpuestas en el tiempo que pueden durar varios meses o años. Estas etapas se denominan inflamación, epitelización y remodelación de tejido; normalmente siguen un esquema definido. Entrando en más detalle, diferentes procesos biológicos, químicos y mecánicos pueden ser identificados dentro de cada etapa. Estos procesos suelen estar guiados por la interacción entre células, factores químicos y estímulos mecánicos y el proceso de cicatrización no se puede completar en ausencia de cualquiera de esos agentes.

Existe muchos tipos diferentes de heridas que dependiendo de su severidad se curan más rápido o más lento. Por ejemplo, cortes o abrasiones superficiales curan rápidamente siguiendo la progresión habitual. En otras ocasiones, cuando no se sigue el esquema temporal normal o la persona lesionada sufre de algún tipo de trastorno fisiológico, la curación puede llevar a dificultades tales como cicatrices patológicas (cicatrices hipertróficas y queloides) o heridas crónicas, que tardan más en curarse o incluso pueden llegar a no sanar completamente.

La investigación en el campo de la cicatrización de heridas se ha centrado en trabajos experimentales y computacionales que intentan comprender la influencia de las diferentes variables en el proceso. Las diferencias entre los tipos de heridas y geometrías requieren un procedimiento general y adaptable, que se pueda aplicar para analizar diferentes heridas. Para ello, los modelos computacionales son una alternativa complementaria a los métodos experimentales, ya que pueden ser fácilmente particularizados a la geometría y las características de la herida deseada. Los modelos computacionales de cicatrización de heridas se han estudiado ampliamente en los últimos años, a partir de modelos con geometrías sencillas, incluyendo una variable única y han evolucionado a modelos más complejos con múltiples variables y diferentes geometrías. Sin embargo, estos modelos han sido prácticamente limitados a las geometrías planas en dos dimensiones, y sólo algunos de ellos reproducen heridas profundas. Por otra parte, los modelos existentes tienen otras limitaciones que reducen su potencial predictivo. Por ejemplo, la mayoría de los modelos existentes consideran la

piel como un material isótropo viscoelástico o hiperelástico, dejando de lado su anisotropía debida fundamentalmente a las contribuciones de las fibras de colágeno y su orientación.

Por lo tanto, el objetivo de esta tesis es el estudio de la cicatrización de heridas en la piel a través de la simulación computacional y el uso de un enfoque multifísico. Con el fin de lograr este objetivo, se ha propuesto e implementado un modelo computacional que permite reproducir la cicatrización de heridas en diferentes condiciones. Más concretamente, el modelo propuesto se centra en la fase de contracción de la herida, ya que tiene un fuerte componente mecánico. El modelo también permite incluir más procesos que tienen lugar de forma simultánea a la contracción de la herida, por ejemplo la angiogénesis. El modelo propuesto incluye factores biológicos (especies celulares, factores de crecimiento y colágeno) y también factores mecánicos (caracterización de las propiedades mecánicas de la piel y contracción celular). Se ha utilizado una formulación basada en observaciones físicas de mecanorregulación y mecanotransducción celular para definir la generación de tensiones por las células y la diferenciación celular. El modelo constitutivo de la piel se ha actualizado partiendo del material viscoelástico comúnmente utilizado hasta una descripción más realista utilizando un modelo hiperelástico anisótropo. Las ecuaciones resultantes se resuelven a través del método de los elementos finitos, y su formulación se ha implementado en dos y tres dimensiones con el fin de poder estudiar cualquier geometría de la herida. Con todas estas características, el modelo aquí presentado permite analizar la cicatrización de heridas desde una perspectiva mucho más amplia, teniendo en cuenta no sólo los aspectos morfológicos, sino también las aspectos específicos de la bioquímica y la biomecánica que influyen en la evolución de las células y los tejidos.

Palabras clave: cicatrización de heridas, piel, contracción, angiogénesis, multifísica, matriz extracelular, biomecánica, fibroblastos, miofibroblastos, células endoteliales, colágeno, factor de crecimiento, mecanorregulación, mecanotransducción, rigidez de la matriz, modelo constitutivo, viscoelasticidad, anisotropía, hiperelasticidad, fibras, tensión celular, convección-difusión-reacción, elementos finitos, formulación en tres dimensiones.

Abstract

Wound healing is an important health matter that affects millions of patients and generates high costs to the health system and society. Wounds appear in the skin as a consequence of damage in traumatic accidents but also as a result of surgery incisions, which sometimes are not easy to heal.

Wound healing is usually divided into three stages overlapped in time that can lasts for several months or years. These stages are named inflammation, tissue formation and tissue remodeling and they normally follow a predictable progress. Going into more detail, different biological, chemical and mechanical processes can be identified inside every stage. These processes are usually guided by the interaction between cells, chemical factors and mechanical stimulus and the healing process can not be completed in the absence of any of those agents.

There exists many different wound types which depending on their severeness heal faster or slower. For instance, superficial cuts or abrasions heal quickly following the usual progression. In other occasions, if the regular time scheme is not followed or the injured person suffers from any kind of physiological disorder, healing can lead into difficulties such as pathological scars (hypertrophic scars and keloids) or chronic wounds, which take longer to heal or even never heal completely.

Research in the wound healing field has been focused in experimental and computational works that try to understand the influence of the different variables in the process. Differences between wound types and geometries require a general procedure, customizable, that can be applied to analize different wounds. To this purpose, computational models are the best approach, as they can be easily particularized to the desired wound geometry and characteristics. Computational models of wound healing have been widely studied during the lasts years, from simple geometry models including a unique variable to more complex models with several variables and different geometries. However, these models have been barely extended out of the two-dimensional planar geometries and just a few of them reproduced deep wounds. Moreover, existing models have other limitations that reduce their predictive potential. For instance, most of the existent models consider the skin as a viscoelastic or hyperelastic isotropic material, neglecting the contributions of the collagen fibers and their orientation.

Thus, the aim of this thesis is the study of wound healing in the skin through computational simulation and using a multiphysics approach. In order to achieve

this objective, a computational model that allows to reproduce wound healing under different conditions has been proposed and implemented. More specifically, the proposed model focuses on the wound contraction phase, as it has a strong mechanical component. The model also allows to include more processes that take place simultaneously to wound contraction, for instance angiogenesis. The proposed model includes biological factors (cellular species, growth factors and collagen) and also mechanical factors (characterization of the skin mechanical properties and cellular contraction). A physically based formulation of cell mechanosensing and mechanotransduction has been used to describe both cell-exerted stresses and cell differentiation signals. The constitutive model of the skin has been updated from the commonly used viscoelasticy to a more realistic anisotropic hyperelastic description. The resulting governing equations are solved through the Finite Elements Method, and its formulation has been implemented in two and three dimensions in order to be able to study any wound geometry. With all these characteristics, the model here presented allows to analyze wound healing evolution from a much wider perspective, taking into account not only morphological aspects but also specific characteristics of the chemical and mechanical cues on cellular and tissue evolution.

Keywords: wound healing, skin, contraction, angiogenesis, ECM collagen matrix, biomechanics, fibroblasts, myofibroblasts, endothelial cells, collagen, growth factor, mechanosensing, mechanotransduction, matrix stiffness, constitutive model, viscoelasticity, anisotropy, hyperelasticity, fibers, cell-traction, cell-induced stress, convection-diffusion-reaction, finite elements, three-dimensional formulation, multiphisics

Agradecimientos

En primer lugar, me gustaría dar las gracias a mis directoras, *Mª José* y *Etel* por su constante apoyo durante este tiempo. Por estar en todo momento disponibles para atender mis dudas y ofrecer ayuda y consejo ante todas las incertidumbres que han aparecido a lo largo de estos cuatro años. No sólo por ofrecerme soluciones ante las dificultades, si no también por ayudarme a aprender a encontrar las soluciones por mí misma.

También quiero expresar mi agradecimiento a *Manu*, que siempre ha estado dispuesto a ayudarme en lo que hiciera falta y encontrar un momento para atender a mis preguntas. Gracias también a *Mª Ángeles* por estar ahí y preocuparse siempre por saber si todo iba bien.

Me gustaría especialmente agradecer a los profesores Krishna Garikipati de la Universidad de Michigan y Andreas Menzel de la TU de Dortmund, que me acogieron en sus grupos de investigación durante varios meses. Las estancias en sus grupos me permitieron no sólo ampliar mi experiencia investigadora, sino también disfrutar de una experiencia difícilmente repetible

Belén, Carmelo, Héctor, María, Marta, Noelia, Rosa, Samuel, Sara,... que durante estos años no sólo han demostrado ser buenos amigos en los buenos momentos, sino también apoyo en los momentos de mayor dificultad. Por todas las tardes de quedadas, viajes para desconectar y conversaciones para desahogarnos. Gracias por hacer que estos años hayan sido fáciles.

No me olvido tampoco de todos los compañeros que a lo largo de estos años han formado parte del grupo de becarios del área, hayamos coincidido más o menos tiempo, de todos guardo buen recuerdo. Hemos compartido los momentos duros y estresantes que todos pasamos a lo largo de la tesis pero también buenos ratos, dentro y fuera de la universidad. Con estos me quedo.

Finalmente, me gustaría agradecer a mi familia, que me han apoyado en todo momento siendo una motivación constante. Gracias por entender lo que es importante para mí.

Índice general - Table of contents

INTRODUCCIÓN GENERAL Y CONCLUSIONES

Modelado mecanoquímico de la cicatrización de heridas: simulación multifísica con elementos finitos.

CAPÍTULO 1

Introducción

Las heridas en la piel son lesiones que la mayoría de las personas sufren a lo largo de la vida. Cuando la persona herida no tiene problemas serios de salud y la herida no es muy profunda, las heridas se curan sin implicaciones más relevantes que una cicatriz en la piel. Sin embargo, cuando el proceso de curación no sigue su evolución natural puede dar lugar a diferentes complicaciones, tales como heridas crónicas y otros problemas. Las heridas crónicas afectan a 6,5 millones de pacientes en los Estados Unidos generando un coste anual de 25000 millones de dólares (Sen et al., 2009), reducir estos números es un objetivo permanente del sistema de salud.

Encontrar cómo mejorar el proceso de curación necesita una inversión de tiempo y un elevado gasto económico. Además, las implicaciones éticas están siempre presentes cuando los experimentos implican seres vivos. Por ello, los modelos matemáticos de curación de heridas han aumentado su popularidad en las últimas décadas. Los modelos matemáticos permiten estudiar un amplio número de casos modificando parámetros con un reducido coste económico y de tiempo, añadiendo la posibilidad de estudiar casos específicos, individualizados para cada paciente. Por ello, el objetivo de esta tesis es el desarrollo de un modelo de cicatrización de heridas para predecir la evolución de la cicatrización de heridas bajo diferentes condiciones y que permita el estudio de un amplio rango de heridas y factores que influyen en su curación.

1.1 La piel

La piel es la cubierta exterior de los animales vertebrados y presenta diferente estructura y propiedades en cada especie. En los humanos, la piel es el órgano más grande y representa el 8 % de la masa corporal (Gray et al., 1995). La piel cubre la

totalidad del cuerpo humano y su espesor varía según la parte del cuerpo (Odland, 1991), entre 1,5 mm y 4 mm considerando la epidermis y la dermis. El tejido inferior tiene una gran variabilidad en cuanto a su profundidad y composición en función de su localización anatómica. La piel se clasifica normalmente en dos tipos: fina y gruesa. La piel fina se encuentra en partes tales como los párpados o zonas donde hay folículos capilares, mientras que la piel gruesa no presenta normalmente folículos capilares y está localizada principalmente en las palmas de las manos y las suelas de los pies. La piel constituye una interfaz entre el cuerpo y el medio ambiente, es una barrera natural que protege los órganos internos de agresiones externas. Además de ser una barrera física, la piel tiene varias funciones; evita la deshidratación regulando la pérdida de agua y actúa como barrera térmica. Los mecanismos que la piel utiliza para regular la temperatura corporal son principalmente la evaporación de sudor y la convección, regulando el flujo sanguíneo en la superficie corporal. Una de las funciones más importantes de la piel es su papel como parte del sistema inmunológico, evitando la entrada de partículas extrañas y patógenos (cualquier agente que pueda causar daño) en el cuerpo (Fore-Pfliger, 2004). Además, numerosos sistemas fisiológicos necesarios para el funcionamiento correcto del cuerpo, tales como nervios, capilares o el sistema linfático, están localizados en la piel. Por lo tanto, mantener la estabilidad de la piel y evitar cualquier factor que pueda reducir sus propiedades es altamente importante. Además, también es de gran importancia conseguir una recuperación rápida y funcional de la piel cuando sufre daño.

1.1.1 Estructura de la piel

La piel humana está formada por colágeno, elastina y un número variable de especies celulares (Tabla 1.1). Está organizada en tres capas principales, desde la más externa a la más interna: epidermis, dermis e hipodermis (Wilkes et al., 1973).

Las heridas en la piel normalmente atraviesan la epidermis y alcanzan la dermis. La **epidermis** es la capa más externa de la piel y es la que está en contacto con el medio ambiente, y por lo tanto tiene un papel principal en la función protectora de la piel. La epidermis constituye una barrera frente a la pérdida de agua y la entrada de substancias extrañas. A pesar del papel importante de la epidermis, ésta es también la capa más fina de la piel, con un espesor de entre 75-150μm (Odland, 1991), y se divide en 5 capas: *Stratum corneum, Stratum lucidum, Stratum granulosum, Stratum spinosum* y *Stratum germinativum* (Figura 1.1). La epidermis está constituida principalmente por keratinocitos, que son también parte del sistema inmunitarios y producen mediadores anti-inflamatorios. Puesto

que la epidermis está en contacto directo con el medio ambiente, su capacidad de autorrenovación es crucial; la producción y muerte de células en la epidermis se encuentran en equilibrio.

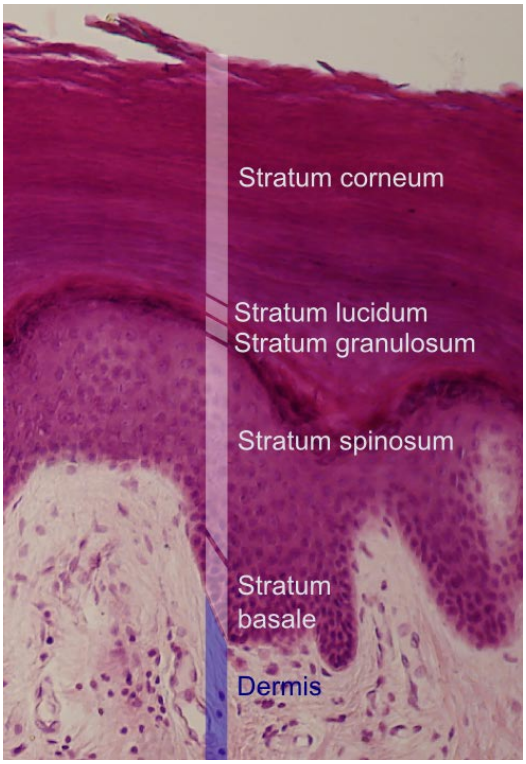

Figura 1.1: Imagen histológica de las capas de la dermis. Fuente: http://en.wikipedia.org/wiki/File:Epidermal_layers.png

La **dermis** es la capa intermedia de la piel y se encuentra conectada a la epidermis por la membrana basal. Tiene un espesor variable de entre 1-4*mm* y por lo general se divide en dos regiones, la *región papilar* y la *región reticular* (Figura 3.2). La dermis está compuesta principalmente de colágeno tipo I y III embebido en una sustancia fundamental compuesta de proteoglicanos, fibronectina (Gray et al., 1995) y especies celulares variables (fibroblastos, miofibroblastos, células endoteliales, macrófagos, neutrófilos o linfocitos entre otros (Tabla 1.1)). Mientras que algunas especies celulares, como los fibroblastos, están naturalmente en la piel otras especies sólo aparecen cuando se necesitan. Éste es el caso de los miofibroblastos, que sólo aparecen cuando se produce una lesión, o los macrófagos que migran a los lugares donde hay patógenos para eliminarlos. Uno de los principales componentes de la dermis es el colágeno. El colágeno es la proteína más abundante en la piel y se organiza por lo general

en una red de fibras con propiedades elásticas proporcionando integridad a la piel. De hecho, la resistencia a tracción de la piel se debe a esta red de colágeno.

Los cortes y heridas profundas penetran en la dermis y pueden llegar a la capa subyacente, la hipodermis, que se encuentra debajo de la *región reticular* de la piel.

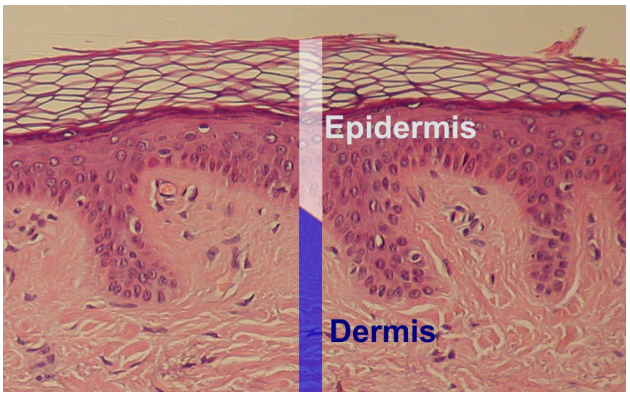

Figura 1.2: Imagen histológica de la epidermis y las capas de la dermis. Fuente: http://upload.wikimedia.org/wikipedia/commons/8/84/Epidermis-delimited.JPG

La **hipodermis**, también llamada tejido subcutáneo o fascia superficial, es la capa más profunda de la piel y su espesor puede alcanzar el orden de los centímetros, dependiendo de su localización anatómica. Por lo general, se compone de grasa subcutánea y tejido conectivo y contiene numerosos sistemas fisiológicos importantes, como vasos sanguíneos (ver Figura 1.3) y nervios. Además, como la epidermis y la dermis, la hipodermis contiene varias especies celulares, principalmente fibroblastos, células adiposas y macrófagos. Los huesos, músculos y órganos internos se encuentran bajo la hipodermis, haciendo necesaria la rápida recuperación de la hipodermis después del daño para recuperar la estabilidad fisiológica.

Nombre	Función	Localización	Etapa de curación de heridas	Otros
Células adiposas/Adipocitos	Almacenan energía en forma de grasa	Hipodermis	Todas	Síntesis de diferentes hormonas
Células endoteliales	Formación de nuevos capilares durante la angiogénesis	Vasos sanguíneos	Epitelización	Células móviles que migran a la herida durante la etapa de epitelización
Fibroblastos	Síntesis de colágeno de tipo III Generación de fuerzas de contracción	Dermis Hipodermis	Epitelización Contracción	Células móviles que migran a la herida durante la etapa de epitelización
Keratinocitos	Componente principal de la epidermis Barrera ante agresiones ambientales Regulación del sistema inmune mediante la producción de factores anti-inflamatorios	Epidermis	Epitelización	Células móviles que migran a la herida durante la etapa de epitelización
Macrófagos	Fagocitosis Destrucción de bacterias y células muertas en los lugares dañados	Dermis Hipodermis	Inflamación	Derivados de monocitos sanguíneos Entran a la herida a través del endotelio de los capilares Atraídos quimiotacticamente a la herida por los citokinos liberados por células dañadas Parte del sistema inmunológico

Continúa en la página siguiente

Tabla 1.1 – *Continúa en la página siguiente*

Nombre	**Función**	**Localización**	**Etapa de curación de heridas**	**Otros**
Miofibroblastos	Síntesis de colágeno de tipo III Generación de fuerzas de contracción Producción de factores que inducen la angiogénesis	Dermis	Epitelización Contracción Angiogénesis	Fibroblastos diferenciados No-móviles
Neutrófilos	Destrucción de bacterias y células muertas en los lugares dañados	Torrente sanguíneo	Inflamación	Atraídos por factores inflamatorios Parte del sistema inmunológico
Plaquetas	Prevención del sangrado formando un cierre donde se ha producido daño vascular Coagulación de la sangre	Dermis	Hemostasis	Secretan PDGF

Tabla 1.1: Lista de las especies celulares que participan en la curación de heridas.

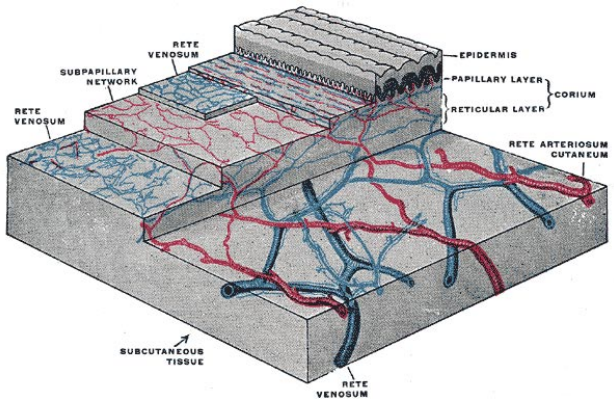

Figura 1.3: Imagen esquemática del sistema circulatorio a través de las capas de la piel (Gray et al., 1995).

La función combinada de las tres capas es crucial para el funcionamiento del cuerpo, y el mantenimiento de la integridad de toda la estructura es necesaria para la vida. Por lo tanto, conservar la piel sin daño y con buenas propiedades mecánicas es una de las cuestiones de salud más importantes.

1.1.2 Propiedades mecánicas de la piel

Las propiedades mecánicas de la piel han sido estudiadas desde hace siglos. Uno de los primeros experimentos en este campo lo llevó a cabo Langer (1861), mostrando que la piel está naturalmente sometida a tensión anisótropa. La pretensión de la piel se observa claramente cuando se produce una herida y la piel se relaja, causando un aumento del tamaño inicial del defecto.

Además, las propiedades mecánicas de la piel varían no solo dependiendo de la ubicación, orientación y profundidad de la piel, sino que también dependen de la edad del sujeto; la piel pierde su elasticidad y capacidad de recuperación a lo largo de tiempo (Escoffier et al., 1989). La mayoría de las propiedades mecánicas de la piel se deben a las fibras que componen su matriz extracelular (ECM), que tiene un módulo elástico de 150-300 kPa (Wilkes et al., 1973). Las fibras de la matriz tienen una alta resistencia a la tracción derivada de la organización en forma de hélice de tres proteínas primarias (colágeno, elastina y fibrina) (Kerr, 2010). El componente principal de estas fibras es el colágeno, que da la mayor parte de la resistencia a la tracción a la ECM. El segundo componente principal de la ECM es la elastina que da propiedades elásticas a la piel y permite que se recupere su estado original después de ser estirada.

Las fibras de proteínas están embebidas en una sustancia fundamental compuesta de proteoglicanos y fibronectinas (Gray et al., 1995), que ayuda a las células a moverse a través de las fibras. Las fibras de colágeno se alinean en la piel siguiendo las líneas de tensión o líneas de Langer, que están presentes en la superficie del cuerpo y fueron descubiertas por Langer (1861). En su investigación, Langer realizó cortes circulares en la piel a lo largo de toda la superficie del cuerpo, encontrando que estos cortes se convertían en elipses alineadas con las líneas de tensión cuando la piel se relajaba. La orientación de estos cortes define la orientación natural de las fibras de colágeno, por lo general paralela a los músculos subyacentes (Figura 1.4). La importancia de estas líneas se ha demostrado experimentalmente en algunos procesos como la cicatrización de heridas, donde se ha encontrado que las heridas se curan de manera diferente en función de su orientación relativa respecto a las líneas de Langer. La posición relativa de las heridas en la piel ha mostrado que las heridas paralelas a las líneas de Langer curan mejor y producen menos cicatrización mientras que las heridas que son perpendiculares a las líneas de Langer presentan más dificultades para curarse (Motegi et al., 1977).

Por otra parte, la magnitud de la pretensión de la piel descrita por Langer (1861) ha sido medida en el brazo y el antebrazo por Flynn et al. (2011a), donde se encontraron valores que van desde 28 hasta 92 kPa.

El conocimiento de las propiedades de la piel ha sido una cuestión de estudio importante en las investigaciones experimentales, en las que se han desarrollado numerosos métodos de medición. Durante las últimas décadas, se han diseñado tanto estudios *in-vivo* como *in-vitro* para caracterizar el comportamiento mecánico de la piel y encontrar valores precisos de los parámetros necesarios para el modelado y desarrollo de sustitutos de la piel.

La mayor parte de los estudios *in-vivo* para medir las propiedades de la piel se llevan a cabo en el antebrazo o la parte superior del brazo utilizando diferentes ensayos mecánicos, tales como extensión, indentación, aspiración o torsión. Diridollou et al. (2000) utilizó pruebas de succión en el antebrazo y un método inverso para identificar los parámetros que caracterizaban la piel como un material no lineal. Para ello aplicaron una presión negativa en la superficie de la piel y midieron la deformación de la misma, encontrando que la piel se vuelve más rígida para deformaciones mayores. Boyer et al. (2007) estudió las propiedades mecánicas de la epidermis y la dermis utilizando un dispositivo de micro ranura y lo caracterizó como un material viscoelástico, encontrando que el módulo complejo alcanza valores de 47,3 a 128,3 N/m, donde el módulo complejo

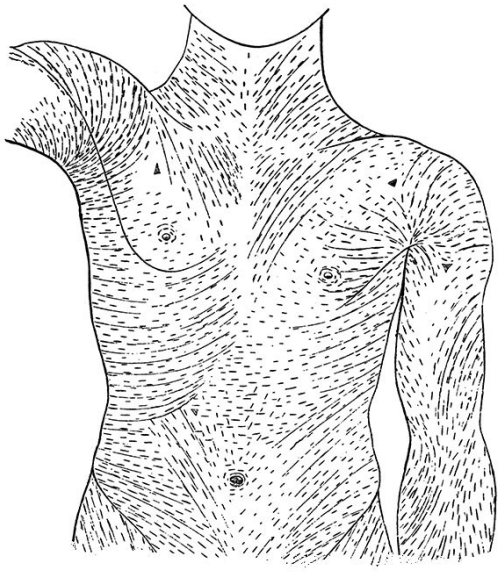

Figura 1.4: Distribución de las líneas de tensión en el tronco del cuerpo humano (Langer, 1861).

es definido como una variable que tiene una parte independiente y otra parte dependiente de la frecuencia.

Silver et al. (2001) estudió las propiedades viscoelásticas de los componentes de la piel a partir de datos experimentales (Dunn and Silver, 1983), estimando que la constante elástica para el colágeno de la piel es de 4,4 GPa y para la elastina es 4,0 MPa. Para realizar los ensayos de tensión-deformación utilizaron piel del tórax y del abdomen.

Otros trabajos caracterizan la piel como un material hiperelástico. Estos materiales no muestran propiedades elásticas lineales en su relación tensión-deformación y permiten definir otras propiedades del material tales como anisotropía o incompresibilidad. Flynn et al. (2011a) midieron la relación fuerza-desplazamiento en la piel del antebrazo al aplicar deformaciones. Más tarde, encontraron los parámetros del material que se ajustan al modelo hiperelástico de Ogden y al modelo de Tong y Fung (Flynn et al., 2011b). Gahagnon et al. (2012) estudiaron la anisotropía de la piel del antebrazo *in-vivo* usando pruebas elastográficas. Para ello estiraron la piel paralela y perpendicularmente a las líneas de Langer encontrando comportamiento anisótropo.

Los ensayos *in-vivo* para determinar las propiedades de la piel son difíciles de realizar y la variabilidad entre los sujetos es alta. El amplio rango de valores obtenidos se debe a las diferentes localizaciones anatómicas de la piel, la unión de la dermis con el tejido subyacente y las características específicas del paciente, lo que hace difícil encontrar una caracterización única válida para todas las pieles.

Mientras que los estudios *in-vivo* proporcionan información acerca de la piel en su entorno natural, sin la eliminación de los procesos naturales, los estudios *in-vitro* proporcionan experimentos más controlados, donde diferentes aspectos pueden ser aislados y se pueden realizar ensayos destructivos. Por lo tanto, los ensayos *in-vitro* dan información acerca de diferentes propiedades tales como la resistencia o la elasticidad de la piel, mientras que los ensayos *in-vivo* muestran la reacción de la piel frente a cargas externas en situaciones reales (Edwards and Marks, 1995). Annaidh et al. (2012b) investigaron la influencia de la ubicación y la orientación de la piel en sus propiedades, centrándose en la anisotropía de la piel. Realizaron ensayos *in-vitro* de tracción a muestras de piel humana obtenidas de diferentes partes de la espalda (Figura 1.5), encontrando una correlación entre la orientación de las líneas de Langer y las fibras de colágeno. Más tarde, Annaidh et al. (2012a) relacionaron sus resultados con el modelo hiperelástico desarrollado por Gasser et al. (2006).

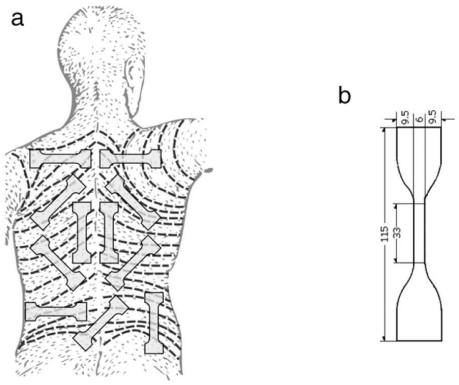

Figura 1.5: Orientación de las muestras de la espalda estudiadas por Annaidh et al. (2012b) con respecto a las líneas de Langer (Langer, 1861). (b) Dimensiones de la probeta (mm) utilizada por Annaidh et al. (2012b)

Groves et al. (2013) realizaron ensayos de tracción utilizando probetas circulares de piel humana para medir las propiedades de la piel. Para observar el efecto de la anisotropía realizaron pruebas a lo largo de tres ejes de carga diferentes. Encontraron que la piel tiene un comportamiento hiperelástico

anisótropo y utilizaron el modelo de Weiss et al. (1996) para caracterizar este comportamiento.

Otros estudios se han centrado en investigar fenómenos puntuales que se producen en procesos como la cicatrización de heridas. Hinz et al. (2001) estudió el efecto de la tensión en el tejido granular y en la diferenciación de los fibroblastos a miofibroblastos, mientras que Graham et al. (2004) estudiaron el comportamiento de las fibras de colágeno cuando se someten a distintas deformaciones.

A pesar de la gran cantidad de datos que se ha generado como resultado de los estudios anteriormente mencionados, la búsqueda de un conjunto único de parámetros para definir las propiedades de la piel humana es casi imposible debido a la alta variabilidad de los resultados entre los diferentes sujetos y localizaciones anatómicas y la dificultad de preservar la piel sin necesidad de modificar sus propiedades.

1.2 Cicatrización de heridas

La cicatrización de heridas es un tema de salud importante que afecta a millones de pacientes y genera un alto coste para el sistema sanitario y la sociedad (Sen et al., 2009). Cada año se realizan millones de procedimientos quirúrgicos con el posterior tratamiento de la herida creada y las cicatrices. También se estima que alrededor de 6,5 millones de pacientes se ven afectados por heridas crónicas en EE.UU., lo que genera un coste de 25000 millones de dólares al año. Se calcula también que el cuidado de cicatrices en la piel genera un gasto anual de alrededor de 12000 millones de dólares.

Las heridas pueden aparecer como consecuencia de daños en accidentes traumáticos, pero también como resultado de las incisiones necesarias en cirugía, que muchas veces no son fáciles de curar. Por otra parte, las heridas como las *úlceras por presión* pueden aparecer a causa de largos períodos de inmovilidad y pueden conducir a infecciones y complicaciones más graves, incluso la muerte. Las complicaciones en la curación de heridas tienden a aparecer en personas con enfermedades crónicas como la diabetes y la obesidad, que presentan dificultades para una correcta cicatrización.

La cicatrización de heridas se produce después de que ocurra el daño en la piel. Las heridas leves se cicatrizan generalmente a través de una serie de procesos bien

organizados sin necesidad de tratamiento especial, pero en aquellos casos en los que las heridas causan un daño excesivo es necesario aplicar diferentes técnicas para lograr su curación. Además, los procesos de curación anormales, como lesiones fibroproliferativas (*queloides* o *cicatrices hipertróficas*) o las heridas crónicas (*úlceras venosas*, *úlceras por presión*, y *úlceras de pie diabético*), no pueden lograr una cicatrización adecuada sin ayuda externa debido a su incorrecta actividad fisiológica. Por lo tanto, es de gran importancia entender los mecanismos de cicatrización con el fin de proponer nuevas técnicas que favorezcan el proceso de cicatrización y prevenir la aparición de complicaciones. Estos avances incluyen la aplicación de diferentes factores de crecimiento o fármacos a los pacientes, la elección de una geometría de la incisión que facilite la cicatrización en los procedimientos de cirugía, creando menos cicatrización, o el desarrollo de técnicas de sutura que permitan reducir al mínimo la formación de la cicatriz (Hall-Findlay, 1999; Pollock and Pollock, 2000). Sin embargo, cuando no se produce la cicatrización normal ni siquiera con ayuda, deben aplicarse otras técnicas más complejas y costosas.

1.2.1 Etapas de la cicatrización de heridas

La cicatrización de heridas se suele dividir en tres etapas superpuestas en el tiempo que pueden durar varios meses o años (Figura 3.6). Estas etapas se denominan: **inflamación**, **epitelización** y **remodelación** (Singer and Clark, 1999). Los procesos bien definidos que tienen lugar durante cada etapa se explican a continuación:

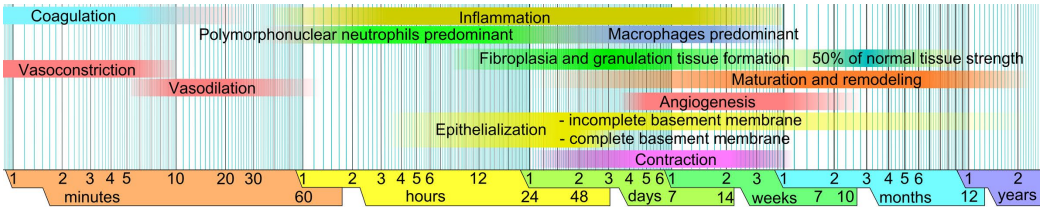

Figura 1.6: Distribución temporal de las fases de cicatrización de heridas, incluyendo los procesos más importantes, a lo largo del tiempo. Fuente: http://commons.wikimedia.org/wiki/$File$: $Wound\_healing\_phases$.png.

1. **Inflamación:** Esta etapa comienza cuando aparece la lesión. Cuando se produce una herida, la matriz extracelular se sustituye por un coágulo de sangre proveniente de los vasos rotos, y factores inflamatorios tales como el factor de crecimiento derivado de las plaquetas (PDGF) (Figura 1.7(a)) para estimular la actividad celular. Posteriormente, los vasos se cierran

para detener el sangrado (hemostasia) y un coágulo de fibrina reemplaza el coágulo de sangre (Gurtner et al., 2008). En este punto, el oxígeno ha desaparecido del tejido de la herida induciendo hipoxia, y no puede volver a ser suministrado ya que los capilares no se han regenerado todavía. Las células inflamatorias (neutrófilos y macrófagos) limpian la herida y eliminan bacterias, tejido muerto y otras partículas extrañas (Singer and Clark, 1999). La inflamación dura aproximadamente 48 horas, hasta que se eliminan todas las partículas extrañas. Al final de la fase inflamatoria se liberan factores de crecimiento tales como el TGF-β y VEGF, necesarios para guiar la actividad de las células en la siguiente etapa (Gray et al., 1995).

2. **Epitelización:** La epitelización o formación de nuevo tejido comienza algunas horas después de que aparezca la herida y se superpone con la etapa final de la inflamación, durando habitualmente entre 2 y 10 días (Gurtner et al., 2008). Esta etapa se caracteriza por la migración y proliferación de varias especies celulares, principalmente fibroblastos y células endoteliales, a la zona de la herida, atraídas por los factores de crecimiento liberados al final de la fase inflamatoria. El coágulo de fibrina es eliminado y reemplazado por tejido granular (Figura 1.7(b)). Más tarde, el tejido de granulación es sustituido por una nueva matriz extracelular constituida principalmente por colágeno. Los fibroblastos que se han infiltrado en el sitio de la herida se activan y diferencian a miofibroblastos. Ambas especies celulares secretan colágeno, inicialmente de tipo III, que se sustituye a lo largo del tiempo por colágeno más fuerte, de tipo I, el cual forma inicialmente una red de fibras desorganizada, que da soporte mecánico para la formación del nuevo tejido. En esta etapa, las células epiteliales estimuladas por el VEGF forman nuevos vasos sanguíneos a partir de los dañados, en el proceso llamado angiogénesis (Risau, 1997). Este proceso permite restablecer el flujo normal de sangre y nutrientes al tejido (Gray et al., 1995) y también el suministro de oxígeno necesario para la actividad celular. Sin embargo, la angiogénesis también es un fenómeno importante en otros procesos fisiológicos tales como la embriogénesis y la formación de tumores (Carmeliet and Jain, 2000), que puede resultar negativo cuando es excesivo.

   Por otra parte, en esta etapa se produce la contracción de la nueva matriz extracelular que contiene los nuevos capilares y varios tipos de células. La contracción del tejido se debe a las fuerzas que las células (fibroblastos y miofibroblastos) ejercen en respuesta al cambio en las propiedades del material en la zona dañada. De hecho, los miofibroblastos son capaces de ejercer fuerzas de tracción más elevadas que los fibroblastos. Por lo tanto, una proporción adecuada entre ambos tipos de células es crucial

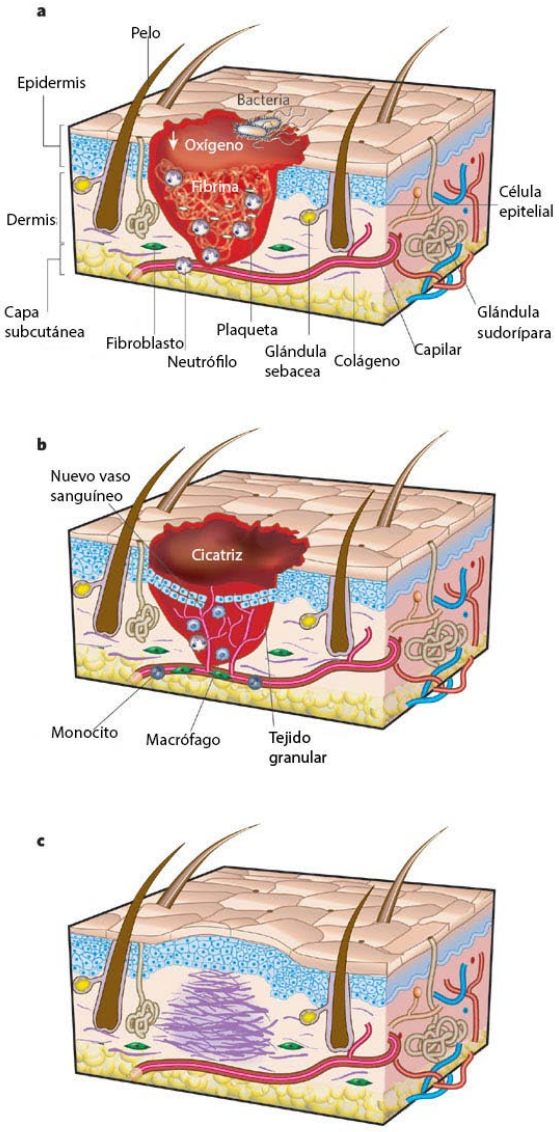

Figura 1.7: Etapas de la cicatrización de heridas a) inflamación, b) epitelización, c) remodelación. Dibujo de Gurtner et al. (2008).

para evitar trastornos en la cicatrización. Al final de la reepitelización las células innecesarias desaparecen del tejido de granulación, principalmente por apoptosis. Una vez concluido este proceso, se forma la cicatriz inicial.

Nombre	Función	Etapa de curación de heridas / Proceso	Otros
Factor de crecimiento epidérmico (EGF)	Estimula la proliferación y diferenciación de células epiteliales y mesenquimales Formación de tejido granular	Proliferación	Producido por macrófagos y keratinocitos
Factor de crecimiento de fibroblastos (FGFs)	Quimiotaxis y proliferación de los fibroblastos Migración y proliferación de los keratinocitos Estimula la angiogénesis, contracción de heridas y deposición de matriz	Angiogénesis	Producido por macrófagos, células endoteliales y fibroblastos entre otros
Factor de crecimiento de keratinocitos (KGF)	Migración, proliferación y diferenciación de keratinocitos	Epitelización	Producido por keratinocitos
Factor de crecimiento derivado de los macrófagos (MDGF)	Estimula la proliferación de fibroblastos, células de músculo liso y células endoteliales	Inflamación-Epitelización	Liberado por macrófagos
Factor de crecimiento derivado de plaquetas (PDGF)	Estimula la proliferación de fibroblastos Regula el crecimiento y división de múltiples células Influye en la formación de vasos sanguíneos (angiogénesis) y la remodelación de tejido	Inflamación/Hemostasis	Producido por plaquetas

Continúa en la página siguiente

Tabla 1.2 – *Continúa de la página anterior*

Nombre	**Función**	**Etapa de curación de heridas / Proceso**	**Otros**
Factor de crecimiento transformante beta (TGF-β)	Estimula la diferenciación de fibroblastos a miofibroblastos Controla la proliferación, diferenciación, apoptosis y otras funciones en la mayoría de las células Estimula la producción de ECM	Epitelización/Diferenciación	Producido por fibroblastos, miofibroblastos y macrófagos entre otros
Factor de crecimiento endotelial vascular (VEGF)	Estimula la angiogénesis y vasculogénesis, dirige la formación de capilares Promueve la migración de células endoteliales y fibroblastos Quimiotáctico para los macrófagos	Hipoxia-Angiogénesis	Producido por células que reciben oxígeno insuficiente

Tabla 1.2: Lista de factores de crecimiento químicos que intervienen en la curación de heridas.

3. **Remodelación:** Una vez que el nivel de colágeno en la herida recupera el de la piel sana, el colágeno comienza a reorganizarse. Al comienzo del proceso, las fibras de colágeno están orientadas aleatoriamente. Sin embargo, las fibras de colágeno tienden a orientarse con el tiempo a lo largo de direcciones preferenciales, por lo general paralelas a las líneas de tensión de la piel. Las propiedades del tejido evolucionan aumentando su resistencia a tracción. Sin embargo, la funcionalidad del tejido se recupera después de varios meses o años dependiendo de la herida (Figura 1.7 (c)) aunque una recuperación completa nunca se logra debido a que las propiedades del tejido recién formado siguen siendo ligeramente inferiores a las propiedades del tejido sano.

Durante cada etapa tienen lugar simultáneamente varios fenómenos que se rigen por la presencia de especies celulares y factores de crecimiento (ver Figura 3.6). La mayoría de los procesos celulares que ocurren durante la curación de heridas, tales como la proliferación, la diferenciación y el crecimiento, están altamente influenciados por factores de crecimiento. Los factores de crecimiento son sustancias químicas secretadas normalmente por las células, que también estimulan la actividad de estas. Se ha incluido una lista de los principales factores de crecimiento que guían los procesos de cicatrización de heridas (Tabla 1.2).

1.2.2 Complicaciones en la cicatrización de heridas

Las etapas de la cicatrización de heridas normalmente siguen un esquema predecible. Los cortes o abrasiones superficiales se curan rápidamente siguiendo la progresión habitual. Si esta progresión temporal normal no se sigue o si la persona lesionada sufre algún tipo de trastorno fisiológico pueden aparecer complicaciones en la cicatrización como cicatrices patológicas (*cicatrices hipertróficas* y *queloides*) o heridas crónicas (tales como *úlceras por presión*, *úlceras de pie diabético* y *úlceras venosas*).

La cicatrización de heridas termina con la creación de la cicatriz, que se compone de una masa no-funcional de tejido fibrótico (Gurtner et al., 2008). Este tejido está compuesto principalmente por fibroblastos y matriz extracelular que contiene la misma proteína (colágeno) que el tejido sano pero con una composición diferente (Gauglitz et al., 2011). Las cicatrices anormales pueden aparecer cuando la producción y la degradación de ECM no están bien equilibradas. Los trastornos fibroproliferativos generan cicatrización excesiva, que puede conducir a diferentes tipos de cicatrices caracterizadas por la cantidad y el tipo de colágeno sobreproducido. Mientras que las *cicatrices hipertróficas*

están formadas por colágeno tipo III, las *queloides* contienen colágeno de tipo I y tipo III. Las *cicatrices hipertróficas* están causadas por una producción excesiva de colágeno. Se producen cuando hay una lesión grave en la piel, como infección de la herida o tensión excesiva en la herida (Gauglitz et al., 2011) y el40-70 % de las cicatrices quirúrgicas puede conducir a *cicatrices hipertróficas*. Las *cicatrices hipertróficas* normalmente sólo crecen hacia arriba, mientras que las *queloides* son un tipo de *cicatrices hipertróficas* tumorales caracterizadas por su crecimiento excesivo, que afecta a los tejidos que en un principio no pertenecían a la herida. Estas cicatrices suelen aparecer en zonas de elevada tensión y causar contractura, con la consiguiente disminución de la calidad de vida del paciente (Gauglitz et al., 2011).

Igualmente problemático que la cicatrización excesiva es la cicatrización impedida, que da lugar a las heridas crónicas. Las heridas crónicas tardan más tiempo en curarse que las heridas normales y por lo general no se curan completamente sin ayuda. Hay una serie de factores que contribuyen a la aparición de heridas crónicas tales como enfermedades sistémicas (diabetes), insuficiencia arterial, infecciones o la edad avanzada. La primera causa de las heridas crónicas son las *úlceras venosas* (Snyder, 2005), causadas por el mal funcionamiento de las válvulas venosas y un crecimiento vascular no adecuado. Las *úlceras venosas* suelen aparecer en las piernas, son más probables en pacientes diabéticos y en casos críticos pueden terminar en la amputación de la extremidad. Los pacientes diabéticos tienen alrededor de un 15% de probabilidades de sufrir una *úlcera de pie diabético*, una llaga abierta situada en la parte inferior del pie. Los principales factores que dan lugar al *pie diabético* son la diabetes y las neuropatías vasculares, que producen disminución de la sensación de dolor causada por el daño de los nervios después de mantenerse los niveles de glucosa en sangre excesivamente altos. Por otra parte, la diabetes afecta a la evolución normal del proceso de curación, prolongando la fase inflamatoria, lo que retrasa la formación de tejido de granulación y reduce la fuerza de contracción en la herida (Ogawa and Hsu, 2013). Debido a su alto impacto, se han desarrollado una serie de soluciones para el tratamiento de heridas crónicas en pacientes diabéticos, incluida la aplicación de factores de crecimiento, el uso de sustitutos de la piel, las terapias de presión negativa y la terapia hiperbárica de oxígeno (HBOT) .

Las *úlceras por presión* son también una de las heridas más complicadas de curar, y se producen generalmente cuando el paciente debe permanecer inmóvil durante largos períodos de tiempo, sobre todo en cama o silla de ruedas. Por este motivo, las *úlceras por presión* aparecen por lo general en lugares donde hay una prominencia ósea, tales como el sacro, el coxis, las caderas o los talones,

como resultado de la presión constante que se aplica al tejido blando (Bluestein and Javaheri, 2008). Como consecuencia, el flujo sanguíneo se reduce dando lugar a isquemia y necrosis de los tejidos. A medida que la *úlcera por presión* evoluciona (Figura 3.8), el espesor del tejido se reduce hasta que se destruye la dermis y la grasa subyacente queda expuesta. En las etapas más graves (3 y 4) de las *úlceras por presión*, la grasa también desaparece y los huesos y los músculos quedan al descubierto (Topman et al., 2012). Las primeras etapas de la *úlcera por presión* aparecen después de unas pocas horas de inmovilidad. Por lo tanto, la mejor manera de evitar que se produzcan es un cambio constante de la posición del paciente, por lo general cada dos horas (Bluestein and Javaheri, 2008), para permitir un cambio en la distribución de la presión. El tratamiento más extendido para las *úlceras de presión* consiste en el desbridamiento del tejido necrótico para evitar el crecimiento bacteriano .

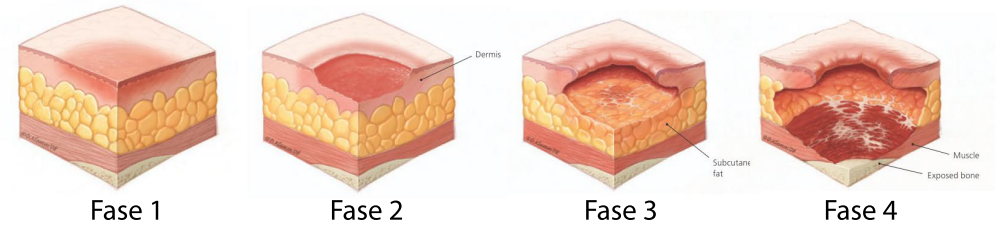

Figura 1.8: Etapas de la úlcera por presión (Gauglitz et al., 2011)

Por último, otra de las complicaciones que pueden surgir de la cicatrización de heridas es la *contractura* del tejido. Se produce cuando el tejido cicatrizado de la dermis continúa contrayéndose después de que la cicatrización haya concluido debido a la presencia de un exceso de miofibroblastos (Tomasek et al., 2002; Li and Wang, 2011). Las fuerzas generadas por los miofibroblastos dan lugar a una contractura excesiva permanente que disminuye la funcionalidad de los tejidos reduciendo su movilidad en casos extremos.

Estas complicaciones se encuentran resumidas junto con sus tratamientos en la Tabla 1.3.

Complicación	**Causa**	**Efecto**	**Tratamiento**
CICATRICES PATOLÓGICAS			
Cicatrices hipertróficas	Desórdenes fibroproliferativos	Cicatrización excesiva hacia arriba Dolor Contractura	Terapia de presión (HBOT) Suturas y recubrimientos
Queloides (cicatrices hipertróficas tumorales)	Desórdenes fibroproliferativos	Cicatrización excesiva fuera de la herida Dolor Contractura	Suturas y recubrimientos
HERIDAS CRÓNICAS			
Úlceras por presión	Inmovilidad del paciente	Isquemia Necrosis	Cambio de la posición del paciente Desbridamiento del tejido necrótico
Úlceras venosas	Mal funcionamiento de las válvulas venosas		Injertos de piel
Úlcera de pie diabético	Enfermedades vasculares Diabetes	Llaga abierta en el talón del pie	Injertos de piel
Contractura	Población excesiva de miofibroblastos	Acortamiento del tejido cicatrizado Disminución de la funcionalidad del tejido	

Tabla 1.3: Lista de complicaciones en la cicatrización y sus tratamientos.

1.2.3 Tratamientos para la cicatrización

Prevenir la aparición de complicaciones en la cicatrización es la primera estrategia para una recuperación adecuada tras una lesión. Una de las terapias más extendidas para estimular la cicatrización cuando ésta se ve dificultada es la aplicación de injertos de piel, que consiste en el trasplante de tejidos del mismo paciente o de otro sujeto de la misma o diferente especie a la zona afectada (Billingham and Medawar, 1951). Se utiliza normalmente en el tratamiento del *pie diabético*, *úlceras venosas* o heridas de microcirugía (Lineaweaver, 2013). En este procedimiento, la piel dañada se retira del paciente y se sustituye por el nuevo tejido. Los implantes pueden tener el espesor parcial o total de la piel cuando las heridas son más complicadas (Rose et al., 2014). Con menor frecuencia, se realiza el trasplante de tejidos creados artificialmente con un propósito específico en lugar de los naturales (Tauzin et al., 2014). Algunas de las complicaciones que pueden surgir de esta técnica son infecciones, daño a los nervios o rechazo de los tejidos.

Debido a que la curación de heridas tiene un alto componente mecánico, un gran número de tratamientos están basados en cambiar las condiciones mecánicas en las que la herida cicatriza, modificando el estado mecánico de la herida. Se ha demostrado que el uso de dispositivos que permiten fijar la herida como suturas, cintas o láminas que limitan estiramiento de la piel reducen la tensión en la herida para evitar la aparición de *cicatrices hipertróficas* (Visscher et al., 2001; Widgerow et al., 2000). Sin embargo, existen un gran número de tratamientos disponibles cuando no es posible evitar que estas heridas aparezcan.

Uno de los dispositivos más aplicados es el cierre asistido por vacío (VAC), que consiste en un recubrimiento de espuma que se coloca sobre la herida y se sella con una lámina. Utilizando una bomba de vacío y un tubo de drenaje se aplica presión negativa para estimular el crecimiento más rápido del tejido (Argenta and Morykwas, 1997; Scherer et al., 2002). Estos dispositivos permiten regular los gradientes de presión hidrostática y las tensiones tangenciales.

Otra terapia basada en el uso de diferentes presiones es la terapia de oxígeno hiperbárico (HBOT), que consiste en aplicar oxígeno al 100% de concentración a una presión superior a una atmósfera. Se ha aplicado a diversos tipos de heridas, en heridas graves, heridas crónicas y heridas diabéticas (Eskes et al., 2011). Eskes et al. (2011) realizaron un estudio para analizar el efecto de la HBOT en las heridas graves, encontrando que la HBOT es beneficiosa en pacientes con lesiones por aplastamiento y quemaduras, y es más eficaz cuando se aplica junto con injertos de piel. La terapia de oxígeno hiperbárico tiene múltiples efectos positivos, tales

como la reducción de la infección y la muerte celular, la generación de radicales libres de oxígeno, la inhibición de las funciones bacterianas y la mejora del transporte de ciertos antibióticos. Por otra parte, la HBOT amplifica los gradientes de oxígeno alrededor de las heridas isquémicas y mejora la formación de colágeno (Gill and Bell, 2004). Los principales efectos negativos de la HBOT son la elevada presión y la hiperoxia, que pueden causar problemas en el sistema auditivo y en la vista.

Uno de los métodos más utilizados para el tratamiento de cicatrices hipertróficas es la terapia de presión. Los efectos de esta terapia son principalmente la aceleración del proceso de remodelación y la reducción del espesor de la cicatriz junto con una disminución de la rigidez.

Por último, aunque aún no ha sido aplicada a los seres humanos, se ha observado que el uso de factores de crecimiento específicos para promover la cicatrización de la herida resulta eficaz. Kwon et al. (2006) estudió el efecto de la aplicación de un factor de crecimiento epidérmico (factor de crecimiento epidérmico humano recombinante EGFhr) en ratas. Kwon et al. (2006) aplicaron por vía tópica el EGF, encontrando que el cierre de la herida era mayor en presencia del factor de crecimiento. El uso de EGF incrementó la proliferación de miofibroblastos y la tasa de producción de colágeno. Por otra parte, se ha demostrado que el EGF disminuye la formación de cicatrices.

1.2.4 Propiedades mecánicas del tejido cicatrizado

Cuando una herida se cura, el nuevo tejido creado no tiene las mismas propiedades que el inicial. Se ha observado que el tejido de la herida muestra sólo alrededor del 20% de su resistencia en las tres primeras semanas. Además, el tejido cicatrizado sólo presenta alrededor del 70% de la resistencia mecánica del tejido sano (Levenson et al., 1965).

Aunque no hay muchos trabajos experimentales que midan las propiedades del tejido de la cicatriz algunos autores lo han hecho. Entre ellos, Clark et al. (1996) midieron el módulo elástico y la deformación de la piel para determinar la severidad de cicatrices hipertróficas derivadas de quemaduras. Las cicatrices hipertróficas presentan propiedades diferentes de las cicatrices normales, presentado mayor rigidez y menor elasticidad conforme la cicatriz es más severa. Clark et al. (1996) eligió grandes cicatrices en el brazo y el antebrazo y realizó pruebas extensómetricas de las cicatrices y de la piel sana del brazo no afectado cuando fue posible para su comparación.

1.2.5 Mecanorrecepción y mecanotransducción en cicatrización de heridas

Los procesos fisiológicos dependen de múltiples factores biológicos y químicos. Por ejemplo, Vaughan et al. (2000) estudiaron el efecto del factor de crecimiento transformante-β_1 (TGF-β_1) en los miofibroblastos. Encontraron que la fuerza generada por los miofibroblastos depende de la dosis de TGF$-\beta_1$, ya que regula la expresión de actina $\alpha-$SM. Por otra parte, el TGF$-\beta_1$ también estimula la diferenciación de los fibroblastos en miofibroblastos y aumenta la producción de colágeno (Petrov et al., 2002).

Aunque estos factores bioquímicos tienen un papel fundamental en la cicatrización, no son el único factor regulador. Múltiples estudios han demostrado la influencia de la mecánica en los procesos biológicos. Los estímulos mecánicos como la tensión y la compresión, entre otras, son percibidas por los mecanorreceptores celulares (Ogawa, 2011).

Hinz et al. (2001) investigó si la tensión mecánica influía en la diferenciación de los fibroblastos *in-vivo*. Para ello, estudió heridas de espesor completo en ratas, usando un marco de plástico en algunas heridas para estirarlas e inducir en ellas una tensión mecánica superior. Hinz et al. (2001) encontró que el aumento de la tensión inducía una mayor contractilidad del tejido y de los miofibroblastos, como consecuencia de la formación de fibras de estrés. Además, la expresión de $\alpha-$SMA se ve favorecida por la tensión mecánica (Grinnell, 2000).

La observaciones experimentales sugieren que las células sienten y reaccionan ante los estímulos mecánicos de su entorno (mecanorrecepción) para regular su actividad y modificar su entorno para hacerlo más cómodo. Análogamente, las células pueden traducir información bioquímica en actividad mecánica (mecanotransducción). Se ha demostrada que procesos como la migración celular, la diferenciación o la generación de fuerzas se ven modificados por los estímulos mecánicos.

Uno de los factores mecánicos más estudiado es la rigidez del tejido. La atracción de las células a los sustratos rígidos se llama durotaxis, y es uno de los mecanismos implicados en el crecimiento de tumores (Harland et al., 2011). Pelham and Wang (1997) investigaron la movilidad de los fibroblastos en sustratos con diferente rigidez. Su hipótesis es que las células son capaces de evaluar la rigidez del sustrato que les rodea empujando y tirando de sus receptores de integrina. Esta observación es consistente con la idea de que las

células evalúan su entorno mecánico a través de su mecanismo de actina-miosina. Por otra parte, observaron que las adhesiones focales se hacían más estables al aumentar la rigidez del sustrato. Las células se anclan al sustrato a través de las adhesiones focales (FA), que muestran diferentes comportamientos dependiendo de las propiedades mecánicas del sustrato. Discher et al. (2005) estudiaron la influencia de la rigidez del sustrato en la actividad celular. Por otra parte, las células se adhieren sólo a los sustratos que tienen una rigidez superior a un valor umbral, las adhesiones focales creadas en sustratos rígidos resultan más estables y la regulación de la generación de la fuerza en respuesta a la resistencia del sustrato. Wells (2008) también recogió el efecto de la modificación de la rigidez del sustrato en funciones celulares tales como la diferenciación y la proliferación, encontrando en las células del hígado conclusiones similares a Pelham and Wang (1997).

Mitrossilis et al. (2009) también demostraron que las células sobre sustratos elásticos modifican su actividad en función de la rigidez. Mitrossilis et al. (2009) quería dilucidar si la respuesta celular se determina por la rigidez o las fuerzas, aplicando una tracción uniaxial a una única célula viva. Sus experimentos *in-vitro* demostraron que las fuerzas ejercidas por las células aumentan a medida que el sustrato se vuelve más rígido, y que se alcanza un nivel límite de fuerza de saturación. Finalmente, Jones and Ehrlich (2011) realizaron pruebas *in-vitro* en superficies de colágeno de diferente rigidez. Sus resultados demostraron que la rigidez del sustrato condiciona la secreción de integrinas.

1.3 Modelos computacionales de cicatrización de heridas

Durante las últimas décadas, se han desarrollado modelos matemáticos para estudiar diferentes procesos biológicos y fisiológicos, tales como el daño en tejidos y su recuperación. En particular, un número elevado de estos modelos se han centrado en la piel y la curación de heridas en la piel. Estos modelos teóricos son de gran importancia, ya que pueden ayudar a dilucidar por qué una herida se cura correctamente o evoluciona a una herida crónica. Por otra parte, los modelos teóricos ofrecen la posibilidad de estudiar los factores que tienen influencia en la cicatrización de heridas. Estos factores pueden ser analizados aislados o junto con otros factores y de esta manera es posible entender qué factores son más importantes.

Durante los últimos años la curación heridas y, concretamente, algunos procesos tales como la contracción de heridas y la angiogénesis han sido ampliamente modelados utilizando modelos continuos. Sin embargo, no se ha desarrollado todavía un modelo que incluya todas las etapas de la cicatrización, ya que el número de procesos y variables que intervienen es demasiado grande, y requeriría una elevada capacidad computacional y grandes tiempos de cálculo.

Los aspectos más relevantes de los modelos revisados se resumen en la Tabla 1.4.

1.3.1 Modelos de cicatrización de heridas epidérmicas

El primer trabajo sobre la cicatrización de heridas epidérmicas fue desarrollado por Sherratt and Murray (1990). El cierre de heridas epidérmicas se debe sólo a la migración de células epidérmicas y no se ve afectado por la contracción de la herida, que sólo tiene lugar cuando las capas más profundas de la piel se ven afectadas. Sherratt and Murray (1990) propusieron un modelo continuo de reacción-difusión estableciendo que un factor de crecimiento químico producido por las células epidérmicas difundía a través del tejido. Además, la variación de la cantidad de células proviene de la migración y la mitosis regulada por el factor producido y también por la apoptosis de las células (Clark, 1988; Folkman and Moscona, 1978). El modelo se utilizó para predecir la cicatrización de una herida epidérmica con geometría circular considerando que la herida estaba cicatrizada al alcanzar una densidad celular superior al 80% de la densidad de células del tejido sano. Sherratt and Murray (1990) compararon sus resultados con uno de los pocos trabajos experimentales existentes sobre la cicatrización de heridas epidérmicas, realizado por Van den Brenk (1956) en orejas de conejo. Sherratt and Murray (1990) propusieron el primer modelo incorporando el control químico, y este ha sido la base para la mayoría de los modelos de curación y contracción de heridas. Además, su modelo ha sido adaptado también para simular la cicatrización de heridas en otros tejidos. Por ejemplo, Dale et al. (1994) lo adaptó para estudiar la cicatrización de heridas epiteliales en la cornea en función del factor de crecimiento epitelial (EGF). Además, la cicatrización de heridas epidérmicas se ha simulado junto con otros procesos que tienen lugar al mismo tiempo, tales como la angiogénesis (Maggelakis, 2003).

Autor	Procesos simulados	Variables del modelo	Modelo mecánico	Geometría	Comparación con trabajos experimentales
Sherratt and Murray (1990)	Curación de heridas epidérmicas	Células epidérmicas Factor de crecimiento regulador de la mitosis	No incluido	Heridas superficiales circulares simplificadas en un modelo axisimétrico 1D	Validado en conejo (Van den Brenk, 1956)
Tranquillo and Murray (1992)	Curación de heridas en la dermis Contracción de heridas	Fibroblastos Matriz de colágeno Desplazamientos de la matriz Factor de crecimiento genérico	Viscoelástico	Heridas superficiales circulares simplificadas en un modelo axisimétrico 1D	Validado en rata (McGrath and Simon, 1983)
Dale et al. (1994)	Curación de heridas epiteliales en la córnea	Células EGF	No incluido	Heridas superficiales circulares simplificadas en un modelo axisimétrico 1D	Validado en conejo

Continúa en la página siguiente

Tabla 1.4 – *Continúa de la página anterior*

Autor	Procesos simulados	Variables del modelo	Modelo mecánico	Geometría	Comparación con trabajos experimentales
Olsen et al. (1995)	Contracción de heridas	Fibroblastos Miofibroblastos Factor de crecimiento genérico Matriz de colágeno	Viscoelástico	Heridas superficiales circulares simplificadas en un modelo axisimétrico 1D	Validado en rata (McGrath and Simon, 1983)
Pettet et al. (1996a)	Angiogénesis	Fuentes de vasos sanguíneos Factor quimioatrayente Vasos sanguíneos	No incluido	Heridas superficiales circulares simplificadas en un modelo axisimétrico 1D	Validado en conejo (Van den Brenk, 1956)
Pettet et al. (1996b)	Angiogénesis	Fuentes de vasos sanguíneos Fibroblastos MDGF Oxígeno Matriz de colágeno	No incluido	Heridas superficiales circulares simplificadas en un modelo axisimétrico 1D	Validado en conejo (Van den Brenk, 1956)

Continúa en la página siguiente

Tabla 1.4 – *Continúa de la página anterior*

Autor	Procesos simulados	Variables del modelo	Modelo mecánico	Geometría	Comparación con trabajos experimentales
Maggelakis (2003)	Angiogénesis Curación de heridas epidérmicas	Oxígeno MDGF Capilares	No incluido	Heridas superficiales circulares simplificadas en un modelo axisimétrico 1D	No se incluye validación con resultados experimentales
Manoussaki (2003)	Angiogénesis Vasculogénesis	Células endoteliales Colágeno Factor angiogénico	Viscoelástico	Cuadradas en 2D	No se incluye validación con resultados experimentales
Javierre et al. (2008)	Cierre de heridas Angiogénesis Curación de heridas epidérmicas	Oxígeno MDGF Capilares EGF	No incluido	Heridas superficiales en 2D	No se incluye validación con resultados experimentales

Continúa en la página siguiente

Tabla 1.4 – *Continúa de la página anterior*

Autor	Procesos simulados	Variables del modelo	Modelo mecánico	Geometría	Comparación con trabajos experimentales
Schugart et al. (2008)	Angiogénesis	Fuentes de vasos sanguíneos Oxígeno Células inflamatorias Quimioatrayente Fibroblastos Miofibroblastos Matriz de colágeno	Heridas superficiales circulares simplificadas en un modelo axisimétrico 1D	No se incluye validación con resultados experimentales	
Flegg et al. (2009)	Angiogénesis en curación de heridas (aplicacion de terapia de oxígeno hiperbárico)	Oxígeno Capillary tips Vasos sanguíneos	No incluido	Heridas superficiales circulares simplificadas en un modelo axisimétrico 1D	No se incluye validación con resultados experimentales

Continúa en la página siguiente

Tabla 1.4 – *Continúa de la página anterior*

Autor	Procesos simulados	Variables del modelo	Modelo mecánico	Geometría	Comparación con trabajos experimentales
Javierre et al. (2009)	Contracción de heridas	Fibroblasts Miofibroblastos Matriz de colágeno Factor de crecimiento genérico Desplazamiento de la matriz	Viscoelástico	Heridas superficiales en 2D	No se incluye validación con resultados experimentales
Xue et al. (2009)	Cierre de heridas	Oxígeno PDGF VEGF Macrófagos Fibroblastos Matriz de colágeno Puntas de capilares	Viscoelástico	Heridas superficiales circulares simplificadas en un modelo axisimétrico 1D	Validado en cerdo (Roy et al., 2009)

Continúa en la página siguiente

Tabla 1.4 – *Continúa de la página anterior*

Autor	Procesos simulados	Variables del modelo	Modelo mecánico	Geometría	Comparación con trabajos experimentales
Flegg et al. (2010)	Angiogénesis en curación de heridas	Oxígeno Quimioatrayente Puntas de capilares Vasos sanguíneos Fibroblastos ECM	No incluido	Heridas superficiales circulares simplificadas en un modelo axisimétrico 1D	No se incluye validación con resultados experimentales
Vermolen and Javierre (2010)	Contracción de heridas Cierre de heridas Angiogénesis	Células epidérmicas Capilares Matriz de colágeno Fibroblastos Oxígeno VEGF	Viscoelástico	Heridas profundas en 2D	No se incluye validación con resultados experimentales

Continúa en la página siguiente

Tabla 1.4 – *Continúa de la página anterior*

Autor	Procesos simulados	Variables del modelo	Modelo mecánico	Geometría	Comparación con trabajos experimentales
Friedman and Xue (2011)	Cierre de heridas (en heridas crónicas)	Macrófagos Oxígeno PDGF VEGF Fibroblastos Matriz de colágeno Velocidad del contorno Fuentes de vasos sanguíneos	Viscoelástico	Heridas en 2D con simetría radial Heridas tridimensionales con simetría axial	Validado en cerdo (Roy et al., 2009)
Murphy et al. (2011)	Curación de heridas dérmincas Contracción de heridas	Fibroblastos Miofibroblastos Matriz de colágeno TGF$-\beta$	Elástico	Heridas superficiales circulares simplificadas en un modelo axisimétrico 1D	Validado en rata (McGrath and Simon, 1983)
Murphy et al. (2012)	Cierre de heridas Curación de heridas dérmicas	Fibroblastos Miofibroblastos TGF$-\beta$ PDGF Matriz de colágeno Colagenasa	Viscoelástico	Heridas superficiales circulares simplificadas en un modelo axisimétrico 1D	Validado en humano (Catty, 1965) y rata McGrath and Simon (1983)

Continúa en la página siguiente

Tabla 1.4 – *Continúa de la página anterior*

Autor	Procesos simulados	Variables del modelo	Modelo mecánico	Geometría	Comparación con trabajos experimentales
Vermolen and Javierre (2012)	Contracción de heridas Cierre de heridas Angiogénesis Regeneración dérmica	Células epidérmicas Capilares ECM Fibroblastos Oxígeno VEGF EGF	Viscoelástico	Heridas profundas bidimensionales	No se incluye validación con resultados experimentales

Tabla 1.4: Lista de modelos previos de curación de heridas y sus caracteristicas.

1.3.2 Modelos de contracción de heridas

Aunque las heridas epidérmicas representan una buena primera aproximación para el estudio de la cicatrización de heridas, las heridas que afectan a las capas más profundas y presentan más dificultades para cicatrizar también son más interesantes para estudiar. Se ha observado que las heridas que llegan a la dermis no se curan sólo con el efecto de la migración celular y son necesarios mecanismos más complejos para una curación exitosa.

La contracción de heridas es uno de los procesos más importantes durante la cicatrización de heridas dérmicas y está fuertemente influenciada por la mecánica. La reducción del tamaño de la herida es debida en parte a la retracción del contorno de la herida hacia adentro. Este desplazamiento es creado por el equilibrio entre las fuerzas que generan las células en el tejido en el que están alojadas y la resistencia que ofrece el tejido a ser deformado.

El primer modelo de contracción de heridas fue propuesto por Tranquillo and Murray (1992). Este ha sido la base para la mayoría de los modelos de contracción de heridas hasta el momento. El modelo está compuesto por un conjunto de ecuaciones diferenciales que describen la conservación de una especie celular (fibroblastos) y la densidad de colágeno de la ECM y el momento lineal de la matriz. Tranquillo and Murray (1992) incluyeron el efecto de la proliferación celular, la migración y la difusión junto con la convección pasiva debida al movimiento de la ECM. En una primera aproximación se consideró que la variación de ECM se debía sólo a su convección pasiva. Más tarde, propusieron una ley de evolución de la ECM más realista que incluía la síntesis de ECM por los fibroblastos. Por otra parte, en el mismo trabajo propusieron un modelo bioquímico más completo incluyendo el efecto quimiotáctico de un factor de crecimiento químico. La ley de momento lineal incluye el equilibrio de fuerzas entre la matriz (caracterizado como un material viscoelástico) y las fuerzas de tracción ejercidas por las células. Consideraron un dominio de estudio dividido en dos partes, la herida y la piel sana circundante. El modelo se utilizó para el estudio de heridas unidimensionales y se siguió el desplazamiento del margen de la herida durante el tiempo para medir el tamaño de la herida.

El modelo de Tranquillo and Murray (1992) fue extendido más tarde por Olsen et al. (1995). Olsen et al. (1995) propusieron un modelo de contracción de heridas que incluía el desplazamiento del tejido contraído y lo aplicaron a heridas normales y patológicos. Una de las principales diferencias entre los trabajos de Tranquillo and Murray (1992) y Olsen et al. (1995) es la incorporación

del efecto de los miofibroblastos en el proceso de contracción por Olsen et al. (1995). Los miofibroblastos son fibroblastos activados no móviles que, debido a sus similitudes con las células musculares son capaces de ejercer fuerzas de tracción superiores a las que crean los fibroblastos. Se ha observado que un nivel de contracción adecuado no se puede alcanzar sin las fuerzas ejercidas por los miofibroblastos (Tomasek et al., 2002). El modelo de Olsen et al. (1995) describe la evolución temporal de los fibroblastos, miofibroblastos, un factor de crecimiento y la matriz extracelular durante la contracción de la herida. Para modelar la evolución celular se incluye la mitosis celular, la diferenciación, la apoptosis, la convección pasiva para ambas especies y la migración de fibroblastos debido a la dispersión aleatoria y a la quimiotaxis. El modelo predice la evolución de la herida hasta alcanzar un estado de equilibrio. Siguiendo a Tranquillo and Murray (1992), se aplicó el modelo a geometrías unidimensionales, lo que reduce su aplicabilidad a heridas circulares asumiendo axisimetría.

Cook (1995) propuso un modelo mecanoquímico para la reparación dérmica incluyendo la contracción del tejido. Cook (1995) utilizó la hipótesis del estado de tensión nula, que asume un estado sin tensiones para todos los elementos, respecto a los cuales se miden las deformaciones.

A pesar de que estos modelos incluyen un gran número de los factores que guían la cicatrización de heridas, la contracción de la herida está altamente influenciada no sólo por estímulos celulares y químicos, sino también por la mecánica. Las células son capaces de sentir el entorno mecánico dónde están y regulan su actividad, por ejemplo para la generación de fuerzas, en función de ciertas propiedades mecánicas o estímulos. Se ha demostrado que procesos como la migración celular, la diferenciación o la generación de fuerzas se ven influenciados por estímulos mecánicos (Discher et al., 2005; Mitrossilis et al., 2009; Harland et al., 2011). Por lo tanto, los modelos de curación y contracción de heridas han evolucionado incluyendo el efecto regulador de las variables mecánicas en diferentes procesos bioquímicos (Javierre et al., 2009; Murphy et al., 2011, 2012). Sin embargo, no hay una opinión común sobre cual es el estímulo mecánico que regula el mecanismo mecanosensor celular.

Siguiendo el trabajo de Olsen et al. (1995), Javierre et al. (2009) propusieron un modelo matemático de contracción de heridas incluyendo fibroblastos, miofibroblastos, colágeno, un factor de crecimiento genérico y los desplazamientos del tejido. El modelo incluye el efecto de la tensión mecánica para regular los procesos celulares, definiendo las tensiones de tracción generadas por las células a través del concepto de tensión neta de un fibroblasto por unidad de matriz in-

troducido por Moreo et al. (2008). Moreo et al. (2008) propusieron un modelo mecanosensor aplicable a procesos celulares, tales como la migración o proliferación, basado en el modelo de Hill para el comportamiento del músculo esquelético. En su trabajo, se propone un modelo para evaluar las tensiones octaédricas ejercidas por las células en función de la rigidez del tejido. La tensión se evalúa por medio de dos componentes. Las primera mide las tensiones de contracción generadas por el mecanismo de miosina transmitidas a través de los haces de actina y el segundo término está relacionado con la tensión contráctil soportada por la resistencia pasiva de la célula (absorbida por los microtúbulos). Estas dos contribuciones dan lugar a la tensión que la célula transmite eficazmente a la ECM. Este enfoque considera que la deformación que el sustrato y la célula sufren es la misma. Javierre et al. (2009) también incluyó este factor en la expresión de la diferenciación de fibroblastos en miofibroblastos, ya que se había observado experimentalmente que la diferenciación es guiada por la tensión mecánica (Hinz and Gabbiani, 2003; Tomasek et al., 2002). Javierre et al. (2009) centraron también su modelo en el estudio de diferentes geometrías de la herida, creando uno de los primeros modelos mecanoquímicos de heridas en 2D. Con este modelo se estudió cómo la elongación de las heridas elípticas afecta a la contracción de la herida.

Siguiendo a Cook (1995), Murphy et al. (2011) desarrollaron un modelo 1D para reproducir la interacción entre los fenómenos celulares, químicos y mecánicos añadiendo nuevos factores. Como se ha demostrado que el TGF-β es crítico en la reparación dérmica (Shah et al., 1992), Murphy et al. (2011) incluyeron su cinética en su modelo. Murphy et al. (2011) propusieron un mecanismo de diferenciación de fibroblastos a miofibroblastos, activado por el TGF-β y la tensión de los tejidos. Aplicaron el modelo para investigar cómo se curan las heridas al producirse ciertos trastornos. Cuando hay un exceso de TGF-β esto da lugar a *contractura* causada por las fuerzas excesivas de los miofibroblastos. Por otra parte, la herida contrae insuficientemente cuando el TGF-β desaparece demasiado rápido y no hay suficientes miofibroblastos para generar fuerzas. Observaron el mismo efecto cuando la cinética de los miofibroblastos se modifica cambiando su diferenciación desde fibroblastos o la tasa de muerte. Como principal diferencia con los modelos anteriores, Murphy et al. (2011) utilizaron la elasticidad lineal para modelar el comportamiento de la piel en lugar del modelo viscoelástico elegido por otros autores (Tranquillo and Murray, 1992; Olsen et al., 1995).

Siguiendo el trabajo de Tranquillo and Murray (1992), Murphy et al. (2012) propusieron un modelo más complejo que incluía el efecto de más factores.

Además de la cinética del TGF-β, añadieron el efecto de la colagenasa (una enzima que contribuye a la formación de nuevo tejido) en la concentración de colágeno. Una de las principales diferencias del modelo de Murphy et al. (2012) con modelos anteriores era el mecanismo de diferenciación de los fibroblastos a miofibroblastos. El modelo establece que el estímulo mecánico que guía la diferenciación es la tensión elástica positiva. Esta idea fue introducida por primera vez por Hall (2008), mientras que los enfoques anteriores proponían que este estímulo era la tracción celular (Javierre et al., 2009). Murphy et al. (2012) siguieron el enfoque propuesto por Tranquillo and Murray (1992) para evaluar las fuerzas de tracción ejercidas por las células, considerándolas proporcionales a la densidad del colágeno y de la concentración de células y despreciando los términos de saturación que dependen de las densidades de células (Tranquillo and Murray, 1992) o la densidad de ECM (Olsen et al., 1995; Javierre et al., 2009). Como diferencia principal con los modelos anteriores (Olsen et al., 1995; Javierre et al., 2009), Murphy et al. (2012) consideraron que los miofibroblastos generan fuerzas de tracción, incluso en ausencia de fibroblastos, tal como se pone de manifiesto experimentalmente (Tomasek et al., 2002). También supusieron que no hay diferenciación inversa de miofibroblastos a fibroblastos. Siguiendo a Olsen et al. (1995), consideraron que la piel es un material viscoelástico, aunque Murphy et al. (2012) utilizaron una ley evolutiva para evaluar el módulo de elasticidad proporcional a la concentración de colágeno. Al igual que en los modelos anteriores, estudiaron heridas circulares superficiales aproximadas por un modelo axisimétrico unidimensional.

1.3.3 Modelos computacionales de angiogénesis durante la cicatrización de heridas

El crecimiento vascular también ha sido ampliamente modelado y simulado, principalmente la angiogénesis y la vasculogénesis. Mientras que la vasculogénesis es la formación de nuevos vasos sanguíneos cuando no hay vasculatura preexistente, la angiogénesis consiste en la formación de nuevos vasos sanguíneos a partir de los vasos preexistentes, siendo este el fenómeno que se produce durante la cicatrización de heridas. La angiogénesis también está involucrada en otros procesos biológicos, por ejemplo, el crecimiento de tumores o la embriogénesis, y por su impacto la mayoría de los trabajos computacionales sobre angiogénesis se centran en la simulación de la angiogénesis en el cáncer (Anderson and Chaplain, 1998; Chaplain, 2000; Mantzaris et al., 2004). Sin embargo, la angiogénesis en la cicatrización de heridas ha sido también ampliamente modelada. Pettet et al. (1996a) presentaron el primer modelo de angiogénesis aplicado a la cicatrización de heridas, basándose en el modelo de crecimiento fúngico de Edelstein (1982).

El modelo se compone de un conjunto de ecuaciones diferenciales para modelar la evolución de las células endoteliales de las fuentes de los capilares que migran quimiotácticamente hacia un quimioatrayente derivado de los macrófagos regulado por la densidad de la vasculatura. El suministro de oxígeno no se incluyó en el modelo y los niveles de oxígeno se suponían proporcionales a la densidad de los vasos. Más tarde la densidad de oxígeno se incluyó como una variable principal en un modelo extendido (Pettet et al., 1996b), en el que también se incluyó el efecto de los fibroblastos y la matriz extracelular. Ambos modelos reproducían geometrías en dos dimensiones aproximadas por un modelo unidimensional y permitían simular la evolución de heridas normales y también de heridas que no cicatrizan.

Maggelakis (2003) desarrolló un modelo de angiogénesis incluyendo el efecto de factores de crecimiento derivados de macrófagos (MDGF), la densidad capilar y la concentración de oxígeno en el tejido, en una dimensión. Maggelakis (2003) propuso que el oxígeno es proporcionado a la herida por los capilares y es consumido por los macrófagos, que aparecen cuando hay una baja concentración de oxígeno y secretan MDGF, al mismo tiempo que se difunde a través del tejido. Por último, los altos niveles de MDGF mejoraron la aparición de capilares, regulados también por un bucle de retroalimentación negativa hasta alcanzar la capacidad máxima. El modelo fue utilizado para estudiar la dependencia de la curación de una herida circular con el suministro de oxígeno. Un modelo posterior fue propuesto por Javierre et al. (2008), agregando una nueva variable: el factor de crecimiento epidérmico (EGF). Javierre et al. (2008) propuso un acoplamiento entre la angiogénesis y una interfaz de la herida debido a la migración celular para estudiar el efecto de la disponibilidad de oxígeno durante la cicatrización de heridas epidérmicas en dos dimensiones.

Uno de los factores que impide la cicatrización de heridas es la hipoxia, falta del oxígeno necesario para la actividad celular (Schreml et al., 2010). El oxígeno se suministra principalmente por los capilares y por lo tanto la angiogénesis es crucial para restaurar el flujo regular de oxígeno. Por lo tanto, muchos autores han propuesto modelos de angiogénesis centrados en el papel del oxígeno durante la angiogénesis. Schugart et al. (2008), propusieron un modelo de siete variables siguiendo a Pettet et al. (1996b) y añadiendo el efecto de los macrófagos. Se estudió por primera vez el papel de la tensión de oxígeno del tejido en el proceso de cicatrización de la herida y se estableció que existe un nivel óptimo de hipoxia para el crecimiento vascular y la cicatrización de heridas. En algunos casos, el suministro de oxígeno natural no es suficiente para una curación adecuada, causando hipoxia y terminando posteriormente en la aparición de heridas crónicas.

Flegg et al. (2009) simularon una de las técnicas que se utilizan para el tratamiento de esta patología, la terapia de oxígeno hiperbárico (HBOT), que consiste en la elevación de los niveles de oxígeno de manera deliberada. Se estudió el efecto de la HBOT en la angiogénesis en heridas graves y crónicas. En un primer modelo Flegg et al. (2009) estudiaron la evolución de la densidad de oxígeno, fuentes de capilares y vasos sanguíneos. Flegg et al. (2009) predijeron que la HBOT intermitente ayuda a curar a las heridas crónicas, pero el oxígeno normobárico no tiene efectos positivos. Más tarde, Flegg et al. (2010) ampliaron el modelo incluyendo el efecto de un quimioatrayente, los fibroblastos y la matriz extracelular, y lo aplicaron a las heridas crónicas causadas por la diabetes. Ellos estudiaron el efecto de diferentes presiones, porcentaje de oxígeno, tiempo de exposición de la herida y frecuencia de aplicación. En todos los casos estudiados se encontró que el tratamiento es beneficioso sólo bajo ciertas condiciones.

De la misma manera que la contracción de la herida depende de factores mecánicos, la angiogénesis también se ve influida por la mecánica. Aunque existen múltiples modelos mecanoquímicos de curación de heridas (Tranquillo and Murray, 1992; Olsen et al., 1995; Javierre et al., 2009; Murphy et al., 2011, 2012) el número de modelos mecanoquímicos de angiogénesis durante la contracción de heridas es reducido. Vermolen and Javierre (2010) desarrollaron un modelo incluyendo angiogénesis, contracción y el cierre de la herida. Para ello combinaron el modelo de Tranquillo and Murray (1992) para modelar el proceso de contracción y el de Maggelakis (2003) para el proceso de la angiogénesis. Sin embargo, estos procesos son tratados de manera aislada, sin tener en cuenta su interacción. Se estudiaron los procesos por separado en la dermis y la epidermis permitiendo el estudio de heridas profundas. Más tarde, Vermolen and Javierre (2012) modificaron el modelo añadiendo el proceso de regeneración dérmica acoplado con el proceso de angiogénesis .

Manoussaki (2003) desarrolló un modelo mecanoquímico de la angiogénesis teniendo en cuenta las fuerzas de tracción ejercidas por las células en la matriz, modelada como un material viscoelástico. Por otra parte, el movimiento de las células es causado por quimiotaxis guiadas por un factor químico regulado por sí mismas. Aunque Manoussaki (2003) no se centró en la cicatrización de heridas, su modelo podría ser adaptado a esta aplicación. Xue et al. (2009) extendieron el modelo de Schugart et al. (2008) incorporando el comportamiento mecánico de la piel.

1.3.4 Limitaciones de los modelos existentes

Los modelos matemáticos de procesos biológicos normalmente proceden de un mismo modelo inicial. Aunque los autores extienden y modifican este modelo inicial añadiendo nuevos factores y variables, muchas veces no se centran en resolver las limitaciones del modelo original, y estas se transmiten de un modelo a los siguientes.

Una de las limitaciones principales de los modelos de contracción de heridas es que suelen limitarse a geometrías unidimensionales (Murray et al., 1998; Sherratt and Murray, 1990; Schugart et al., 2008; Murphy et al., 2011; Olsen et al., 1995, 1996; Murphy et al., 2012). Estas geometrías son útiles para estudiar heridas simples con geometrías axisimétricas ya que permiten reducir el problema a un modelo unidimensional, con un menor coste de tiempo y recursos. Sin embargo, esta simplificación de la geometría real de la morfología de la herida limita el poder predictivo del modelo. En este sentido, algunos trabajos recientes estudian geometrías en dos dimensiones (Javierre et al., 2008, 2009; Vermolen and Javierre, 2010, 2012), acercando los modelos a situaciones reales, sin embargo los modelos en tres dimensiones son necesarios para obtener una representación fiel de los procesos que suceden.

Otra de las limitaciones de los modelos existentes es que la mayoría se centran en el estudio de heridas superficiales atendiendo a la evolución de su área superficial y sin tener en cuenta la influencia de la profundidad de la herida en la contracción. Por lo tanto, Olsen et al. (1995); Javierre et al. (2009); Murphy et al. (2012) utilizan la hipótesis de tensión plana para simplificar la geometría real de las heridas. Sin embargo, los fenómenos que tienen lugar a lo largo de la profundidad de la herida son igualmente importantes, aunque no han sido modelados por su complejidad. Por lo que nosotros sabemos, sólo Vermolen and Javierre (2012) han estudiado heridas profundas utilizando hipótesis de deformación plana para reducir la geometría de la herida a dos dimensiones. El uso de geometrías tridimensionales proporcionaría los resultados más realistas, sin embargo, utilizar el modelo de deformación plana para estudiar las heridas a lo largo de su profundidad puede revelar información útil sin la complejidad y el coste computacional de los modelos tridimensionales.

Existen algunas diferencias cuando se consideran las simplificaciones de tensión plana y deformación plana. En primer lugar, cuando se simulan heridas profundas, una parte de la frontera no está rodeado por la piel, mientras que las heridas superficiales están completamente rodeadas por tejido sano. La parte de la

frontera que está en contacto con el aire está representada por una frontera libre. La implicación principal es que se puede mover libremente, ya que no hay tejido unido a él. Cuando se formula el modelo matemático, esta frontera libre debe ser tratada de manera diferente al resto del contorno. Algunas de las simplificaciones supuestas para el contorno no libre no son aplicables a esta frontera libre. Desde una perspectiva numérica las heridas planas bajo hipótesis de tensión plana son más fáciles de modelar ya que no es necesario tener en cuenta las condiciones de contorno naturales.

Otra diferencia entre el estudio de heridas planas y profundas es la consideración de las distintas capas de la piel. Cuando se simulan heridas planas solo las propiedades de la capa más superficial de la piel se consideran, como es el caso de los modelos de curación de heridas epidérmicas (Sherratt and Murray, 1990; Maggelakis, 2003; Javierre et al., 2008) y algunos modelo de cicatrización de heridas dérmicas (Tranquillo and Murray, 1992; Murphy et al., 2011, 2012). Cuando se simulan heridas profundas, dependiendo de la profundidad considerada de la herida, no es posible caracterizar toda la geometría con las mismas propiedades. Se sabe que la capa más externa de la piel, la epidermis, tiene un espesor de micrómetros. Sin embargo, la dermis por lo general tiene un espesor de 1,5 mm a 4 mm y la hipodermis alcanza diferentes profundidades dependiendo de la parte considerada del cuerpo. Por lo tanto, cuando se estudian heridas profundas las propiedades de las diferentes capas de la piel deben ser consideradas con el fin de obtener resultados más realistas.

Por último, uno de los aspectos más limitantes en el modelado de la cicatrización de heridas es la caracterización mecánica de la piel. Tradicionalmente, se ha utilizado un modelo de material viscoelástico para modelar el comportamiento mecánico de la piel. Este material reproduce con exactitud algunas de las propiedades de la piel que dependen del tiempo, pero también presenta algunas limitaciones. Se ha demostrado experimentalmente que el modelo constitutivo hiperelástico encaja mejor en el comportamiento de la piel, aunque su caracterización es más complicada. La mayoría de los modelos de cicatrización de heridas que incluyen aspectos mecánicos (deformación del tejido) han considerado la piel (o sus capas) como un material viscoelástico (Olsen et al., 1995; Javierre et al., 2009; Murphy et al., 2012). Sin embargo, la simulación de la piel como un material hiperelástico permitiría reproducir el comportamiento de la piel con más precisión, incluyendo la posibilidad de añadir anisotropía tejido.

1.4 Trabajos experimentales

A pesar de la existencia de un gran número de modelos computacionales que simulan los diferentes aspectos de la curación de heridas, el número de estudios experimentales en el campo para validar los resultados computacionales es muy reducido.

Debido a razones éticas, los experimentos de cicatrización de heridas en sujetos vivos no son frecuentes, casi inexistentes en seres humanos. En consecuencia, los ensayos con animales son la mejor opción a pesar de que también son objeto de consideraciones éticas. Por otra parte, la piel de los mamíferos presenta diferentes propiedades mecánicas a las de la piel humana, y los resultados obtenidos en estos experimentos sólo se pueden utilizar como un patrón cualitativo para los seres humanos.

Uno de los primeros estudios experimentales se debe a Van den Brenk (1956). Van den Brenk (1956) estudió heridas epidérmicas en orejas de conejo. Sus resultados fueron utilizados para la validación de los resultados de Sherratt and Murray (1990).

McGrath and Simon (1983) estudiaron la influencia de la forma y el tamaño de las heridas profundas en ratas. Observaron la evolución de heridas con tres geometrías distintas: una herida cuadrada pequeña y otra grande y una herida circular con la misma superficie que la herida cuadrada grande. Para medir el tamaño de la herida, McGrath and Simon (1983) siguieron el movimiento de algunos puntos que definían la frontera de la herida. Diferenciaron la curación debida a la contracción de la herida y a la epitelización. Después de una distracción rápida de la herida y una fase de seis días sin variaciones, las heridas se contrajeron durante alrededor de 30 días, y posteriormente permanecieron prácticamente sin variaciones. McGrath and Simon (1983) observaron que después de 70 días todas las heridas habían experimentado una tasa de contracción similar, reduciendo su tamaño al 35% del tamaño inicial.

La mayoría de los mamíferos tales como ratas y conejos presentan una piel más flexible y más elástica que los seres humanos, y los niveles de contracción que estos experimentan no son comparables con los de los seres humanos. Sin embargo, la piel del cerdo presenta una estructura más similar a la de la piel humana, por lo tanto el modelo porcino es ampliamente aceptado para las comparaciones. Roy et al. (2009) observaron la evolución de heridas circulares isquémicas y no isquémicas en cerdos. Se realizaron incisiones y mientras algunas

heridas se dejaron curar normalmente, en otras se introdujeron láminas de silicona entre la dermis y el tejido subyacente. De esta manera se pudieron reproducir las heridas isquémicas, en las que la re-epitelización está impedida. Roy et al. (2009) fueron capaces de medir la concentración de oxígeno y la presión parcial de oxígeno en la herida, encontrando niveles de saturación de oxígeno más elevados en las heridas no isquémicas. También observaron el cierre de la herida a lo largo de 31 días, cuando la herida no isquémica casi había cerrado pero la herida isquémica solo había logrado alrededor del 80% del cierre.

Al comparar los resultados experimentales con modelos humanos, hay que tener en cuenta que cada especie tiene diferentes parámetros, debido a sus diferentes cinéticas celulares y tisulares (Reina-Romo et al., 2010). Por lo tanto, si se obtiene una equivalencia adecuada entre especies, es posible la comparación de los resultados experimentales en animales y los resultados obtenidos computacionalmente en los modelos humanos.

1.5 Objetivos

El objetivo principal de esta tesis es el estudio de la cicatrización de heridas en la piel a través de la simulación computacional y el uso de un enfoque multidisciplinar. Con el fin de lograr este objetivo, se ha propuesto e implementado un modelo computacional que permite reproducir la cicatrización de heridas en diferentes condiciones. Más concretamente, el modelo propuesto se centra en la fase de contracción de la herida, ya que tiene un fuerte componente mecánico. El modelo también permite incluir más procesos que tienen lugar de forma simultánea a la contracción de la herida, tales como la angiogénesis. El modelo propuesto incluye factores biológicos (especies celulares, factores de crecimiento y colágeno) y también factores mecánicos (caracterización de las propiedades mecánicas de la piel y contracción celular). Para encontrar la solución del problema resultante, se aplica el método de los elementos finitos (MEF). El modelo está constituido por dos partes, una relacionada con el análisis bioquímico del proceso y otra en relación al análisis mecánico de la piel. En primer lugar, la evolución de las especies bioquímicas se evalúa con un sistema de ecuaciones de reacción-difusión. En segundo lugar, el comportamiento mecánico de la piel se modela teniendo en cuenta las relaciones mecánicas fundamentales para el modelo de material constitutivo elegido para caracterizarla. Las dos partes están relacionadas a través de un mecanismo mecanosensor y mecanotransductor, que regula el comportamiento de las células en función de las variables mecánicas. El modelo permitirá estudiar diferentes casos de curación y diferentes tipos de heridas. Los objetivos principales se resumen a continuación:

- Adaptación del modelo para el estudio de heridas planas y heridas profundas en dos dimensiones. Las heridas planas se caracterizan por su área superficial, utilizando hipótesis de tensión plana. Las heridas largas y profundas se estudian a través de su sección transversal, bajo un enfoque de deformación plana y teniendo en cuenta las diferentes capas de la piel que se ven afectadas por la lesión.

- Utilización de varios modelos constitutivos (viscoelástico, hiperelástico isótropo e hiperelástico anisótropo) para caracterizar el comportamiento mecánico de la piel. Los materiales viscoelásticos son una buena opción para reproducir el comportamiento de la piel. Por otra parte, los materiales viscoelásticos se pueden utilizar cuando se aplica la teoría de las pequeñas deformaciones, pero no cuando el material trabaja con grandes deformaciones. En este caso, se deben utilizar materiales hiperelásticos.

- Incorporación de otros fenómenos que tienen lugar de forma simultánea a la contracción de la herida, como la angiogénesis. Como se sabe, todos los fenómenos que tiene lugar durante la cicatrización están relacionados entre sí, por lo que la inclusión de la mayor cantidad de procesos proporciona un modelo más completo y realista. El principal inconveniente es el aumento de los recursos necesarios para resolver el problema al incrementar la precisión del modelo.

- Incorporación de nuevas leyes de cinética celular en función de evidencias físicas, basadas en estudios experimentales en lugar de las leyes fenomenológicas propuestas hasta ahora.

- Resolución de los problemas bioquímicos y mecánicos utilizando un enfoque totalmente acoplado o un enfoque no acoplado. Si bien un enfoque totalmente acoplado permite resolver todo el problema al mismo tiempo, un enfoque no acoplado permite dividir el problema y resolverlo en diferentes etapas. Esto es especialmente útil para separar el análisis bioquímico y el análisis mecánico debido a sus diferentes escalas de tiempo. Por otra parte, permite utilizar un lagrangiano actualizado y la actualización de determinadas variables entre las dos etapas.

- Aplicación del modelo a heridas con diferentes tamaños y formas en dos dimensiones, tanto heridas planas como profundas. La capacidad del modelo para reproducir geometrías complejas, tales como las consideradas en trabajos experimentales, permite una validación más completa de los resultados.

- Aplicación del modelo para simular heridas en tres dimensiones, en las que el efecto de la forma superficial y profundidad de la herida se examinan simultáneamente.
- Incorporación de las fibras de colágeno en la piel sana. Las fibras de colágeno permiten simular la anisotropía real de la piel en lugar de utilizar simplificaciones isótropas, lo cual es importante en la piel sana que rodea a la herida.

1.6 Financiación

Los estudios incluidos en esta tesis han sido financiados por:

- El Ministerio Español de Ciencia e Innovación a través de la beca BES2010-037281 y el proyecto DPI2009-07514. Este proyecto fue parcialmente financiado por la Unión Europea (a través de los fondos FEDER).
- El Ministerio Español de Economía y Competitividad a través del proyecto DPI2012-32888. Este proyecto está parcialmente financiado por la unión europea (a través de los fondos FEDER).
- El Consejo Europeo de Investigación (ERC) a través del proyecto ERC-2012-StG 306751.

CAPÍTULO 2

Conclusiones

La motivación principal de esta tesis es el estudio de la piel después de sufrir una lesión. Entender el proceso de cicatrización de la herida con el fin de reproducirla mediante modelos computacionales es fundamental para avanzar en el desarrollo de soluciones curativas y procedimientos quirúrgicos. Para lograr este objetivo, se ha propuesto e implementado un modelo de contracción de heridas en piel humana para ayudar a entender el proceso y sus posibles soluciones cuando este no sigue la evolución normal.

El trabajo se ha centrado en el punto de vista teórico del problema, incluyendo ecuaciones espacio-temporales de difusión-convección para describir el problema biológico combinado con la formulación del problema mecánico.

2.1 Conclusiones generales

Las conclusiones principales que se han obtenido de esta tesis, considerando los estudios numéricos realizados, se presentan a continuación. Teniendo en cuenta que las heridas que se contraen en menor medida generan cicatrices más pequeñas, lo cual es muy conveniente, las principales conclusiones desde el punto de vista biológico, son las siguientes:

- Cuando se estudian heridas profundas a través de su sección transversal, se observa que las heridas con la misma área pero diferente longitud de superficie libre presentan diferentes porcentajes de contracción. Las heridas que son más profundas y más estrechas se contraen menos que las heridas más anchas y menos profundas.
- Cuando la contracción de la herida y la angiogénesis son simuladas juntas en heridas planas, se ha encontrado que las heridas más alargadas (elípticas)

muestran una vascularización más rápida que las circulares. Sin embargo, la contracción experimentada por ambas heridas estudiadas, en comparación con el tamaño inicial, es similar. La mayor rapidez de los procesos bioquímicos en la herida elíptica pueden ser causados por la difusión más rápida de las sustancias, debido a la relación más elevada de contorno respecto a la superficie de la herida.

- Cuando se analiza el efecto del tamaño en las heridas planas, se observa que las heridas grandes comienzan a contraerse antes en el tiempo. Sin embargo, al final del proceso de contracción estas heridas han contraído menos que las heridas más pequeñas, en relación con el tamaño inicial de la herida.

- En heridas profundas, es muy importante tener en cuenta las diferentes capas de la piel. La dermis y los tejidos subyacentes tienen diferentes propiedades mecánicas y la dermis es más rígida que el tejido subyacente.

En relación al modelo, su implementación y sus aspectos numéricos, las conclusiones más importantes son:

- Cuando las heridas se analizan en dos dimensiones, la decisión más importante es elegir el estudio de la herida bajo un enfoque de deformación plana o de tensión plana. Esto implica el estudio de la herida a través de su sección transversal o de su área superficial. La selección entre los dos enfoques depende de qué tipo de herida se está estudiando.

- El modelo mecánico constitutivo del material determina altamente la evolución del proceso de contracción. El uso de modelos más realistas, como el hiperelástico ayuda a obtener también resultados más realistas. Incluir las fibras en el modelo hiperelástico de la piel permite modelar el comportamiento anisótropo real de la piel. Se ha encontrado que la orientación de las fibras en la piel no modifica altamente la tasa de contracción de la herida, pero modifica la distribución de las deformaciones volumétricas alrededor de la herida.

- Las variables mecánicas influyen en procesos biológicos como la diferenciación celular y la generación de tensiones. Se ha postulado que la deformación volumétrica es el estímulo mecánico que regula este proceso, ya que depende de la rigidez del tejido.

- La inclusión de leyes basadas en evidencias experimentales en lugar de las leyes fenomenológicas existentes proporciona resultados igualmente buenos.

2.2 Contribuciones originales

El desarrollo de esta tesis ha dado como resultado un modelo computacional para simular la curación de heridas que permite incluir diferentes procesos y estudiar distintas variables y su efecto en el proceso de curación. Los aspectos de esta tesis que son completamente nuevos y que no han sido incluidos en modelos previos de cicatrización de heridas, por lo que sabemos, son:

- La tensión generada por las células se ha modelado a través de una nueva ley basada en evidencias experimentales. Los mecanismos considerados anteriormente para representar estas tensiones eran principalmente fenomenológicos, y aunque los resultados son igualmente buenos, no existía justificación física para estas leyes. El modelo propuesto generaliza los modelos anteriores con un mecanismo de regulación de la actividad celular regulado por la rigidización de la matriz extracelular.

- La ley fenomenológica de diferenciación de fibroblastos también se ha actualizado por una ley basada en evidencias físicas. Una vez más, la ley propuesta sigue observaciones experimentales regulándose a través de la rigidez del tejido, fácilmente medible.

- Se ha presentado un modelo de cicatrización de heridas, que incluye la angiogénesis y la contracción de la herida en tres dimensiones. La mayoría de los modelos existentes reproducen geometrías bidimensionales, utilizando simplificaciones de tensión plana o de deformación plana o incluso simplificaciones unidimensionales. El desarrollo de un modelo tridimensional para estudiar la cicatrización permite reproducir geometrías más complejas y realistas; también analizar el comportamiento global de la herida.

- Se ha utilizado un material hiperelástico que incorpora el efecto anisótropo de las fibras de colágeno para modelar el comportamiento de la piel. Los modelos existentes de cicatrización de heridas no tienen en cuenta este comportamiento, que en parte regula el proceso de curación.

Desde el punto de vista numérico las contribuciones principales son:

- Se ha formulado el problema de manera totalmente acoplada y por otra parte de manera desacoplada. La forma tradicional de resolver este tipo de problema es utilizando la implementación totalmente acoplada, que permite evaluar los problemas bioquímico y mecánico al mismo tiempo. La contribución de este trabajo es el desacoplamiento de los dos modelos.

Este enfoque permite hacer frente a las dos escalas de tiempo diferentes de los problemas bioquímico y mecánico. Además, permite actualizar las variables entre la solución de los dos problemas.

- Se ha implementado la actualización de la malla para resolver el problema de manera más precisa, mediante un algoritmo lagrangiano actualizado, necesario para utilizar las hipótesis de pequeñas deformaciones. Utilizando esta técnica se evita que las deformaciones sufridas por la malla sean mayores que las permitidas cuando se utilizan las hipótesis de pequeñas deformaciones.

- Se ha implementado una subrutina de elemento de usuario utilizando el programa comercial de elementos finitos Abaqus® (Hibbit et al., 2008). Este elemento incorpora las ecuaciones del modelo que describen el problema y las condiciones de contorno del problema, que se resuelve con el método de los elementos finitos. Por otra parte, la aplicación de las condiciones de contorno naturales para un problema con frontera libre se han incluido en la formulación. El elemento desarrollado permite elegir entre los enfoques de tensión y deformación plana en dos dimensiones, permitiendo simular heridas planas y heridas profundas.

2.2.1 Publicaciones y comunicaciones

El trabajo desarrollado en esta tesis ha dado lugar a tres artículos publicados en revistas JCR y otro artículo que se encuentra en el proceso de revisión. Además, un quinto artículo ha sido publicado en una revista JCR, como resultado del trabajo desarrollado durante una estancia de investigación en los EE.UU. Estos documentos se enumeran en la Tabla 2.1.

Además de estos artículos, se han presentado un total de 12 contribuciones en congresos nacionales e internacionales. Las contribuciones están detalladas en la Tabla 2.2.

Finalmente, se recibió la invitación para la colaboración en la escritura de un capítulo de libro con los resultados de este trabajo:

Autores: E. Reina-Romo, **C. Valero**, C. Borau, R. Rey, E. Javierre, M.J. Gómez-Benito, J. Domínguez, J.M. García-Aznar
Título: Mechanobiological modelling of angiogenesis: impact on tissue engineering and bone regeneration
Libro: Computational Modeling in Tissue Engineering, pp.379-404
Fecha: 01/2013

DOI:10.1007/8415_2011_111 ISBN: 978-3-642-32562-5
Editorial: Springer-Verlag Berlin Heidelberg
Editor: Liesbet Geris.

2.3 Líneas futuras

Teniendo en cuenta los resultados y las conclusiones obtenidas a partir de los trabajos desarrollados en esta tesis y sus limitaciones, se definen algunas líneas de trabajo futuro:

- Extensión del modelo de contracción bidimensional a tres dimensiones. El uso de las hipótesis de deformación plana y de tensión plana permite estudiar un gran número de geometrías y casos de heridas, pero también implica la pérdida de información en el proceso de simulación. El modelo tridimensional actual incluye la angiogénesis y la contracción de la herida guiada solamente por los fibroblastos. El modelo está listo para ser ampliado con los miofibroblastos y la cinética de colágeno.

- El comportamiento volumétrico de la célula se podría mejorar utilizando una descripción más completa, teniendo en cuenta el comportamiento anisótropo de la célula. El modelo propuesto en la tesis considera que las células ejercen la misma tracción en todas las direcciones independientemente de la dirección en la que la célula se ha deformado. Un modelo más evolucionado distinguirá la magnitud en la que la célula se ha deformado a lo largo de cada dirección y, por lo tanto, podrá regular las fuerzas ejercidas como consecuencia de estas diferentes deformaciones.

- Incorporación de los fenómenos de remodelación en el tejido de la herida después de la curación. El modelo actual incluye el efecto de las fibras en la piel sana, pero no reproduce la producción y la remodelación de las fibras en la herida cicatrizada. Un enfoque más realista incluirá la producción de fibras y su orientación en el tejido, siempre y cuando se alcance un nivel de curación adecuado. Por otra parte, la orientación de las fibras será regulada por la dirección de los mayores niveles de tensión.

- Incorporación de todas las capas de la piel en la geometría tridimensional. De igual manera que la dermis y el tejido subyacente se modelan separadamente en el modelo de deformación plana, estas capas se pueden separar en el modelo de tres dimensiones, incluyendo sus diferentes propiedades. Esta modificación proporcionará un comportamiento más realista.

- Estudio de patologías de la herida, en las que la cicatrización está impedida, es excesiva o presenta otras dificultades tales como las úlceras por presión o queloides. El estudio de estos casos podría ser simulado ajustando adecuadamente la cinética bioquímica o las propiedades de la piel.
- Estudio de diferentes tratamientos, tales como suturas u otros dispositivos que modifican las condiciones mecánicas en las que se curan las heridas. La simulación de estos fenómenos será importante para ayudar a los médicos en la elección de soluciones favorables en casos específicos.

Trabajo	**Título**	**Autores**	**Revista**	**IF***	**Fecha de publicación**
1	Nonlinear finite element simulations of injuries with free boundaries: Application to surgical wounds	**C.Valero**, E. Javierre, J.M. García Aznar, M.J. Gómez-Benito	Int. J. Numer. Meth. Biomed. Engng. (2014). DOI: 10.1002/cnm.2621	1.310	En línea
2	Numerical modelling of the angiogenesis process in wound contraction	**C.Valero**, E. Javierre, J.M. García Aznar, M.J. Gómez-Benito	Biomech Model Mechanobiol. DOI: 10.1007/s10237-012-0403-x	3.331	
3	A cell-regulatory mechanism involving feedback between contraction and tissue formation guides wound healing progression	**C.Valero**, E. Javierre, J.M. García Aznar, M.J. Gómez-Benito	PLOS ONE. DOI:10.1371/journal.pone.0092774	3.730	En línea
4	Modeling anisotropic wound healing: effect of the relative position of wounds with respect to collagen fibers orientation	**C.Valero**, E. Javierre, J.M. García Aznar, M.J. Gómez-Benito, A. Menzel	Journal of the Mechanics and Physics of Solids	3.406	En revisión
5	A computational study of stress fiber-focal adhesion dynamics governing cell contractility	M.Maraldi, **C.Valero**, K.Garikipati	Biophysical Journal	3.668	Aceptado para publicación

*Factor de impacto de la revista.

Tabla 2.1: Artículos publicados como resultado del trabajo realizado en esta tesis.

	Título	Autores	Congreso	Lugar y fecha	Participación
1	Finite element modelling of wound contraction: a non-linear mechano-chemical approach	**C. Valero**, J.M. García Aznar, M.J. Gómez-Benito, E. Javierre	Congress on Numerical Methods in Engineering CMNE 2011	Junio 2011, Coimbra (Portugal)	Ponente
2	Three dimensional modelling of wound contraction.	**C. Valero**, J.M. García Aznar, M.J. Gómez-Benito, E. Javierre	XXIII congress International Society of Biomechanics (ISB 2011)	Julio 2011, Bruselas (Bélgica)	Ponente
3	Finite Element Analysis of the angiogenesis process in wound healing	**C. Valero**, E. Javierre, M.J. Gómez-Benito	XVIII congress of the European Society of Biomechanics (ESB 2012)	Julio 2012, Lisboa (Portugal)	Ponente
4	Modelling skin healing: Effect of cell traction	**C. Valero**, E. Javierre, J.M. García Aznar, M.J. Gómez-Benito	XIVrd congress of the European Society of Biomechanics (ESB 2013)	Agosto 2013, Patras (Grecia)	Ponente
5	A cell-regulatory mechanism between wound contraction and tissue formation	**C. Valero**, E. Javierre, J.M. García Aznar, M.J. Gómez-Benito	V International Conference on Computational Bioengineering (ICCB 2013)	Septiembre 2013, Lovaina (Bélgica)	Coautor
6	Modelado multifísico de la contracción de heridas (Multi-physical modeling of wound contraction)	**C. Valero**, E. Javierre.	XV Reunión de Usuarios del Programa	Octubre 2010, Madrid (España)	Ponente

Continúa en la página siguiente

Tabla 2.2 – *Continúa de la página anterior*

	Título	Autores	Congreso	Lugar y fecha	Participación
7	Simulación por elementos finitos del proceso de angiogénesis aplicado a la cicatrización de heridas	**C. Valero**, E. Javierre, J.M. García Aznar, M.J. Gómez-Benito	Reunión del Capítulo de la ESB	Noviembre 2011, Zaragoza (España)	Ponente
8	In-silico Models of Wound and Bone Healing: Examples from Nature	M.J. Gómez-Benito , **C. Valero**, E. Reina-Romo, J.M. García Aznar, E. Javierre	Euro Bio-inspired Materials - International School and Conference on Biological Materials Science.	Marzo 2012, Potsdam (Alemania)	Coautor
9	Stress Evaluation During Angiogenesis in Skin Wound Healing	**C. Valero**, E. Javierre, J.M. García Aznar, M.J. Gómez-Benito	10th International Symposium Computer Methods in Biomechanics and Biomedical Engineering (CMBBE 2012)	Abril 2012, Berlin (Alemania)	Coautor
10	A Mechano-Chemical Model of Wound Contraction for Superficial and Acute Wounds	E. Javierre, **C. Valero**, M.J. Gómez-Benito, J.M. García-Aznar	. XVIIIrd congress of the European Society of Biomechanics (ESB 2012)	Julio 2012, Lisboa (Portugal)	Coautor
11	Mathematical analysis of physiological and pathological wound healing. Application to diabetic foot ulcers	E. Javierre, **C. Valero**, M.J. Gómez-Benito, F.J. Vermolen	Mathematical Modelling in Engineering & Human Behavior	Septiembre 2012, Valencia (España)	Coautor

Continúa en la página siguiente

Tabla 2.2 – *Continúa de la página anterior*

	Título	**Autores**	**Congreso**	**Lugar y fecha**	**Participación**
12	Finite element analysis of the mechanoc-chemical regulation of the wound contraction in surgical wounds	E. Javierre, **C. Valero**, M.J. Gómez-Benito, J.M. García-Aznar	Conference on the Mathematics of Finite Elements and Applications MAFELAP 2013	Junio 2013, Uxbridge (Reino Unido)	Coautor

Tabla 2.2: Trabajos presentados en congresos nacionales e internacionales.

GENERAL INTRODUCTION AND CONCLUSIONS

Mechanochemical modeling of wound healing: multiphysics finite element simulations.

CHAPTER 3

Introduction

Wounds in the skin are a major health matter that most people suffer along their live. When the injured person has not serious health problems wounds heal without more relevant implications than leaving a scar in the skin. Nevertheless, when the healing process does not follow its natural evolution several complications arise from it, leading to chronic wounds and other healing disorders. Chronic wounds affect around 6.5 million patients in the United States with an annual cost of US$25 billion (Sen et al., 2009) and reducing these numbers is a permanent objective for the health system.

Finding healing improvements is time consuming and has high economic cost. Moreover, ethical implications are always present when experiments involve living subjects. Thus, mathematical models of wound healing have become more popular during the last decades. Mathematical models allow to study a wide number of cases varying parameters with a low time and economic cost, adding the possibility of studying specific cases for individual patients. Therefore, the goal of this thesis is the development of a wound healing model to predict the healing evolution of wounds under different conditions and that allows the study of a wide range of wounds and factors influencing healing.

3.1 The skin

Skin is the outer coverage of vertebrate animals and presents different structure and properties in every species. In humans, skin is the largest organ in the body and it represents 8 % of the body mass (Gray et al., 1995). Skin covers the whole human body and its thickness varies in every anatomical location (Odland, 1991), ranging from 1,5 mm to 4 mm considering the epidermis and the dermis. The underlying tissue has a highly variable thickness and composition depending on the

anatomical location. Skin is usually classified into two types: thin and thick. Thin skin is found in parts such as the eyelids or where hair follicles are present, while thick skin is usually hairless and it is mainly located on the hand palms or the feet soles. Skin constitutes the interface between the body and the environment and it is a natural barrier that protects internal organs from external aggressions. More than just a physical barrier, skin has several functions; it avoids dehydration regulating water loss and acts as a thermal barrier. The mechanisms that skin uses to regulate the body temperature are mainly the evaporation of sweat and convection, regulating the blood flow along the body surface. One of the most important functions of the skin is its role as a part of the immune system, it avoids the entrance of strange particles and pathogens (any agent that can cause disease) in the body (Fore-Pfliger, 2004). In addition, several physiological systems necessary for the proper body functioning, such as nerves, capillary and lymphatic systems, are allocated in the skin. Thus, keeping the skin stability and avoiding any factor that would decrease its properties is highly important. Moreover, it is also crucial to achieve a fast and functional recovery of the skin when it suffers a damage.

3.1.1 Structure of the skin

Human skin consists of collagen, elastin and a variable number of cellular species (Table 3.1). It is organized into three main layers, from the more external to the more internal: epidermis, dermis and hypodermis (Wilkes et al., 1973).

Wounds in the skin usually go through the epidermis and reach the dermis. The **epidermis** is the most external layer and it is in contact with the environment, which makes it to have the principal role in the protection function of the skin. Epidermis constitutes a barrier against water loss and against the entrance of external substances. Despite of its important role, epidermis is also the thinnest layer, presenting a thickness of 75-150μm (Odland, 1991), and it is divided into five layers: *Stratum corneum, Stratum lucidum, Stratum granulosum, Stratum spinosum* and *Stratum germinativum* (Figure 3.1). Epidermis is mainly constituted by keratinocytes, which are also part of the immune system and produce anti-inflammatory mediators. As it is in direct contact with the environment, the epidermis capacity of self-renovation is crucial; it presents equal cell production and cell death rates in equilibrium.

The **dermis** is the intermediate skin layer and it is connected to the epidermis by the basement membrane. It has a variable thickness of 1-4mm and it is usually divided into two regions, the *papillary region* and the *reticular region* (Figure 3.2). The dermis is mainly made of collagen type I and III embedded on a ground

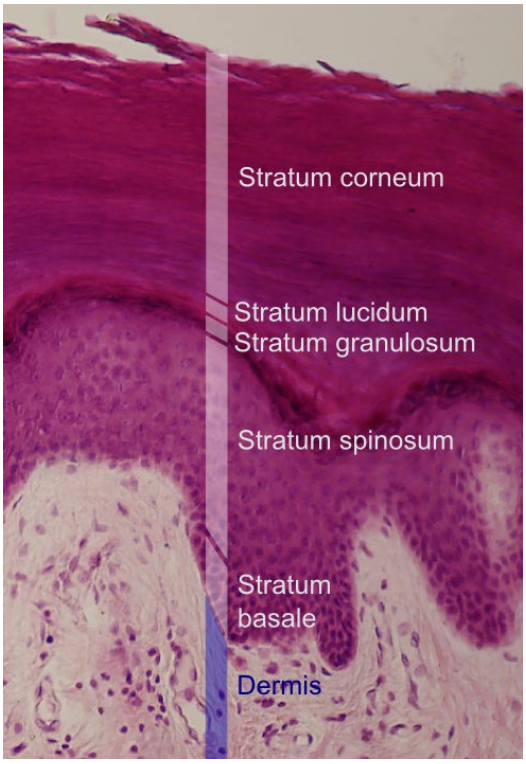

Figure 3.1: Histologic image of the epidermis layers. Source: http://en.wikipedia.org/wiki/File:Epidermal_layers.png

substance composed of proteoglicans, fibronectins (Gray et al., 1995) and variable cellular species (fibroblasts, myofibroblasts, endothelial cells, macrophages, neutrofils or linfocits among others (Table 3.1)). While some cellular species, such as fibroblasts, are naturally in the skin other species appear only when they are needed. This is the case of myofibroblasts, that only appear when an injury is produced, or macrophages that migrate to the locations where there are pathogens to eliminate them. One of the main components of the dermis is collagen. Collagen is the most abundant protein in the skin and it is usually organized in a fiber network with elastic properties that gives integrity to the skin. In fact, the mechanical tensile strength of the skin is due to this collagen lattice.

Deep cuts and wounds penetrate the dermis and reach the underlying layer, the hypodermis, which is located under the *reticular region* of the skin.

Name	Function	Location	Wound healing stage/process	Others
Adipose cells/Adipocytes	Store energy as fat.	Hypodermis		Synthesize several hormones.
Endothelial cells	Form new capillaries during angiogenesis.	Blood vessels	Epithelialization	Motile cells that migrate to the wound site during the epithelialization stage.
Fibroblasts	Synthesize collagen type III. Generate contraction forces.	Dermis Hypodermis	Epithelialization Contraction	Motile cells that migrate to the wound site during the epithelialization stage.
Keratinocytes	Main constituent of the epidermis. Form a barrier against environmental damage. Modulates the immune system producing anti-inflammatory mediators.	Epidermis	Epithelialization	Motile cells that migrate to the wound site during the epithelialization stage.
Macrophages	Phagocytosis. Eliminate bacteria and dead cells at injured sites.	Dermis Hypodermis	Inflammation	Derived from blood monocytes. Enter the damaged site through the endothelium of blood vessels. Chemotactically attracted to the wound site by cytokines released from damaged cells. Part of the immune system.

Continued on next page

Table 3.1 – *Continued from previous page*

Name	**Function**	**Location**	**Wound healing stage/process**	**Others**
Myofibroblasts	Synthesize collagen type III. Generate contraction forces. Secrete factors that induce angiogenesis.	Dermis	Epithelialization Contraction Angiogenesis	Differentiated fibroblasts. Non-motile.
Neutrophils	Eliminate bacteria and dead cells at injured sites.	Bloodstream	Inflammation	Attracted by inflammation factors. Part of the immune system.
Platelets	Prevent bleeding forming a plug where there is vascular endothelial damage. Blood coagulation.	Dermis	Hemostasis	Release PDGF.

Table 3.1: List of cellular species involved in wound healing.

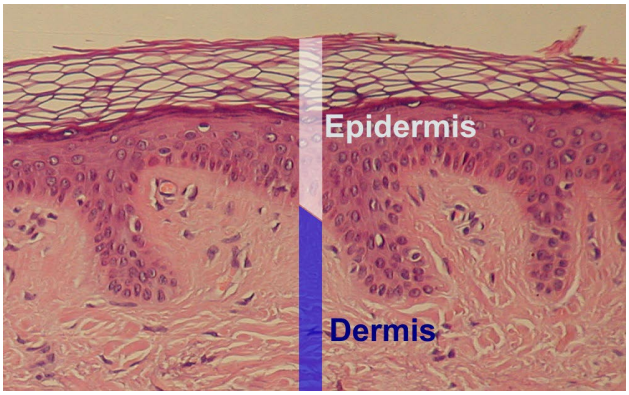

Figure 3.2: Histologic image of the epidermis and the dermis layers. Source: http://upload.wikimedia.org/wikipedia/commons/8/84/Epidermis-delimited.JPG

The **hypodermis**, also called subcutaneous tissue or superficial fascia, is the deepest layer and its thickness can reach the order of the centimeters depending on the anatomical location. It usually consists of subcutaneous fat and connective tissue and it also contains many important physiological systems, such as blood vessels (see Figure 3.3) and nerves. Furthermore, as the epidermis and the dermis, the hypodermis contains several cellular species, mainly fibroblasts, adipose cells and macrophages. Bones, muscles and internal organs lay under the hypodermis, making its recovery after damage to be necessary for a global physiological stability.

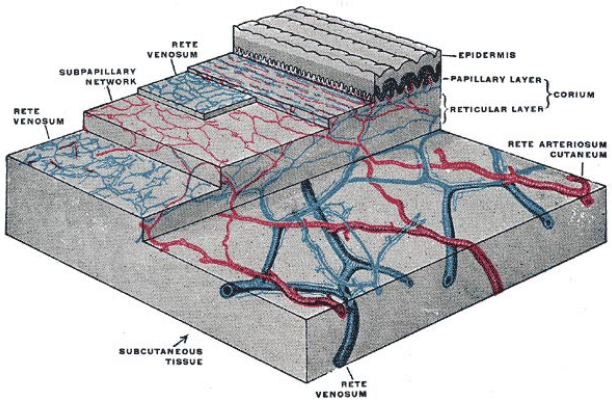

Figure 3.3: Schematic image of the vascular system through the skin layers, (Gray et al., 1995).

The combined function of the three layers is crucial for the body functioning, and maintaining the integrity of the whole structure is necessary for living. Therefore, preserving the skin undamaged and with a good mechanical properties is one of the most important health matters.

3.1.2 Mechanical properties of the skin

The mechanical properties of the skin have been studied since centuries ago. One of the first experiments on this field was performed by Langer (1861), illustrating that skin is naturally subjected to anisotropic stress. Skin's pre-stress is clearly observed when a wound occurs and the skin relaxes and looses, causing that the initial defect size increases.

In addition to that, the mechanical properties of the skin vary depending on the skin location, orientation and depth but also on the age; skin loses its elasticity and recovery capacity along time (Escoffier et al., 1989). Most of the mechanical properties of the skin are due to the fibers that compose its extracellular matrix (ECM), which have an elastic modulus of 150-300 kPa (Wilkes et al., 1973). Matrix fibers have a high tensile strength derived from the organization of three primary proteins chain (collagen, elastin and fibrin) into a superhelix (Kerr, 2010). The main component of these fibers is collagen, that gives most of the tensile strength to the ECM. The second main component of the ECM is elastin which gives elastic properties to the skin and allows it to recover its original state after being stretched.

Protein fibers are embedded on a ground substance made of proteoglicans and fibronectins (Gray et al., 1995), that help cells to move through the fibers. Collagen fibers align in the skin following the stress lines or Langer lines, which are present in the body surface and were discovered by Langer (1861). In his research, Langer (1861) performed circular cuts in the skin in all the body surface, finding that these cuts turned into ellipses aligned with tension lines when the skin relaxed. The orientation of these cuts defined the natural orientation of collagen fibers, usually parallel to the underlying muscles (Figure 3.4). The importance of these lines has been experimentally proved in some processes like wound healing, where it has been found that wounds heal differently depending on their relative orientation to Langer lines. The relative position of wounds in the skin has shown that wounds parallel to Langer lines heal better and produce less scaring while wounds that are perpendicular to Langer lines present more difficulties to heal (Motegi et al., 1977).

Moreover, the magnitude of the skin pre-stress found in Langer (1861) experiments has been measured in the arm and forearm by Flynn et al. (2011a), where they found values ranging from 28 to 92 kPa.

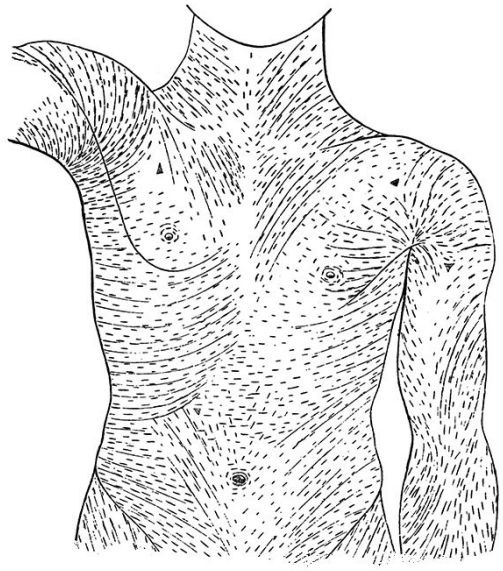

Figure 3.4: Distribution of the stress lines in the human trunk (Langer, 1861).

Further knowledge of the skin properties has been an important issue for experimental researches, and several measurement methods have been reported. During the last decades, both *in-vivo* and *in-vitro* experiments have been designed to characterize the mechanical behavior of the skin and find accurate parameter values, necessary for modeling and developing skin substitutes.

Most of the *in-vivo* studies to measure skin properties are carried out in the forearm or the upper arm and use different mechanical assays such as extension, indentation, suction or torsion. Diridollou et al. (2000) used suction tests in the forearm and an inverse method to identify the nonlinear material parameters of the skin. They applied negative pressure at the skin surface and measured the skin deflection, finding that the skin becomes stiffer for higher strains. Boyer et al. (2007) studied the mechanical properties of the epidermis and the dermis using a micro indentation device and characterized it as a viscoelastic material, finding that the complex modulus has values of 47.3 to 128.3 N/m. They defined the complex modulus as a variable that has a part which is independent of the frequency and other part dependent of the frequency.

Silver et al. (2001) studied the viscoelastic properties of the skin components from experimental data (Dunn and Silver, 1983), and estimated that the elastic constant for skin collagen is 4.4 GPa and for the elastin is 4.0 MPa. They used thoracic and abdominal skin to perform their stress-strain tests.

Other works characterize skin as a hyperelastic material. These materials do not show linear elastic properties in their strain-stress relationship and allow to describe other material properties such as anisotropy or incompressibility. Flynn et al. (2011a) measured the force-displacement response in the forearm skin when three-dimensional deformations were applied. Later, they found the material parameters that fit the Ogden hyperelastic model and the Tong and Fung model (Flynn et al., 2011b).

Gahagnon et al. (2012) studied the anisotropy of forearm skin *in-vivo* using elastographic tests. They stretched the skin parallel and perpendicularly to Langer's lines finding anisotropic behavior.

In-vivo assays to determine the skin properties are difficult to perform and variability between subjects is high. The wide range of values obtained is due to the different anatomical locations of the skin, the attachment of the dermis to the underlying tissue and patient specific characteristics, which makes difficult to find a unique characterization valid for every skin.

While *in-vivo* studies provide information about the skin in its natural environment, without eliminating natural processes, *in-vitro* studies provide more controlled experiments, where different aspects can be isolated and more destructive essays can be performed. Thus, *in-vitro* tests give information about different properties such as strength or elasticity, whereas *in-vivo* tests show the reaction of the skin against external loads (Edwards and Marks, 1995). Annaidh et al. (2012b) investigated the influence of location and orientation of the skin on its properties, focusing on skin anisotropy. They performed *in-vitro* tensile tests to human skin samples obtained from different parts of the back (Figure3.5), finding a correlation between the orientation of Langer lines and collagen fibers. Later, Annaidh et al. (2012a) fit their results with the hyperelastic model developed by Gasser et al. (2006).

Groves et al. (2013) used tensile test on circular human skin specimens to measure the skin properties. To find skin anisotropy they performed the test along three different load axes. They found that skin has anisotropic hyperelastic behavior and used the model by Weiss et al. (1996) to characterize it.

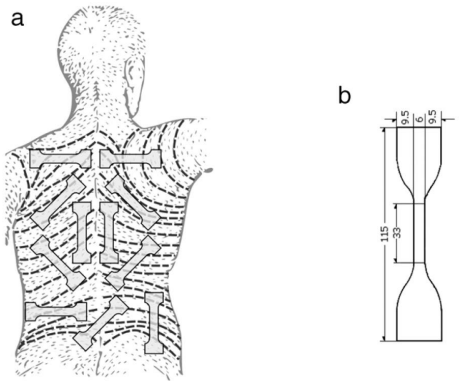

Figure 3.5: Orientation of samples from the back studied by Annaidh et al. (2012b) with respect to the Langer lines (Langer, 1861). (b) Dimensions of custom made dye (mm) used by Annaidh et al. (2012b)

Other studies have focused on punctual phenomena that take place in processes like wound healing. Hinz et al. (2001) studied the effect of tension in the granular tissue and in myofibroblasts differentiation, while Graham et al. (2004) studied the behavior of collagen fibers when they are subjected to deformations.

Despite the large amount of data that has been generated with all the abovementioned studies, finding a unique set of parameters to define human skin properties is almost impossible due to the high variability of the results among different subjects and anatomical locations and the difficulty of preserving skin without modifying its properties.

3.2 Wound healing

Wound healing is an important health matter that affects millions of patients and generates high costs to the health system and society (Sen et al., 2009). Millions of surgical procedures are performed every year with the subsequent wound and scar treatment. It is also estimated that around 6.5 million patients are affected of chronic wounds in the U.S., which generates a cost of US $25 billion every year. It is also calculated that skin scarring care generates an annual cost of around US $12 billions.

Wounds can appear as a consequence of damage in traumatic accidents but also as a result of surgery incisions, which sometimes are not easy to heal. Moreover, wounds such as *pressure ulcers* can appear caused by long periods of immobility

and may lead into infections and more severe complications, even death. Complicated wounds are more likely to appear also in people with chronic diseases such as diabetes and obesity, presenting difficulties for a proper healing.

Wound healing takes place after damage occurs in the skin. Minor wounds heal usually through a series of well organized processes without special treatment, but in those cases in which wounds cause an excessive damage it is necessary to apply different techniques to achieve healing. Besides, abnormal healing processes, such as fibroproliferative diseases (*keloids* or *hypertrophic scars*) or chronic wounds (*venous ulcers*, *pressure ulcers*, and *diabetic foot ulcers*), can not achieve a proper healing without external help due to their aberrant physiological activity.

Thus, it is of great importance understanding the healing mechanisms in order to propose new techniques that favor the healing process and prevent the appearance of complications. These advances include applying different growth factors or drugs to patients, choosing in surgery procedures a better incision geometry that helps healing, creating less scaring, or developing suture techniques that allow to minimize the scar formation (Hall-Findlay, 1999; Pollock and Pollock, 2000). Nevertheless, when normal healing does not occur, not even with aid, more complex and expensive techniques must be applied.

3.2.1 Stages of wound healing

Wound healing is usually divided into three stages overlapped in time that can lasts for several months or years. These stages are named: **inflammation**, **tissue formation** and **tissue remodeling** (Singer and Clark, 1999). The well-defined processes that take place during each stage are here explained:

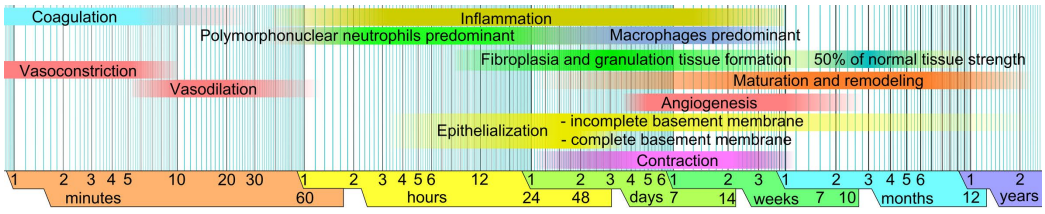

Figure 3.6: Temporal distribution of wound healing phases, including the most important phenomena along time. Source: http://commons.wikimedia.org/wiki/*File* : *Wound_healing_phases*.png.

1. **Inflammation:** This stage begins when the injury appears. After a wound is produced, extracellular matrix is replaced by a blood clot made of blood

from disrupted vessels, and inflammatory factors such as platelet derived growth factor (PDGF) which are secreted by platelets (Figure 3.7(a)) to stimulate cellular activity. Subsequently, vessels are closed, stopping bleeding (hemostasis) and a hypoxic fibrin clot replaces the blood clot (Gurtner et al., 2008). At this point oxygen has disappeared from the wound tissue, inducing hypoxia, and cannot be supplied, as vessels have not grown again yet. Inflammatory cells (neutrophils and macrophages) clean the wound site and eliminate bacteria, dead tissue and other strange particles (Singer and Clark, 1999). Inflammation lasts approximately 48 hours, until all strange particles are removed. At the end of the inflammatory phase, growth factors such as TGF-β and VEGF, necessary to promote cell activity in the next stage, are released (Gray et al., 1995).

2. **Epithelialization:** Epithelialization or new tissue formation begins some hours after the wound appears and it overlaps with the final stage of inflammation, lasting from 2 to 10 days (Gurtner et al., 2008). This stage is characterized by migration and proliferation of several cellular species, mainly fibroblasts or endothelial cells to the wound site, driven by the growth factors released at the end of the inflammatory stage. The fibrin clot is removed and replaced by granulation tissue (Figure 3.7(b)). Later, the granulation tissue is substituted by a new extracellular matrix mainly made of collagen. Fibroblasts that have infiltrated the wound site are activated and differentiate into myofibroblasts. Both cellular species initially secrete collagen type III which is replaced in time by stronger collagen type I. Collagen forms initially a disorganized fiber network, that gives mechanical support to the new tissue. In this stage, epithelial cells stimulated by VEGF form new blood vessels from the damaged ones, in the process called angiogenesis (Risau, 1997). This process allows to reestablish the normal blood and nutrients flux to the tissue (Gray et al., 1995) and also the oxygen supply necessary for cellular activity. Nevertheless, angiogenesis is also a crucial phenomena in other physiological processes such as embryogenesis and tumor formation (Carmeliet and Jain, 2000), resulting negative when excessive.
   Moreover, the new extracellular matrix that contains vessels and several cell types is contracted in this stage. The contraction of the tissue is due to the forces that cells (fibroblasts and myofibroblasts) exert in response to the change in the material properties in the damaged area. Indeed, myofibroblasts are able of exerting higher traction forces than fibroblasts. Thus, an adequate proportion between both cell types is crucial for avoiding healing disorders. After reepithelialization superfluous cells disappear from the granulation tissue, mainly by apoptosis. Once this process is concluded, an initial scar is formed.

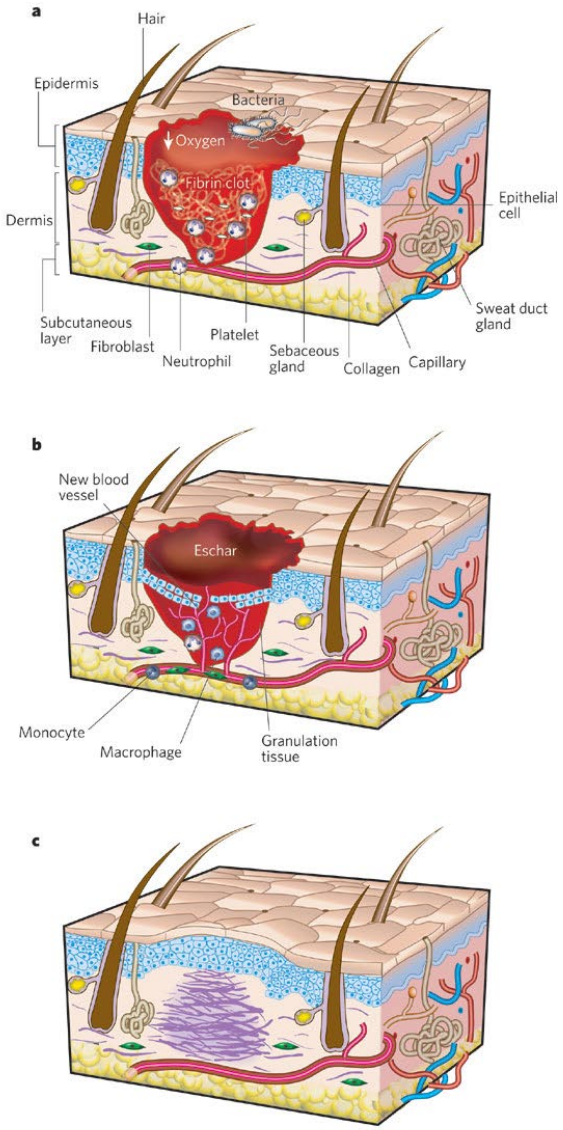

Figure 3.7: Phases of wound healing. a) inflammation, b) epithelialization, c) remodeling. Picture from Gurtner et al. (2008).

3. **Remodeling:** Once the collagen level in the wound reaches that of the undamaged skin, collagen begins to reorganize. At the beginning of the process, collagen fibers are randomly oriented. However, as time evolves, collagen fibers tend to orientate along preferred directions, usually parallel to the skin tension lines. Tissue properties evolve increasing its tensile strength towards that of healthy skin. Despite tissue functionality is mostly recovered after several months to years (Figure 3.7(c)), a complete recovery

is never achieved because the properties of the newly formed tissue remain slightly lower than the properties of the healthy tissue.

During each stage several phenomena governed by cellular species and growth factors take place simultaneously (see Figure 3.6). Most of the cellular processes that occur during wound healing, such as proliferation, differentiation and growth, are highly influenced by growth factors (GF's). Growth factors are chemical substances usually secreted by cells, that also stimulate cell activity. A list of the principal growth factors that guide wound healing processes is included in Table 3.2.

3.2.2 Complications of wound healing

Wound healing stages normally follow a predictable progress. Superficial cuts or abrasions heal quickly following the usual progression. If the regular time scheme is not followed or the injured person suffers from any kind of physiological disorder, healing can lead into healing difficulties such as pathological scars (*hypertrophic scars* and *keloids*) or chronic wounds (such as *pressure ulcers*, *diabetic foot ulcers* and *venous ulcers*).

Wound healing ends with the creation of the scar, which is composed of a non-functioning mass of fibrotic tissue (Gurtner et al., 2008). This tissue is made mainly of fibroblasts and extracellular matrix which contains the same protein (collagen) as the unwounded tissue but with a different composition (Gauglitz et al., 2011). Abnormal scars can appear when the production and degradation of ECM is not well balanced. Fibroproliferative disorders generate excessive scarring, which can lead into different scar types characterized by the amount and type of overexpressed collagen. While *hypertrophic scars* are made of type III collagen, *keloids* contain type I and type III collagen. *Hypertrophic scars* are caused by an excessive collagen production. They occur when there is a traumatic skin injury, such as wound infection or excessive wound tension (Gauglitz et al., 2011) and 40-70% of surgery scar can lead into hypertrophic scars. Hypertrophic scars usually grow only upwards, whereas *keloids* are a type of tumoral *hypertrophic scars* characterized by their excessive growth, affecting tissue that initially did not belong to the wound. This aberrant scars usually appear in zones with high tension and cause pain, pruritus and contracture, decreasing the quality of life of the patient (Gauglitz et al., 2011).

Name	Function	Wound healing stage / Process	Others
Epidermal growth factor (EGF)	Stimulates proliferation and differentiation of epithelial and mesenchymal cells. Granulation tissue formation.	Epithelialization	Secreted by macrophages and keratinocytes.
Fibroblasts growth factors (FGFs)	Fibroblast chemotaxis and proliferation. Keratinocyte migration and proliferation. Stimulates angiogenesis, wound contraction and matrix deposition.	Angiogenesis	Secreted by macrophages, endothelial cells and fibroblasts among others.
Keratinocyte growth factor (KGF)	Keratinocyte migration, proliferation and differentiation.	Epithelialization	Secreted by keratinocytes.
Macrophage derived growth factor (MDGF)	Stimulates the proliferation of fibroblasts, smooth muscle cells and endothelial cells.	Inflammation-Epithelialization	Secreted by macrophages.
Platelet derived growth factor (PDGF)	Stimulates fibroblasts proliferation. Regulates growth and division of multiple cells. Influences blood vessel formation (angiogenesis) and tissue remodeling.	Inflammation/Hemostasis	Secreted by platelets.

Continued on next page

Table 3.2 – *Continued from previous page*

Name	**Function**	**Wound healing stage / Process**	**Others**
Transforming growth factor beta (TGF-β)	Stimulates the differentiation of fibroblasts into myofibroblasts. Controls proliferation, differentiation, apoptosis and other functions in most cells. Stimulates ECM production.	Epithelialization / Differentiation	Secreted by fibroblasts, myofibroblasts and macrophage among others.
Vascular endothelial growth factor (VEGF)	Stimulates angiogenesis and vasculogenesis, directs the sprouting of capillaries. Promotes migration of endothelial cells and fibroblasts. Chemotactic for macrophages.	Hipoxia-Angiogenesis	Produced by cells receiving insufficient oxygen.

Table 3.2: List of growth factors involved in wound healing.

Equally problematic than excessive scarring is impaired wounding, which give place to chronic wounds. Chronic wounds take longer than normal wounds to heal and usually they do not heal completely without help. There are a number of factors that contribute to the occurrence of chronic wounds such as systemic diseases (diabetes), arterial insufficiency, infection or advanced age. The first cause of chronic wounds are *venous ulcers* (Snyder, 2005), caused by the malfunction of venous valves and a non adequate vascular ingrowth. *Venous ulcers* usually appear in the legs, are more likely in diabetic patients and in critical cases they end in the amputation of the limb. Diabetic patients have around 15% of probability of suffering a *diabetic foot ulcer*, an open sore located in the bottom of the foot. The main factors that give place to *diabetic foot* are vascular disease and diabetes neuropathy, a decrease in sensing pain caused by nerve damage after maintained high blood glucose levels. Moreover, diabetes impairs the normal evolution of the healing process, prolonging the inflammatory stage, which delays the formation of granulation tissue and reduces wound tensile strength (Ogawa and Hsu, 2013). Due to its high impact, a number of solutions have been developed to treat chronic wounds in diabetic patients, including the application of growth factors, the use of skin substitutes, negative pressure therapies and hyperbaric oxygen therapy (HBOT).

Pressure ulcers are also one of the most complicated wounds to heal, and are produced usually when the patient must stay immobile for long periods of time, mostly in bed or wheelchair. Thus, *pressure ulcers* appear usually in places where there is a bony prominence, such as the sacrum, coccyx, hips or heels, as a result of the constant pressure that is applied to the soft tissue (Bluestein and Javaheri, 2008). As a consequence, blood flow is decreased, leading to ischemia and tissue necrosis. As the *pressure ulcer* evolves (Figure 3.8), tissue thickness is reduced until the dermis is destroyed and the underlying fat is exposed. In the most severe stages (3 and 4) of *pressure ulcer*, fat also disappears and bones and muscles are uncovered (Topman et al., 2012). The first stages of pressure ulcer appear after a few hours of immobility. Therefore, the best way to prevent them is a constant change of the patient position, usually every two hours (Bluestein and Javaheri, 2008), to allow a change in the pressure distribution. The most extended treatment for *pressure ulcers* consists on the debridement of the necrotic tissue to avoid bacterial growth.

Finally, another complication that can arises from wound healing is tissue *contracture*. It is caused when dermal scar tissue continues shortening after healing by shortening of the ECM material caused by an excessive myofibroblasts population (Tomasek et al., 2002; Li and Wang, 2011). The forces generated by my-

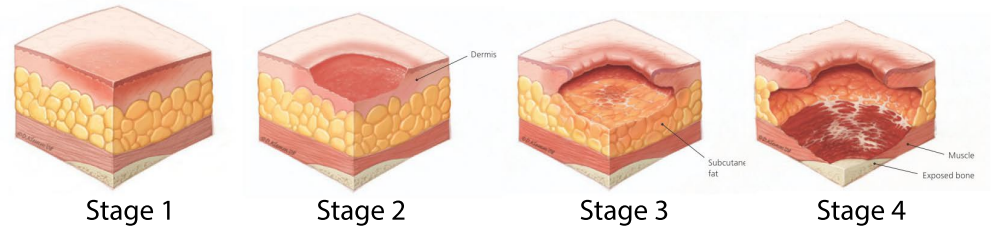

Figure 3.8: Pressure ulcer stages (Gauglitz et al., 2011)

ofibroblasts give place to a permanent excessive contracture that decreases tissue functionality reducing the tissue mobility in extreme cases.

These healing disorders together with their solutions are summarized in Table 3.3.

3.2.3 Healing strategies

Preventing the appearance of healing complications is the first strategy for a proper recovery after injury. One of the most extended therapies to help impaired healing is applying skin grafts, which consists on the transplantation of tissues from the same patient or from another subject of the same or different species (Billingham and Medawar, 1951) to the affected area. It is usually used in *diabetic foot* disease, *venous ulcers* or microsurgery wounds (Lineaweaver, 2013). In this procedure, damaged skin is removed from the patient and replaced by the new tissue. Implants can be half-skin thickness or full-skin thickness when wounds are more complicated (Rose et al., 2014). Less frequently, tissues artificially created with a specific purpose are transplanted instead of the natural ones (Tauzin et al., 2014). Some complications that can arise from this technique are infection, nerve damage or tissue rejection.

As it is known that wound healing has a high mechanical component, there exist a number of mechanical-based solutions, that modify the mechanical state of the wound. It has been proved that the use of fixable materials such as sutures, tapes or sheetings that limit skin stretching and reduce tension in the wound help to avoid the appearance of *hypertrophic scars* (Visscher et al., 2001; Widgerow et al., 2000). Nevertheless, when it is not possible to avoid this wounds to appear a number of treatments are available.

Disorder	**Cause**	**Effect**	**Treatment**
PATHOLOGICAL SCARS			
Hypertrophic scars	Fibroproliferative disorders	Excessive scaring upward Pain Contracture	Pressure therapy HBOT Sutures, tapes and sheetings
Keloids (tumoral hypertrophic scars)	Fibroproliferative disorders	Excessive scaring outward of the wound Pain Contracture	Sutures, tapes and sheetings
CHRONIC WOUNDS			
Pressure ulcers	Patient immobility	Ischemia Tissue necrosis	Change of patient position Debridement of necrotic tissue
Venous ulcers	Malfunction of venous ulcers		Skin grafts
Diabetic foot ulcer	Vascular disease Diabetes	Open sore in the bottom of the foot	Skin grafts
Contracture	Excessive myofibroblasts population	Shortening of the scar tissue. Decrease of tissue functionality	

Table 3.3: List of healing disorders and their treatment.

One of the most applied devices is the vacuum assisted closure (VAC), which consist on a foam cover that is laid over the wound and sealed with a film. Negative pressure is applied using a vacuum pump and a drainage tube to promote faster tissue growth (Argenta and Morykwas, 1997; Scherer et al., 2002). Hydrostatic pressure gradients and shear forces can be regulated with these devices.

Another therapy based on the use of different pressures is the hyperbaric oxygen therapy (HBOT), that consists on applying 100% oxygen to the body at a pressure higher to 1 atmosphere. It has been applied to various wound types, for instance acute wounds, chronic wounds and diabetic wounds (Eskes et al., 2011). Eskes et al. (2011) performed a review to find the effect of HBOT on acute wounds. They found that HBOT is beneficial in patients with crush injuries or burns, and it is more effective when applied together with skin grafts. HBOT has multiple positive effects such as reducing infection and cell death, generation of oxygen free radicals, inhibition of bacterial functions and the improvement of the transport of certain antibiotics. Moreover, HBOT amplifies oxygen gradients around ischemic wounds and improve the formation of collagen matrix (Gill and Bell, 2004). The main negative effects of HBOT are elevated pressure and hyperoxia, which can cause problems in the photoreceptor and hearing system.

One of the most used methods for treating hypertrophic scars is pressure therapy. the effects of this therapy are mainly acceleration of the remodeling process and reduction of the scar thickness together with a stiffness decreasing.

Finally, although it has not been yet applied to humans, the use of specific growth factors to promote wound healing has been seen to be effective. Kwon et al. (2006) studied the effect of applying certain epidermal growth factor (recombinant human epidermal growth factor rhEGF) in full thickness wounds in rats. They applied EGF topically, finding that wound closure was higher in presence of the growth factor. The use of EGF increased the proliferation of myofibroblasts and the rate of collagen production. Moreover, it has been proved that EGF decreases scar formation.

3.2.4 Scar mechanical properties

After a wound heals, the newly created tissue has not the same properties as the initial one. It has been reported that wound tissue shows only about 20 % of their normal strength in the first three weeks. Moreover, healed tissue only presents around 70 % of the resistance of the undamaged tissue (Levenson et al., 1965).

Although there are not many experimental works that measure the scar tissue properties, some authors have done it. Among them, Clark et al. (1996) used the elastic modulus and the strain of the skin to determine the severeness of post-burning hypertrophic scars. Hypertrophic scars present different properties from normal scars, becoming stiffer and less extensible as long as the scar is more severe. Clark et al. (1996) chose large scars on the arm and forearm and performed extensometer test of the scars and healthy skin of the unaffected arm when possible.

3.2.5 Mechanosensing and mechanotransduction in wound healing

Physiological processes are dependent of multiple biological and chemical factors. For example, Vaughan et al. (2000) studied the effect of transforming growth factor-β_1 (TGF-β_1) on myofibroblasts. They found that the force generated by myofibroblasts is dependent of the TGF$-\beta_1$ dose, as it regulates the expression of $\alpha-$SM actin. Moreover, TGF$-\beta_1$ also stimulates fibroblasts differentiation into myofibroblasts and increases collagen production (Petrov et al., 2002).

Although these biochemical factors, have a crucial role in physiology, they are not the only regulatory factor. Multiple studies have shown evidence about the influence of mechanics on these processes. Mechanical forces such as stretching tension, shear force, scratch and compression, among others, are perceived by cellular mechanoreceptors/mechanosensors (Ogawa, 2011).

Hinz et al. (2001) elucidated whether mechanical tension enhanced fibroblasts differentiation in vivo. With this purpose, they studied full-thickness wounds in rats, using a plastic frame in some wounds to splint them and induce a higher mechanical tension. Hinz et al. (2001) found that higher tension induced greater tissue contractility and myofibroblasts markers, which should be a consequence of the formation of stress fibers. Furthermore, $\alpha-$SMA expression is favored by mechanical tension (Grinnell, 2000).

Experimental evidence suggest that cells feel and react to mechanical stimuli from their environment (mechanosensing) to regulate their activity and to turn their environment into a more comfortable one. Analogously, cells can translate biochemical information into mechanical activity (mechanotransduction). Processes like cell migration, differentiation or force generation have been proved to be influenced by mechanical stimuli.

One of the most studied mechanical stimuli is tissue stiffness. The attraction of cells to rigid substrates is called durotaxis, and it is though to be one of the mechanisms involved in tumor growth (Harland et al., 2011).

Pelham and Wang (1997) investigated the motility of fibroblasts on substrates with different stiffness. They hypothesized that cells evaluate the stiffness by pushing and pulling their integrin receptors. This observation is consistent with the idea that the mechanical environment is evaluated by the cell through their actin-myosin mechanism. Moreover, they observed that focal adhesions became more stable when the substrate stiffness was increased. Cells are anchored to the substrate through focal adhesions (FA) and show different behaviors depending on the mechanical properties of the substrate. Discher et al. (2005) reviewed the influence of the substrate stiffness in cellular activity. Cells generate contractile forces through their actin and myosin filaments. Moreover, cells adhere only to substrates that have a stiffness higher than a threshold value, creating more stable focal adhesions in stiffer substrates and regulating the force generation in response to the resistance of the substrate. Wells (2008) also summarizes the effect on cell functions such as differentiation and proliferation when the substrate (ECM) stiffness is modified, finding in liver cells similar conclusions to Pelham and Wang (1997).

Mitrossilis et al. (2009) also demonstrated that cells on elastic substrates modify their activity according to the substrate stiffness. Mitrossilis et al. (2009) wanted to elucidate whether cellular response was determined by stiffness or forces by applying a uniaxial traction to a single living cell. Their in-vitro experiments demonstrated that the forces exerted by cells increase as the substrate becomes stiffer, and that a saturation force level is reached.

In addition, Jones and Ehrlich (2011) performed in-vitro tests on collagen surfaces of different stiffness. Their results demonstrate that substrate stiffness conditions the secretion of integrins.

3.3 Computational models of wound healing

For the last decades, mathematical models have been developed to study different biological and physiological processes such as tissues damage and recovery. In particular, a number of these models have focused on skin and wound healing. Theoretical models are of great importance, they can help to elucidate why a wound heals properly or leads into a chronic wound. Moreover, theoretical

models offer the possibility of studying the factors that have influence in wound healing. These factors can be analyzed isolated or together with other factors and it is possible to elucidate which factors are more important.

During the last few years wound healing and more particularly some processes such as wound contraction and angiogenesis have been broadly modeled using continuous models. Nevertheless, a model that includes all the wound healing stages has not been developed yet, as the number of processes and variables involved is too large and it would require a high computational capacity and would take large calculation times.

The most relevant aspects of the reviewed models are summarized in Table 3.4.

3.3.1 Epidermal wound healing models

A first work about epidermal wound healing was developed by Sherratt and Murray (1990). Epidermal wound closure is due only to epidermal cells migration and it is not affected by wound contraction, that only takes place when deeper layers of the skin are affected. Sherratt and Murray (1990) proposed a continuous reaction-diffusion model setting that a chemical growth factor produced by epidermal cells diffuses through the tissue. Furthermore, cell variation comes from migration and mitosis regulated by the produced chemical factor and also by apoptosis (Clark, 1988; Folkman and Moscona, 1978). The model was applied to predict epidermal wound healing in a circular wound considering that the wound had healed when it reached a cell density higher than the 80 % of the cell density of the healthy tissue. Sherratt and Murray (1990) compared their results with one of the few experimental works about epidermal wound healing, performed by Van den Brenk (1956) in rabbits ears. Sherratt and Murray (1990) proposed the first model including chemical control, and it has been the base for most of the subsequent wound healing and contraction models. Moreover, their model has been also adapted to simulate wound healing in other tissues. For instance, Dale et al. (1994) adapted it to study corneal epithelial wound healing as a function of the epithelial growth factor (EGF). In addition, epidermal wound healing has been simulated together with other processes that take place simultaneously, such as angiogenesis (Maggelakis, 2003).

Author	Simulated processes	Model variables	Mechanical model	Geometry	Validation with experimental works
Sherratt and Murray (1990)	Epidermal wound healing	Epidermal cells Mitosis-regulating GF	Not considered	Superficial circular wounds simplified by 1D axisymmetric approach	Validated with rabbit (Van den Brenk, 1956)
Tranquillo and Murray (1992)	Dermal wound healing Wound contraction	Fibroblasts Collagen ECM ECM displacement Generic chemical growth factor	Viscoelastic	Superficial circular wounds simplified by 1D axisymmetric approach	Validated with rat (McGrath and Simon, 1983)
Dale et al. (1994)	Corneal epithelial wound healing	Cells EGF	Not considered	Superficial circular wounds simplified by 1D axisymmetric approach	None

Continued on next page

Table 3.4 – *Continued from previous page*

Author	**Simulated processes**	**Model variables**	**Mechanical model**	**Geometry**	**Validation with experimental works**
Olsen et al. (1995)	Wound contraction	Fibroblasts Myofibroblasts Generic chemical GF Collagen ECM ECM displacement	Viscoelastic	Superficial circular wounds simplified by 1D axisymmetric approach	Validated with rat (McGrath and Simon, 1983)
Pettet et al. (1996a)	Angiogenesis	Capillary tips Chemoattractant Blood vessels	Not considered	Superficial circular wounds simplified by 1D axisymmetric approach	Validated with rabbit (Van den Brenk, 1956)
Pettet et al. (1996b)	Angiogenesis	Capillary tips Capillary sprouts Fibroblasts MDGF Oxygen Collagen ECM	Not considered	Superficial circular wounds simplified by 1D axisymmetric approach	Validated with rabbit (Van den Brenk, 1956)

Continued on next page

Table 3.4 – *Continued from previous page*

Author	Simulated processes	Model variables	Mechanical model	Geometry	Validation with experimental works
Maggelakis (2003)	Angiogenesis Epidermal wound healing	Oxygen MDGF Capillaries	Not considered	Superficial circular wounds simplified by 1D axisymmetric approach	None
Manoussaki (2003)	Angiogenesis Vasculogenesis	Endothelial cells Collagen Angiogenic factor	Viscoelastic	Plain stress 2D square	None
Javierre et al. (2008)	Wound closure Angiogenesis Epidermal wound healing	Oxygen MDGF Capillaries EGF	Not considered	Superficial 2D wounds	None

Continued on next page

Table 3.4 – *Continued from previous page*

Author	Simulated processes	Model variables	Mechanical model	Geometry	Validation with experimental works
Schugart et al. (2008)	Angiogenesis	Capillary tips Capillary sprouts Oxygen Inflammatory cells Chemoattractant Fibroblasts Myofibroblasts Collagen ECM	Not considered	Superficial circular wounds simplified by 1D axisymmetric approach	None
Flegg et al. (2009)	Angiogenesis in wound healing (application of hyperbaric oxygen therapy)	Oxygen Capillary tips Blood vessels	Not considered	Superficial circular wounds simplified by 1D axisymmetric approach	None
Javierre et al. (2009)	Wound contraction	Fibroblasts Myofibroblasts Collagen ECM Generic GF ECM displacement	Viscoelastic	Superficial 2D wounds	None

Continued on next page

Table 3.4 – *Continued from previous page*

Author	Simulated processes	Model variables	Mechanical model	Geometry	Validation with experimental works
Xue et al. (2009)	Wound closure	Oxygen PDGF VEGF Macrophages Fibroblasts Collagen ECM Capillary tips Capillary sprouts	Viscoelastic	3D wounds simplified by 1D approach	Validated with pig (Roy et al., 2009)
Flegg et al. (2010)	Angiogenesis in wound healing	Oxygen Chemoattractant Capillary tips Blood vessels Fibroblasts ECM	Not considered	Superficial circular wounds simplified by 1D axisymmetric approach	None
Vermolen and Javierre (2010)	Wound contraction Wound closure Angiogenesis	Epidermal cells Capillaries Collagen ECM Fibroblasts Oxygen VEGF ECM displacement	Viscoelastic	2D deep wounds	None

Continued on next page

Table 3.4 – *Continued from previous page*

Author	**Simulated processes**	**Model variables**	**Mechanical model**	**Geometry**	**Validation with experimental works**
Friedman and Xue (2011)	Wound closure (in chronic wounds)	Macrophages Oxygen PDGF VEGF Fibroblasts Collagen ECM Capillary tips Capillary sprouts	Viscoelastic	2D radially symmetric wounds 3D axial symmetric wounds	Validated with pigs (Roy et al., 2009)
Murphy et al. (2011)	Dermal wound healing Wound contraction	Fibroblasts Myofibroblasts Collagen ECM TGF$-\beta$ ECM displacement	Elastic	Superficial circular wounds simplified by 1D axisymmetric approach	Validated with rat (McGrath and Simon, 1983)
Murphy et al. (2012)	Wound closure Dermal wound healing	Fibroblasts Myofibroblasts TGF$-\beta$ PDGF Collagen ECM Collagenase	Viscoelastic	Superficial circular wounds simplified by 1D axisymmetric approach	Validated with human (Catty, 1965) and rat (McGrath and Simon, 1983)

Continued on next page

Table 3.4 – *Continued from previous page*

Author	**Simulated processes**	**Model variables**	**Mechanical model**	**Geometry**	**Validation with experimental works**
Vermolen and Javierre (2012)	Wound contraction Wound closure Angiogenesis Dermal regeneration	Epidermal cells Capillaries ECM Fibroblasts Oxygen VEGF EGF ECM displacement	Viscoelastic	2D deep wounds	None provided

Table 3.4: List of previous wound healing models and their description.

3.3.2 Wound contraction models

Although epidermal wounds represent a good first approach to study wound healing, those wounds that affect deeper layers and present more difficulties to heal are also more interesting to study. It has been observed that wounds that reach the dermis do not heal only with the effect of cell migration and more complex mechanisms are needed for a success healing.

Wound contraction is one of the most important processes during dermal wound healing and it is highly influenced by mechanics. The reduction of the wound size is due in part to the retraction of the wound contour inward. This displacement is created by the balance between the forces that cells generate in the tissue where they are embedded and the resistance that the tissue offers to be deformed.

The first wound contraction model was proposed by Tranquillo and Murray (1992) and it has been the base for most wound contraction models until now. The model was composed by a set of differential equations describing the conservation of a cellular species (fibroblasts) and the collagen density of the ECM and the linear momentum of the matrix. Tranquillo and Murray (1992) included the effect of cell growth, migration and diffusion together with the passive convection due to the ECM movement. On a first approach they considered that the ECM variation was due only to its passive convection. Later, they proposed a more realistic ECM evolution law that includes ECM synthesis by fibroblasts. Moreover, in the same work they proposed a more complete biochemical model including the chemotactic effect of a chemical growth factor. The linear momentum law included a force balance between the matrix (characterized as a viscoelastic material) and the traction forces exerted by cells. They considered a domain divided into two parts, the wound and the surrounding healthy skin. The model investigated one dimensional wounds and followed the displacement of the wound margin during time to measure the wound size.

The model of Tranquillo and Murray (1992) was later extended by Olsen et al. (1995). Olsen et al. (1995) proposed a wound contraction model that included the displacement of the contracted tissue and applied it to normal and pathological wounds. One of the main differences between the works of Tranquillo and Murray (1992) and Olsen et al. (1995) is the incorporation of the effect of myofibroblasts in the contraction process by Olsen et al. (1995). Myofibroblasts are non-motile activated fibroblasts that due to their similarities to muscle cells are able to exert higher traction forces than fibroblasts. It has been reported that a proper contraction level is not reached without myofibroblasts forces (Tomasek

et al., 2002). Olsen et al. (1995) model describes the temporal evolution of fibroblasts, myofibroblasts, a chemical growth factor and the extracellular matrix during wound contraction. To model the cellular evolution they included cell mitosis, differentiation, apoptosis, passive convection for both species and fibroblasts migration due to random dispersal and chemotaxis. They predicted the evolution of the wound until reaching a steady state. Following Tranquillo and Murray (1992), they applied the model to unidimensional geometries, which reduces its applicability to circular wounds assuming axisymmetry.

Cook (1995) proposed a mechanochemical model for dermal repair accounting tissue contraction. Cook (1995) uses the zero stress state approach, that assumes an unstressed state for all the elements, to which a relative strain is measured.

Despite, these models included a great number of the factors that guide wound healing, wound contraction is highly influenced not only by cellular and chemical stimuli, but also mechanics. Cells are able to feel the mechanical environment where they are and regulate their activity, for instance force generation, in function of certain mechanical properties or stimuli. Processes like cell migration, differentiation or force generation have been proved to be influenced by mechanical stimuli (Discher et al., 2005; Mitrossilis et al., 2009; Harland et al., 2011).

Therefore, wound healing and wound contraction models have evolved including the regulatory effect of mechanical variables in different biochemical processes (Javierre et al., 2009; Murphy et al., 2011, 2012). Nevertheless, there is not a common opinion about which is the involved mechanical stimulus that regulates the cellular mechanosensing mechanism.

Following the work of Olsen et al. (1995), Javierre et al. (2009) proposed a mathematical model of wound contraction including fibroblasts, myofibroblasts, collagen, a generic growth factor and the tissue displacements. They included the effect of mechanical stress to regulate cellular processes, defining the traction stresses generated by cells through the concept of net stress of one fibroblasts cell per unit of ECM matrix introduced by Moreo et al. (2008). Moreo et al. (2008) proposed a mechanosensing model applicable to cellular processes such as migration or proliferation, based on the Hill's model for skeletal muscle behavior. On their work, they proposed a model to evaluate the octahedral stresses exerted by cells as a function of the tissue stiffness. They evaluated this stress trough two components. The first measures the contractile stresses generated by the myosin machinery transmitter thorough actin bundles and a term related to the contractile stress supported by the passive resistance of the cell (absorbed by the micro-

tubules). These two contributions give place to the stress that the cell effectively transmit to the ECM. This approach considers that the strain that the substrate and the cell suffer is the same. They also included this factor in the expression of fibroblasts differentiation into myofibroblasts, as it had been experimentally observed that differentiation is guided by mechanical tension (Hinz and Gabbiani, 2003; Tomasek et al., 2002). Javierre et al. (2009) also focused their model on the study of different wound geometries, creating one of the first 2D wound contraction mechanochemical models. Thus, they studied how the elongation of elliptical wounds affects the wound contraction.

Following Cook (1995), Murphy et al. (2011) developed a 1D model reproducing the interaction between the cellular, chemical and mechanical phenomena adding new factors. As it has been proved that TGF-β is critical in dermal repair (Shah et al., 1992), they included its kinetics on their model. They proposed a differentiation mechanism, from fibroblasts to myofibroblasts, activated by TGF-β and tissue stress. They applied the model to investigate how the wound heals producing certain disorders. When there is excessive TGF-β it gives place to *contracture* caused by excessive myofibroblasts forces. On the other hand, the wound contracts insufficiently when TGF-β disappears too fast and there are not enough myofibroblasts to generate forces. They found the same effect when the myofibroblasts kinetics were modified by changing its differentiation from fibroblasts and death rate. As a main difference with previous models, Murphy et al. (2011) used linear elasticity to model the skin behaviour instead of the viscoelastic model chosen by other authors (Tranquillo and Murray, 1992; Olsen et al., 1995).

Following the work by Tranquillo and Murray (1992), Murphy et al. (2012) proposed a more complex model that included the effect of more factors. In addition to the TGF-β kinetics, they added the effect of collagenase (an enzyme that contributes to new tissue formation) on the collagen concentration. One of the main differences of Murphy et al. (2012) model with previous models was the differentiation mechanism from fibroblasts to myofibroblasts. They set that the mechanical stimuli which guides differentiation was the positive elastic stress. This idea was first introduced by Hall (2008), while previous approaches proposed that this stimulus was cell traction stress (Javierre et al., 2009). They followed the approach proposed by Tranquillo and Murray (1992) to evaluate the traction forces exerted by cells, taking them proportional to the collagen density and cell concentration and neglecting the saturation terms dependent on cell densities (Tranquillo and Murray, 1992) or ECM densities (Olsen et al., 1995; Javierre et al., 2009). As a main difference with previous models (Olsen et al., 1995; Javierre et al., 2009), Murphy et al. (2012) assumed that myofibroblasts generate traction forces even

in the absence of fibroblasts, as it is experimentally evidenced (Tomasek et al., 2002). They also assumed that there is not differentiation back from myofibroblasts to fibroblasts. Following Olsen et al. (1995) they considered the skin to be a viscoelastic material, although Murphy et al. (2012) uses a evolutive law to evaluate the elastic modulus proportional to the collagen concentration. As in previous models, they studied superficial circular wounds approximated by an unidimensional axisymmetric model.

3.3.3 Computational models of angiogenesis during wound healing

Vascular growth has been also broadly modeled and simulated, mainly angiogenesis and vasculogenesis. While vasculogenesis is the formation of new blood vessels when there is no pre-existing vasculature, angiogenesis consists on the formation of new blood vessels from pre-existing ones, being this the case during wound healing. Angiogenesis is also involved in other biological processes, for instance tumor growth or embryogenesis, and most of the computational works about angiogenesis are focused on simulating angiogenesis in cancer (Anderson and Chaplain, 1998; Chaplain, 2000; Mantzaris et al., 2004) due to its social impact nowadays. Nevertheless, angiogenesis in wound healing has been also broadly modeled. Pettet et al. (1996a) presented the first angiogenesis model applied to wound healing, based on the fungal growth model of Edelstein (1982). It comprises a set of differential equations to model the evolution of capillary-tip endothelial cells migrating chemotactically to a macrophage-derived chemoattractant regulated by the vasculature density. Oxygen supply was not included in the model and oxygen levels were assumed proportional to the vessel density and later included as a primary variable in a model extension (Pettet et al., 1996b), in which they also included the effect of fibroblasts and the extracellular matrix. Both models were used to reproduce two-dimensional wound geometries approximated by a one-dimensional model, and allowed to reproduce the evolution of normal wounds and also non-healing wounds.

Maggelakis (2003) developed an angiogenesis model that included the effect of macrophage-derived growth factors (MDGF), the capillary density and the tissue oxygen concentration in one dimension. She proposed that oxygen is provided to the wound by capillaries and consumed by macrophages, that appear when there is a low oxygen concentration and secrete MDGF, at the same time that diffuses through the tissue. Finally, high levels of MDGF enhanced the appearance of capillaries regulated also by a negative feedback loop until reaching the maximum capacity. The model was applied to study the dependence of the healing of a circu-

lar wound with the oxygen supply. A subsequent model was proposed by Javierre et al. (2008), adding a new variable: the epidermal growth factor (EGF) concentration. They proposed a coupling between angiogenesis and a wound interface due to cell migration to study the effect of oxygen availability on cell function during epidermal wound healing in two dimensions.

One of the factors that impairs wound healing is hypoxia (the lack of oxygen) (Schreml et al., 2010), which is necessary for cellular activity. Oxygen is mainly supplied by capillaries and thus angiogenesis is crucial for restoring the regular oxygen flux. Therefore, many authors have proposed angiogenesis models focused on the role of oxygen during angiogenesis. Schugart et al. (2008), proposed a seven-variables model, following Pettet et al. (1996b), adding the effect of macrophages. They studied for the first time the role of the tissue oxygen tension in the wound healing process and set that there is an optimal level of hypoxia for vascular growth and wound healing. In some cases, natural oxygen supply is not enough for an adequate healing, causing hipoxia and ending subsequently in chronic wounds. Flegg et al. (2009) simulated one of the techniques used to treat this pathology, the Hyperbaric Oxygen Therapy (HBOT) which consist on the deliberated elevation of oxygen levels. They studied the effect of the HBOT in angiogenesis in acute and chronic wounds. On a first approach Flegg et al. (2009) studied the evolution of oxygen density, capillary tips and blood vessels. They predicted that intermittent HBOT helps chronic wounds to heal but normobaric oxygen has not positive effects. Later, Flegg et al. (2010) expanded the model including the effect of a chemoattractant, fibroblasts and the ECM, and applied it to chronic diabetic wounds. They studied the effect of different pressures, oxygen percentage, exposition time and frequency. From all the studied cases they found that the therapy is beneficial only under certain conditions.

In a similar way that wound contraction depends on mechanical factors, angiogenesis is also influenced by mechanics. Although there exist multiple mechanochemical wound healing models (Tranquillo and Murray, 1992; Olsen et al., 1995; Javierre et al., 2009; Murphy et al., 2011, 2012) there is still a lack of mechanochemical models of angiogenesis in wound contraction. Vermolen and Javierre (2010) developed a model including angiogenesis, wound contraction and wound closure. They combined the model by Tranquillo and Murray (1992) to model the contraction process and Maggelakis (2003) model for the angiogenesis process. However, they treated these processes isolated, without considering their interaction. They studied the processes separately in the dermis and the epidermis, which allows the study of deep wounds. Later, Vermolen and Javierre (2012) modified the model adding the dermal regeneration process coupling it with the angiogenesis process.

Manoussaki (2003) developed a mechanochemical model of angiogenesis taking into account the traction forces exerted by cells on the ECM, which was modeled as a viscoelastic material. Moreover, cells movement was caused by chemotaxis guided by a chemical factor regulated by themselves. Although Manoussaki (2003) did not focused on wound healing, her model could be adapted to this application. Xue et al. (2009) extended the model by Schugart et al. (2008) incorporating the mechanical behaviour of the skin.

3.3.4 Limitations of existing models

Mathematical models of biological processes usually come from a same initial model. Although authors extend these models adding new factors and variables, sometimes they do not focus their effort on solving model limitations, that are transmitted from one model to the subsequent ones.

One of the main limitations of wound contraction models is that they are limited to one dimensional geometries (Murray et al., 1998; Sherratt and Murray, 1990; Schugart et al., 2008; Murphy et al., 2011; Olsen et al., 1995, 1996; Murphy et al., 2012). This is useful for studying simple axisymmetric geometries because they allow the spatial problem to be reduced to a one-dimensional model, which is less time and resources consuming. However, this oversimplification of the real wound morphology limits their true predictive capacity. In this direction, some recent works allow to study two dimensional geometries (Javierre et al., 2008, 2009; Vermolen and Javierre, 2010, 2012), bringing models closer to realistic situations, despite three dimensional models are required to obtain accurate representation of the involved phenomena.

Another limitation of prior wound healing works is that they are focused on tracking the evolution of superficial wounds, studying the evolution of the superficial area and not taking into account the influence of wound depth on the contraction kinetics. Thus, Olsen et al. (1995); Javierre et al. (2009); Murphy et al. (2012) use a plane stress approach to simplify the geometry of real wounds. However, the phenomena that take place along the wound depth are equally important, although have not been modeled due to its complexity. To our knowledge, only Vermolen and Javierre (2012) study deep wounds, though the plane strain hypotheses are adopted to reduce the wound geometry to two dimensions. As a matter of fact, while using three dimensional geometries is the most realistic approach, using a plane strain approach to study wounds along its depth can reveal useful information without the complexity and computational cost of three-dimensional models.

There are some main differences when plane stress and plane strain approaches are assumed. In first place, when simulating deep wounds there is part of the boundary that is not surrounded by skin, while plane wounds are completely surrounded by non-wounded tissue. This part of the boundary is in contact with the air and it is represented by a free boundary. The major implication to this is that it can move freely, as there is no tissue attached to it. When the mathematical model is formulated, this free boundary must be treated differently to the constrained boundaries. Some of the simplifications that are assumed for the attached boundaries are not applicable to this free boundary. From a numerical perspective planar wounds under plane stress hypotheses are easier to model as natural boundary conditions do not need to be taken into account.

Another difference between the study of planar and deep wounds is the consideration of the different skin layers involved in the model. When plane wounds are simulated only the properties of the most superficial layer of the skin are taken into account, as it has been the case in models of epidermal wound healing (Sherratt and Murray, 1990; Maggelakis, 2003; Javierre et al., 2008) and some models of dermal wounds healing (Tranquillo and Murray, 1992; Murphy et al., 2011, 2012). When deep wounds are represented, depending on the depth of the considered injury it is not possible to characterize the whole geometry with the same properties. It is known that the most external layer of the skin, the epidermis, has a thickness of micrometres. However, the dermis usually has a thickness from 1,5 mm to 4 mm and the hypodermis reaches different depths depending on the considered part of the body. Thus, when deep wounds are studied and the properties of the different skin layers need to be considered in order to obtain more realistic results.

Finally, one of the most limiting aspects in wound healing modeling is the mechanical characterization of the skin. Traditionally, a viscoelastic material model has been used for modeling the mechanical behavior of the skin. This approach captures accurately some time-dependent properties of the skin but also presents some limitations. It has been experimentally proved that a hyperelastic constitutive model fits better the skin behavior, although its characterization is more complicated. Most of the wound healing models that include mechanics (tissue deformation) have treated the skin (or its layers) as a viscoelastic material (Olsen et al., 1995; Javierre et al., 2009; Murphy et al., 2012). However, implementing skin as a hyperelastic material would allow to reproduce the skin behavior more accurately, including the possibility of adding tissue anisotropy.

3.4 Experimental works

Despite there is a high number of computational models that simulate different aspects of wound healing, there is a lack of experimental works in the field that can help to corroborate the computational outcomes.

Because of ethical reasons, wound healing experiments in living subjects are not frequent, almost inexistent in humans. Consequently, animal assays are the best approach although they are also subjected to strong ethical considerations. Moreover, mammals skin presents different mechanical properties to human skin, and results obtained in these experiments can be used only as a qualitative pattern for humans.

One of the firsts experimental studies is due to Van den Brenk (1956). Van den Brenk (1956) studied epidermal wounds in rabbits ears. Their results were used to validate Sherratt and Murray (1990) results.

McGrath and Simon (1983) studied the influence of shape and size in deep wounds on rats. They observed the evolution of three wound geometries: a small square, a large square and a circular wound with the same area as the large square. To measure the wound size, McGrath and Simon (1983) tracked the movement of some points defining the wound border. They differentiated healing due to wound contraction and epithelialization. After a rapid wound distraction and a six-days plateau phase, the wounds contracted during around 30 days, followed by a long almost steady plateau. McGrath and Simon (1983) observed that after 70 days all the wounds had experienced a similar contraction rate, reducing its size to the 35% of the initial size.

Additionally, most mammals such as rats and rabbits present a looser and more elastic skin than humans, and the contraction levels are not comparable with those from humans. However, pigs present a skin structure more similar to human, thus the porcine model is widely accepted for comparisons. Roy et al. (2009) observed the evolution of ischemic and non-ischemic circular wounds in pigs. They performed the incisions and while some wounds were left to heal normally, others were disrupted introducing silicon sheets between the dermis and the underlaying tissue. In this way, ischemic wounds -in which re-epithelialization is impaired- were reproduced. Roy et al. (2009) were able to measure the oxygen concentration and the partial oxygen pressure in the wound, finding higher oxygen saturation levels in the non-ischemic wounds. They observed also wound closure along

31 days, when the non-ischemic wound had almost closed but the ischemic wound had achieved only around 80% of closure.

When comparing experimental results with human models, it must be taken into consideration that each species has different time parameters due to their different cellular and tissue kinetics (Reina-Romo et al., 2010). Thus, if a proper equivalence between species is obtained, it is possible the comparison of experimental results on animals to computational results on human models.

3.5 Objectives

The main objective of this thesis is the study of wound healing in the skin through computational simulation and using a multiphysics approach. In order to achieve this objective, a computational model that allows to reproduce wound healing under different conditions has been proposed and implemented. More specifically, the proposed model focuses on the wound contraction phase, as it has a strong mechanical component. The model also allows to include more processes that take place simultaneously to wound contraction, for instance angiogenesis. The proposed model includes biological factors (cellular species, growth factors and collagen) and also mechanical factors (characterization of the skin mechanical properties and cellular contraction). To find the solution of the resulting governing equations, the finite element method (FEM) is applied. The model is constituted by two parts, one related to the biochemical analysis of the process and the other regarding the mechanical analysis of the skin. First, the evolution of the biochemical species is evaluated with a reaction-diffusion system of equations. Second, the mechanical behavior of the skin is modeled assuming the fundamental mechanical relationships for the constitutive material model chosen to characterize it. The two parts are related through a mechanosensing and mechanotransductor mechanism, that regulates the behavior of the cells as a function of mechanical variables. The model will allow to study different healing cases and different wound types. The main objectives are summarized next:

- Adaptation of the model for the study of planar and deep wounds, in two dimensions. Planar wounds are characterized by their superficial area, using plane stress approach. Long and deep wounds can be studied through their transversal section, under a plane strain approach and taking into account the different skin layers that are affected by the injury.

- Use of several constitutive models (viscoelastic, hyperelastic isotropic and hyperelastic anisotropic) to characterize the mechanical behavior of the skin.

Viscoelastic materials are a good approximation to reproduce skin behavior. Moreover, viscoelastic materials can be used when small deformations theory is applied but not when the material works with large deformations. In this case, hyperelastic materials should be used.

- Inclusion of other phenomena that take place simultaneously to wound contraction, such as angiogenesis. As it is known that every phenomena which takes place during healing are interrelated, the inclusion of as much processes as possible gives a more complete and realistic model. As a disadvantage, the resources needed to solve the problem increase together with the model precision.

- Incorporation of new cellular kinetics laws depending on physical evidences, based on experimental studies instead of the phenomenological laws proposed until now.

- Solving the biochemical and mechanical problems with a fully coupled approach or a non-coupled approach. While a fully-coupled approach allows to solve the whole problem at the same time, a non-coupled approach allows to divide the problem and solve it in different stages. This is specially useful to separate the biochemical and the mechanical analysis due to their different time scales. Moreover, it allows us to use an updated Lagrangian and updating certain variables between the two stages.

- Application of the model to different size and shape wounds in two dimensions, both planar and deep wounds. The model capacity of reproducing complex geometries, such as those considered in experimental works, allows for a more thorough validation of the results.

- Application of the model to simulate three-dimensional wounds, in which the effect of the superficial shape and wound depth are considered simultaneously.

- Incorporation of the collagen fibers in the healthy skin. Collagen fibers allow to simulate the real anisotropy of the skin instead of isotropic simplifications, which is important in the healthy skin surrounding the wound.

3.6 Financial support

The research included in this thesis was supported by:

- The Spanish Ministry of Science and Innovation through grant BES2010-037281 and project DPI2009-07514. This project was partly financed by the European Union (through the European Regional Development Fund).
- The Spanish Ministry of Economy and Competitiveness through project DPI2012-32888. This project is partly financed by the European Union (through the European Regional Development Fund).
- The European Research Council(ERC) through project ERC-2012-StG 306751.

CHAPTER 4

Conclusions

The main motivation of this thesis is the study of the skin after suffering an injury. Understanding the wound healing process in order to reproduce it by computational models is crucial for advancing in developing healing solutions and surgical procedures. To achieve this goal, a wound contraction model for human skin has been proposed and developed to help in the understanding of the process and its possible solutions when it does not follow the normal evolution.

The work has been focused on the theoretical point of view of the problem, including spatio-temporal convection diffusion equations to describe the biological problem combined with the formulation of the mechanical problem.

4.1 General conclusions

The main conclusions that have been obtained from this thesis, considering the conducted numerical studies, are now summarized. Taking into account that wounds that contract less will generate smaller scars, which is highly desirable, the main conclusions from the biological point of view are the following:

- When deep wounds are studied through their transversal section, it is found that wounds with the same area but different free surface length present different contraction rates. Wounds that are deeper and narrower contract less than wider and shallower wounds.

- When wound contraction and angiogenesis are simulated together in planar wounds, it is found that more elongated planar wounds (elliptical) show a faster vascularization than circular wounds. However, the contraction experienced by both wounds, in comparison with the initial size, is similar. Faster biochemical processes in the elliptical wound can be caused by the

faster diffusion of substances in that case, thanks to the higher relation of contour respect to the wound surface.

- When the effect of size is analyzed in planar wounds, it is found that large wounds begin to contract earlier in time. However, at the end of the contraction process they have contracted less than smaller wounds, in relation to the initial wound size.

- In deep wounds it is very important to take into account the different skin layers. The dermis and the underlying tissues have different mechanical properties and the dermis is stiffer than the underlying tissue.

Regarding the model and its implementation and numerical aspects, the most important conclusions are:

- When wounds are analyzed under two dimensional simplifications, the most important decision is whether to study the wound under a plane strain or plane stress approach. This means, studying the wound through its transversal or superficial area and geometry. The selection between the two approaches depends on what type of wound is being studied.

- The mechanical material constitutive model highly determines the evolution of the contraction process. The use of more realistic models such as the hyperelastic gives also more realistic results. Including the fibers into the hyperelastic model of the skin allows to model its real anisotropic behavior. It has been found that the orientation of the fibers in the skin does not modified highly the contraction rate but modifies the volumetric strain distribution.

- Mechanical variables influence biological processes such as cell differentiation and stresses generation. It has been postulated that the volumetric strain is the mechanical stimulus that regulates this process as it depends on the tissue stiffness.

- Inclusion of evidence-based laws instead of the existing phenomenological ones provides results equally good but without the assumption component.

4.2 Original contributions

The development of this thesis has given as a result a computational model to simulate wound healing that allows to include different processes and to study a number of variables and their effect in the healing process. Aspects of this thesis

that are completely new and had not been included in existing wound healing models, as far as I know, are:

- The stress generation by the cells was modeled through a new law based on experimental evidences. The previous mechanisms to represent these stresses were mainly phenomenological, and although they provided good results, there was no physical justification for them. The proposed model generalizes from previous models with a cell-regulatory mechanism that handles ECM rigidization and its impact on cell function.

- The phenomenological law for fibroblasts differentiation has been also updated by a physical evidence-based law. Again, the proposed law follows experimental observations using the tissue stiffness, which is easily measurable, as the guiding variable.

- A wound healing model that includes angiogenesis and wound contraction in three dimensions has been presented. Most of the existing models reproduce two-dimensional geometries, using plane stress or plane strain approaches or by one-dimensional simplifications. The development of a three-dimensional model allows to study more complex and realistic geometries and also to analyze the global wound behavior.

- A hyperelastic material including the anisotropic effect of the collagen fibers has been used to model the skin behavior. Existing wound healing models do not take into account this behavior that clearly regulates the healing process.

From a numerical point of view the main contributions are:

- A fully coupled approach and a fully decoupled approach have been formulated to solve the problem. The traditional way of solving these kind of problem is using the fully coupled implementation, that allows to evaluate the biochemical and the mechanical problems at the same time. The contribution from this work is the decoupling of the two models. This approach allows to deal with the two different time scales of the biochemical and the mechanical problems. Moreover, it allows to update variables between the solution of the biochemical and the mechanical problems.

- A mesh update has been implemented for solving the problem on a more accurate way. An updated Lagrangian algorithm has been used to upgrade the mesh, which is needed to use the small strains approach. As the mesh can suffer deformations higher than the allowed for the small strains approach, considering the incremental deformations avoid this problem.

- A user element subroutine has been implemented using Abaqus® Hibbit et al. (2008). This element incorporates the model equations that describe the problem and the boundary conditions of the problem, which is solved with the finite element method. Moreover, the implementation of the boundary natural conditions for a problem with a free boundary has been included in the formulation. Plain stress and plain strain approaches are included in the two-dimensional element, which allows to simulate planar and deep wounds.

4.2.1 Publications and communications

The work developed in this thesis has given place to three papers, published in JCR journals and other paper is at the moment in the submission procedure. Moreover a fifth paper has been published in a JCR journal as a result of the work developed during a research stay in the USA. These papers are listed in Table

In addition to that, a total of 12 contributions have been presented in national and international conferences. These contributions are listed in Table 4.2.

Finally, we have been invited to write a book chapter as a result of this work

Authors: E. Reina-Romo, **C. Valero**, C. Borau, R. Rey, E. Javierre, M.J. Gómez-Benito, J. Domínguez, J.M. García-Aznar
Title: Mechanobiological modelling of angiogenesis: impact on tissue engineering and bone regeneration
Book: Computational modeling in tissue engineering, pp.379-404
Date: 01/2013
DOI:10.1007/8415_2011_111 ISBN: 978-3-642-32562-5
Editorial: Springer-Verlag Berlin Heidelberg
Editors: Liesbet Geris.

Work	**Title**	**Authors**	**Journal**	**IF***	**Publication date**
1	Nonlinear finite element simulations of injuries with free boundaries: Application to surgical wounds	**C.Valero**, E. Javierre, J.M. García Aznar, M.J. Gómez-Benito	Int. J. Numer. Meth. Biomed. Engng. (2014). DOI: 10.1002/cnm.2621	1.310	Online
2	Numerical modelling of the angiogenesis process in wound contraction	**C.Valero**, E. Javierre, J.M. García Aznar, M.J. Gómez-Benito	Biomech Model Mechanobiol. DOI: 10.1007/s10237-012-0403-x	3.331	
3	A cell-regulatory mechanism involving feedback between contraction and tissue formation guides wound healing progression	**C.Valero**, E. Javierre, J.M. García Aznar, M.J. Gómez-Benito	PLOS ONE. DOI:10.1371/journal.pone.0092774	3.730	Online
4	Modeling anisotropic wound healing: effect of the relative position of wounds with respect to collagen fibers orientation	**C.Valero**, E. Javierre, J.M. García Aznar, M.J. Gómez-Benito, A. Menzel	Journal of the Mechanics and Physics of Solids	3.406	Submitted
5	A computational study of stress fiber-focal adhesion dynamics governing cell contractility	M.Maraldi, **C.Valero**, K.Garikipati	Biophysical Journal	3.668	Accepted for publication

*Journal Impact Factor.

Table 4.1: Articles included in this thesis.

	Title	Authors	Conference	Date and Place	Participation
1	Finite element modelling of wound contraction: a non-linear mechano-chemical approach	**C. Valero**, J.M. García Aznar, M.J. Gómez-Benito, E. Javierre	Congress on Numerical Methods in Engineering CMNE 2011	June 2011, Coimbra (Portugal)	Speaker
2	Three dimensional modelling of wound contraction.	**C. Valero**, J.M. García Aznar, M.J. Gómez-Benito, E. Javierre	XXIII congress International Society of Biomechanics (ISB 2011)	July 2011, Brussels (Belgium)	Speaker
3	Finite Element Analysis of the angiogenesis process in wound healing	**C. Valero**, E. Javierre, M.J. Gómez-Benito	XVIII congress of the European Society of Biomechanics (ESB 2012)	July 2012, Lisbon (Portugal)	Speaker
4	Modelling skin healing: Effect of cell traction	**C. Valero**, E. Javierre, J.M. García Aznar, M.J. Gómez-Benito	XIVrd congress of the European Society of Biomechanics (ESB 2013)	August 2013, Patras (Greece)	Speaker
5	A cell-regulatory mechanism between wound contraction and tissue formation	**C. Valero**, E. Javierre, J.M. García Aznar, M.J. Gómez-Benito	V International Conference on Computational Bioengineering (ICCB 2013)	September 2013, Leuven (Belgium)	Coauthor
6	Modelado multifísico de la contracción de heridas (Multi-physical modeling of wound contraction)	**C. Valero**, E. Javierre.	XV Reunión de Usuarios del Programa	October 2010	Speaker

Continued on next page

Table 4.2 – *Continued from previous page*

	Title	Authors	Conference	Date and Place	Participation
7	Simulación por elementos finitos del proceso de angiogénesis aplicado a la cicatrización de heridas	**C. Valero**, E. Javierre, J.M. García Aznar, M.J. Gómez-Benito	Reunión del Capítulo de la ESB	November 2011, Zaragoza (Spain)	Speaker
8	In-silico Models of Wound and Bone Healing: Examples from Nature	M.J. Gómez-Benito , **C. Valero**, E. Reina-Romo, J.M. García Aznar, E. Javierre	Euro Bio-inspired Materials - International School and Conference on Biological Materials Science.	March 2012, Potsdam (Germany)	Coauthor
9	Stress Evaluation During Angiogenesis in Skin Wound Healing	**C. Valero**, E. Javierre, J.M. García Aznar, M.J. Gómez-Benito	10th International Symposium Computer Methods in Biomechanics and Biomedical Engineering (CMBBE 2012)	April 2012, Berlin (Germany)	Coauthor
10	A Mechano-Chemical Model of Wound Contraction for Superficial and Acute Wounds	E. Javierre, **C. Valero**, M.J. Gómez-Benito, J.M. García-Aznar	XVIIIrd congress of the European Society of Biomechanics (ESB 2012)	July 2012, Lisbon (Portugal)	Coauthor
11	Mathematical analysis of physiological and pathological wound healing. Application to diabetic foot ulcers	E. Javierre, **C. Valero**, M.J. Gómez-Benito, F.J. Vermolen	Mathematical Modelling in Engineering & Human Behavior	September 2012, Valencia (Spain)	Coauthor

Continued on next page

Table 4.2 – *Continued from previous page*

	Title	Authors	Conference	Date and Place	Participation
12	Finite element analysis of the mechanoc-chemical regulation of the wound contraction in surgical wounds	E. Javierre, **C. Valero**, M.J. Gómez-Benito, J.M. García-Aznar	Conference on the Mathematics of Finite Elements and Applications MAFELAP 2013	June 2013, Uxbridge (United Kindom)	Coauthor

Table 4.2: Contributions in national and international conferences.

4.3 Future lines

Considering the results and conclusions obtained from the work developed in this thesis and its limitations, some lines of future work could be defined:

- Extension of the contraction two-dimensional model to three dimensional geometries. The use of plane strain and plane stress simplifications allow to study a large number of wound geometries and cases, but they also imply loss of information in the simulation process. The actual three-dimensional model includes angiogenesis and wound contraction guided only by the fibroblasts. The model is ready to be extended with the myofibroblasts and collagen kinetics.

- The volumetric cell behavior could be improved by a more complete approach, considering the anisotropic cell behavior. The model proposed in the thesis considers that cells exert the same traction in every direction independently of the direction in which they are been deformed. A more evolved model will distinguish the magnitude in which the cell is been deformed along each direction and thus will regulate the forces exerted as a result of these different strains.

- Incorporation of the remodeling phenomena in the wound tissue after healing. The actual model includes the fibers effect in the dermis while the wound heals, but it does not reproduce the production and remodeling of fibers in the healed wound. A more realistic approach will include the fiber production and orientation in the tissue as long as it presents an adequate healing level. Moreover, the fiber orientation will be regulated by the direction of higher stress levels.

- Include all the skin layers in the three dimensional geometry. In a same way than the dermis and the underlying tissue are distinguish in the plane strain model, these layers can be separated in the three dimensional model, presenting different properties. This modification will provide a more realistic behavior.

- Study of wound pathologies, in which healing is impaired, excessive or presents other difficulties such as pressure ulcers or keloids. The study of these cases could be simulated by properly adjusting the biochemical kinetics or the skin properties.

- Study of different healing solutions, such as sutures or other devices that modify the mechanical conditions in which wounds are healed. The simulation of these phenomena will be of great help for clinicians to choose favorable solutions in specific cases.

Bibliography

Anderson, A., Chaplain, M., 1998. Continuous and discrete mathematical models of tumor-induced angiogenesis rid a-5355-2010. Bulletin of Mathematical Biology 60 (5), 857–899.

Annaidh, A. N., Bruyere, K., Destrade, M., Gilchrist, M. D., Maurini, C., Ottenio, M., Saccomandi, G., 2012a. Automated estimation of collagen fibre dispersion in the dermis and its contribution to the anisotropic behaviour of skin. Annals of Biomedical Engineering 40 (8), 1666–1678.

Annaidh, A. N., Bruyere, K., Destrade, M., Gilchrist, M. D., Ottenio, M., 2012b. Characterization of the anisotropic mechanical properties of excised human skin. Journal of the Mechanical Behavior of Biomedical Materials 5 (1), 139–148.

Argenta, L., Morykwas, M., 1997. Vacuum-assisted closure: A new method for wound control and treatment: Clinical experience. Annals of Plastic Surgery 38 (6), 563–576.

Billingham, R., Medawar, P., 1951. The technique of free skin grafting in mammals. Journal of Experimental Biology 28 (3), 385–402.

Bluestein, D., Javaheri, A., 2008. Pressure ulcers: Prevention, evaluation, and management. American Family Physician 78 (10), 1186–1194.

Boyer, G., Zahouani, H., Le, B. A., Laquieze, L., 2007. In vivo characterization of viscoelastic properties of human skin using dynamic micro-indentation. 2007 Annual International Conference of the Ieee Engineering in Medicine and Biology Society, Vols 1-16, 4584–4587.

Carmeliet, P., Jain, R., 2000. Angiogenesis in cancer and other diseases. Nature 407 (6801), 249–257.

Catty, R. H. C., 1965. Healing and contraction of experimental full-thickness wounds in human. British Journal of Surgery 52 (7), 542.

Chaplain, M., 2000. Mathematical modelling of angiogenesis rid a-5355-2010. Journal of Neuro-Oncology 50 (1-2), 37–51.

Clark, J. A., Cheng, J. C. Y., Leung, K. S., 1996. Mechanical properties of normal skin and hypertrophic scars. Burns 22 (6), 443–446.

Clark, R., 1988. Overview and general considerations of wound repair. In: Clark, R., Henson, P. (Eds.), The Molecular and Cellular Biology of Wound Repair. Springer US, pp. 3–33.

Cook, J., 1995. A mathematical model for dermal wound healing: wound contraction and scar formation. Ph.D. thesis.

Dale, P., Maini, P., Sherratt, J., 1994. Mathematical-modeling of corneal epithelial wound-healing. Mathematical Biosciences 124 (2), 127–147.

Diridollou, S., Patat, F., Gens, F., Vaillant, L., Black, D., Lagarde, J., Gall, Y., Berson, M., 2000. In vivo model of the mechanical properties of the human skin under suction. Skin Research and Technology 6 (4), 214–221.

Discher, D., Janmey, P., Wang, Y., 2005. Tissue cells feel and respond to the stiffness of their substrate. Science 310 (5751), 1139–1143.

Dunn, M., Silver, F., 1983. Viscoelastic behavior of human connective tissues - relative contribution of viscous and elastic components. Connective tissue research 12 (1), 59–70.

Edelstein, L., 1982. The propagation of fungal colonies - a model for tissue-growth. Journal of theoretical biology 98 (4), 679–701.

Edwards, C., Marks, R., 1995. Evaluation of biomechanical properties of human skin. Clinics in dermatology 13 (4), 375–380.

Escoffier, C., Derigal, J., Rochefort, A., Vasselet, R., Leveque, J., Agache, P., 1989. Age-related mechanical-properties of human-skin - an invivo study. Journal of Investigative Dermatology 93 (3), 353–357.

Eskes, A. M., Ubbink, D. T., Lubbers, M. J., Lucas, C., Vermeulen, H., 2011. Hyperbaric oxygen therapy: Solution for difficult to heal acute wounds? systematic review. World journal of surgery 35 (3), 535–542.

Flegg, J. A., Byrne, H. M., McElwain, L. S., 2010. Mathematical model of hyperbaric oxygen therapy applied to chronic diabetic wounds. Bulletin of mathematical biology 72 (7), 1867–1891.

Flegg, J. A., McElwain, D. L. S., Byrne, H. M., Turner, I. W., 2009. A three species model to simulate application of hyperbaric oxygen therapy to chronic wounds. Plos Computational Biology 5 (7), e1000451.

Flynn, C., Taberner, A., Nielsen, P., 2011a. Measurement of the force-displacement response of in vivo human skin under a rich set of deformations. Medical engineering& physics 33 (5), 610–619.

Flynn, C., Taberner, A., Nielsen, P., 2011b. Modeling the mechanical response of in vivo human skin under a rich set of deformations. Annals of Biomedical Engineering 39 (7), 1935–1946.

Folkman, J., Moscona, A., 1978. Role of cell-shape in growth-control. Nature 273 (5661), 345–349.

Fore-Pfliger, J., 2004. The epidermal skin barrier: implications for the wound care practitioner, part i. Advances in Skin & Wound Care 17 (8), 417–425.

Friedman, A., Xue, C., 2011. A mathematical model for chronic wounds. Mathematical Biosciences and Engineering 8 (2), 253–261.

Gahagnon, S., Mofid, Y., Josse, G., Ossant, F., 2012. Skin anisotropy in vivo and initial natural stress effect: A quantitative study using high-frequency static elastography. Journal of Biomechanics 45 (16), 2860–2865.

Gasser, T., Ogden, R., Holzapfel, G., 2006. Hyperelastic modelling of arterial layers with distributed collagen fibre orientations. Journal of the Royal Society Interface 3 (6), 15–35.

Gauglitz, G. G., Korting, H. C., Pavicic, T., Ruzicka, T., Jeschke, M. G., 2011. Hypertrophic scarring and keloids: Pathomechanisms and current and emerging treatment strategies. Molecular Medicine 17 (1-2), 113–125.

Gill, A., Bell, C., 2004. Hyperbaric oxygen: its uses, mechanisms of action and outcomes. Qjm-an International Journal of Medicine 97 (7), 385–395.

Graham, J., Vomund, A., Phillips, C., Grandbois, M., 2004. Structural changes in human type i collagen fibrils investigated by force spectroscopy. Experimental cell research 299 (2), 335–342.

Gray, H., Williams, P., Bannister, L., 1995. Gray's Anatomy: The Anatomical Basis of Medicine and Surgery. Gray's Anatomy. Churchill Livingstone.

Grinnell, F., 2000. Fibroblast-collagen-matrix contraction: growth-factor signalling and mechanical loading. Trends in cell biology 10 (9), 362–365.

Groves, R. B., Coulman, S. A., Birchall, J. C., Evans, S. L., 2013. An anisotropic, hyperelastic model for skin: Experimental measurements, finite element modelling and identification of parameters for human and murine skin. Journal of the Mechanical Behavior of Biomedical Materials 18, 167–180.

Gurtner, G. C., Werner, S., Barrandon, Y., Longaker, M. T., 2008. Wound repair and regeneration. Nature 453 (7193), 314–321.

Hall, C. L., 2008. Modelling of some biological materials using continuum mechanics. Ph.D. thesis, Queensland University of Technology.

Hall-Findlay, E., 1999. A simplified vertical reduction mammaplasty: Shortening the learning curve. Plastic and Reconstructive Surgery 104 (3), 748–759.

Harland, B., Walcott, S., Sun, S. X., 2011. Adhesion dynamics and durotaxis in migrating cells. Physical Biology 8 (1), 015011.

Hibbit, Karlsonn, Sorensen, 2008. Abaqus user´s guide, v.6.9. Pawtucket, RI, HKS Inc.

Hinz, B., Gabbiani, G., 2003. Mechanisms of force generation and transmission by myofibroblasts. Current opinion in biotechnology 14 (5), 538–546.

Hinz, B., Mastrangelo, D., Iselin, C., Chaponnier, C., Gabbiani, G., 2001. Mechanical tension controls granulation tissue contractile activity and myofibroblast differentiation. American Journal of Pathology 159 (3), 1009–1020.

Javierre, E., Moreo, P., Doblare, M., Garcia-Aznar, J. M., 2009. Numerical modeling of a mechano-chemical theory for wound contraction analysis. International Journal of Solids and Structures 46 (20), 3597–3606.

Javierre, E., Vermolen, F. J., Vuik, C., van der Zwaag, S., 2008. Numerical Modelling of Epidermal Wound Healing. Springer-Verlag Berlin, Berlin; Heidelberg Platz 3, D-14197 Berlin, Germany.

Jones, C., Ehrlich, H. P., 2011. Fibroblast expression of alpha-smooth muscle actin, alpha 2 beta 1 integrin and alpha v beta 3 integrin: Influence of surface rigidity. Experimental and molecular pathology 91 (1), 394–399.

Kerr, J., 2010. Functional Histology. Elsevier Mosby Australia.

Kwon, Y., Kim, H., Roh, D., Yoon, S., Baek, R., Kim, J., Kweon, H., Lee, K., Park, Y., Lee, J., 2006. Topical application of epidermal growth factor accelerates wound healing by myofibroblast proliferation and collagen synthesis in rat. Journal of Veterinary Science 7 (2), 105–109.

Langer, K., 1861. Zur anatomie und physiologie de haut 1. ueber der spaltbarkeit der cutis. Sitzungsbericht der Akademie der Wissenschaften in Wien 44, 19.

Levenson, S., Geever, E., Crowley, L., Oates, J., Berard, C., Rosen, H., 1965. Healing of rat skin wounds. Annals of Surgery 161 (2), 293.

Li, B., Wang, J. H. ., 2011. Fibroblasts and myofibroblasts in wound healing: Force generation and measurement. Journal of tissue viability 20 (4), 108–120.

Lineaweaver, W. C., 2013. Skin graft coverage of critical marginal wounds in microsurgical cases. Microsurgery 33 (4), 315–317.

Maggelakis, S., 2003. A mathematical model of tissue replacement during epidermal wound healing. Applied Mathematical Modelling 27 (3), 189–196.

Manoussaki, D., 2003. A mechanochemical model of angiogenesis and vasculogenesis. Esaim-Mathematical Modelling and Numerical Analysis-Modelisation Mathematique Et Analyse Numerique 37 (4), 581–599.

Mantzaris, N., Webb, S., Othmer, H., 2004. Mathematical modeling of tumor-induced angiogenesis. Journal of mathematical biology 49 (2), 111–187.

McGrath, M., Simon, R., 1983. Wound geometry and the kinetics of wound contraction. Plastic and Reconstructive Surgery 72 (1), 66–72.

Mitrossilis, D., Fouchard, J., Guiroy, A., Desprat, N., Rodriguez, N., Fabry, B., Asnacios, A., 2009. Single-cell response to stiffness exhibits muscle-like behavior. Proceedings of the National Academy of Sciences of the United States of America 106 (43), 18243–18248.

Moreo, P., Garcia-Aznar, J. M., Doblare, M., 2008. Modeling mechanosensing and its effect on the migration and proliferation of adherent cells rid f-8256-2010. Acta Biomaterialia 4 (3), 613–621.

Motegi, K., Azumi, Y., Ueno, T., 1977. Postoperative scars and cleavage lines. The Bulletin of Tokyo Medical and Dental University 24 (2), 163–168.

Murphy, K. E., Hall, C. L., Maini, P. K., McCue, S. W., McElwain, D. L. S., 2012. A fibrocontractive mechanochemical model of dermal wound closure incorporating realistic growth factor kinetics. Bulletin of mathematical biology 74 (5), 1143–1170.

Murphy, K. E., Hall, C. L., McCue, S. W., McElwain, D. L. S., 2011. A two-compartment mechanochemical model of the roles of transforming growth factor beta and tissue tension in dermal wound healing. Journal of theoretical biology 272 (1), 145–159.

Murray, J. D., Cook, J., Tyson, R., Lubkin, S. R., 1998. Spatial pattern formation in biology: I. dermal wound healing. ii. bacterial patterns. Journal of the Franklin Institute-Engineering and Applied Mathematics 335B (2), 303–332.

Odland, G., 1991. Structure of the skin. In: Goldsmith, L.A. (editor) Physiology, biochemistry, and molecular biology of the skin. Oxford University Press, Oxford.

Ogawa, R., 2011. Mechanobiology of scarring. Wound Repair and Regeneration 19, S2–S9.

Ogawa, R., Hsu, C.-K., 2013. Mechanobiological dysregulation of the epidermis and dermis in skin disorders and in degeneration. Journal of Cellular and Molecular Medicine 17 (7), 817–822.

Olsen, L., Sherratt, J. A., Maini, P. K., 1995. A mechanochemical model for adult dermal wound contraction and the permanence of the contracted tissue displacement profile. Journal of theoretical biology 177 (2), 113–128.

Olsen, L., Sherratt, J. A., Maini, P. K., 1996. A mathematical model for fibroproliferative wound healing disorders. Bulletin of mathematical biology 58 (4), 787–808.

Pelham, R., Wang, Y., 1997. Cell locomotion and focal adhesions are regulated by substrate flexibility. Proceedings of the National Academy of Sciences of the United States of America 94 (25), 13661–13665.

Petrov, V., Lijnen, P., Fagard, R., 2002. Stimulation of collagen production by tgf-beta 1 during differentiation of cardiac fibroblasts to myofibroblasts. Journal of hypertension 20, S29–S29.

Pettet, G., Byrne, H., Mcelwain, D., Norbury, J., 1996a. A model of wound-healing angiogenesis in soft tissue. Mathematical biosciences 136 (1), 35–63.

Pettet, G., Chaplain, M., McElwain, D., Byrne, H., 1996b. On the role of angiogenesis in wound healing rid a-5355-2010. Proceedings of the Royal Society of London Series B-Biological Sciences 263 (1376), 1487–1493.

Pollock, H., Pollock, T., 2000. Progressive tension sutures: A technique to reduce local complications in abdominoplasty. Plastic and Reconstructive Surgery 105 (7), 2583–2586.

Reina-Romo, E., Gomez-Benito, M. J., Garcia-Aznar, J. M., Dominguez, J., Doblare, M., 2010. An interspecies computational study on limb lengthening.

Proceedings of the Institution of Mechanical Engineers Part H-Journal of Engineering in Medicine 224 (H11), 1245–1256.

Risau, W., 1997. Mechanisms of angiogenesis. Nature 386 (6626), 671–674.

Rose, J. F., Giovinco, N., Mills, J. L., Najafi, B., Pappalardo, J., Armstrong, D. G., 2014. Split-thickness skin grafting the high-risk diabetic foot. Journal of Vascular Surgery.

Roy, S., Biswas, S., Khanna, S., Gordillo, G., Bergdall, V., Green, J., Marsh, C. B., Gould, L. J., Sen, C. K., 2009. Characterization of a preclinical model of chronic ischemic wound. Physiological Genomics 37 (3), 211–224.

Scherer, L., Shiver, S., Chang, M., Meredith, J., Owings, J., 2002. The vacuum assisted closure device - a method of securing skin grafts and improving graft survival. Archives of Surgery 137 (8), 930–933.

Schreml, S., Szeimies, R. M., Prantl, L., Karrer, S., Landthaler, M., Babilas, P., 2010. Oxygen in acute and chronic wound healing. British Journal of Dermatology 163 (2), 257–268.

Schugart, R. C., Friedman, A., Zhao, R., Sen, C. K., 2008. Wound angiogenesis as a function of tissue oxygen tension: A mathematical model. Proceedings of the National Academy of Sciences of the United States of America 105 (7), 2628–2633.

Sen, C. K., Gordillo, G. M., Roy, S., Kirsner, R., Lambert, L., Hunt, T. K., Gottrup, F., Gurtner, G. C., Longaker, M. T., 2009. Human skin wounds: A major and snowballing threat to public health and the economy. Wound Repair and Regeneration 17 (6), 763–771.

Shah, M., Foreman, D., Ferguson, M., 1992. Control of scarring in adult wounds by neutralizing antibody to transforming growth-factor-beta. Lancet 339 (8787), 213–214.

Sherratt, J., Murray, J., 1990. Models of epidermal wound-healing. Proceedings of the Royal Society B-Biological Sciences 241 (1300), 29–36.

Silver, F., Freeman, J., DeVore, D., 2001. Viscoelastic properties of human skin and processed dermis. Skin Research and Technology 7 (1), 18–23.

Singer, A., Clark, R., 1999. Mechanisms of disease - cutaneous wound healing. New England Journal of Medicine 341 (10), 738–746.

Snyder, R., 2005. Treatment of nonheating ulcers with allografts. Clinics in dermatology 23 (4), 388–395.

Tauzin, H., Rolin, G., Viennet, C., Saas, P., Humbert, P., Muret, P., 2014. A skin substitute based on human amniotic membrane. Cell and Tissue Banking, 1–9.

Tomasek, J., Gabbiani, G., Hinz, B., Chaponnier, C., Brown, R., 2002. Myofibroblasts and mechano-regulation of connective tissue remodelling. Nature Reviews Molecular Cell Biology 3 (5), 349–363.

Topman, G., Lin, F.-H., Gefen, A., 2012. The influence of ischemic factors on the migration rates of cell types involved in cutaneous and subcutaneous pressure ulcers. Annals of Biomedical Engineering 40 (9), 1929–1939.

Tranquillo, R., Murray, J., 1992. Continuum model of fibroblast-driven wound contraction - inflammation-mediation. Journal of theoretical biology 158 (2), 135.

Van den Brenk, H., 1956. Studies in restorative growth processes in mammalian wound healing. British Journal of Surgery 43 (181), 525–550.

Vaughan, M., Howard, E., Tomasek, J., 2000. Transforming growth factor-beta 1 promotes the morphological and functional differentiation of the myofibroblast. Experimental cell research 257 (1), 180–189.

Vermolen, F. J., Javierre, E., 2010. Computer simulations from a finite-element model for wound contraction and closure. Journal of tissue viability 19 (2), 43–53.

Vermolen, F. J., Javierre, E., 2012. A finite-element model for healing of cutaneous wounds combining contraction, angiogenesis and closure. Journal of mathematical biology 65 (5), 967–996.

Visscher, M., Hoath, S., Conroy, E., Wickett, R., 2001. Effect of semipermeable membranes on skin barrier repair following tape stripping. Archives of Dermatological Research 293 (10), 491–499.

Weiss, J., Maker, B., Govindjee, S., 1996. Finite element implementation of incompressible, transversely isotropic hyperelasticity. Computer Methods in Applied Mechanics and Engineering 135 (1-2), 107–128.

Wells, R. G., 2008. The role of matrix stiffness in regulating cell behavior. Hepatology 47 (4), 1394–1400.

Widgerow, A., Chait, L., Stals, R., Stals, P., 2000. New innovations in scar management. Aesthetic Plastic Surgery 24 (3), 227–234.

Wilkes, G., Brown, I., Wildnauer, R., 1973. The biomechanical properties of skin. Critical Reviews in Bioengineering, 453–495.

Xue, C., Friedman, A., Sen, C. K., 2009. A mathematical model of ischemic cutaneous wounds. Proceedings of the National Academy of Sciences of the United States of America 106 (39), 16782–16787.

COMPENDIUM OF PUBLICATIONS

Mechanochemical modeling
of wound healing:
multiphysics finite element simulations.

Work 1: Nonlinear finite element simulations of injuries with free boundaries: Application to surgical wounds

Journal: *International Journal for Numerical Methods in Biomedical Engineering*(2014). Published online in Wiley Online Library (wileyonlinelibrary.com).
DOI: 10.1002/cnm.2621
Journal Impact factor: 1.310

Contribution of the author of the thesis: the author was in charge of rewriting the formulation for the plane strain approach, making a review of the existing literature, choosing the mechanical variables, performing all the computational simulations, analyzing the results and determining their implications. Everything was done under the supervision of the other authors.

INTERNATIONAL JOURNAL FOR NUMERICAL METHODS IN BIOMEDICAL ENGINEERING
Int. J. Numer. Meth. Biomed. Engng. (2014)
Published online in Wiley Online Library (wileyonlinelibrary.com). DOI: 10.1002/cnm.2621

Nonlinear finite element simulations of injuries with free boundaries: Application to surgical wounds

C. Valero [1,*,†], E. Javierre [2], J. M. García-Aznar [1] and M. J. Gómez-Benito [1]

[1] *Multiscale in Mechanical and Biological Engineering, Aragón Institute of Engineering Research, University of Zaragoza, Zaragoza, Spain*
[2] *Centro Universitario de la Defensa, Academia General Militar, Zaragoza, Spain*

SUMMARY

Wound healing is a process driven by biochemical and mechanical variables in which a new tissue is synthesised to recover original tissue functionality. Wound morphology plays a crucial role in this process, as the skin behaviour is not uniform along different directions. In this work, we simulate the contraction of surgical wounds, which can be characterised as elongated and deep wounds. Because of the regularity of this morphology, we approximate the evolution of the wound through its cross section, adopting a plane strain hypothesis. This simplification reduces the complexity of the computational problem; while allows for a thorough analysis of the role of wound depth in the healing process, an aspect of medical and computational relevance that has not yet been addressed. To reproduce wound contraction, we consider the role of fibroblasts, myofibroblasts, collagen and a generic growth factor. The contraction phenomenon is driven by cell-generated forces. We postulate that these forces are adjusted to the mechanical environment of the tissue where cells are embedded through a mechanosensing and mechanotransduction mechanism. To solve the nonlinear problem, we use the finite element method (FEM) and an updated Lagrangian approach to represent the change in the geometry. To elucidate the role of wound depth and width on the contraction pattern and evolution of the involved species, we analyse different wound geometries with the same wound area. We find that deeper wounds contract less and reach a maximum contraction rate earlier than superficial wounds.

Received 13 May 2013; Revised 12 November 2013; Accepted 20 November 2013

KEY WORDS: finite elements; free boundary problem; wound healing; nonlinear convection-diffusion-reaction; mechanosensing and mechanotransduction

1. INTRODUCTION

Skin is the protective barrier between internal organs and external aggressions. Occasionally, this barrier is damaged and a number of complicated processes are needed to recover the initial functionality of the skin. Different injuries such as burns, cuts, ulcers and surgery scars cause a reduction in skin quality, making the wound healing process to recover the appropriate properties [1].

Wound healing is mainly driven by different cellular species (fibroblasts, myofibroblasts, epithelial cells and macrophages) and growth factors (macrophage-derived growth factor, transforming growth factor (TGF)$-\alpha$, TGF$-\beta$, platelet-derived growth factor and vascular endothelial growth factor). These species undergo several processes (proliferation, differentiation, migration and apoptosis) that modify their concentration, regulating the evolution of the wound. Wound healing is usually divided into three stages: inflammation, tissue formation and scar remodelling [2]. During the inflammation stage, a fibrin clot is formed at the wound site and a number of growth factors are released. During the second stage, different cellular species are attracted to the clot by the growth

*Correspondence to: C. Valero, Multiscale in Mechanical and Biological Engineering, Aragón Institute of Engineering Research, University of Zaragoza, Maria de Luna s/n, 50018 Zaragoza, Spain.

†E-mail: claraval@unizar.es

factors released during inflammation. Epidermal cells proliferate into the wound area, granulation tissue appears and new blood vessels begin to grow to supply oxygen and nutrients to the new tissue [1]. Fibroblasts secrete collagen to create a new extracellular matrix (ECM) that will replace the temporary fibrin clot. In this stage, the wound reduces its size and acquires a tensional state that will slowly relax. Finally, in the remodelling stage, previously synthesised collagen fibres align with tension lines in such a way that the damaged tissue gradually recovers most of its initial functionality. In the last stage, previously initiated processes end, and cell types that are no longer needed die and are removed.

Wound contraction is one of the most important processes during wound healing. This process is strongly influenced by not only cellular and chemical species but also mechanics. Cells feel the mechanical changes on the substrate in which they are embedded and regulate the forces they exert corresponding to this mechanical environment [3–5]. Therefore, most wound healing studies include both biological and mechanical factors in their models [6–10]. In addition, wound geometry is one of the most important characteristics in determining the evolution of the healing process. Wounds in the skin can be classified according to their dimensions. Wounds with a large superficial area and a shallow depth should be treated differently than deep wounds with a relevant depth.

For a number of years, mathematical models have been developed to study different biological and physiological processes [11]. Prior wound healing works have focused on tracking the wound superficial area over time, neglecting any influence of wound depth on the contraction kinetics [6, 9, 12]. Previous works on wound healing [8, 13–15] and wound contraction [9, 12, 16] have mostly studied wounds from a one-dimensional (1-D) perspective or under the assumption of plane stress. These models consider simple axisymmetric geometries and allow the spatial problem to be reduced to a 1-D model. Recent works have considered more realistic wound geometries [6, 10], solving the two-dimensional (2-D) spatial problem but neglecting the wound depth. 2-D models allow the study of complex wounds with more realistic geometries. From a numerical perspective, planar wounds are easier to model as the boundary conditions are the same for the whole boundary and the natural boundary conditions do not need to be taken into account. Therefore, in this work, we focus on the numerical solution of the governing system without boundary simplification to obtain a model applicable to both wound types. Hence, we present a mathematical model that can reproduce the evolution of both (superficial and deep) wounds. We focus on the simulation of deep and elongated wounds to consider the different behaviours of wounds along different directions. The healing of deep and elongated wounds varies from that of planar wounds because all involved phenomena mainly occur along the wound depth. From a mechanical perspective, the hypotheses of plane strain and a free boundary on the top surface of the wound are adopted. Note, moreover, that this approach to wound healing is the closest approximation to a three-dimensional spatial model of wound healing. Three-dimensional models are desirable to capture more realistic and complex wound morphologies. However, they are much more complex to develop and more expensive computationally. There are still many hypotheses on cell and tissue behaviour that need to be properly addressed using the predictive power of three-dimensional wound healing models. Therefore, from a modelling and simulation point of view, 2-D models present the most affordable option with less simplification of hypotheses than 1-D models. To the best of our knowledge, a model with these characteristics has not been developed previously.

The FEM is used to conveniently manage the complex wound geometries and free boundary. A nonlinear finite element is implemented to solve the mechanical equilibrium of the tissue and evolution of the chemical and cellular species simultaneously. The finite element approximation of the highly nonlinear and coupled convection-diffusion-reaction governing equations allows us to propose a strict linearisation of the governing equations, which yields a linear system of equations that are easy to solve on each time increment.

2. MATHEMATICAL MODEL

The aim of this work is to address the difference between planar and long deep wounds, specifically the effects of wound morphology and mechanical behaviour. Superficial wounds are studied

DOI: 10.1002/cnm

assuming a plane stress approach because their depths are much smaller than their other dimensions. In contrast, long deep wounds are studied under a plane strain approach because the wound behaviour is assumed to be the same along their lengths, and thus, only the transversal section should be studied. Furthermore, in long deep wounds, the upper part of the wound edge is in contact with the external environment with no constrains on its movement, which allows a different contraction pattern.

In this work, we present the formulation and numerical solution of a model that reproduces the contraction of elongated and deep wounds. The model formulation used here, based on the mechanochemical coupling of different cellular species, growth factors and the ECM, is similar to those in earlier works [6, 9, 12], but fewer simplifications are assumed in its implementation than in previous models.

Thus, to reproduce the wound status over time, we take into account biological and mechanical factors that affect both the cellular kinetics and ECM mechanical evolution. This mechanochemical coupling is supported by experimental results proving that cells not only respond to biochemical stimulus but also modify their behaviour depending on the mechanical evolution of the skin [3, 4]. Moreover, the mechanical contribution of the skin determines the way the wound contracts, a crucial element of the healing process.

2.1. Governing equations

The model reproduces the temporal and spatial evolution of four different species within the wound space and surrounding tissue. Following previous works [6, 9, 12], we considered two different cellular species: fibroblasts and myofibroblasts. Fibroblasts (n) are motile cells inside the skin that secrete ECM and exert traction forces on the tissue in which they are embedded. Myofibroblasts (m) are nonmotile cells that appear in the skin because of the combined action of inflammatory growth factors and mechanical stimulus and amplify the forces exerted by fibroblasts [17, 18]. The secreted ECM is mainly composed of collagen (ρ), which gives structural support to the skin and determines its mechanical properties. Collagen forms fibres that are synthesised and degraded by fibroblasts and myofibroblasts [19]. Thus, we assume that collagen is the main component in the skin that causes the stiffening effect of the newly synthesised ECM. The elastic modulus (E) is therefore dependent on the collagen density through the equation $E = E_0\rho/\rho_0$, where E_0 and ρ_0 are the elastic modulus and collagen density of the undamaged skin, respectively, considering that the skin becomes stiffer as the collagen density increases [20, 21]. Finally, we consider a generic growth factor (c) accumulated at the wound site during the inflammatory phase that regulates cell migration and cell function during the contraction process.

Each of the aforementioned cellular and chemical species follows a conservation law that incorporates the biological cues previously described. In general terms, this conservation law can be expressed as

$$\frac{\partial Q}{\partial t} + \nabla \cdot \mathbf{J}_Q = f_Q, \tag{1}$$

where $\mathbf{J}_Q$ denotes the net flux of the species Q and its net production, f_Q.

If we single out this equation for each of the four species, we find that the corresponding laws can be written for fibroblasts (Eqn (2)), myofibroblasts (Eqn (3)), collagen (Eqn (4)) and growth factor (Eqn (5)) as follows,

$$\frac{\partial n}{\partial t} + \nabla \cdot \left(\underbrace{-D_n \nabla n}_{\text{random migration}} + \underbrace{\frac{a_n}{(b_n + c)^2} n \nabla c}_{\text{chemotaxis}} + \underbrace{n \frac{\partial \mathbf{u}}{\partial t}}_{\text{passive convection}} \right) = \underbrace{\left(r_n + \frac{r_{n,max} c}{C_{1/2} + c} \right) n \left(1 - \frac{n}{K} \right)}_{\text{proliferation}}$$
$$\underbrace{- \frac{k_{1,max} c}{C_k + c} \frac{p_{cell}(\theta)}{\tau_d + p_{cell}(\theta)} n}_{\text{differentiation}} + \underbrace{k_2 m}_{\text{dedifferentiation}} - \underbrace{d_n n}_{\text{death}} \tag{2}$$

DOI: 10.1002/cnm

$$\frac{\partial m}{\partial t} + \nabla \cdot \left(\underbrace{m \frac{\partial \mathbf{u}}{\partial t}}_{\text{passive convection}} \right) = \underbrace{\epsilon_r \left(r_n + \frac{r_{n,max} c}{C_{1/2} + c} \right) m \left(1 - \frac{m}{K} \right)}_{\text{proliferation}} + \underbrace{\frac{k_{1,max} c}{C_k + c} \frac{p_{cell}(\theta)}{\tau_d + p_{cell}(\theta)} n}_{\text{differentiation}} - \underbrace{k_2 m}_{\text{dedifferentiation}} - \underbrace{d_m m}_{\text{death}} \tag{3}$$

$$\frac{\partial \rho}{\partial t} + \nabla \cdot \left(\underbrace{\rho \frac{\partial \mathbf{u}}{\partial t}}_{\text{passive convection}} \right) = \underbrace{\left(r_\rho + \frac{r_{\rho,max} c}{C_\rho + c} \right) \frac{n + \eta_b m}{R_\rho^2 + \rho^2}}_{\text{production}} - \underbrace{d_\rho \left(n + \eta_d m \right) \rho}_{\text{degradation}} \tag{4}$$

$$\frac{\partial c}{\partial t} + \nabla \cdot \left(\underbrace{-D_c \nabla c}_{\text{diffusion}} + \underbrace{c \frac{\partial \mathbf{u}}{\partial t}}_{\text{passive convection}} \right) = \underbrace{\frac{k_c (n + \zeta m) c}{\Gamma + c}}_{\text{production}} - \underbrace{d_c c}_{\text{degradation}} \tag{5}$$

where $\mathbf{u}$ represents the tissue displacements. The parameter values and descriptions can be found in Tables I and II.

As the model reproduces wound contraction, we consider that wound healing is driven by not only biochemical laws but also mechanical stimuli. Regarding the mechanical behaviour of the system, we express the balance between the internal stresses and the external forces as

$$\nabla \cdot (\boldsymbol{\sigma}_{ecm} + \boldsymbol{\sigma}_{cell}) = \mathbf{f}_{ext}, \tag{6}$$

where $\boldsymbol{\sigma}_{ecm}$ denotes the ECM stress contribution. Following most works in wound contraction [6, 9, 12], we assume that the skin behaves as a viscoelastic material. Therefore, $\boldsymbol{\sigma}_{ecm}$ can be written as

$$\boldsymbol{\sigma}_{ecm} = \mu_1 \frac{\partial \boldsymbol{\varepsilon}}{\partial t} + \mu_2 \frac{\partial \theta}{\partial t} \mathbf{I} + \frac{E}{1 + \nu} \left(\boldsymbol{\varepsilon} + \frac{\nu}{1 - 2\nu} \theta \mathbf{I} \right), \tag{7}$$

Table I. List of model parameters related to fibroblasts and myofibroblasts kinetics.

Parameter	Description	Value	Observations
n_0	Fibroblasts density in undamaged dermis	10^4 cells/cm^3	[12]
D_n	Fibroblasts diffusion rate	$2{\cdot}10^{-2}$ cm^2/day	[22]†
a_n	Together with b_n determines the maximal chemotaxis rate per unit of GF concentration	$4{\cdot}10^{-10}$ g/cm day	[6]
b_n	GF concentration that produces 25% of the maximal chemotactic response	$2{\cdot}10^{-9}$ g/cm^3	[6]
r_n	Fibroblasts proliferation rate	0.832 day^{-1}	[22]
$r_{n,max}$	Maximal rate of GF-induced fibroblasts proliferation	0.3 day^{-1}	[6]
$C_{1/2}$	Half-maximal GF enhancement of fibroblasts proliferation	10^{-8} g/cm^3	[12]
K	Fibroblasts maximal capacity in dermis	10^7 cells/cm^3	[12]
$k_{1,max}$	Maximal rate of fibroblasts differentiation	0.8 day^{-1}	[6]
C_k	Half-maximal GF enhancement of fibroblasts differentiation	10^{-8} g/cm^3	[6]
k_2	Myofibroblasts dedifferentiation rate	0.693 day^{-1}	[6]
d_n	Fibroblasts death rate	0.831 day^{-1}	$d_n = r_n \left(1 - \frac{n_0}{K}\right)$‡
ϵ_r	Proportionality factor	0.5	[12]
d_m	Myofibroblasts death rate	$2.1{\cdot}10^{-2}$ day^{-1}	[6]

GF, growth factor.

† Adjusted to fit reported migration rate with a traveling wave model.

‡ Determined fibroblasts proliferation kinetics to remain in equilibrium away from the wound.

DOI: 10.1002/cnm

Table II. List of model parameters related to collagen and growth factor kinetics.

Parameter	Description	Value	Observations
ρ_0	Collagen concentration in undamaged dermis	0.1 g/cm^3	[12]
ρ_{ini}	Initial collagen concentration in the wound	10^{-3} g/cm^3	[12]
c_0	GF concentration in the wound	10^{-8} g/cm^3	[12]
r_ρ	Collagen production rate	$7.59{\cdot}10^{-10}$ g^3 $/cm^6$ cell day	$r_\rho = d_\rho \rho_0 \left(R_\rho^2 + \rho_0^2\right)^{\ddagger}$
$r_{\rho,max}$	Maximal rate of GF-induced collagen production	$7.59{\cdot}10^{-9}$ g^3 $/cm^6$ cell day	[12]
C_ρ	Half-maximal GF enhancement of collagen synthesis	10^{-9} g/cm^3	[12]
η	Proportionality factor	2	[12]
R_ρ	Half-maximal collagen enhancement of ECM deposition	0.3 g/cm^3	[12]
d_ρ	Collagen degradation rate per unit of cell density	$7.59{\cdot}10^{-8}$ cm^3/cell day	[12]
D_c	GF diffusion rate	$5{\cdot}10^{-2}$ cm^2/day	[12]
k_c	GF production rate per unit of cell density	$7.5{\cdot}10^{-6}$ cm^3/cell day	[6]§
ζ	Proportionality factor	1	[12]
Γ	Half-maximal enhancement of net GF production	10^{-8} g/cm^3	[12]
d_c	GF decay rate	0.693 day^{-1}	[6]

GF, growth factor; ECM, extracellular matrix.

‡ Determined collagen degradation kinetics to remain in equilibrium away from the wound.

§ Downestimated to prevent fibro-proliferative disorders [16] with the used GF decay rates.

where the elastic modulus of the ECM varies with the collagen density, θ denotes the volumetric strain of the ECM, $\boldsymbol{\varepsilon}$ denotes the ECM deformation and $\mathbf{I}$ refers to the second-order identity tensor. In contrast, $\boldsymbol{\sigma}_{cell}$ represents the stress exerted by the cells in the ECM

$$\boldsymbol{\sigma}_{cell} = p_{cell}(\theta)\,(1 + \xi m)\,\frac{n\rho}{R_\tau^2 + \rho^2}\mathbf{I}. \tag{8}$$

Cell densities play a crucial role in determining the contractile stress [18, 19], which is limited by the collagen density and modulated by a mechanical stimulus, p_{cell}. This stimulus represents the net stress of one cell per unit of ECM [23] and is a function of the matrix volumetric strain (θ),

$$\begin{aligned} p_{cell}(\theta) = {} & \frac{K_{act}\,p_{max}}{K_{act}\theta_1 - p_{max}}\,(\theta_1 - \theta)\,\chi_{[\theta_1,\theta^*]}(\theta) \\ & + \frac{K_{act}\,p_{max}}{K_{act}\theta_2 - p_{max}}\,(\theta_2 - \theta)\,\chi_{(\theta^*,\theta_2]}(\theta) + K_{pas}\theta. \end{aligned} \tag{9}$$

In this expression, the contributions of two different components of the cell to the generation of stresses are considered, following the assumptions proposed by Moreo *et al.* (2008) [23]. The active contribution is a linear stiffness-dependent actuator that corresponds to the contractile mechanism, simulating the force provided by the actin and myosin cross-bridges at the sarcomere level during shortening. In fact, p_{max} is the maximum force provided by the actomyosin system. Following this approach, the series element K_{act} corresponds to the stiffness of the actin components that are aligned with the actomyosin motors. This model also considers a parallel component, K_{pas}, which corresponds to the stiffness of different mechanical components of cells, such as the membrane, microtubules and cytoplasm.

DOI: 10.1002/cnm

Table III. List of model parameters related to the mechanical behaviour of cells and extracellular matrix.

Parameter	Description	Value	Observations
p_{max}	Maximal cellular active stress per unit of ECM	10^{-5} N g$/cm^2$ cell	[6]
K_{pas}	Volumetric stiffness moduli of the passive components of the cell	$2{\cdot}10^{-5}$ N g$/cm^2$ cell	[23]
K_{act}	Volumetric stiffness moduli of the actin filaments of the cell	10^{-4} N g$/cm^2$ cell	[23]
θ_1	Shortening strain of the contractile element	-0.6	[6]
θ_2	Lengthening strain of the contractile element	0.5	[23]
τ_d	Half-maximal mechanical enhancement of fibroblast differentiation	10^{-5} N g$/cm^2$ cell	[6]
μ_1	Undamaged skin shear viscosity	200 N day/cm^2	[6]
μ_2	Undamaged skin bulk viscosity	200 N day/cm^2	[6]
E_d	Dermis Young's modulus	33.4 N/cm^2	[24]
ν_d	Dermis skin Poisson's ratio	0.3	[24]
E_{ut}	Underlying tissue Young's modulus	0.82 N/cm^2	[25]
ν_{ut}	Underlying tissue Poisson's ratio	0.459	[26]
ξ	Myofibroblasts enhancement of traction per unit of fibroblasts density	10^{-3} cm^3/g	[12]
R_τ	Traction inhibition collagen density	$5{\cdot}10^{-4}$ g/cm^3	[12]
s	Dermis tethering factor	10^{-1} N/cm g	Estimated

ECM, extracellular matrix.

Finally, $\mathbf{f_{ext}}$ denotes the tethering forces created by the attachments to the underlying tissue, which are proportional to the collagen density and the tissue displacements,

$$\mathbf{f}_{ext} = s\rho\mathbf{u}. \tag{10}$$

The parameter values and descriptions of the mechanical equilibrium equations can be found in Table III.

2.2. *Boundary conditions*

When modelling deep wounds, special attention should be paid to the evolution of species and mechanical tension along the wound depth. Thus, detailed descriptions of the boundary conditions for the different species are given in this section.

Given the fixed morphology of the wound (deep and elongated), we assume that the mechanical evolution of the wound follows the plane strain hypotheses, neglecting deformations along its longitudinal direction. Furthermore, we simulate only the cross section of the wound. The wound is assumed to behave in the same way in all its cross sections, except near the two ends, considering the wound length is much larger than its other two dimensions (Figure 1). Let us denote the computational domain as Ω (Figure 1). The computational domain consists of two parts, the wound and the surrounding undamaged tissue. The undamaged tissue consists of two layers, the dermis and the underlying tissue. The boundary of the domain $\partial\Omega$ consists of two distinct and nonintersecting parts: the free boundary ($\Gamma_\mathbf{t}$), which is in contact with the environment and can move freely, and the fixed boundary ($\Gamma_\mathbf{u}$), which is attached to the underlying tissue. Mathematically, it can be written as $\partial\Omega = \Gamma_\mathbf{u} \cup \Gamma_\mathbf{t}$ with $\Gamma_\mathbf{u} \cap \Gamma_\mathbf{t} = \emptyset$.

The computational domain Ω is large enough so that boundary effects on the evolution of the species can be disregarded. Hence, on the outer boundary $\Gamma_\mathbf{u}$, diffusive fluxes and displacements are not allowed:

$$\nabla Q \cdot \mathbf{n}_\perp = 0 \quad \text{and} \quad \mathbf{u} = \mathbf{0} \quad \text{on } \Gamma_\mathbf{u}, \tag{11}$$

for all species Q that migrate or diffuse through the tissue (that is, fibroblasts n and the generic growth factor c). Here, $\mathbf{n}_\perp$ denotes the normal vector pointing out from Ω. On the upper boundary

DOI: 10.1002/cnm

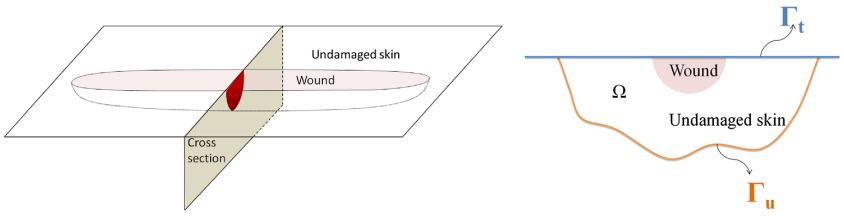

Figure 1. Boundary conditions.

$\Gamma_{\mathbf{t}}$, the situation is slightly different. The mass conservation of species Q implies, again, that there is no diffusive flux. However, there is no constrain on the displacement profile. Consequently, the stress vector $\mathbf{t} = \sigma \mathbf{n}_{\perp}$ should be zero, which yields

$$\nabla Q \cdot \mathbf{n}_{\perp} = 0 \quad \text{and} \quad \mathbf{t} = \mathbf{0} \quad \text{on} \ \Gamma_{\mathbf{t}}. \tag{12}$$

Hence, $\Gamma_{\mathbf{t}}$ behaves as a free boundary. Note that models focusing on the evolution of the wound surface do not address this moving boundary; therefore, the boundary conditions in those cases are given in Eqn (11) for the complete boundary.

2.3. *Initial conditions*

We initialise the analysis at the beginning of the proliferative stage, when cells have not yet begun to appear in the wound site. As initial conditions, we fix the concentration of the species in the entire domain. The cellular species, fibroblasts and myofibroblasts are not yet present in the wound. However, the undamaged tissue is full of fibroblasts; myofibroblasts are not present here because they only appear where damage has occurred. The new ECM has not begun to form in the wound site; thus, there is only a small concentration of collagen belonging to the temporary fibrin clot. The undamaged tissue has a normal collagen density. Finally, because during the previous stages different growth factors were released into the wound site, we initiate our analysis with the wound site full of growth factors but no growth factors present in the undamaged skin.

3. NUMERICAL METHOD

3.1. *Weak formulation*

Using Gauss' theorem, the integrals over the domain of computation of Eqns (1) and (6) multiplied by sufficiently smooth weighting function υ_Q and $\boldsymbol{v}$, respectively, result in

$$\int_{\Omega} \frac{\partial Q}{\partial t} \upsilon_Q d\Omega - \int_{\Omega} \mathbf{J}_Q \cdot \nabla \upsilon_Q d\Omega = \int_{\Omega} f_Q \upsilon_Q d\Omega - \int_{\partial\Omega} \mathbf{J}_Q \cdot \mathbf{n}_{\perp} \upsilon_Q d\Gamma, \tag{13}$$

$$\int_{\Omega} \boldsymbol{\sigma} : \frac{1}{2} \left(\nabla \boldsymbol{v} + \nabla \boldsymbol{v}^T \right) d\Omega = \int_{\Omega} \mathbf{f}_{ext} \cdot \boldsymbol{v} d\Omega + \int_{\partial\Omega} \mathbf{t} \cdot \boldsymbol{v} d\Gamma, \tag{14}$$

where $\mathbf{n}_{\perp}$ denotes the normal vector pointing out from Ω and $\boldsymbol{\sigma}$ comprises the ECM stress contribution and the stress exerted by the cells

$$\boldsymbol{\sigma} = \boldsymbol{\sigma}_{ecm} + \boldsymbol{\sigma}_{cell}. \tag{15}$$

DOI: 10.1002/cnm

For all considered species, the flux term $\mathbf{J}_Q$, consists of a passive convection term $Q\frac{\partial \mathbf{u}}{\partial t}$ and additional diffusive fluxes. Given that there are no diffusive fluxes across the boundaries $\Gamma_\mathbf{u}$ and $\Gamma_\mathbf{t}$, and $\mathbf{u} = \mathbf{0}$ on $\Gamma_\mathbf{u}$, we can write the boundary integral in Eqn (13) as

$$\int_{\partial\Omega} \mathbf{J}_Q \cdot \mathbf{n}_\perp v_Q \, d\Gamma = \int_{\Gamma_\mathbf{t}} Q v_Q \frac{\partial \mathbf{u}}{\partial t} \cdot \mathbf{n}_\perp \, d\Gamma \tag{16}$$

without a loss of generality. Because of the boundary conditions, $\boldsymbol{v}$ satisfies $\boldsymbol{v} = \mathbf{0}$ on $\Gamma_\mathbf{u}$ and $\mathbf{t} = \mathbf{0}$ on $\Gamma_\mathbf{t}$. Hence, the boundary integral in Eqn (14) vanishes

$$\int_{\partial\Omega} \mathbf{t} \cdot \boldsymbol{v} \, d\Gamma = \int_{\Gamma_\boldsymbol{v}} \mathbf{t} \cdot \boldsymbol{v} \, d\Gamma + \int_{\Gamma_\mathbf{t}} \mathbf{t} \cdot \boldsymbol{v} \, d\Gamma = 0. \tag{17}$$

Therefore, the weak formulation of the problem results in

$$\begin{aligned} \int_\Omega \frac{\partial Q}{\partial t} v_Q \, d\Omega - \int_\Omega \mathbf{J}_Q \cdot \nabla v_Q \, d\Omega = \int_\Omega f_Q v_Q \, d\Omega - \int_{\Gamma_\mathbf{t}} Q v_Q \frac{\partial \mathbf{u}}{\partial t} \cdot \mathbf{n}_\perp \, d\Gamma, \\ \int_\Omega \sigma : \frac{1}{2}\left(\nabla \boldsymbol{v} + \nabla \boldsymbol{v}^T\right) \, d\Omega = \int_\Omega \mathbf{f}_{ext} \cdot \boldsymbol{v} \, d\Omega, \end{aligned} \tag{18}$$

for all weighting functions v_Q and $\boldsymbol{v}$ that are sufficiently differentiable and satisfy $\boldsymbol{v} = \mathbf{0}$ on $\Gamma_\mathbf{u}$. Note that because of the considered wound morphology, an integral over the free boundary of the domain arises. As the wound geometry dynamically changes, the position of $\Gamma_\mathbf{t}$ and the computation of the normal vector $\mathbf{n}_\perp$ need to be updated for each time increment. We nevertheless assume a small deformation approach during each time increment. The geometry was updated after each time increment using an updated Lagrangian approximation to take the change in the normal outward vector and the change in the wound geometry into account.

We implement and calculate all integrals that are not present in existing wound contraction works due to their plane stress assumptions. Nevertheless, it is necessary to calculate these terms only for those elements that belong to the free boundary in the plane strain or three-dimensional simulations. In this work, this effect cannot be neglected as the boundary is moving and its contribution is significant.

3.2. Finite element approximation

To reach the finite element approximation, it is necessary to express the primary unknowns in terms of their nodal values through their associated shape functions [27]:

$$Q^h(\mathbf{x}, t) = \mathbf{N}_Q(\mathbf{x})\mathbf{Q}(t), \quad \mathbf{u}^h(\mathbf{x}, t) = \mathbf{N}_\mathbf{u}(\mathbf{x})\mathbf{U}(t), \tag{19}$$

where the finite element solution is denoted by the superscript h. The final discrete and nonlinear system of equations is reached by substituting these approximations into the weak formulation (Eqn(13) and Eqn(14)) and setting the weighting functions equal to the shape functions. The time-dependent nodal values of the primary unknowns are determined from the resulting system of equations, which can be expressed as a balance of internal and external forces matrices

$$\mathbb{F}\left(\mathbb{Z}_{n+1}\right) := \mathbb{F}^{int}\left(\mathbb{Z}_{n+1}\right) - \mathbb{F}^{ext}\left(\mathbb{Z}_{n+1}\right) = \mathbf{0}, \tag{20}$$

where $\mathbb{F}^{int}$ comprises the temporal derivative and flux terms and $\mathbb{F}^{ext}$ the reaction terms on the governing equations. The vector of unknowns, $\mathbb{Z}$, denotes the ordered primary variables nodal values

$$\mathbb{Z} = \left(\mathbf{n}^T \ \mathbf{m}^T \ \boldsymbol{\rho}^T \ \mathbf{c}^T \ \mathbf{U}^T\right)^T. \tag{21}$$

DOI: 10.1002/cnm

Hence, nodal submatrices for the fibroblasts are given by

$$\mathbf{F}_n^{int} = \int_\Omega \mathbf{N}_n^T \frac{\partial n}{\partial t}\, d\Omega + \int_\Omega \nabla \mathbf{N}_n^T \left[D_n \nabla n - \frac{a_n}{(b_n + c)^2} n \nabla c - n \frac{\partial \mathbf{u}}{\partial t} \right] d\Omega + \int_{\Gamma_t} \mathbf{N}_n^T n \frac{\partial \mathbf{u}}{\partial t} \mathbf{n}_\perp d\Gamma \tag{22}$$

$$\mathbf{F}_n^{ext} = \int_\Omega \mathbf{N}_n^T \left[\left(r_n + \frac{r_{n,max} c}{C_{1/2} + c} \right) n \left(1 - \frac{n}{K} \right) - \frac{k_{1,max} c}{C_k + c} \frac{p_{cell}(\theta)}{\tau_d + p_{cell}(\theta)} n + k_2 m \right] d\Omega - \int_\Omega \mathbf{N}_n^T d_n n\, d\Omega. \tag{23}$$

The remainder matrices are included in Appendix A. To obtain the solution of the resulting non-linear system of equations we use an explicit time integration method [28] and a Newton–Raphson linearisation. The non-zero entries of the Jacobian matrices $\frac{\partial \mathbb{F}^{int}}{\partial \mathbb{Z}}$ and $\frac{\partial \mathbb{F}^{ext}}{\partial \mathbb{Z}}$ are presented in Appendix A.

To properly reproduce the natural boundary conditions on the free boundary, it is necessary to compute the corresponding boundary integrals. As our model is 2-D, the element integrals are surface integrals, and the boundary integrals are line integrals. To determine the boundary conditions, we need to calculate the boundary integrals only for those elements that belong to the free boundary and only in those element faces that belong to the boundary, as they are zero in the rest of the domain.

The finite element formulation is implemented using an updated Lagrangian approach. Hence, the reference configuration is updated after each time increment, even though a small strain assumption is considered. This update is needed to accurately compute the boundary conditions effect on the process, which depends strongly on the surface of the wound, as the natural boundary conditions contribution changes along the outwards normal direction. To perform the calculation process, we initially have the wound geometry, the species densities along the entire wound and the boundary conditions. We simulate the wound evolution over 30 days, in shorter steps of 0.1 day, to obtain an accurate model of the evolution of the geometry. After the first analysis (corresponding to one step of 0.1 day), we update the wound geometry and perform a new analysis. This process can be repeated as many times as needed to complete the total time studied.

4. EXAMPLE OF APPLICATION

Two different wound geometries are studied in this work: two long wounds with a semicircular or semielliptical transverse section. These wounds are characterised by having a large length and a nondepreciable depth. Therefore, the wounds can be studied through their transverse sections using the plane strain approach (Figure 2). The semicircular wound has a diameter (d) of 0.5 cm, whereas the semielliptical wound has an aspect ratio of two, that is, its depth (b) is twice its width (a). The dimensions of the semielliptical wound are such that it has the same cross-sectional area as the semicircular wound. Both wounds are surrounded by healthy skin, with the domain being sufficiently large to neglect the boundary effects. The undamaged tissue consists of two different layers: the dermis and the underlying tissue. Human dermis varies in depth depending on its anatomical location; it can have a thickness between 1 and 4 mm [29]. Here, we assume that the dermis has a depth of 1.5 mm and that the simulated wounds are deep enough to penetrate the dermis. Considering the symmetry of the wound and the surrounding skin, we simulate half of the entire geometry.

5. RESULTS

First, we study the spatial contraction and temporal evolution of the wound. In Figure 3, we present the normalised contraction curve for the two studied geometries. In this curve, we represent the area

DOI: 10.1002/cnm

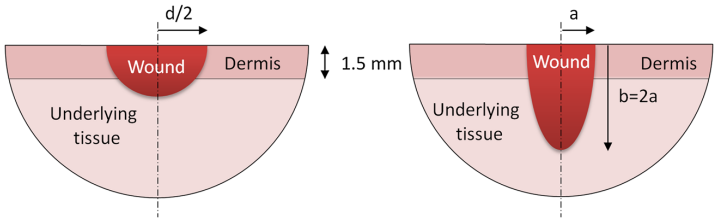

Figure 2. Scheme of the semicircular and the semielliptical wounds.

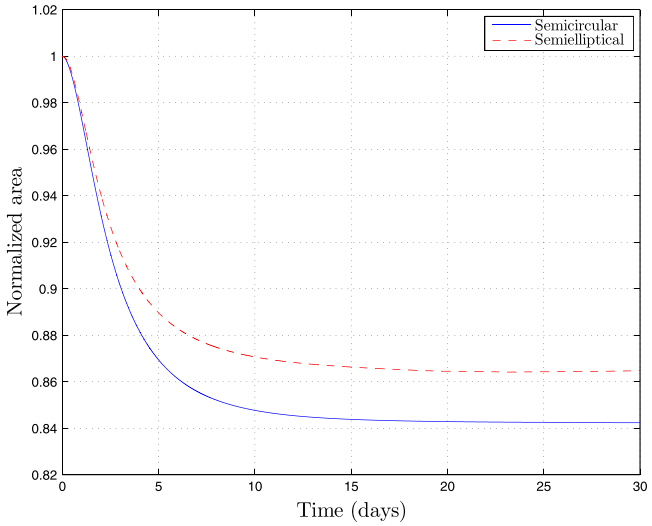

Figure 3. Normalised contraction curve for the semicircular and the semielliptical wounds.

of the simulated domain (half of the wound) during the simulated time (30 days) with respect to its initial area. We observe that, for both wounds, the main part of the contraction occurs during the first few days, after which the wound contracts more slowly. The highest contraction percentage occurs around day 10 in the semielliptical wound and around day 12 in the semicircular wound. From this point to the end of the 30 days, the wounds expand slowly. If we compare the contraction of both wounds, we see that the semicircular wound contracts more than the semielliptical one, reducing its size to 84.2% of its initial area, whereas the semielliptical wound contracts to 86.5% of its initial size. In the early stages of wound contraction (5 days), the semicircular wound contracts faster than the semielliptical wound. After this transitory phase, both wounds seem to reach a stationary state at the same time. We observe that the wound centre (Figure 2) is the point where the downward boundary displacement is the highest, approximately 0.66 mm in the semicircular wound and 0.82 mm in the semielliptical one. We also observe that the further we move from this point, the smaller the downward displacement of the free surface is.

Regarding the final geometry of the wound, Figure 4 shows the evolution of the wound geometry at different times and how the free boundary of the wound moves down due to the myofibroblasts contraction forces. Observing the evolution of different species in the wound (Figure 4), we see fibroblasts invade the wound site as the wound heals. The fibroblast's movement in the semielliptical wound is faster than in the semicircular wound; the semielliptical wound site is almost saturated

DOI: 10.1002/cnm

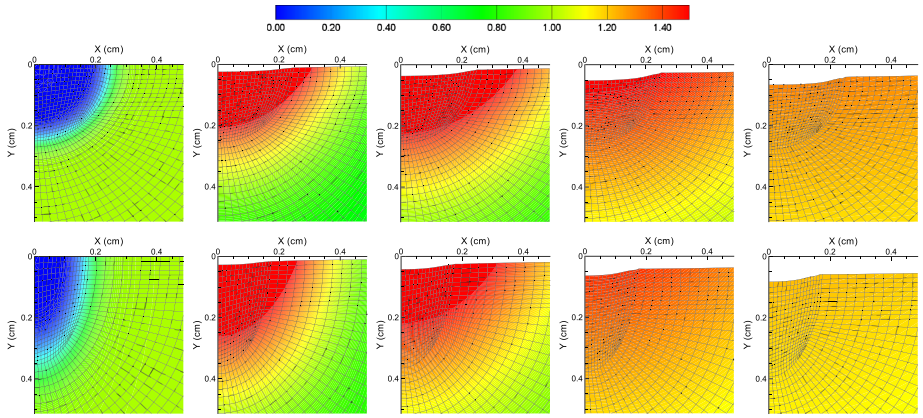

Figure 4. Fibroblast concentration in the semicircular (top) and semielliptical (bottom) wounds at different time points (from left to right; days 0, 3, 6, 15 and 30).

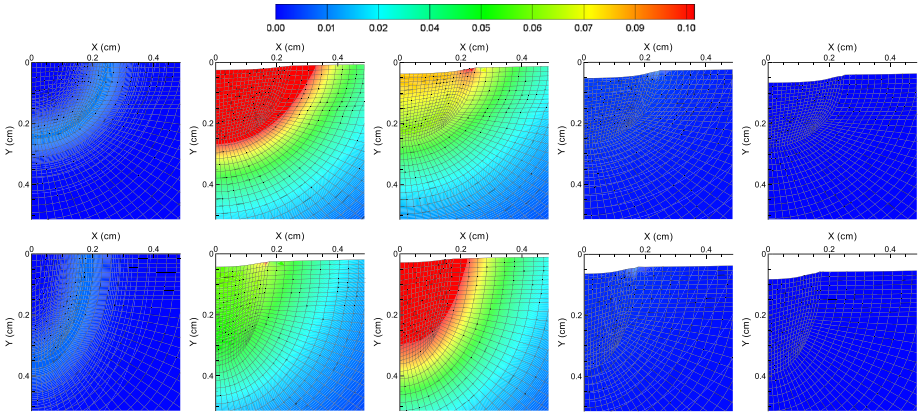

Figure 5. Myofibroblast concentration in the semicircular (top) and semielliptical (bottom) wounds at different time points (from left to right; days 0, 3, 6, 15 and 30).

with fibroblasts by day 3, whereas the semicircular one never reaches this level within the simulated period. The fibroblast's concentration far from the wound site remains invariable during the entire process. Similarly, we observe the evolution of myofibroblasts in both wounds (Figure 5). Myofibroblasts quickly appear in the wound and in the closest healthy skin when there is damage and disappear after contraction. We observe that the higher contractions occur while myofibroblasts are in the tissue, and the wound stabilises when they disappear.

Finally, we observe how the volumetric strain of the wound and the surrounding tissue evolves (Figure 6) over time. The volumetric strain (θ) denotes how much the tissue has deformed (contracted or expanded) from its initial state. During the entire process, the tissue that is far from the wound does not experience any contraction. Inside the wound site, we observe that contraction begins at the boundary between the wound and healthy skin. Furthermore, as the cell concentration increases and cells invade the wound centre, the wound contracts. We observe that the final contraction is highest in the wound centre. The distributions remain without changes from the moment that the contraction becomes stabilised in the contraction curve (Figure 3).

DOI: 10.1002/cnm

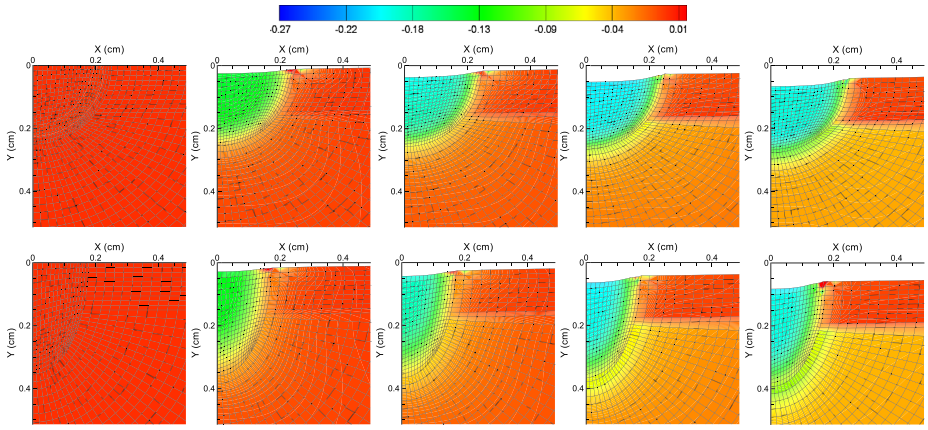

Figure 6. Total volumetric deformation in the semicircular (top) and semielliptical (bottom)wounds at different time points (from left to right; days 0, 3, 6, 15 and 30).

6. DISCUSSION

Computational models have become more important during recent years [11, 30]. These models can reproduce the evolution of wounds, which has not been deeply studied experimentally. There are few computational studies on human wounds, and those in the literature have mostly studied planar wounds. Long, deep wounds are more difficult to study computationally than planar wounds. Because long deep wounds are more complex, a deeper knowledge of the different phenomena that occur during wound healing is essential to establish a successful healing model. In this work, we present a model that predicts how deep elongated wounds contract depending on how different species that are present in the skin evolve and behave. Our work follows the work of Javierre *et al*. [6], which was based on a previous biochemical wound contraction model developed [12]. Javierre *et al.* [6] studied the behaviour of 2-D planar wounds with different sizes and geometries. There are a number of models [9, 12, 15] that also studied planar wounds but took a 1-D perspective with simpler and more restrictive models. Although those models properly reproduce the healing process, they are only useful for a small number of wound geometries (straight and circular); they are not applicable to real complex wounds.

All the previous 1-D and 2-D models only reproduced the behaviour of planar wounds. These wounds are superficial, and their area determines the healing process of the wound.

There are few animal models for the study of wound contraction [31, 32]. Most of them study superficial wounds, not examining the processes that occur along the transversal section of the wound. The present model elucidates the role of wound depth on contraction kinetics; hence, one of the most relevant outcomes of this work is the direct relationship among wound morphology, wound contraction and scar formation. As wound contraction represents an intermediate step between healing and scar formation, the results here obtained could predict the final scar aspect from wound geometry. Wound contraction will determine the posterior size and shape of the scar. In fact, we expect that deeper wounds will lead into more pronounced scars, because the downward tissue displacement is higher in deeper wounds. Thus, scars from deeper wounds are expected to be more perceptible. This model is a step forward to analyse suture patterns in a three dimensional model. This relationship could be used to identify a suture pattern that minimises the contraction of the wound and consequently results in a smaller scar [33]. This prediction would be of special interest in plastic surgery, where the size and visibility of scars is one of the most important factors.

More serious wounds, such as ulcers and surgery scars are not comparable with planar wounds. In these wounds, the transversal behaviour (along its depth) is more relevant than the superficial behaviour. Most of the change in the geometry is due to the movement of the free boundary, which

DOI: 10.1002/cnm

is in contact with the environment and can move without any constraint. These wounds have more importance as they more closely resemble real clinical wounds, which are often difficult to heal and usually require help to heal properly. Previous models cannot reproduce these wounds as they do not mimic the real behaviour of the species in the free boundary. A first attempt to study deep wounds was made in [7]. However, this work focused on the coupling of wound closure, angiogenesis and contraction.

In this work, we present a model to simulate deep wounds and reproduce the behaviour along their depths. Although these wounds are more similar to real wounds, their behaviour is also much more difficult to reproduce. Mathematically, the difficulty of these wounds is translated into a higher number of terms in the weak formulation. As the effect of the free boundary is not negligible, it is necessary to solve both the element and the boundary integrals that define the problem. In planar wounds, the boundary integrals vanish during the formulation. To the best of our knowledge, long deep wounds have not been previously studied, and these equations have not been solved without neglecting the natural boundary conditions term and updating the geometry using an updated Lagrangian approach. Wounds with different areas and same depth were also analysed (not included in the paper). Results for those geometries show a similar evolution of the wound area (normalised with respect to the initial wound size). From this observation, we can conclude that wound depth has a larger influence on the contraction kinetics than wound width. Deeper wounds, with less area in contact with the surrounding environment with respect to its depth, contract less than wider wounds, similar to semicircular wounds. Although there are no other studies on the wound contraction process in deep wounds our results qualitatively agree with experimental works [34, 35] and computational [12, 13] results for the contraction curves of planar wounds. The major difference in these curves is that the contraction is faster in deep wounds.

To perform this analysis, several simplifications were needed. First, the model considers a small strain approach and uses an updated Lagrangian approach; we update the reference configuration every time increment. The deformations in the tissue are small enough to satisfy the small strain hypothesis (lower than 0.6% at all time increments).

The contraction process is also known to be influenced by the relative position of the wound with the skin tension lines. Wounds parallel to tension lines heal better, creating smaller scars, whereas wounds perpendicular to tension lines generate larger scars [36]. Another limitation of the model is that we neglect the effect of the collagen fibres orientation in the tissue, which would modify the effect of the stress exerted by cells. Including the effect of these fibres would provide the model with more realistic anisotropic behaviour. In the simulated contraction stage, the wound fibres are randomly dispersed in the matrix; however, its reorganisation takes several months [14]. Thus, the effect of the collagen fibres would be more important during the remodelling phase.

Wound healing in the skin is one of today's major medical challenges. Although surgery techniques have improved and surgeons can now perform a number of different surgeries, the most severe difficulties, caused by scarring, usually occur after surgery. Moreover, ulcers and cuts are difficult wounds to control. Thus, mathematical models that reproduce the healing process can help us to understand the healing mechanism and learn how to improve it.

APPENDIX A: MATRICES OF THE INTERNAL AND EXTERNAL FORCES

The matrices of the internal and external forces appearing in Eqn(20) can be written as

$$\mathbf{F}_n^{int} = \int_\Omega \mathbf{N}_n^T \frac{\partial n}{\partial t}\, d\Omega + \int_\Omega \nabla \mathbf{N}_n^T \left(D_n \nabla n - \frac{a_n}{(b_n + c)^2} n \nabla c - n \frac{\partial \mathbf{u}}{\partial t} \right) d\Omega + \int_{\Gamma_t} \mathbf{N}_n^T n \frac{\partial \mathbf{u}}{\partial t} \mathbf{n}_\perp d\Gamma \tag{24}$$

$$\mathbf{F}_m^{int} = \int_\Omega \mathbf{N}_m^T \frac{\partial m}{\partial t} d\Omega - \int_\Omega \nabla \mathbf{N}_m^T m \frac{\partial \mathbf{u}}{\partial t} d\Omega + \int_{\Gamma_t} \mathbf{N}_m^T m \frac{\partial \mathbf{u}}{\partial t} \mathbf{n}_\perp d\Gamma \tag{25}$$

DOI: 10.1002/cnm

$$\mathbf{F}_{\rho}^{int} = \int_{\Omega} \mathbf{N}_{\rho}^{T} \frac{\partial \rho}{\partial t} d\Omega - \int_{\Omega} \nabla \mathbf{N}_{\rho}^{T} \rho \frac{\partial \mathbf{u}}{\partial t} d\Omega + \int_{\Gamma_t} \mathbf{N}_{\rho}^{T} \rho \frac{\partial \mathbf{u}}{\partial t} \mathbf{n}_{\perp} d\Gamma \tag{26}$$

$$\mathbf{F}_{c}^{int} = \int_{\Omega} \mathbf{N}_{c}^{T} \frac{\partial c}{\partial t} d\Omega + \int_{\Omega} \nabla \mathbf{N}_{c}^{T} \left(D_c \nabla c - c \frac{\partial \mathbf{u}}{\partial t} \right) d\Omega + \int_{\Gamma_t} \mathbf{N}_{c}^{T} c \frac{\partial \mathbf{u}}{\partial t} \mathbf{n}_{\perp} d\Gamma \tag{27}$$

$$\mathbf{F}_{\mathbf{u}}^{int} = \int_{\Omega} \mathbf{B}_{\mathbf{u}}^{T} \left[\mathbf{D}_{elas} \frac{\rho}{\rho_0} \mathbf{B}_{\mathbf{u}} \mathbf{U} + \mathbf{D}_{visco} \mathbf{B}_{\mathbf{u}} \dot{\mathbf{U}} + p_{cell}(\theta)(1 + \xi m) \frac{n\rho}{R_{\tau}^2 + \rho^2} \mathbf{I} \right] d\Omega \tag{28}$$

and

$$\mathbf{F}_{n}^{ext} = \int_{\Omega} \mathbf{N}_{n}^{T} \left[\left(r_n + \frac{r_{n,max} c}{C_{1/2} + c} \right) n \left(1 - \frac{n}{K} \right) - \frac{k_{1,max} c}{C_k + c} \frac{p_{cell}(\theta)}{\tau_d + p_{cell}(\theta)} n + k_2 m \right] d\Omega - \int_{\Omega} \mathbf{N}_{n}^{T} d_n n \, d\Omega \tag{29}$$

$$\mathbf{F}_{m}^{ext} = \int_{\Omega} \mathbf{N}_{m}^{T} \epsilon_r \left(r_n + \frac{r_{n,max} c}{C_{1/2} + c} \right) m \left(1 - \frac{m}{K} \right) d\Omega + \int_{\Omega} \mathbf{N}_{m}^{T} \frac{k_{1,max} c}{C_k + c} \frac{p_{cell}(\theta)}{\tau_d + p_{cell}(\theta)} n d\Omega - \int_{\Omega} \mathbf{N}_{m}^{T} (k_2 m + d_m m) \, d\Omega \tag{30}$$

$$\mathbf{F}_{\rho}^{ext} = \int_{\Omega} \mathbf{N}_{\rho}^{T} \left[\left(r_\rho + \frac{r_{\rho,max} c}{C_\rho + c} \right) \frac{n + \eta_b m}{R_\rho^2 + \rho^2} - d_\rho (n + \eta_d m) \rho \right] d\Omega \tag{31}$$

$$\mathbf{F}_{c}^{ext} = \int_{\Omega} \mathbf{N}_{c}^{T} \left(\frac{k_c (n + \zeta m) c}{\Gamma + c} - d_c c \right) d\Omega \tag{32}$$

$$\mathbf{F}_{\mathbf{u}}^{ext} = - \int_{\Omega} \mathbf{N}_{\mathbf{u}}^{T} s \rho \mathbf{u} d\Omega, \tag{33}$$

where all the terms containing $\mathbf{n}_{\perp}$ refer to the boundary and are the terms that allow us to reproduce the boundary behaviour. To obtain the solution of the resulting system of equations, we use an explicit integration method taking the nonzero entries of the Jacobian matrices $\frac{\partial \mathbb{F}^{int}}{\partial \mathbb{Z}}$ and $\frac{\partial \mathbb{F}^{ext}}{\partial \mathbb{Z}}$.

$$\frac{\partial \mathbf{F}_{n}^{int}}{\partial \mathbf{n}} = \frac{1}{\Delta t} \int_{\Omega} \mathbf{N}_{n}^{T} \mathbf{N}_n d\Omega + \int_{\Omega} \nabla \mathbf{N}_{n}^{T} D_n \nabla \mathbf{N}_n d\Omega - \int_{\Omega} \nabla \mathbf{N}_{n}^{T} \left[\frac{a_n}{(b_n + c)^2} \nabla c + \frac{\partial \mathbf{u}}{\partial t} \right] \mathbf{N}_n d\Omega + \int_{\Gamma_t} \mathbf{N}_{n}^{T} \mathbf{N}_n \frac{\partial \mathbf{u}}{\partial t} \mathbf{n}_{\perp} d\Gamma \tag{34}$$

$$\frac{\partial \mathbf{F}_{n}^{int}}{\partial \mathbf{c}} = - \int_{\Omega} \nabla \mathbf{N}_{n}^{T} \frac{a_n}{(b_n + c)^2} n \nabla \mathbf{N}_c d\Omega + \int_{\Omega} \nabla \mathbf{N}_{n}^{T} \frac{2 a_n}{(b_n + c)^3} n \nabla c \mathbf{N}_c d\Omega$$
$$\frac{\partial \mathbf{F}_{n}^{int}}{\partial \mathbf{U}} = - \frac{1}{\Delta t} \int_{\Omega} \nabla \mathbf{N}_{n}^{T} n \mathbf{N}_{\mathbf{u}} d\Omega + \frac{1}{\Delta t} \int_{\Gamma_t} \mathbf{N}_{n}^{T} n \mathbf{N}_{\mathbf{u}} \mathbf{n}_{\perp} d\Gamma \tag{35}$$

$$\frac{\partial \mathbf{F}_{m}^{int}}{\partial \mathbf{m}} = \frac{1}{\Delta t} \int_{\Omega} \mathbf{N}_{m}^{T} \mathbf{N}_m d\Omega - \int_{\Omega} \nabla \mathbf{N}_{m}^{T} \frac{\partial \mathbf{u}}{\partial t} \mathbf{N}_m d\Omega + \int_{\Gamma_t} \mathbf{N}_{m}^{T} \mathbf{N}_m \frac{\partial \mathbf{u}}{\partial t} \mathbf{n}_{\perp} d\Gamma \tag{36}$$

DOI: 10.1002/cnm

$$\frac{\partial \mathbf{F}_m^{int}}{\partial \mathbf{U}} = -\frac{1}{\Delta t}\int_\Omega \nabla \mathbf{N}_m^T m \mathbf{N}_\mathbf{u} d\Omega + \frac{1}{\Delta t}\int_{\Gamma_t} \mathbf{N}_m^T m \mathbf{N}_\mathbf{u} \mathbf{n}_\perp d\Gamma \tag{37}$$

$$\frac{\partial \mathbf{F}_\rho^{int}}{\partial \boldsymbol{\rho}} = \frac{1}{\Delta t}\int_\Omega \mathbf{N}_\rho^T \mathbf{N}_\rho d\Omega - \int_\Omega \nabla \mathbf{N}_\rho^T \frac{\partial \mathbf{u}}{\partial t} \mathbf{N}_\rho d\Omega + \int_{\Gamma_t} \mathbf{N}_\rho^T \mathbf{N}_\rho \frac{\partial \mathbf{u}}{\partial t} \mathbf{n}_\perp d\Gamma \tag{38}$$

$$\frac{\partial \mathbf{F}_\rho^{int}}{\partial \mathbf{U}} = \frac{-1}{\Delta t}\int_\Omega \nabla \mathbf{N}_\rho^T \rho \mathbf{N}_\mathbf{u} d\Omega + \frac{1}{\Delta t}\int_{\Gamma_t} \mathbf{N}_\rho^T \rho \mathbf{N}_\mathbf{u} \mathbf{n}_\perp d\Gamma \tag{39}$$

$$\frac{\partial \mathbf{F}_c^{int}}{\partial \mathbf{c}} = \frac{1}{\Delta t}\int_\Omega \mathbf{N}_c^T \mathbf{N}_c d\Omega + \int_\Omega \nabla \mathbf{N}_c^T D_c \nabla \mathbf{N}_c - \int_\Omega \nabla \mathbf{N}_c^T \frac{\partial \mathbf{u}}{\partial t} \mathbf{N}_c d\Omega \quad + \int_{\Gamma_t} \mathbf{N}_c^T \mathbf{N}_c \frac{\partial \mathbf{u}}{\partial t} \mathbf{n}_\perp d\Gamma$$

$$\frac{\partial \mathbf{F}_c^{int}}{\partial \mathbf{U}} = \frac{-1}{\Delta t}\int_\Omega \nabla \mathbf{N}_c^T c \mathbf{N}_\mathbf{u} d\Omega + \frac{1}{\Delta t}\int_{\Gamma_t} \mathbf{N}_c^T c \mathbf{N}_\mathbf{u} \mathbf{n}_\perp d\Gamma \tag{40}$$

$$\frac{\partial \mathbf{F}_\mathbf{u}^{int}}{\partial \mathbf{n}} = \int_\Omega \mathbf{B}_\mathbf{u}^T p_{cell}(\theta)(1+\xi m)\frac{\rho}{R_\tau^2+\rho^2} \mathbf{I} \mathbf{N}_n d\Omega \tag{41}$$

$$\frac{\partial \mathbf{F}_\mathbf{u}^{int}}{\partial \mathbf{m}} = \int_\Omega \mathbf{B}_\mathbf{u}^T p_{cell}(\theta)\frac{\xi n \rho}{R_\tau^2+\rho^2} \mathbf{I} \mathbf{N}_m d\Omega \tag{42}$$

$$\frac{\partial \mathbf{F}_\mathbf{u}^{int}}{\partial \boldsymbol{\rho}} = \int_\Omega \mathbf{B}_\mathbf{u}^T \left[\mathbf{D}_{elas}\frac{1}{\rho_0}\mathbf{B}_\mathbf{u}\mathbf{U} + p_{cell}(\theta)(1+\xi m)\frac{n}{\left(R_\tau^2+\rho^2\right)^2}\left(R_\tau^2-\rho^2\right)\mathbf{I}\right] \mathbf{N}_\rho d\Omega \tag{43}$$

$$\frac{\partial \mathbf{F}_\mathbf{u}^{int}}{\partial \mathbf{U}} = \frac{1}{\Delta t}\int_\Omega \mathbf{B}_\mathbf{u}^T \mathbf{D}_{visco} \mathbf{B}_\mathbf{u} d\Omega + \int_\Omega \mathbf{B}_\mathbf{u}^T \mathbf{D}_{elas}\frac{\rho}{\rho_0}\mathbf{B}_\mathbf{u} d\Omega + \int_\Omega \mathbf{B}_\mathbf{u}^T K_{cell}(\theta)(1+\xi m)\frac{n\rho}{R_\tau^2+\rho^2}\mathbf{I}\tilde{\nabla}\mathbf{N}_\mathbf{u} d\Omega \tag{44}$$

$$\frac{\partial \mathbf{F}_n^{ext}}{\partial \mathbf{n}} = \int_\Omega \mathbf{N}_n^T \left(r_n + \frac{r_{n,max}c}{C_{1/2}+c}\right)\left(1-\frac{2n}{K}\right)\mathbf{N}_n d\Omega - \int_\Omega \mathbf{N}_n^T \left(\frac{k_{1,max}c}{C_k+c}\frac{p_{cell}(\theta)}{\tau_d+p_{cell}(\theta)} + d_n\right)\mathbf{N}_n d\Omega \tag{45}$$

$$\frac{\partial \mathbf{F}_n^{ext}}{\partial \mathbf{m}} = \int_\Omega \mathbf{N}_n^T k_2 \mathbf{N}_m d\Omega \tag{46}$$

$$\frac{\partial \mathbf{F}_n^{ext}}{\partial \mathbf{c}} = \int_\Omega \mathbf{N}_n^T \left[\frac{r_{n,max}C_{1/2}}{(C_{1/2}+c)^2} n\left(1-\frac{n}{K}\right) - \frac{k_{1,max}C_k}{(C_k+c)^2}\frac{p_{cell}(\theta)}{\tau_d+p_{cell}(\theta)} n\right]\mathbf{N}_c d\Omega \tag{47}$$

$$\frac{\partial \mathbf{F}_n^{ext}}{\partial \mathbf{U}} = -\int_\Omega \mathbf{N}_n^T \frac{k_{1,max}c}{C_k+c}\frac{\tau_d K_{cell}(\theta)}{(\tau_d+p_{cell}(\theta))^2} n \tilde{\nabla}\mathbf{N}_\mathbf{u} d\Omega \tag{48}$$

$$\frac{\partial \mathbf{F}_m^{ext}}{\partial \mathbf{n}} = \int_\Omega \mathbf{N}_m^T \frac{k_{1,max}c}{C_k+c}\frac{p_{cell}(\theta)}{\tau_d+p_{cell}(\theta)} \mathbf{N}_n d\Omega \tag{49}$$

DOI: 10.1002/cnm

$$\frac{\partial \mathbf{F}_m^{ext}}{\partial \mathbf{m}} = \int_\Omega \mathbf{N}_m^T \left[\epsilon_r \left(r_n + \frac{r_{n,max} c}{C_{1/2} + c} \right) \left(1 - \frac{2m}{K} \right) - k_2 - d_m \right] \mathbf{N}_m d\Omega \tag{50}$$

$$\frac{\partial \mathbf{F}_m^{ext}}{\partial \mathbf{c}} = \int_\Omega \mathbf{N}_m^T \left[\epsilon_r \frac{r_{n,max} C_{1/2}}{(C_{1/2} + c)^2} m \left(1 - \frac{m}{K} \right) + \frac{k_{1,max} C_k}{(C_k + c)^2} \frac{p_{cell}(\theta)}{\tau_d + p_{cell}(\theta)} n \right] \mathbf{N}_c d\Omega \tag{51}$$

$$\frac{\partial \mathbf{F}_m^{ext}}{\partial \mathbf{U}} = \int_\Omega \mathbf{N}_m^T \frac{k_{1,max} c}{C_k + c} \frac{\tau_d K_{cell}(\theta)}{(\tau_d + p_{cell}(\theta))^2} n \tilde{\nabla} \mathbf{N}_\mathbf{u} d\Omega \tag{52}$$

$$\frac{\partial \mathbf{F}_\rho^{ext}}{\partial \mathbf{n}} = \int_\Omega \mathbf{N}_\rho^T \left(r_\rho + \frac{r_{\rho,max} c}{C_\rho + c} \right) \frac{1}{R_\rho^2 + \rho^2} \mathbf{N}_n d\Omega - \int_\Omega \mathbf{N}_\rho^T d_\rho \rho \mathbf{N}_n d\Omega \tag{53}$$

$$\frac{\partial \mathbf{F}_\rho^{ext}}{\partial \mathbf{m}} = \int_\Omega \mathbf{N}_\rho^T \left(r_\rho + \frac{r_{\rho,max} c}{C_\rho + c} \right) \frac{\eta_b}{R_\rho^2 + \rho^2} \mathbf{N}_m d\Omega - \int_\Omega \mathbf{N}_\rho^T d_\rho \eta_d \rho \mathbf{N}_m d\Omega \tag{54}$$

$$\frac{\partial \mathbf{F}_\rho^{ext}}{\partial \boldsymbol{\rho}} = - \int_\Omega \mathbf{N}_\rho^T \left(r_\rho + \frac{r_{\rho,max} c}{C_\rho + c} \right) \frac{n + \eta_b m}{\left(R_\rho^2 + \rho^2 \right)^2} 2\rho \mathbf{N}_\rho d\Omega \tag{55}$$

$$\frac{\partial \mathbf{F}_\rho^{ext}}{\partial \mathbf{c}} = \int_\Omega \mathbf{N}_\rho^T \frac{r_{\rho,max} C_\rho}{\left(C_\rho + c \right)^2} \frac{n + \eta_b m}{R_\rho^2 + \rho^2} \mathbf{N}_c d\Omega \tag{56}$$

$$\frac{\partial \mathbf{F}_c^{ext}}{\partial \mathbf{n}} = \int_\Omega \mathbf{N}_c^T \frac{k_c}{\Gamma + c} c \mathbf{N}_n d\Omega \tag{57}$$

$$\frac{\partial \mathbf{F}_c^{ext}}{\partial \mathbf{m}} = \int_\Omega \mathbf{N}_c^T \frac{k_c \xi}{\Gamma + c} c \mathbf{N}_m d\Omega \tag{58}$$

$$\frac{\partial \mathbf{F}_c^{ext}}{\partial \mathbf{c}} = \int_\Omega \mathbf{N}_c^T \left(\frac{k_c (n + \zeta m) \Gamma}{(\Gamma + c)^2} - d_c \right) \mathbf{N}_c d\Omega \tag{59}$$

$$\frac{\partial \mathbf{F}_\mathbf{u}^{ext}}{\partial \boldsymbol{\rho}} = - \int_\Omega \mathbf{N}_\mathbf{u}^T s \mathbf{u} \mathbf{N}_\rho d\Omega \tag{60}$$

$$\frac{\partial \mathbf{F}_\mathbf{u}^{ext}}{\partial \mathbf{U}} = - \int_\Omega \mathbf{N}_\mathbf{u}^T s \rho \mathbf{N}_\mathbf{u} d\Omega \tag{61}$$

ACKNOWLEDGEMENTS

This research was supported by the Spanish Ministry of Economy and Competitiveness (Grant DPI2012-32880 and BES2010-037281). The financial support of the European Research Council (ERC) through project ERC-2012-StG 306751 is gratefully acknowledged.

DOI: 10.1002/cnm

REFERENCES

1. Singer AJ, Clark RAF. Mechanisms of disease—cutaneous wound healing. *New England Journal of Medicine* SEP 2 1999; **341**(10):738–746.
2. Gurtner GC, Werner S, Barrandon Y, Longaker MT. Wound repair and regeneration. *Nature* MAY 15 2008; **453**(7193):314–321.
3. Discher DE, Janmey P, Wang YL. Tissue cells feel and respond to the stiffness of their substrate. *Science* NOV 18 2005; **310**(5751):1139–1143.
4. Mitrossilis D, Fouchard J, Guiroy A, Desprat N, Rodriguez N, Fabry B, Asnacios A. Single-cell response to stiffness exhibits muscle-like behavior. *Proceedings of the National Academy of Sciences of the United States of America* OCT 27 2009; **106**(43):18 243–18 248.
5. Harland B, Walcott S, Sun SX. Adhesion dynamics and durotaxis in migrating cells. *Physical Biology* FEB 2011; **8**(1):015011.
6. Javierre E, Moreo P, Doblare M, Garcia-Aznar JM. Numerical modeling of a mechano-chemical theory for wound contraction analysis rid f-8256-2010. *International Journal of Solids and Structures* OCT 1 2009; **46**(20): 3597–3606.
7. Vermolen FJ, Javierre E. A finite-element model for healing of cutaneous wounds combining contraction, angiogenesis and closure. *Journal of Mathematical Biology* NOV 2012; **65**(5):967–996.
8. Murphy KE, Hall CL, McCue SW, McElwain DLS. A two-compartment mechanochemical model of the roles of transforming growth factor beta and tissue tension in dermal wound healing. *Journal of theoretical biology* MAR 7 2011; **272**(1):145–159.
9. Murphy KE, Hall CL, Maini PK, McCue SW, McElwain DLS. A fibrocontractive mechanochemical model of dermal wound closure incorporating realistic growth factor kinetics. *Bulletin of Mathematical Biology* MAY 2012; **74**(5):1143–1170.
10. Valero C, Javierre E, García-Aznar J, Gómez-Benito M. Numerical modelling of the angiogenesis process in wound contraction. *Biomechanical Modeling and Mechanobiology* 2013; **12**(2):349–360.
11. Fusi L. Macroscopic models for fibroproliferative disorders: a review. *Mathematical and Computer Modelling* NOV 2009; **50**(9-10):1474–1494.
12. Olsen L, Sherratt JA, Maini PK. A mechanochemical model for adult dermal wound contraction and the permanence of the contracted tissue displacement profile. *Journal of Theoretical Biology* NOV 21 1995; **177**(2):113–128.
13. Murray JD, Cook J, Tyson R, Lubkin SR. Spatial pattern formation in biology: I. Dermal wound healing. II. Bacterial patterns rid f-8802-2011. *Journal of the Franklin Institute-Engineering and Applied Mathematics* MAR 1998; **335B**(2):303–332.
14. Sherratt JA, Dallon JC. Theoretical models of wound healing: past successes and future challenges. *Comptes Rendus Biologies* MAY 2002; **325**(5):557–564.
15. Schugart RC, Friedman A, Zhao R, Sen CK. Wound angiogenesis as a function of tissue oxygen tension: a mathematical model. *Proceedings of the National Academy of Sciences of the United States of America* FEB 19 2008; **105**(7):2628–2633.
16. Olsen L, Sherratt JA, Maini PK. A mathematical model for fibro-proliferative wound healing disorders. *Bulletin of Mathematical Biology* JUL 1996; **58**(4):787–808.
17. Hinz B, Gabbiani G. Mechanisms of force generation and transmission by myofibroblasts. *Current Opinion in Biotechnology* OCT 2003; **14**(5):538–546.
18. Tomasek JJ, Gabbiani G, Hinz B, Chaponnier C, Brown RA. Myofibroblasts and mechano-regulation of connective tissue remodelling. *Nature Reviews Molecular Cell Biology* MAY 2002; **3**(5):349–363.
19. Li B, Wang JH. Fibroblasts and myofibroblasts in wound healing: force generation and measurement. *Journal of Tissue Viability* NOV 2011; **20**(4):108–120.
20. Graham J, Vomund A, Phillips C, Grandbois M. Structural changes in human type I collagen fibrils investigated by force spectroscopy. *Experimental Cell Research* OCT 1 2004; **299**(2):335–342.
21. Roeder B, Kokini K, Sturgis J, Robinson J, Voytik-Harbin S. Tensile mechanical properties of three-dimensional type I collagen extracellular matrices with varied microstructure. *Journal of Biomechanical Engineering-Transactions of the Asme* APR 2002; **124**(2):214–222.
22. Ghosh K, Pan Z, Guan E, Ge S, Liu Y, Nakamura T, Ren XD, Rafailovich M, Clark RAF. Cell adaptation to a physiologically relevant ecm mimic with different viscoelastic properties. *Biomaterials* FEB 2007; **28**(4): 671–679.
23. Moreo P, Garcia-Aznar JM, Doblare M. Modeling mechanosensing and its effect on the migration and proliferation of adherent cells rid f-8256-2010. *Acta Biomaterialia* MAY 2008; **4**(3):613–621.
24. Khatyr F, Imberdis C, Vescovo P, Varchon D, Lagarde JM. Model of the viscoelastic behaviour of skin in vivo and study of anisotropy. *Skin Research and Technology* MAY 2004; **10**(2):96–103.
25. Tran HV, Charleux F, Rachik M, Ehrlacher A, Ho Ba Tho MC. In vivo characterization of the mechanical properties of human skin derived from mri and indentation techniques. *Computer Methods in Biomechanics and Biomedical Engineering* 2007 Dec (Epub 2007 Sep 24) 2007; **10**(6):401–407.
26. Levy A, Kopplin K, Gefen A. Simulations of skin and subcutaneous tissue loading in the buttocks while regaining weight-bearing after a push-up in wheelchair users. *Journal of the Mechanical Behavior of Biomedical Materials* April 2013:S1751-6161(13)00138-0, 436–447. DOI: 10.1016/j.jmbbm.2013.04.015.

27. Zienkiewicz OC, Taylor RL. *The Finite Element Method*, 5th edn, Vol. 1. Butterworth Heinemann: Oxford, 2000. O.C. Zienkiewicz, R.L. Taylor; ;24 cm; Indices. – Bibliografa en cada captulo; Ed. orig. publicada en 1967 por McGrawHill. En la 4a ed. el tt. vol.: Basic formulation and linear problems.
28. Zienkiewicz OC, Taylor RL. *The Finite Element Method*, 5th edn, Vol. 2. Butterworths Heinemann: Oxford, 2000. O.C. Zienkiewicz, R.L. Taylor; ;26 cm; ndices; Ed. orig. publicada en 1967 por McGrawHill.
29. Odland G. Structure of the skin. In *Physiology, Biochemistry, and Molecular Biology of the Skin*, Goldsmith LA (ed.). Oxford University Press: Oxford, 1991.
30. Geris L, Schugart R, Van Oosterwyck H. In silico design of treatment strategies in wound healing and bone fracture healing. *Philosophical Transactions of the Royal Society A: Mathematical, Physical and Engineering Sciences* 2010; **368**(1920):2683–2706.
31. McGrath M, Simon R. Wound geometry and the kinetics of wound contraction. *Plastic and Reconstructive Surgery* 1983; **72**(1):66–72.
32. Roy S, Biswas S, Khanna S, Gordillo G, Bergdall V, Green J, Marsh CB, Gould LJ, Sen CK. Characterization of a preclinical model of chronic ischemic wound. *Physiological Genomics* MAY 2009; **37**(3):211–224.
33. Yannas IV. *Tissue and Organ Regeneration in Adults*. Springer: New York, 2001. Ioannis V. Yannas.; Includes bibliographical references (p. 328-366) and index.; 1. The Irreversibility of Injury – 2. Nonregenerative Tissues – 3. Anatomically Well-Defined Defects – 4. The Defect Closure Rule – 5. Regeneration of Skin – 6. Regeneration of a Peripheral Nerve – 7. Irreducible Processes for Synthesis of Skin and Peripheral Nerves – 8. The Antagonistic Relation Between Contraction and Regeneration – 9. Kinetics and Mechanism I: Spontaneous Healing – 10. Kinetics and Mechanism II: Induced Regeneration – App. Method of Estimation of Critical Axon Elongation of an Arbitrary Tubulated Device Bridging Two Nerve Stumps.
34. Catty RHC. Healing and contraction of experimental full-thickness wounds in human. *British Journal of Surgery* 1965 1965; **52**(7). PT: J; TC: 21; UT: WOS:A19656645400014.
35. Vermolen FJ, Gefen A, Dunlop JWC. In vitro "wound" healing: Experimentally based phenomenological modeling. *Advanced Engineering Materials* 2012; **14**(3):B76–B88.
36. Motegi K, Nakano Y, Namikawa A. Relation between cleavage lines and scar tissues. *Journal of maxillofacial surgery* 1984; **12**(1):21–28.

DOI: 10.1002/cnm

Work 2: Numerical modelling of the angiogenesis process in wound contraction

Journal: *Biomechanics and Modeling in Mechanobiology*, 12 (2) (2013) 349-360. DOI 10.1007/s10237-012-0403-x
Journal Impact factor: 3.331

Contribution of the author of the thesis: the author was in charge of writing the formulation for the user element including the angiogenesis process, making a review of the existing literature, choosing the mechanical variables, performing all the computational simulations, analyzing the results and determining their implications. Everything was done under the supervision of the other authors.

Biomech Model Mechanobiol
DOI 10.1007/s10237-012-0403-x

ORIGINAL PAPER

Numerical modelling of the angiogenesis process in wound contraction

C. Valero · E. Javierre · J. M. García-Aznar · M. J. Gómez-Benito

Received: 22 December 2011 / Accepted: 30 April 2012

Abstract Angiogenesis consists of the growth of new blood vessels from the pre-existing vasculature. This phenomenon takes place in several biological processes, including wound healing. In this work, we present a mathematical model of angiogenesis applied to skin wound healing. The developed model includes biological (capillaries and fibroblasts), chemical (oxygen and angiogenic growth factor concentrations) and mechanical factors (cell traction forces and extracellular matrix deformation) that influence the evolution of the healing process. A novelty from previous works, apart from the coupling of angiogenesis and wound contraction, is the more realistic modelling of skin as a hyperelastic material. Large deformations are addressed using an updated Lagrangian approach. The coupled non-linear model is solved with the finite element method, and the process is studied over two wound geometries (circular and elliptical) of the same area. The results indicate that the elliptical wound vascularizes two days earlier than the circular wound but that they experience a similar contraction level, reducing its size by 25 %.

C. Valero · E. Javierre · J. M. García-Aznar · M. J. Gómez-Benito
Multiscale in Mechanical and Biological Engineering (M2BE), Aragón Institute of Engineering Research (I3A), University of Zaragoza, Campus Río Ebro, 50018 Zaragoza, Spain
e-mail: claraval@unizar.es

J. M. García-Aznar
e-mail: jmgaraz@unizar.es

M. J. Gómez-Benito
e-mail: gomezmj@unizar.es

E. Javierre (✉)
Centro Universitario de la Defensa, Academia General Militar, Ctra. Huesca s/n, 50090 Zaragoza, Spain
e-mail: etelvina.javierre@unizar.es

Keywords Angiogenesis · Wound healing · Contraction · Finite element method · Mechanochemical analysis

1 Introduction

Skin is the largest organ of the human body. It covers the whole external body surface and has a critical function in maintaining the integrity of the internal organs and in preventing the transmission of infections and dehydration (Williams and Warwick 1980). Skin consists of various tissue layers: the epidermis, the dermis and the hypodermis and can reach a thickness of 1.5–4 mm depending on the body part. The dermis is an irregular connective soft tissue, with a collagen fibre matrix where nerves, blood vessels and several cellular species are allocated. It provides the skin with high resistance to traction and the ability to contract elastically.

Wounds in the dermis can appear as a result of surgery or traumatic accident. In both cases, successful healing is crucial for a perfect functional and aesthetic recovery. However, in some situations, optimal healing is not possible without appropriate medical treatment (Gurtner et al. 2008).

Wound healing is a natural process in which the damaged skin layers regenerate autonomously through several complex biochemical processes. The different processes taking place during wound healing overlap in time and can be divided into three stages: inflammatory, proliferative and remodelling (Singer and Clark 1999). After wound formation, the wound edge contracts inwards creating mechanical stresses in the surrounding skin and inducing the inflammatory response that initiates the healing process (Murray et al. 1998). After that, several phenomena take place in the proliferative phase: angiogenesis, granulation tissue formation, epithelization and wound contraction (Gurtner et al. 2008). In this stage, new blood vessels and extracellular matrix (ECM)

Published online: 15 May 2012

are created while the wound reduces in size. In the final stage, the collagen fibres are remodelled and realigned and cells that are no longer needed are removed (Singer and Clark 1999).

Angiogenesis involves the formation of new blood vessels from the pre-existing vasculature in response to biochemical and mechanical stimuli (Risau 1997). The growth of the blood vessels is crucial for supplying the necessary blood and nutrients to the tissue and sustaining the healing process. At the beginning of the inflammatory phase, inflammatory cells migrate into the wound site and release angiogenic growth factors (Schugart et al. 2008) that, at the appropriate time, stimulate capillary growth and collagen deposition. In addition, these species cause the appearance of mechanical stresses on the tissue. Cells like fibroblasts have an actomyosin machinery that regulates these stresses depending on the volumetric strain of the surrounding tissue (Moreo et al. 2008). Therefore, it is clear that wound evolution, and in particular wound angiogenesis and contraction, depends both on biochemical signals and on the mechanical properties of the skin.

It should be mentioned here that angiogenesis also occurs in other complex biological phenomena such as bone tissue reconstruction (Glazier and Graner 1993), embryogenesis (Risau 1997) and tumour growth (Carmeliet and Jain 2000). Hence, the work presented here is relevant and could be applied to other important pathologies.

Over recent years, a large number of mathematical models have been proposed to simulate and predict vascular growth. Most of these models focus on angiogenesis in cancer (Anderson and Chaplain 1998; Chaplain 2000; Mantzaris et al. 2004), but there are also a number of angiogenesis models in wound healing. The first continuum model of angiogenesis in wound healing was developed by Pettet et al. (1996a). This model has three variables (capillary-tip endothelial cells, macrophage-derived chemoattractants and the new blood vessels) and it is composed of a number of differential equations that describe its behaviour. The model was used to predict the rate of wound healing through a travelling wave analysis of the governing equations. The model was subsequently expanded adding the influence of fibroblasts, oxygen and the extracellular matrix (Pettet et al. 1996b) in order to analyse the effect of the angiogenic growth factor PDGF (platelet-derived growth factor) on pathological wound healing.

Maggelakis (2003) developed a three-variable model that relates the production of macrophage-derived growth factors (MDGF) with the capillary density and the tissue oxygen concentration in one dimension. This model suggests that wound healing is sustained only at locations where the oxygen supply is sufficient. Javierre et al. (2008) modified this model adding the epidermal growth factor (EGF) concentration. They proposed a coupling between angiogenesis and a wound moving interface caused by cell migration in two dimensions in order to analyse the effect of oxygen availability on the rate of wound closure.

There are also a number of models focusing on the role of oxygen and its influence on the angiogenesis process, as wound healing may be impaired due to the lack of oxygen (Schreml et al. 2010). Schugart et al. (2008) proposed a model with seven variables that relate the angiogenesis process with the tissue oxygen tension. Flegg et al. (2009) proposed a model that simulates the deliberate elevation of oxygen levels at the wound site in order to study angiogenesis in chronic wounds. They recently applied it to predict the treatment for chronic diabetic wounds with hyperbaric oxygen (Flegg et al. 2010).

All the above-mentioned works focus on biochemical aspects of angiogenesis but do not take into account the influence of mechanical signalling on cellular behaviour. There is still a lack of mechanical models of angiogenesis in wound healing. Manoussaki (2003) developed a mechanochemical model of blood vessel formation during vasculogenesis taking into account the traction forces exerted by cells. Xue et al. (2009) extended the angiogenesis model by Schugart et al. (2008) incorporating the mechanical behaviour of the skin.

On the other hand, there is a large number of mechanochemical models of wound healing (Tranquillo and Murray 1992; Olsen et al. 1995; Javierre et al. 2009; Geris et al. 2010; Murphy et al. 2011). However, these models are mostly focused on the contraction stage and do not take into account other processes (such as angiogenesis) taking place simultaneously. Furthermore, all the above mechanical models assume the skin to behave as a viscoelastic material, which is suitable for small deformations but not for the large deformations that take place during wound contraction. In fact, wounds in humans experience a reduction of around 20–30 % of their original size due to contraction (Olsen et al. 1996). Another limitation of previous works is that, in most cases, wound morphology has been idealised to one-dimensional geometries (Olsen et al. 1995; Pettet et al. 1996a,b; Schugart et al. 2008; Flegg et al. 2009, 2010; Olsen et al. 1995; Murphy et al. 2011). This is only valid for simulating linear and circular wounds.

In this work, we have modified the model proposed by Javierre et al. (2008), based on the model of Maggelakis (2003), in order to introduce the effect of fibroblasts on the process. The main advance of this model with respect to that of Javierre et al. (2008) is the replacement of the EGF with the fibroblast density, which allows angiogenesis to be coupled with wound contraction, and the use of a more realistic constitutive model of healthy and damaged skin. We use a hyperelastic model of the skin behaviour, which on the one hand provides a more accurate approximation of the mechanical state of the tissue and on the other hand eases the future incorporation of fibre remodelling in the model (Flynn et al. 2011). Our overall objective is to move forward towards a

more complete model of wound healing incorporating all the phases (inflammation, proliferation and angiogenesis, contraction and remodelling).

The main purpose of this work is the development and implementation of a numerical model that allows the angiogenesis and wound contraction processes taking place in the skin during wound healing to be simulated. We consider the influence of biochemical and mechanical factors, paying special attention to the influence of oxygen availability on the healing kinetics.

2 Materials and methods

In this work, we propose a continuous angiogenesis model that couples biochemical and mechanical factors. We have implemented the biochemical and the mechanical behaviour of the skin separately, due to the different time scales at which these events occur during wound healing. Hence, we first present the biochemical part of the model for the cellular and biological species, followed by the mechanical model for the contractile cells (fibroblasts) and the skin. Finally, we explain how this model has been implemented into a FE code to have a complete approach to the angiogenesis and wound contraction processes.

2.1 Biochemical model of angiogenesis

The proposed biochemical model of angiogenesis includes biological and chemical factors and consists of a number of coupled reaction-diffusion equations. The primary variables of the model are the concentrations of oxygen (u_1), MDGF—such as VEGF (vascular endothelial growth factor) or others, henceforth MDGF—(u_2), capillary density (u_3) and fibroblasts (n). We propose a different conservation law for each species that includes the most important mechanisms of cellular and chemical regulation: production, transport and decay.

2.1.1 Oxygen (u_1)

Oxygen is required for wound healing. Low levels of oxygen impair the healing process (Schreml et al. 2010) since reparative processes such as cell proliferation and angiogenesis require high oxygen availability. We assume that the oxygen transport can be modelled as a diffusion process, that oxygen is supplied by the capillary vasculature (Schugart et al. 2008) and that it is subject to chemical decay. The resulting equation for the oxygen variation is

$$\frac{\partial u_1}{\partial t} + \nabla \cdot \left(u_1 \frac{\partial \mathbf{u}}{\partial t} \right) = D_1 \nabla^2 u_1 + \lambda_{3,1} u_3 - \lambda_{1,1} u_1 \qquad (1)$$

where $\mathbf{u}$ is the ECM displacement vector due to the contraction of the wound, which gives rise to the passive convection term. The values and physiological meaning of the parameters in this and the subsequent equations are given in Table 1.

2.1.2 Macrophage-derived growth factor (MDGF) (u_2)

Macrophages appear at the wound site when the concentration of oxygen is low. Macrophages release chemical substances, MDGFs, that stimulate vessel growth and collagen deposition (Maggelakis 2003). We assume that the transport of MDGFs can be modelled as a diffusion process, that

Table 1 List of normalised model parameters related to the biochemical model

Parameter	Description	Dimensionless value	Reference
D_1	Oxygen diffusion rate	4.32×10^{-3}	Javierre et al. (2008)
$\lambda_{3,1}$	Oxygen supply per unit of capillary density and unit of time	0.864	Javierre et al. (2008)
$\lambda_{1,1}$	Oxygen half life	0.864	Javierre et al. (2008)
D_2	MDGF diffusion rate	0.0864	Javierre et al. (2008)
$\lambda_{1,2}$	MDGF density per unit of time under hypoxia conditions	1.22	Estimated
$\lambda_{2,2}$	MDGF half life	0.864	Javierre et al. (2008)
D_3	Capillaries diffusion rate	4.32×10^{-4}	Estimated
$\lambda_{3,2}$	Capillary production rate per unit of oxygen	1.0	Estimated
$\lambda_{3,3}$	Capillary production rate under normal conditions	1.0	Estimated
u_3^{eq}	Capillary density in undamaged skin	1.0	Javierre et al. (2008)
D_n	Fibroblast diffusion rate	2×10^{-2}	Javierre et al. (2009)
$\lambda_{n,n}$	Fibroblast death rate	0.7488	Javierre et al. (2009)
r_n	Maximal rate of fibroblast proliferation	0.832	Javierre et al. (2009)
K	Fibroblast maximal capacity in dermis	10.0	Javierre et al. (2009)
$u_1^{\beta_2}$	Oxygen concentration below which MDGFs are produced	0.5	Xue et al. (2009)

MDGFs appear at specific locations as a response to the oxygen availability and that, as chemical factors, MDGFs are subject chemical decay. Hence, the equation for the MDGFs is

$$\frac{\partial u_2}{\partial t} + \nabla \cdot \left(u_2 \frac{\partial \mathbf{u}}{\partial t} \right) = D_2 \nabla^2 u_2 + \lambda_{1,2} P(u_1) - \lambda_{2,2} u_2 \quad (2)$$

where P represents the function describing the production of MDGF when the levels of oxygen are low,

$$P(u_1) = \begin{cases} 1 - \frac{u_1}{u_1^{\beta_2}} & \text{if } \; u_1 < u_1^{\beta_2}; \\ 0 & \text{otherwise} \end{cases} \quad (3)$$

and $u_1^{\beta_2}$ is the oxygen concentration below which MDGFs are produced.

2.1.3 Capillary density (u_3)

Capillaries are the smallest blood vessels and are part of the microcirculation system. They are responsible for supplying nutrients and oxygen to the tissue (Singer and Clark 1999). When a wound occurs, capillaries are damaged and their recovery is crucial for correct healing. It is assumed that capillary cells (i.e. the endothelial cells on the capillaries) undergo migration, which is modelled as a diffusion term, and are produced according to a logistic model with the growth rate proportional to the MDGF density (Maggelakis 2003). Hence, the equation for the capillary density is

$$\frac{\partial u_3}{\partial t} + \nabla \cdot \left(u_3 \frac{\partial \mathbf{u}}{\partial t} \right) = D_3 \nabla^2 u_3 + (\lambda_{3,3} + \lambda_{3,2} u_2) u_3 \left(1 - \frac{u_3}{u_3^{\text{eq}}} \right) \quad (4)$$

where u_3^{eq} denotes the maximal capillary density in the undamaged skin.

2.1.4 Fibroblasts (n)

Fibroblasts are motile cells that can exert traction forces on their surrounding tissue. It is known that fibroblasts are responsible for ECM synthesis and serve as an indicator of ECM maturity (Singer and Clark 1999). Hence, as a novelty from the previous model (Javierre et al. 2008), we incorporate the fibroblast density into the angiogenesis model. Fibroblast proliferation is modelled with a logistic term with an oxygen-dependent rate (Schugart et al. 2008). Moreover, the fibroblast migration is modelled as random diffusion, whereas fibroblast net production is due to cell proliferation and death. Therefore, the fibroblast governing equation can be written as

$$\frac{\partial n}{\partial t} + \nabla \cdot \left(n \frac{\partial \mathbf{u}}{\partial t} \right) = D_n \nabla^2 n + r_n u_1 n \left(1 - \frac{n}{K} \right) - \lambda_{n,n} n \quad (5)$$

2.2 Mechanical model of wound contraction

As stated previously, angiogenesis is a biological process that is influenced not only by biochemical factors but also by mechanical stimuli. When mechanical stresses appear in the skin due to its contraction, the geometry of the wound is modified. This also affects the evolution of the biochemical process.

Fibroblasts are the most important cell type in wound contraction as they exert the traction forces deforming the tissue where they are allocated. This mechanical behaviour is due to their actomyosin mechanism (Moreo et al. 2008). From the species density values, we can obtain the net stress of one fibroblast cell per unit of extracellular matrix (ECM), p_{cell}, which, in this work, is considered to be the mechanical stimulus that regulates the forces exerted by the cells. We take p_{cell} following Moreo et al. (2008), where an active mechanosensing model is proposed based on Hill's model for skeletal muscle behaviour, applicable to cell–substrate interaction situations. In this work, p_{cell} is a piecewise linear function depending on the tissue volumetric strain

$$p_{\text{cell}}(\theta) = \begin{cases} K_{\text{pas}}\theta & \theta < \theta_1 \\ \frac{K_{\text{act}} p_{\max}}{K_{\text{act}}\theta_1 - p_{\max}}(\theta_1 - \theta) + K_{\text{pas}}\theta & \theta_1 \le \theta \le \theta^* \\ \frac{K_{\text{act}} p_{\max}}{K_{\text{act}}\theta_2 - p_{\max}}(\theta - \theta_2) + K_{\text{pas}}\theta & \theta^* < \theta \le \theta_2 \\ K_{\text{pas}}\theta & \theta > \theta_2 \end{cases} \quad (6)$$

where θ^* can be defined as $p_{\max}/K_{\text{act}}$.

With this definition, p_{cell} is a mechanosensing variable that depends on the volumetric strain, θ, of the tissue where cells are allocated. As the cell actomyosin machinery responds actively only between certain limits, we have considered θ_1 and θ_2, which are the compression and tension strain limits within which the machinery works. $p_{\max}$ denotes the maximal contractile force that the actomyosin machinery can exert, and K_{act} and K_{pas} the stiffness moduli of the active and passive components of the cell. The values of these parameters (Javierre et al. 2009) are included in Table 2.

Hence, p_{cell} and the ECM and fibroblast densities determine the stresses that cells create in the surrounding tissue. In this work, we have considered that the traction stresses exerted by cells can be written as

$$\boldsymbol{\sigma}_{\text{cell}} = p_{\text{cell}}(\theta) \frac{n \rho_{\text{ecm}}}{R_\tau^2 + \rho_{\text{ecm}}^2} \quad (7)$$

following Javierre et al. (2009). The parameter values are given in Table 2. Hence, we assume cell traction stresses to be isotropic, generated by fibroblasts and inhibited at high ECM density.

In addition, endothelial cells are active in ECM production, and we assume that the ECM density is proportional to the capillary density. Therefore, the ECM density (ρ_{ecm}) is expressed as

Table 2 List of normalised model parameters related to the mechanical behaviour

Parameter	Description	Dimensionless value	Reference
p_{max}	Maximal cellular active stress per unit of ECM	0.25	Estimated
K_{pas}	Volumetric stiffness moduli of the passive components of the cell	2×10^{-1}	Moreo et al. (2008)
K_{act}	Volumetric stiffness moduli of the actin filaments of the cell	1.0	Moreo et al. (2008)
θ_1	Shortening strain of the contractile element	-0.6	Javierre et al. (2009)
θ_2	Lengthening strain of the contractile element	0.5	Moreo et al. (2008)
R_τ	Traction inhibition collagen density	5×10^{-3}	Olsen et al. (1995)
K_{ecm}	ECM production rate per unit of capillary density	1.0	Estimated

Table 3 Values of the hyperelastic parameters

Parameter	μ_1	μ_2	α_1	α_2	**D**
Value	20.764	0.695	1.223	41.672	3.65273

Units are kPa for μ_1, Pa for μ_2 and $mm^2\ N^{-1}$ for D (Flynn et al. 2011; Cheung et al. 2005)

$$\rho_{ecm} = K_{ecm} u_3, \tag{8}$$

where K_{ecm} is a proportionality constant (see Table 2).

2.3 Constitutive model for skin

Skin has been modelled with a large range of material behaviour laws. In wound healing evolutive models, skin is traditionally modelled as a viscoelastic material (Javierre et al. 2009; Manoussaki 2003; Xue et al. 2009), which gives a first-order approximation of the ECM deformation while the focus is placed on the biochemial signalling of different cellular processes. However, other works, focused on skin behaviour, consider it as a hyperelastic material (Linder et al. 2008; Cheung et al. 2005; Lapeer et al. 2011; Hendriks et al. 2003). Nevertheless, Delalleau et al. (2008) found that a Neo-Hookean approach is not suitable for modelling human skin. Thus, in this work, we use an Ogden approach (Flynn et al. 2011) , which is more suitable for modelling skin and whose strain energy function has the form

$$\hat{\psi} = \sum_{i=1}^{N} \frac{2\mu_i}{\alpha_i^2} \left(\lambda_1^{\alpha_i} + \lambda_2^{\alpha_i} + \lambda_3^{\alpha_i}\right) + \frac{1}{D} \sum_{i=1}^{2} (J_{el} - 1)^{2i} \tag{9}$$

where $\hat{\psi}$ is the strain energy per unit of reference volume, μ_i, α_i and D are material parameters and $\lambda_1, \lambda_2, \lambda_3$ are the principal stretches. The values of the material parameters μ_i, α_i and D_i have been taken from previous skin studies (Flynn et al. 2011), where the parameters were obtained in vivo from anterior forearm skin. The values of these parameters are presented in Table 3. As far as we know, there are no works in the literature in which the mechanical properties of damaged skin are determined. Thus, in a first approach, we assume that the mechanical properties of the damaged skin can be determined from the ECM density and the mechanical properties of the undamaged skin through

$$\psi = \hat{\psi} \frac{\rho_{ecm}}{\hat{\rho}_{ecm}} \tag{10}$$

where ψ and ρ_{ecm} are the strain energy function and the matrix density of the wounded skin and $\hat{\rho}_{ecm}$ denotes the ECM density of undamaged skin. Hence, we treat the healing skin as a damaged material that is being repaired. In fact, we propose Eq. (10) in a similar manner to the damage model proposed by Holzapfel (2000), equivalently defining the original reduction factor by $\rho_{ecm}/\hat{\rho}_{ecm}$.

2.4 Numerical implementation of the mechanobiochemical model

The model has been implemented through an Abaqus user subroutine (Hibbit et al. 2011). The weak formulation of the model is included in 'Appendix A'.

The mechanical analysis is performed separately from the biochemical one due to the different time scales at which they occur. However, both parts of the model have some variables in common (displacements, σ_{cell} and matrix composition). These variables are used to couple the biochemical and mechanical parts of the model. The scheme of the implementation is shown in Fig. 1.

In the transport (biochemical) analysis, we evaluate the evolution of the species densities in a fixed geometry. The value of the stresses created by cells depends on the volumetric strain, θ, of their surrounding tissue and it is calculated through a separate mechanical FE analysis. At the beginning of the calculation, θ is zero as the tissue has not yet been deformed.

The value of the stresses σ_{cell} (Eq. (7)) in every node of the mesh is calculated in the biochemical analysis and introduced in the hyperelastic analysis. From the mechanical analysis, we obtain the new position of the mesh nodes, that is, the new (deformed) geometry of the wound and the undamaged surrounding tissue. This new geometry is introduced as the initial geometry of the next biochemical step. Thus, we use

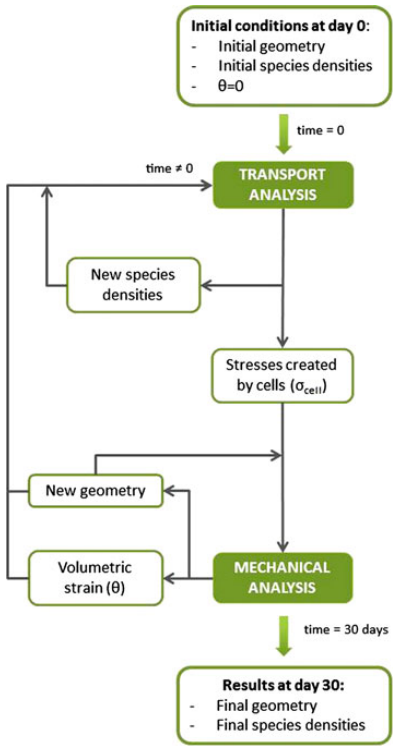

Fig. 1 Scheme of the complete mechanochemical model

an updated Lagrangian formulation. As initial conditions of each transport analysis step, we introduce the node concentrations obtained from the previous transport analysis step, as they are not modified in the mechanical analysis. In this analysis, we also calculate the volumetric deformation θ that the tissue suffers in every node. These nodal values are introduced into the transport analysis to calculate the new stresses and species concentrations. As a first approach, we assume that residual stresses in the damaged skin are relaxed and that when skin is damaged, it loses its 'in vivo' pre-stresses. As the skin recovers its undamaged properties, it can bear stress. The residual stresses in the healthy skin are accumulated after each mechanical analysis and introduced as initial stresses in the subsequent mechanical analysis.

To carry out the full analysis, we alternate the two analyses several times to complete the total desired period of time. In this work, we study a whole time period of 30 days.

In a first approach, a circular and an elliptical wound have been studied. The diameter of the circular wound is 2 cm, and the elliptical wound has the same area as the circular wound with an aspect ratio of 5. In both cases, the wound is surrounded by a sufficiently large circumference of undamaged skin to avoid boundary effects. In both cases, we have simulated one-quarter of the whole geometry as we have considered symmetry in the two axes.

3 Results

The model described above is used to evaluate the angiogenesis progress for two wounds of the same size but different shapes (circular and elliptical).

First, we analyse the distribution of the various biochemical species at the centre of the wound (Fig. 2). The wound centre is the furthest point from the healthy skin and, in normal conditions, the last point to heal. Figure 3 shows the densities of oxygen, MDGF, capillaries and fibroblasts at the wound centre over the simulated period (30 days). The results demonstrate how the oxygen concentration regulates the rest of the variables. While there is no oxygen in the centre of the wound, the level of MDGF increases rapidly,

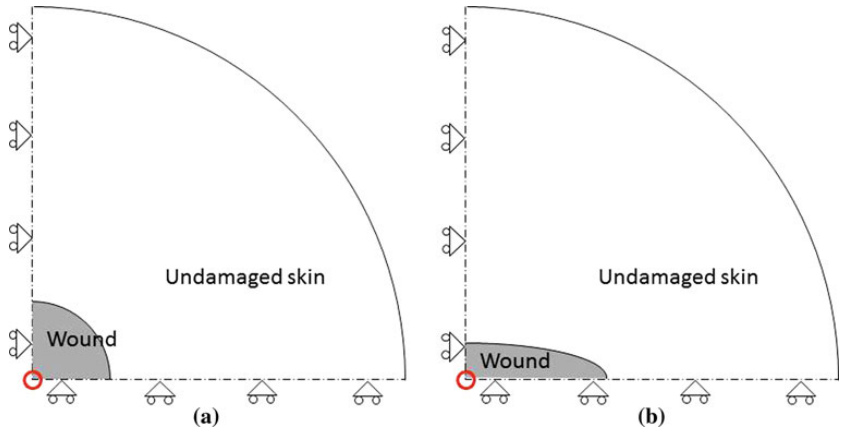

Fig. 2 Scheme of the studied geometries *circular* (**a**) and *elliptical* (**b**) showing the studied point (*red circle*)

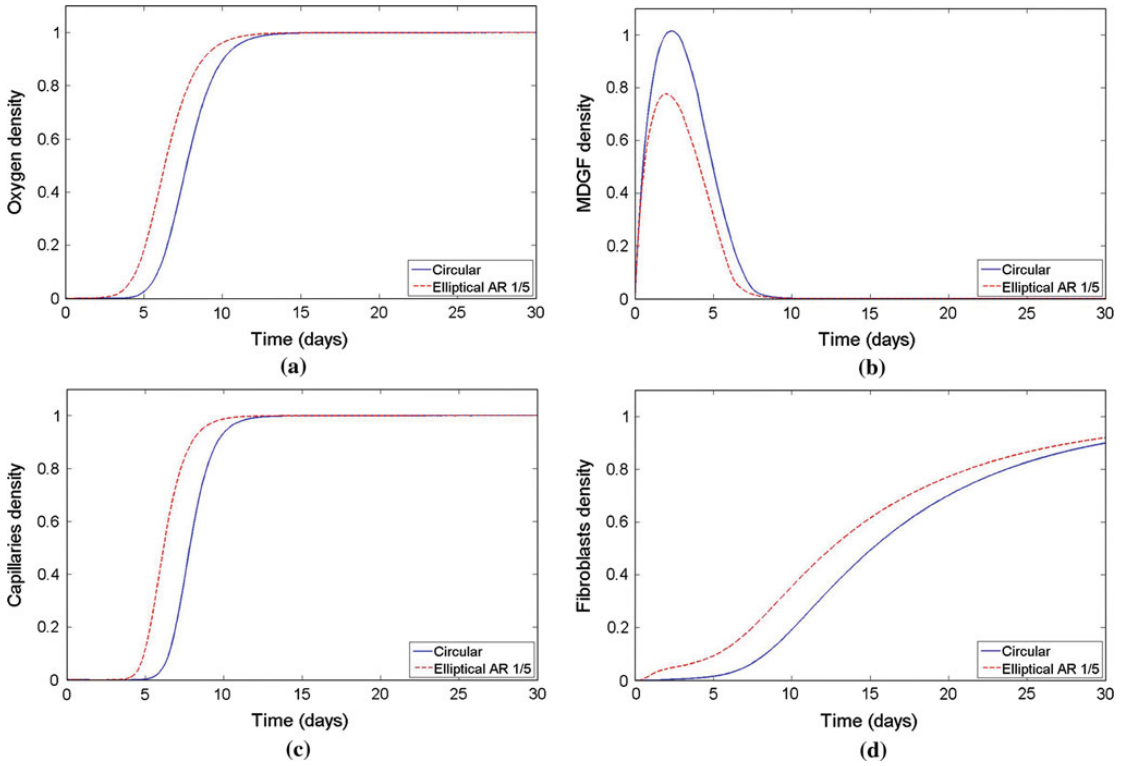

Fig. 3 Evolution of the oxygen density (**a**), MDGF density (**b**), capillary density (**c**) and fibroblast density (**d**) in the centre of the wound during the simulated time

which causes the appearance of capillaries. When the capillary density grows, more oxygen is supplied to the wound centre and the MDGF gradually disappear. The high level of MDGF promotes the rapid growth of capillaries to reach the capillary density of undamaged tissue (u_3^{eq}) and after that the oxygen density stabilises. Finally, when the oxygen density is high enough, the fibroblast density grows indicating that the dermis is being restored.

In addition, the results obtained show a more severe hypoxia at the wound centre for the circular wound, reflected in a higher and more enduring MDGF production. A more thorough analysis of the effect of wound morphology on the progress of wound contraction can be carried out by looking at the contour plots of fibroblasts (n) and fibroblasts-induced traction stresses (σ_{cell}) (Figs. 4, 5). The results show how fibroblasts invade the wound region faster for the elliptical wound. Furthermore, the contraction stresses on the elliptical wound are higher and more localised at the surrounding of the edge wound. However, this does not result in a faster contraction of the elliptical wound. In fact, both wounds seem to contract at a similar rate and to the same extent (Fig. 6a). A comparison with previous experimental and computational results (Fig. 6b) shows a good agreement of the relative uncontracted wound area for the circular wound. This is the difference between the current and the fully contracted wound area divided by the difference between the initial and the fully contracted area. We show our results together with those of Olsen et al. (1995) and McGrath and Simon (1983) in Fig. 6b. It can be observed that initially our results show a faster contraction but as from day 10, they are very similar to the experimental data.

Finally, we present the geometry of the wound at day 30 post-wounding to see how it has evolved. The contraction of the wound is appreciable, at the conclusion of the analysis, as can be seen in Fig. 7. As a result of the stresses in the skin, the geometry of the wound modifies during the simulated time, as can be observed in a real wound. In fact, the circular wound contracts by around 27 % of its original size and the elliptical wound around 24 % of its original size (Fig. 6a).

4 Discussion

Angiogenesis is a relevant process in several important biological processes such as wound healing. A number of studies

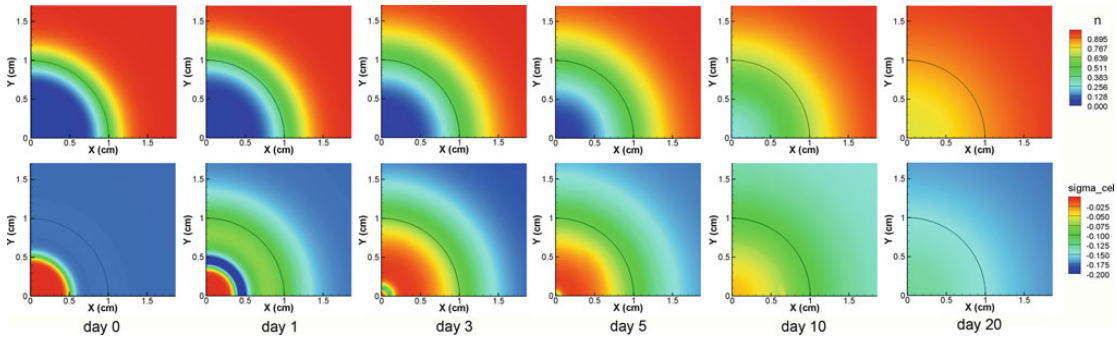

Fig. 4 Evolution of the fibroblast normalised density (*above*) and fibroblasts-induced traction stress (*below*) at different time instants for the circular wound. Units are N/cm^2 for σ_{cell}

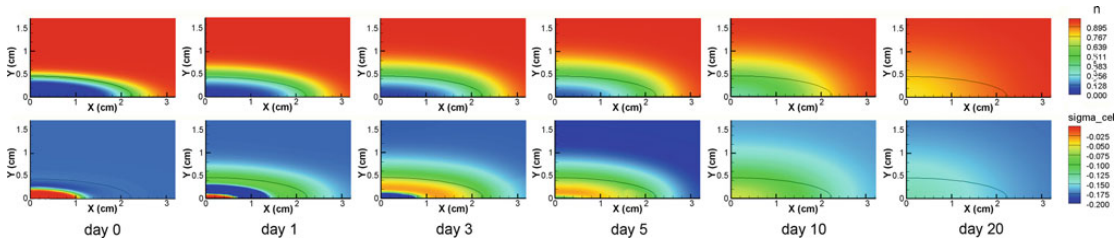

Fig. 5 Evolution of the fibroblast normalised density (*above*) and fibroblasts-induced traction stress (*below*) at different time instants for the elliptical wound. Units are N/cm^2 for σ_{cell}

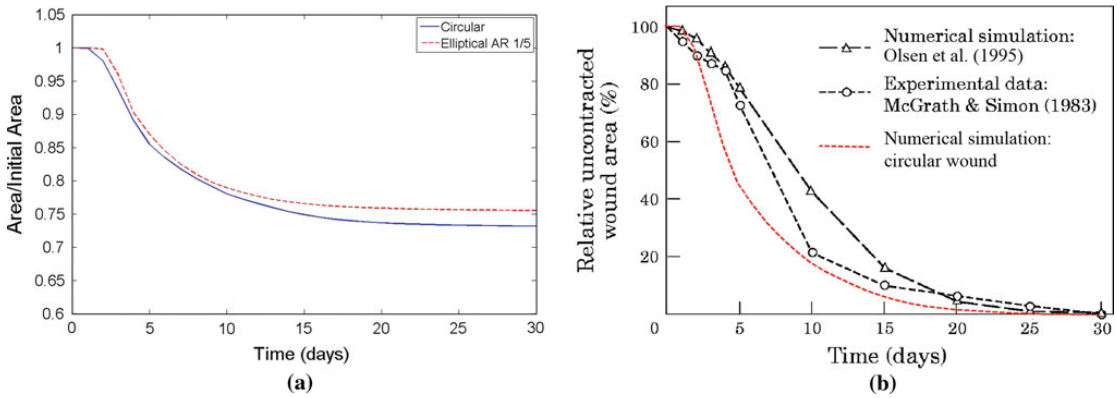

Fig. 6 **a** Evolution of the normalised wound area. **b** Evolution of the relative uncontracted wound area compared to experimental and computational data of our model and previous works (McGrath and Simon 1983; Olsen et al. 1995)

have been carried out to understand and explain the mechanisms of angiogenesis in depth (Risau 1997; Carmeliet and Jain 2000), but there is still a lack of experimental studies due to the complexity of obtaining experimental data of capillary growth. This makes research from an in silico perspective more important. Moreover, the social and economic impact of unsuccessful wound healing and vascular growth adds to the importance of this field. In recent years, a number of mathematical models have been proposed to predict angiogenesis during wound healing (Pettet et al. 1996a; Schugart et al. 2008), but only a few of them incorporate mechanical stimulus as a key factor (Xue et al. 2009).

In this work, we present a model of angiogenesis in wound healing based on the work of Javierre et al. (2008) but incorporating the contraction role of fibroblasts in the model. Among the modifications, the incorporation of the

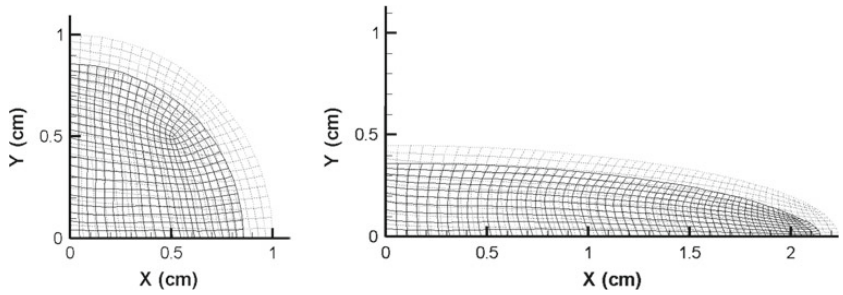

Fig. 7 Initial (day 0) (*doted*) and final (day 30) (*lined*) grids for the circular (*left*) and elliptical wounds (*right*) at day 30

mechanical forces that fibroblasts exert on the surrounding tissue (Moreo et al. 2008) is one of the most important. With this modification, we can reproduce the contraction of the wound as a function of the oxygen tension, which is determined by the angiogenesis progress. We consider in this work that cells (fibroblasts) exert isotropic contraction forces on the surrounding tissue. This hypothesis is a first simplification of the reality, and cell orientation should be incorporated to obtain a more accurate model. However, the goal of this work is to provide a continuous model describing the most relevant features of wound angiogenesis and contraction at the expense of detailed cellular models.

Another novelty in our model, compared to preceding works, is the use of a hyperelastic material model to simulate skin behaviour. Skin is traditionally treated as a viscoelastic material in wound healing models (Manoussaki 2003; Xue et al. 2009). However, adopting a hyperelastic material model is more appropriate for skin (Flynn et al. 2011) as it undergoes large strains, especially during wound contraction. It would also allows for a more straightforward coupling with wound remodelling processes allowing features such as fibre (re)orientation to be incorporated (Flynn et al. 2011). To our knowledge, this is the first wound healing model that assumes skin as a hyperelastic material. In this work, strains are significative and we use an updated Lagrangian approach to model all the full healing event. Maximum strains in a time increment are around 13 % in the first days of the healing process.

Several simplifications had to be made to develop this model. First, the proposed model neglects any anisotropic or viscoelastic effect on the mechanical behaviour of skin despite the fact that recent works include these properties in a hyperelastic constitutive model (Flynn et al. 2011). The incorporation of anisotropy and viscoelasticity would make the proposed model more general, but would also increase the number of model parameters. Second, the properties of the hyperelastic skin were considered as a function of the matrix density instead of the skin composition, which would be more accurate. Third, residual stresses in the damaged skin were assumed to be completely relaxed when the wound occurs. Finally, the model needs a large number of parameters that were taken from the literature when possible but some were estimated. The determination of these parameters is very complicated, especially for human skin for which in vivo studies are not easy to carry out.

In this work, we have proposed a model of angiogenesis and wound contraction to study the effect of the wound shape on both processes. The results show a faster vascularization in the more elongated wound (Fig. 3). However, the contraction experienced by both wounds is similar.

Unfortunately, it is difficult to find experimental data in the literature, especially concerning human skin, to validate the computational results. Several wound contraction experimental studies have, however, been performed with different animal species (mainly rats and pigs). McGrath and Simon (1983) studied wounds in rats and obtained a higher contraction than that predicted with our model, due to the different properties of human and rat skin. However, the contraction curve (Fig. 6b) has a similar shape, although in our model, contraction occurs faster and the wound area stabilizes earlier. McGrath and Simon (1983)'s results also showed that wounds with a relatively larger perimeter to area ratio (in our case the elliptical wound) start the contraction process later, which is also observed in our results. Gross et al. (1995) studied wounds with different geometries in pigs. They also found higher contraction rates than those predicted by our model and also higher than those observed by McGrath and Simon (1983). However, the contraction curve was qualitatively the same. In addition, Roy et al. (2009) presented experimental results for ischaemic and non-ischaemic wounds in pigs. The closure curve is similar to ours, though it should be noted that they represent the ratio of wound closure. Moreover, the macrophage density curve of non-ischaemic wounds is qualitatively equal to ours, showing the highest level between day 2 and 3 in both cases. Therefore, we can conclude that the proposed model captures both phenomena, angiogenesis and wound contraction, in accordance with experimental results.

Regarding computational results, Schugart et al. (2008) studied angiogenesis in wound healing as a function of the oxygen concentration. They show the evolution of the

endothelial cell in time for different constant oxygen concentrations. Comparing the results of Schugart et al. (2008) to ours, we observe for low oxygen levels a similar modification in the capillary density to that observed by them in the endothelial cell. In fact, when an oxygen concentration equal to the unit is reached, we observed a similar steady value for the capillary/endothelial cell density. Schugart et al. (2008) focused on the chemical aspects of the process, in contrast to the model proposed here, and they did not include the influence of mechanics on the angiogenesis process. Like other models, they only simulated one-dimensional geometries.

In this work, we have presented a model that simulates two different processes, angiogenesis and wound contraction, simultaneously. Most of the previous computational models studied only one of these processes. Tranquillo and Murray (1992), Olsen et al. (1995), Javierre et al. (2009), Murphy et al. (2011) presented models of wound contraction in wound healing while Pettet et al. (1996a,b), Schugart et al. (2008), Flegg et al. (2009, 2010) modelled different aspects of angiogenesis in wound healing. Moreover, we present results for two different two-dimensional geometries while past models (Olsen et al. 1995; Pettet et al. 1996a,b; Schugart et al. 2008; Flegg et al. 2009, 2010; Olsen et al. 1995; Murphy et al. 2011) only simulated one-dimensional geometries. The use of two-dimensional models provides additional insights useful for studying more realistic geometries similar to those of real wounds.

In this work, we have gone a step forward in developing a complete model of wound healing. We have proposed a new mechanochemical model which couples angiogenesis and wound contraction processes. Results of these kind of models could help, in the future after further validation, in the prescription of more appropriate healing treatments for each different wound type. These models could also help to understand unsuccessful wound healing process under certain conditions.

Acknowledgments This research was supported by the Spanish Ministry of Science and Innovation (Grant DPI2009-07514 and BES2010-037281). Project partly financed by the European Union (European Regional Development Fund).

Appendix A: Weak formulation of the model

The primary unknowns (u_1, u_2, u_3, n) are interpolated from nodal values through shape functions ($\mathbf{N}$) and the time derivatives are approximated with a generalised trapezoidal method (Hughes 1987).

To obtain the complete coupled non-linear system of equations that describe the biochemical discrete model, we obtain first the weak formulation of the governing equations. For this, we use the Gauss theorem under the assumption of sufficient differentiability. To obtain the weak formulation, we take into account the boundary conditions of the primary unknowns that determine the space of admissible solutions.

The model primary unknowns can be written in function of their nodal values through their associated shape functions (Zienkiewicz and Taylor 2000). For a general species Q, where $\mathbf{x}$ are the node coordinates in a time t, the expression is as follows

$$Q^h(\mathbf{x}, t) = \mathbf{N}_Q(\mathbf{x})\mathbf{Q}(t), \tag{11}$$

where $\mathbf{Q}$ is a vector that comprises the primary unknown species (u_1, u_2, u_3, n) and the superscript h denotes the finite element solution and $\mathbf{N}_{(*)}(\mathbf{x})$ the shape functions. To achieve the algebraic discrete and non-linear system of equations, these approximations are substituted in the weak formulation, choosing the weighting functions equal to the shape functions. The nodal values of the primary time-dependant unknowns can be obtained from the resulting system of equations. This system can be expressed as a balance of internal and external forces:

$$\mathbb{F}(\mathbb{Z}_{n+1}) := \mathbb{F}^{\text{int}}(\mathbb{Z}_{n+1}) - \mathbb{F}^{\text{ext}}(\mathbb{Z}_{n+1}) = \mathbf{0}, \tag{12}$$

where $\mathbb{Z}$ comprises the time-dependant nodal values of the primary variables, expressed as

$$\mathbb{Z} = \left(\mathbf{u_1}^{\mathrm{T}}\ \mathbf{u_2}^{\mathrm{T}}\ \boldsymbol{u_3}^{\mathrm{T}}_{\mathbf{3}}\ \mathbf{n}^{\mathrm{T}}\right)^{\mathrm{T}} \tag{13}$$

and the subscript $(n+1)$ represents the time step where the solution is calculated. The internal and external forces $\mathbb{F}^{\text{int}}$ and $\mathbb{F}^{\text{ext}}$ can be represented in a vectorial form

$$\mathbb{F}^{\text{int}} = \left[\left(\mathbf{F}^{\text{int}}_{u_1}\right)^{\mathrm{T}}\ \left(\mathbf{F}^{\text{int}}_{u_2}\right)^{\mathrm{T}}\ \left(\mathbf{F}^{\text{int}}_{u_3}\right)^{\mathrm{T}}\ \left(\mathbf{F}^{\text{int}}_{n}\right)^{\mathrm{T}}\right]^{\mathrm{T}}, \tag{14}$$

$$\mathbb{F}^{\text{ext}} = \left[\left(\mathbf{F}^{\text{ext}}_{u_1}\right)^{\mathrm{T}}\ \left(\mathbf{F}^{\text{ext}}_{u_2}\right)^{\mathrm{T}}\ \left(\mathbf{F}^{\text{ext}}_{u_3}\right)^{\mathrm{T}}\ \left(\mathbf{F}^{\text{ext}}_{n}\right)^{\mathrm{T}}\right]^{\mathrm{T}}, \tag{15}$$

where the form of the components is calculated in the form

$$\mathbf{F}^{\text{int}}_{u_1} = \int_\Omega \mathbf{N}^{\mathrm{T}}_{u_1}\frac{\partial u_1}{\partial t}\,\mathrm{d}\Omega + \int_\Omega \nabla\mathbf{N}^{\mathrm{T}}_{u_1} D_1 \nabla u_1 \mathrm{d}\Omega \tag{16}$$

$$\mathbf{F}^{\text{int}}_{u_2} = \int_\Omega \mathbf{N}^{\mathrm{T}}_{u_2}\frac{\partial u_2}{\partial t}\mathrm{d}\Omega + \int_\Omega \nabla\mathbf{N}^{\mathrm{T}}_{u_2} D_2 \nabla u_2 \mathrm{d}\Omega \tag{17}$$

$$\mathbf{F}^{\text{int}}_{u_3} = \int_\Omega \mathbf{N}^{\mathrm{T}}_{u_3}\frac{\partial u_3}{\partial t}\,\mathrm{d}\Omega + \int_\Omega \nabla\mathbf{N}^{\mathrm{T}}_{u_3} D_3 \nabla u_3 \mathrm{d}\Omega \tag{18}$$

$$\mathbf{F}^{\text{int}}_{n} = \int_\Omega \mathbf{N}^{\mathrm{T}}_{n}\frac{\partial n}{\partial t}\,\mathrm{d}\Omega + \int_\Omega \nabla\mathbf{N}^{\mathrm{T}}_{n} D_n \nabla n \mathrm{d}\Omega \tag{19}$$

$$\mathbf{F}^{\text{ext}}_{u_1} = \int_\Omega \mathbf{N}^{\mathrm{T}}_{u_1}\lambda_{3,1}u_3\mathrm{d}\Omega - \int_\Omega \mathbf{N}^{\mathrm{T}}_{u_1}\lambda_{1,1}u_1\mathrm{d}\Omega \tag{20}$$

$$\mathbf{F}^{\text{ext}}_{u_2} = \int_\Omega \mathbf{N}^{\mathrm{T}}_{u_2}\lambda_{2,1}P\mathrm{d}\Omega - \int_\Omega \mathbf{N}^{\mathrm{T}}_{u_2}\lambda_{2,2}u_2\mathrm{d}\Omega \tag{21}$$

$$\mathbf{F}_{u_3}^{\text{ext}} = \int_\Omega \mathbf{N}_{u_3}^{\mathrm{T}} \left(1 - \frac{u_3}{u_3^{\text{eq}}}\right)(\lambda_{3,3} + \lambda_{3,2} u_2) u_3 \mathrm{d}\Omega \tag{22}$$

$$\mathbf{F}_{n}^{\text{ext}} = \int_\Omega -\mathbf{N}_{n}^{\mathrm{T}} \lambda_{n,n} n \mathrm{d}\Omega - \int_\Omega r_n n \mathbf{N}_n^{\mathrm{T}} \left(1 - \frac{n}{K}\right) u_1 \mathrm{d}\Omega \tag{23}$$

The Jacobian matrices corresponding to the linearisation of internal and external forces with values resulting from the system of equations are now presented. In the used notation, α represents the characteristic temporal parameter of the trapezoidal integration method. The non-zero terms of the Jacobian matrices $\partial \mathbb{F}^{\text{int}}/\partial \mathbb{Z}$ and $\partial \mathbb{F}^{\text{ext}}/\partial \mathbb{Z}$ are:

$$\frac{\partial \mathbf{F}_{u_1}^{\text{int}}}{\partial \mathbf{u_1}} = \frac{1}{\alpha \Delta t} \int_\Omega \mathbf{N}_{u_1}^{\mathrm{T}} \mathbf{N}_{u_1} \mathrm{d}\Omega + \int_\Omega \nabla \mathbf{N}_{u_1}^{\mathrm{T}} D_1 \nabla \mathbf{N}_{u_1} \mathrm{d}\Omega \tag{24}$$

$$\frac{\partial \mathbf{F}_{u_2}^{\text{int}}}{\partial \mathbf{u_2}} = \frac{1}{\alpha \Delta t} \int_\Omega \mathbf{N}_{u_2}^{\mathrm{T}} \mathbf{N}_{u_2} \mathrm{d}\Omega + \int_\Omega \nabla \mathbf{N}_{u_2}^{\mathrm{T}} D_2 \nabla \mathbf{N}_{u_2} \mathrm{d}\Omega \tag{25}$$

$$\frac{\partial \mathbf{F}_{u_3}^{\text{int}}}{\partial \mathbf{u_3}} = \frac{1}{\alpha \Delta t} \int_\Omega \mathbf{N}_{u_3}^{\mathrm{T}} \mathbf{N}_{u_3} \mathrm{d}\Omega + \int_\Omega \nabla \mathbf{N}_{u_3}^{\mathrm{T}} D_3 \nabla \mathbf{N}_{u_3} \mathrm{d}\Omega \tag{26}$$

$$\frac{\partial \mathbf{F}_{n}^{\text{int}}}{\partial \mathbf{n}} = \frac{1}{\alpha \Delta t} \int_\Omega \mathbf{N}_{n}^{\mathrm{T}} \mathbf{N}_{n} \mathrm{d}\Omega + \int_\Omega \nabla \mathbf{N}_{n}^{\mathrm{T}} D_n \nabla \mathbf{N}_{n} \mathrm{d}\Omega \tag{27}$$

$$\frac{\partial \mathbf{F}_{u_1}^{\text{ext}}}{\partial \mathbf{u_1}} = -\int_\Omega \mathbf{N}_{u_1}^{\mathrm{T}} \mathbf{N}_{u_1} \lambda_{1,1} \mathrm{d}\Omega \tag{28}$$

$$\frac{\partial \mathbf{F}_{u_1}^{\text{ext}}}{\partial \mathbf{u_3}} = \int_\Omega \mathbf{N}_{u_1}^{\mathrm{T}} \mathbf{N}_{u_3} \lambda_{3,1} \mathrm{d}\Omega \tag{29}$$

$$\frac{\partial \mathbf{F}_{u_2}^{\text{ext}}}{\partial \mathbf{u_1}} = \int_\Omega \mathbf{N}_{u_2}^{\mathrm{T}} \mathbf{N}_{u_1} \lambda_{2,1} \left(\frac{-1}{u_1^{\beta_2}}\right) \mathrm{d}\Omega \quad \text{if} \quad u_1 < u_1^{\beta_2} \tag{30}$$

$$\frac{\partial \mathbf{F}_{u_2}^{\text{ext}}}{\partial \mathbf{u_2}} = -\int_\Omega \mathbf{N}_{u_2}^{\mathrm{T}} \mathbf{N}_{u_2} \lambda_{2,2} \mathrm{d}\Omega \tag{31}$$

$$\frac{\partial \mathbf{F}_{u_3}^{\text{ext}}}{\partial \mathbf{u_2}} = \int_\Omega \mathbf{N}_{u_3}^{\mathrm{T}} \mathbf{N}_{u_2} \lambda_{3,2} u_3 \left(1 - \frac{u_3}{u_3^{\text{eq}}}\right) \mathrm{d}\Omega \tag{32}$$

$$\frac{\partial \mathbf{F}_{u_3}^{\text{ext}}}{\partial \mathbf{u_3}} = -\int_\Omega \mathbf{N}_{u_3}^{\mathrm{T}} \mathbf{N}_{u_3} (\lambda_{3,3} + \lambda_{3,2} u_2) \left(1 - \frac{2u_3}{u_3^{\text{eq}}}\right) \mathrm{d}\Omega \tag{33}$$

$$\frac{\partial \mathbf{F}_{n}^{\text{ext}}}{\partial \mathbf{n}} = -\int_\Omega \mathbf{N}_{n}^{\mathrm{T}} \mathbf{N}_{n} \lambda_{n,n} \mathrm{d}\Omega + \int_\Omega r_n \mathbf{N}_n^{\mathrm{T}} \mathbf{N}_n u_1 \left(1 - \frac{2n}{K}\right) \mathrm{d}\Omega \tag{34}$$

$$\frac{\partial \mathbf{F}_{n}^{\text{ext}}}{\partial \mathbf{u_1}} = \int_\Omega r_n \mathbf{N}_n^{\mathrm{T}} \mathbf{N}_{u_1} n \left(1 - \frac{n}{K}\right) \mathrm{d}\Omega \tag{35}$$

From these expressions, it is possible to obtain the necessary block matrices to assemble the global stiffness matrix.

References

Anderson A, Chaplain M (1998) Continuous and discrete mathematical models of tumor-induced angiogenesis RID A-5355-2010. Bull Math Biol 60:857–899. doi:10.1006/bulm.1998.0042

Carmeliet P, Jain R (2000) Angiogenesis in cancer and other diseases. Nature 407:249–257. doi:10.1038/35025220

Chaplain M (2000) Mathematical modelling of angiogenesis RID A-5355-2010. J Neurooncol 50:37–51. doi:10.1023/A:1006446020377

Cheung J, Zhang M, Leung A, Fan Y (2005) Three-dimensional finite element analysis of the foot during standing - a material sensitivity study RID F-8331-2011. J Biomech 38:1045–1054. doi:10.1016/j.jbiomech.2004.05.035

Delalleau A, Josse G, Lagarde J-, Zahouani H, Bergheau J- (2008) A nonlinear elastic behavior to identify the mechanical parameters of human skin in vivo. Skin Res Technol 14:152–164. doi:10.1111/j.1600-0846.2007.00269.x

Flegg JA, McElwain DLS, Byrne HM, Turner IW (2009) A three species model to simulate application of hyperbaric oxygen therapy to chronic wounds. PLoS Comput Biol 5:e1000451. doi:10.1371/journal.pcbi.1000451

Flegg JA, Byrne HM, McElwain LS (2010) Mathematical model of hyperbaric oxygen therapy applied to chronic diabetic wounds. Bull Math Biol 72:1867–1891. doi:10.1007/s11538-010-9514-7

Flynn C, Taberner A, Nielsen P (2011) Modeling the mechanical response of in vivo human skin under a rich set of deformations. Ann Biomed Eng 39: 1935–1946. doi:10.1007/s10439-011-0292-7

Geris L, Schugart R, Van Oosterwyck H (2010) In silico design of treatment strategies in wound healing and bone fracture healing. Philos Trans R Soc A Math Phys Eng Sci 368:2683–2706. doi:10.1098/rsta.2010.0056

Glazier J, Graner F (1993) Simulation of the differential adhesion driven rearrangement of biological cells. Phys Rev E 47:2128–2154. doi:10.1103/PhysRevE.47.2128

Gros J, Farinelli W, Sadow P, Anderson R, Bruns R (1995) On the mechanism of skin wound contraction—a granulation-tissue knockout with a normal phenotype. Proc Natl Acad Sci USA 92:5982–5986. doi:10.1073/pnas.92.13.5982

Gurtner GC, Werner S, Barrandon Y, Longaker MT (2008) Wound repair and regeneration. Nature 453:314–321. doi:10.1038/nature07039

Hendriks F, Brokken D, van Eemeren J, Oomens C, Baaijens F, Horsten J (2003) A numerical-experimental method to characterize

the non-linear mechanical behaviour of human skin. Skin Res Technol 9:274–283. doi:10.1034/j.1600-0846.2003.00019.x
Hibbit D, Karlson B, Sorensen P (2011) Theory manual, version 6.9. HKS inc. Pawtucket
Holzapfel GA (2000) Nonlinear solid mechanics: a continuum approach for engineering. Wiley, Chichester 295–304
Hughes TJR (1987) The finite element method: linear static and dynamic finite element analysis. Prentice Hall International, Englewood Cliffs
Javierre E, Vermolen FJ, Vuik C, van der Zwaag S (2008) Numerical modelling of epidermal wound healing. Springer, Berlin; Heidelberger Platz 3, D-14197 Berlin, Germany
Javierre E, Moreo P, Doblaré M, García-Aznar JM (2009) Numerical modeling of a mechano-chemical theory for wound contraction analysis RID F-8256-2010. Int J Solids Struct 46:3597–3606. doi:10.1016/j.ijsolstr.2009.06.010
Lapeer RJ, Gasson PD, Karri V (2011) A hyperelastic finite-element model of human skin for interactive real-time surgical simulation. IEEE Trans Biomed Eng 58:1013–1022. doi:10.1109/TBME.2009.2038364
Linder-Ganz E, Shabshin N, Itzchak Y, Yizhar Z, Siev-Ner I, Gefen A (2008) Strains and stresses in sub-dermal tissues of the buttocks are greater in paraplegics than in healthy during sitting. J Biomech 41:567–580. doi:10.1016/j.jbiomech.2007.10.011
Maggelakis S (2003) A mathematical model of tissue replacement during epidermal wound healing. Appl Math Model 27:189–196. doi:10.1016/S0307-904X(02)00100-2
Manoussaki D (2003) A mechanochemical model of angiogenesis and vasculogenesis. ESAIM-Math Model Numer Anal Model Math Anal Numer 37:581–599. doi:10.1051/m2an:2003046
Mantzaris N, Webb S, Othmer H (2004) Mathematical modeling of tumor-induced angiogenesis. J Math Biol 49:111–187. doi:10.1007/s00285-003-0262-2
McGrath M, Simon R (1983) Wound geometry and the kinetics of wound contraction. Plast Reconstr Surg 72:66–72
Moreo P, Garcia-Aznar JM, Doblare M (2008) Modeling mechanosensing and its effect on the migration and proliferation of adherent cells RID F-8256-2010. Acta Biomater 4:613–621. doi:10.1016/j.actbio.2007.10.014
Murphy K, Hall C, Maini P, McCue S, McElwain D (2012) A fibrocontractive mechanochemical model of dermal wound closure incorporating realistic growth factor kinetics. Bull Math Biol 74(5):1–28. doi:10.1007/s11538-011-9712-y
Murray J, Cook J, Tyson R, Lubkin S (1998) Spatial pattern formation in biology: I. Dermal wound healing. II. Bacterial patterns RID F-8802-2011. J Frankl Inst Eng Appl Math 335:303–332. doi:10.1016/S0016
Olsen L, Sherratt J, Maini P (1995) A mechanochemical model for adult dermal wound contraction and the permanence of the contracted tissue displacement profile. J Theor Biol 177:113–128. doi:10.1006/jtbi.1995.0230
Olsen L, Sherratt J, Maini P (1996) A mathematical model for fibroproliferative wound healing disorders. Bull Math Biol 58:787–808. doi:10.1007/BF02459482
Pettet G, Byrne H, Mcelwain D, Norbury J (1996a) A model of wound-healing angiogenesis in soft tissue. Math Biosci 136:35–63. doi:10.1016/0025-5564(96)00044-2
Pettet G, Chaplain M, McElwain D, Byrne H (1996b) On the role of angiogenesis in wound healing RID A-5355-2010. Proc R Soc Lond Ser B Biol Sci 263:1487–1493. doi:10.1098/rspb.1996.0217
Risau W (1997) Mechanisms of angiogenesis. Nature 386:671–674
Roy S, Biswas S, Khanna S, Gordillo G, Bergdall V, Green J, Marsh CB, Gould LJ, Sen CK (2009) Characterization of a preclinical model of chronic ischemic wound. Physiol Genomics 37:211–224. doi:10.1152/physiolgenomics.90362.2008
Schreml S, Szeimies RM, Prantl L, Karrer S, Landthaler M, Babilas P (2010) Oxygen in acute and chronic wound healing. Br J Dermatol 163:257–268. doi:10.1111/j.1365-2133.2010.09804.x
Schugart RC, Friedman A, Zhao R, Sen CK (2008) Wound angiogenesis as a function of tissue oxygen tension: a mathematical model. Proc Natl Acad Sci USA 105:2628–2633. doi:10.1073/pnas.0711642105
Singer A, Clark R (1999) Mechanisms of disease—cutaneous wound healing. N Engl J Med 341:738–746
Tranquillo R, Murray J (1992) Continuum model of fibroblast-driven wound contraction—inflammation-mediation. J Theor Biol 158:135–172. doi:10.1016/S0022-5193(05)80715-5
Williams PL, Warwick R (1980) Gray's anatomy. Churchill Livingstone, Edinburgh
Xue C, Friedman A, Sen CK (2009) A mathematical model of ischemic cutaneous wounds. Proc Natl Acad Sci USA 106:16782–16787. doi:10.1073/pnas.0909115106
Zienkiewicz OC, Taylor RL (2000) The finite element method. Butterworth Heinemann, Oxford

Work 3: Stress evaluation during angiogenesis in skin wound healing

Published in: *The Proceedings of the 10th International Symposium on Computer Methods in Biomechanics and Biomedical Engineering*, Berlin, Germany, April 7th-11th, 2012. Published by ARUP; ISBN: 978-0-9562121-5-3.

Contribution of the author of the thesis: the author was in charge of writing the formulation for the user element including the angiogenesis process, making a review of the existing literature, choosing the mechanical variables, performing all the computational simulations, analyzing the results and determining their implications. Everything was done under the supervision of the other authors.

STRESS EVALUATION DURING ANGIOGENESIS IN SKIN WOUND HEALING

C. Valero[1], E.Javierre[1,2], J.M.García-Aznar[1] and M.J. Gómez-Benito[1]

1. ABSTRACT

Several phenomena occur during the wound healing process, including angiogenesis, the formation of new blood vessels from the damaged ones. All these processes are highly influenced by biological factors but also by mechanical stimuli. In this work we present a mathematical model to simulate wound healing angiogenesis taking into account the effect of wound contraction, which causes the modification of the wound geometry during the process. We include biochemical and mechanical factors and consider the skin as a hyperelastic material. We assume that cells in the skin (fibroblasts) are able to exert stresses in the tissue that surrounds them, promoting its contraction. We implement the model using the Finite Element Method and we apply it to two-dimensional wounds with two different geometries, circular and elliptical. The obtained results allow analysing the role of the skin stresses that appear as a consequence of the angiogenesis process together with wound contraction, and also the evolution of the wound geometry during healing.

2. INTRODUCTION

Skin is the largest organ in human body, it covers the whole external body surface and constitutes about the 8% of the human body mass [1]. Skin has a critical function in maintaining the integrity of the internal organs under it and in preventing the transmission of infections and dehydration. Moreover, it is also important its autoregenerative capacity after an injury, getting a perfect healing in almost every case.

Skin consists of various tissue layers: the epidermis, the dermis and the hypodermis. When important injuries occur in the skin, damage can reach the dermis and the hypodermis, and wound healing is more difficult. The dermis is an irregular connective soft tissue, with a collagen fibber matrix where nerves, blood vessels and several cellular species are also located. From a mechanical point of view, the dermis provides to the skin a high resistance to traction and also a high ability to contract elastically, due to the number and location of the collagen fibres.

Wounds in the dermis can appear as a result from a surgery or from a traumatic accident. In both cases, a successful healing is crucial for a perfect functional and

[1]Multiscale in Mechanical and Biological Engineering (M2BE), Aragón Institute of Engineering Research (I3A), University of Zaragoza, Spain
[2] Centro Universitario de la Defensa - Academia General Militar, Spain

aesthetic recovery. However, in some situations an optimal healing without an appropriate medical treatment is not possible. Wound healing is a natural process in which human body has to regenerate the damaged skin. During the tissue recovery process, several complex biochemical processes take place to repair the damage. This phenomena overlap in time and can be divided in three stages: inflammatory, proliferative and remodelling. After the wound formation both sides of the wound contract towards the centre of the wound, creating mechanical stresses in the skin and inducing the inflammatory response that initiates the healing process. After that, several phenomena take place in the proliferative phase: angiogenesis, granulation tissue formation, epithelization and wound contraction. In this stage new blood vessels and extra cellular matrix (ECM) are created while the wound reduces its size. In the final stage, the collagen fibers are remodelled and realigned and cells that are no longer needed are removed.

Angiogenesis involves the formation of new blood vessels from the pre-existing vasculature, where capillaries are formed in response to biochemical and mechanical (external) stimuli and it is present in the wound healing process. When a wound occurs, blood vessels are cut and the wound site is full of blood. To supply the necessary blood and nutrients to the tissue again, the growth and the repair of the blood vessels is crucial. At the beginning of the inflammatory phase cells migrate into the wound site and release angiogenic growth factors [2] that stimulate capillary growth and collagen deposition. This process depends on the biological and chemical species that are present in the skin and the wound. In addition, these species cause the appearance of mechanical stresses in the tissue. Cells like fibroblasts have an actomyosin machinery that regulates these stresses depending on the volumetric strain of the surrounding tissue [3]. Therefore, the evolution of the process depends also on the mechanical properties of the skin. It shall be mentioned here that angiogenesis is also present in other complex biological phenomena such as bone tissue reconstruction [4], embryogenesis and tumour growth. Hence, the work presented here is relevant and applicable to other important pathologies.

During the last years a number of mathematical models have been proposed to simulate and reproduce the vascular growth. Maggelakis [5] developed a three variable model that relates the production of macrophage-derived growth factors (MDGF), with the capillary density and the tissue oxygen concentration in one dimension. This model suggests that the healing of a circular wound depends on the oxygen supply. Javierre et al. [6] modified this model, adding a new variable, the epidermal growth factor (EGF) concentration. They propose a coupling between angiogenesis and a wound moving interface which simulates cell migration in two dimensions. A different kind of models was developed by Pettet et al. [7]. This model has three variables (capillary-tip endothelial cells, macrophage-derived chemoattractants and the new blood vessels) and it is composed by a number of differential equations that describe their behaviour. Later, this model was expanded adding the influence of fibroblasts, oxygen and extracellular matrix [8]. Schugart et al. [2], proposed another model with seven variables that relates the angiogenesis process with the tissue oxygen tension.

The main purpose of this work is the development and implementation of a numerical model that allows simulating the angiogenesis process in the skin, which takes place during the wound healing process. We will study the mechanical stresses created by cells in the skin during the process in two wounds with different geometries of the same

size. The model is used for two dimensional wounds.

3. MATERIALS AND METHODS

In this work, we propose a continuous angiogenesis model that incorporates biological, chemical and mechanical factors, consisting of a number of coupled reaction-diffusion equations. The primary variables of the model are the concentrations of oxygen (u_1), macrophage-derived growth factors -such as VEGF (vascular endothelial growth factor) or others, henceforth MDGF (u_2), capillary density (u_3) and fibroblasts (n). We have modified the model proposed by Javierre et al. [6], based on the model of Maggelakis [5], in order to introduce the effect of fibroblasts in the process.

The evolution of the biological and biochemical species stated above follows a conservation law

$$\frac{\partial Q}{\partial t} + \underline{\nabla} \cdot J_Q = f_Q \qquad (1)$$

where Q denotes the species (u_1, u_2, u_3 or n), J_Q its net flux (which takes into account the dragging term due to ECM deformation) and f_Q its net production [9].

We have also implemented the mechanical behaviour of the skin and cells. Fibroblasts can exert traction forces due to their actomyosin mechanism [3]. The net stress of one fibroblasts cell per unit of extra-cellular matrix is evaluated as

$$\sigma_{cell} = p_{cell}(\theta) \frac{n\rho_{ecm}}{R_\tau^2 + \rho_{ecm}^2} \qquad (2)$$

where p_{cell} is a piecewise linear function depending on the tissue volumetric strain of the tissue, ρ_{ecm} is the density of the extra-cellular matrix and R_τ the traction inhibition collagen density.

In this work we assume that skin behaves as a hyperelastic material, which is more suitable [10, 11] than a viscoelastic approach, which has been usually used to model skin in the wound healing process [7]. We assumed an Ogden energy function.

We have solved the resulting problem using a finite element analysis. It has been implemented through an Abaqus user subroutine.

In this work two wounds with different geometries were studied. The first one is a circular wound with a diameter of 2 cm and the second one is an elliptical wound with the same area and with aspect ratio of 5. Both wounds are surrounded by a sufficiently large circumference of undamaged skin to avoid boundary effects and are evaluated during 30 days.

4. RESULTS

In first place we observe the evolution of the wound area during the studied time. The contraction in both wounds is similar, the circular wound contracts by around 27% of its original size and the elliptical wound around 24% of its original size. We show the initial and the final geometry of both wounds after 30 days in Figure 1. The contraction

ratio experimented by both wounds is very similar.

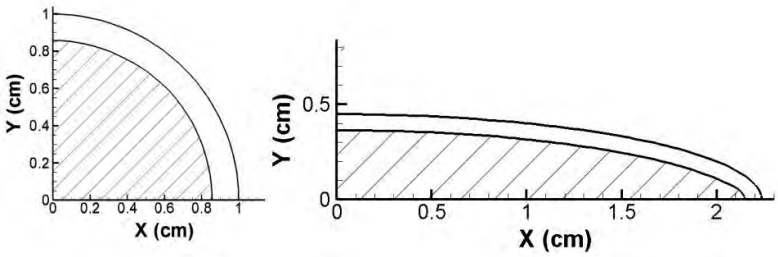

Fig. 1 Initial (day 0) (white) and final (day 30)(lined) geometries for the circular (left) and elliptical wounds (right).

We also include contour plots of the oxygen (Figure 3) and MDGF (Figure 4) concentration at different time instants. We observe how as long as the oxygen concentration increases and the wound heals, the MDGF concentration decreases as they are no longer needed. At the beginning of the process, there are not stresses in the wound and as long as the wound heals and oxygen invades it the wound stresses are higher. We have also observed that stresses around the elliptical wound are higher than around the circular one as the elliptical wound needs higher forces to experience the same contraction.

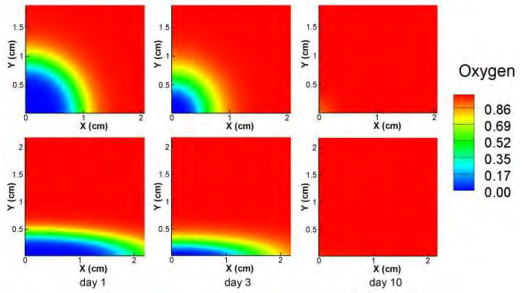

Fig. 3 Oxygen concentration at days 1, 3 and 10 in the circular (above) and the elliptical wound (below).

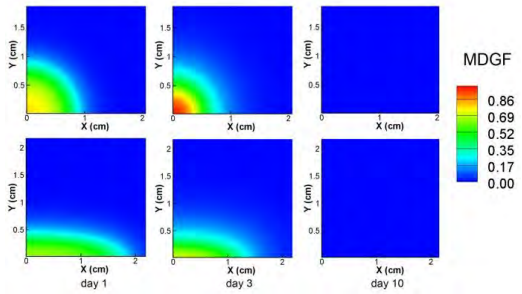

Fig. 4 MDGF concentration at days 1, 3 and 10 in the circular (above) and the elliptical wound (below).

5. DISCUSSION

Wound healing is a complex process crucial in the healing of burns and traumatic and surgical wounds. Angiogenesis is one of the biological processes that take place during wound healing, and it is very important as it involves the formation of new blood

vessels from the pre-existing vasculature, which allows the distribution of oxygen to the new tissue. In the last few years some numerical models that reproduce the angiogenesis process have been proposed. In this work we have presented a model that includes biological and mechanical parameters.

We have studied the effect of mechanics in the angiogenesis process, focusing our attention in the stresses created by cells, which are not frequently studied. The main advantages of the model are the use of a hyperelastic approach and two-dimensional geometries, not included in previous models [2, 5, 6, 7, 8].

From the results we can conclude that mechanics influences the angiogenesis process due to the modification of the wound geometry. It is easy to see that the combination of biochemical and mechanical models in these kinds of processes gives more information that would be lost with the use of just one model. Results of this kind of models can help in the prescription of more appropriate healing treatments for each different wound type. These models can also help to understand unsuccessful wound healing process under certain conditions.

6. REFERENCES

1. Williams, P.L., Anatomía de Gray., 1998, Vol. I. Ed. Elsevier.
2. Schugart, R.C., Friedman, A., Zhao, R., Sen, C.K., Wound angiogenesis as a function of tissue oxygen tension: A mathematical model, Proc. Natl. Acad. Sci. USA, 2008, 105 2628-2633.
3. Moreo, P., García-Aznar, J.M., Doblaré, M., Modeling mechanosensing and its effect on the migration and proliferation of adherent cells, Acta Biomater, 2008, 4 613-621.
4. Glazier, J.A., Graner, F., Simulation of the differential adhesion driven arrangement of biological cells, Phys. Rev. E, 1993, 47 2128-2154.
5. Maggelakis, S., A mathematical model of tissue replacement during epidermal wound healing, . Appl. Math. Model., 27 189-196.
6. Javierre, E., Vermolen, F.J., Vuik, C., Zwaag, S., Numerical Modelling of Epidermal Wound Healing. In: Numerical Mathematics and Advanced Applications, 2008, 83-90. Springer Berlin Heidelberg
7. Pettet, G.J., Byrne, H.M., Mcelwain, D.L.S., Norbury, J., A model of woundhealing angiogenesis in soft tissue. Math Biosci, 1996a, 136 35-63.
8. Pettet, G., Chaplain, M.A.J., Mcelwain, D.L.S., Byrne, H.M., On the role of angiogenesis in wound healing. Proc. R. Soc. London Ser. B, 1996b, 263 1487-1493.
9. Valero, C., Javierre, E., García-Aznar, J.M., Gómez-Benito, M. J., Numerical modelling of the angiogénesis process in wound contraction, Biomech Model Mechan, *Under Review*.
10. Cheung, J., Zhang, M., Leung, A., Fan, Y., 2005. Three-dimensional finite element analysis of the foot during standing - a material sensitivity study. J. Biomech., 2005, 38 1045-1054.
11. Lapeer, R.J., Gasson, P.D., Karri, V., A Hyperelastic Finite-Element Model of Human Skin for Interactive Real-Time Surgical Simulation. IEEE Trans. Biomed. Eng, 2011, 58 1013-1022.

Work 4: A cell-regulatory mechanism involving feedback between contraction and tissue formation guides wound healing progression

Journal: *PLOS ONE*. DOI:10.1371/journal.pone.0092774
Journal impact factor: 3.730

Contribution of the author of the thesis: the author was in charge of rewriting the formulation for the new physical-evidence based laws, making a review of the existing literature, choosing the mechanical variables, performing all the computational simulations, analyzing the results and determining their implications. Everything was done under the supervision of the other authors.

OPEN ACCESS Freely available online

PLOS ONE

A Cell-Regulatory Mechanism Involving Feedback between Contraction and Tissue Formation Guides Wound Healing Progression

Clara Valero[1]*, Etelvina Javierre[2], José Manuel García-Aznar[1], María José Gómez-Benito[1]

1 Multiscale in Mechanical and Biological Engineering (M2BE), Aragón Institute of Engineering Research (I3A), University of Zaragoza, Zaragoza, Spain, **2** Centro Universitario de la Defensa de Zaragoza, Academia General Militar, Zaragoza, Spain

Abstract

Wound healing is a process driven by cells. The ability of cells to sense mechanical stimuli from the extracellular matrix that surrounds them is used to regulate the forces that cells exert on the tissue. Stresses exerted by cells play a central role in wound contraction and have been broadly modelled. Traditionally, these stresses are assumed to be dependent on variables such as the extracellular matrix and cell or collagen densities. However, we postulate that cells are able to regulate the healing process through a mechanosensing mechanism regulated by the contraction that they exert. We propose that cells adjust the contraction level to determine the tissue functions regulating all main activities, such as proliferation, differentiation and matrix production. Hence, a closed-regulatory feedback loop is proposed between contraction and tissue formation. The model consists of a system of partial differential equations that simulates the evolution of fibroblasts, myofibroblasts, collagen and a generic growth factor, as well as the deformation of the extracellular matrix. This model is able to predict the wound healing outcome without requiring the addition of phenomenological laws to describe the time-dependent contraction evolution. We have reproduced two in vivo experiments to evaluate the predictive capacity of the model, and we conclude that there is feedback between the level of cell contraction and the tissue regenerated in the wound.

Citation: Valero C, Javierre E, García-Aznar JM, Gómez-Benito MJ (2014) A Cell-Regulatory Mechanism Involving Feedback between Contraction and Tissue Formation Guides Wound Healing Progression. PLoS ONE 9(3): e92774. doi:10.1371/journal.pone.0092774

Editor: Adam J. Engler, University of California, San Diego, United States of America

Received October 7, 2013; **Accepted** February 25, 2014; **Published** March 28, 2014

Funding: This research was supported by the Spanish Ministry of Economy and Competitiveness (Grant DPI2012-32880 and BES2010-037281) (http://www.mineco.gob.es/portal/site/mineco/?lang_choosen=en). Financial support of the European Research Council (ERC) through project ERC-2012-StG 306751 is gratefully acknowledged (http://erc.europa.eu/). The funders had no role in study design, data collection and analysis, decision to publish, or preparation of the manuscript.

Competing Interests: The authors have declared that no competing interests exist.

* E-mail: claraval@unizar.es

Introduction

Wound healing is an intricate process that combines biological, chemical and mechanical signals for collective cell function. Normal wound healing evolves over three overlapping phases: inflammation, proliferation and remodeling [1,2]. When homeostasis is reached a few hours after wounding, the inflammatory phase begins with neutrophil and macrophage cell invasion and debridement of the wound site [1]. Subsequently, these cell types secrete and/or recruit specialized biochemical growth factors, such as TGF$-\beta$, PDGF and MDGF which control the subsequent stages of the healing process. Re-epithelialization of the wound also occurs during the inflammation phase. Epithelial cells proliferate and move to the top of the wound. During the proliferative phase, biochemical mediators recruited during the inflammatory phase control the migration, proliferation and biosignal production of fibroblasts and endothelial cells. Fibroblasts degrade the initial fibrin blood clot [3] and secrete collagen type III, creating a new extracellular matrix at the wound site that is more resistant than the blood clot but has inferior mechanical properties than the undamaged tissue. The inferior mechanical properties of the granulation tissue are due to, among other factors, the random alignment of the new secreted collagen fibers. Matrix remodeling occurs over a period of months, increasing the proportion of collagen type I and causing the formation of scar tissue that resembles healthy skin. Endothelial cells follow migrating fibroblasts and re-establish the vascular system that provides the oxygen and nutrients required for cell function. There is evidence that both biochemical factors (such as TGF-β) [4] and mechanical stimuli induce the differentiation of fibroblasts into myofibroblasts [5], leading to wound contraction.

Tissue cells are anchored to a substrate and use their actomyosin system to exert and transmit contractile forces to their surroundings [6]. Mechanical stimuli are known to influence several cellular processes such as migration, differentiation and orientation [7–12]. Moreover, there is evidence that the mechanical stimulus that regulates these processes is the stiffness of the substrate that surrounds the cells [5,8,13–17]. To clarify this phenomenon, Mitrossilis et al. [15] demonstrated that cells on elastic substrates modify their activity according to the substrate stiffness. Their in-vitro experiments demonstrated that the forces exerted by cells increase as the substrate becomes stiffer [15], and that a saturation force level is reached. Cells are anchored to the substrate through focal adhesions and show different behaviors depending on the mechanical properties of the substrate; they are stronger on stiffer surfaces.

Computational modeling makes it possible to reproduce and evaluate the wound healing progress under different conditions. To provide valuable predictions, the healing process needs to be fully understood and translated into mathematical equations. Moreover, computational models can be of great aid for the discussion of certain biological hypotheses. Early wound healing models [18–20] could predict the evolution of epidermal wounds. Murray et al. [19] developed the first biochemical model of wound contraction in one dimension, which was used to study the evolution of a cellular species and the extracellular matrix (ECM) density and displacement. Sherratt et al. [20] proposed a biochemical model in which cell proliferation and migration are dictated by a generic growth factor. These models have been further developed to incorporate biophysical evidence acquired from in vitro or animal models. Olsen et al. [21,22] proposed the first mechano-chemical model of wound contraction, in which the major events in fibroplasia and wound contraction are taken into account, including the addition of a new cellular species under study, the myofibroblasts, which have a relevant role in wound contraction. A thorough analysis of these model equations enabled the establishment of the effect of chemical net production on the occurrence of fibroproliferative disorders, particularly the effect of a permanently contracted state. Adam [18] investigated the occurrence of non-healing wounds and the so-called critical size defect with a simple model that describes the evolution of a generic growth factor activating cell proliferation at the wound edge. Olsen's model [21] has been recently revised by different authors [23–25]. These works incorporate the decreased mechanical properties of the granulation tissue and combine for the first time the coupled actions of chemical and mechanical factors on the fibroblast to induce myofibroblast differentiation, although the studies differ in the mechanical stimulus used to drive the differentiation. Both works suggest that differentiation is guided by stress. Whereas Javierre et al. [23] claim that the stress that guides the process is the force exerted by the cells, Murphy et al. [24] propose that this stress comes from the elastic component of the ECM. Additionally, Javierre et al. [23] investigated the effect of wound shape on the contraction kinetics, whereas Murphy et al. [24,25] focused on a more detailed representation of the biochemical signaling of wound contraction. Furthermore, Javierre et al. [23] considered a unique growth factor that regulates differentiation and collagen production, whereas Murphy et al. [25] included the chemical kinetics of two different growth factors (PDGF and TGF-β) separately.

Several cellular mechanisms have been found to be driven by the stiffness of the substrate that surrounds the cells and not by the stresses that the cells support [8,15]. Thus, we propose a differentiation mechanism that combines both chemical factors and a mechanical stimulus, as performed in previous works, but we assume that the mechanical stimulus that regulates the differentiation process is the ECM deformation, which depends directly on the ECM stiffness.

Therefore, in this work, we propose a unified constitutive theory consistent with experimental observations of individual and collective cell populations. This theory is based on a rigidity sensing mechanism that cells use to control the level of contraction that they exert on the ECM to drive its deformation. This deformation of cells is able to indirectly regulate the progression of different cellular events, such as cell differentiation and tissue formation.

Results

Cell traction forces are modulated in response to the rigidity of the surrounding ECM

Early works on wound contraction assumed that cells exert a constant traction force (denoted by τ_0 or λ) on the ECM. This constant traction force is subsequently scaled (or modulated) by the ECM density (ρ) and the cellular densities of fibroblasts (n) and myofibroblasts (m). Traditionally, a linear relationship between cell-induced stresses and cell densities is assumed. Moreover, the myofibroblasts-enhanced traction forces are modeled through the proportionality factor ξ. Finally, the most significant difference between these models arises in the term for the ECM density. This term represents the different properties on the involved tissues (the wound and the partly recovered and healthy skin) during contraction progression. All of these hypotheses have been included through different phenomenological laws, such as [21,23]

$$\sigma_{cell} = \tau_0 \frac{\rho}{R_\tau^2 + \rho^2}(1 + \xi m) n \mathbf{I} \tag{1}$$

or [25]

$$\sigma_{cell} = \lambda \rho (n + \xi m) \mathbf{I} \tag{2}$$

These expressions aim to induce an increase in the cell-exerted stresses in the middle of the wound, creating a stress gradient between the wound and the surrounding healthy tissue. Note that this gradient is therefore dependent on the initial conditions of the model with respect to the ECM density and the cell populations.

Other authors instead proposed phenomenological laws that are non-linear to the cell population. In those cases, the stresses exerted by cells tend to become saturated due to contact inhibition and competition for ECM binding sites at high cell densities [26]

$$\sigma_{cell} = \tau_0 \frac{\rho}{1 + \gamma n^2} n \mathbf{I} \tag{3}$$

However, there are multiple experiments that suggest that the cellular capacity to exert traction forces on the ECM strongly depends on the ECM stiffness [27]. Therefore, in this work we propose a purely mechanical and self-regulated traction force dependent on the ECM stiffness through

$$\sigma_{cell} = p_{cell}(\theta)(n + \xi m) \mathbf{I} \tag{4}$$

In this expression, we consider the role of the ECM stiffness through p_{cell}, which denotes the force that a cell exerts depending on the volumetric strain (θ) of the ECM [28]. Unlike other models, we do not explicitly include the ECM density in the expression for σ_{cell}. However, the ECM density does play an indirect role in cell-induced stresses through the value of p_{cell} (see File S1). As the collagen density increases, the tissue becomes stiffer [29], regulating the volumetric strain of the tissue (θ), which in turn defines the value of p_{cell} and the stresses exerted by the cells on the ECM. We consider also that σ_{cell} depends on the concentration of fibroblasts and myofibroblasts, with a term $(n + \xi m)$ similar to the one proposed by Murphy et al. [25]. Contractile forces exerted by fibroblasts can initiate wound closure and myofibroblasts are

known to contribute to the transmission of these contraction forces [29,30]. Furthermore, any of these species can be present in the absence of the other. Hence, when one of them is not present, the other one can still generate stress [31]. This basic effect is not included in most of the previous models, in which myofibroblasts are not considered [26] or in which the generated forces are always zero in the absence of fibroblasts [21,23].

Figure 1 shows that the initial stress distributions (σ_{cell}) exerted by the cells in the wounded and unwounded tissues are very similar in all considered theories. Therefore, we can conclude that all previous phenomenological laws represent similar behavior and thus, we can find a clear biophysical interpretation of this behavior which is the mechanosensing mechanism provided by cells.

Fibroblast to myofibroblast differentiation is driven by cell deformation

We assume that fibroblasts differentiate into myofibroblasts in response to the strain (θ_{cell}) supported by the fibroblasts. This strain is the same as the strain of the ECM because we consider cells and the ECM to occupy the same domain and because they both support the same strain as the compatibility condition.

This assumption for fibroblast differentiation into myofibroblasts is based on the following phenomena. When a wound occurs and healing events are activated, fibroblasts exert contractile forces as a mechanosensing mechanism. Thus, fibroblasts shrink the external domain of the wound, and consequently, the inner part of the wound is extended. This effect forces the fibroblasts inside the wound to stretch. To overcome this effect, we hypothesize that fibroblasts differentiate into myofibroblasts regulated by the passive stretching that fibroblasts support inside the wound due to the fibroblast contraction in the external part of the wound. This result is consistent with experimental evidence that establishes that mechanical forces such as stretching can drive fibroblasts to differentiate toward a myofibroblast phenotype [29,32,33]. When the population of myofibroblasts inside the wound also exerts contractile stresses, the full contraction of the wound occurs, and the differentiation of fibroblasts to myofibroblasts is stopped.

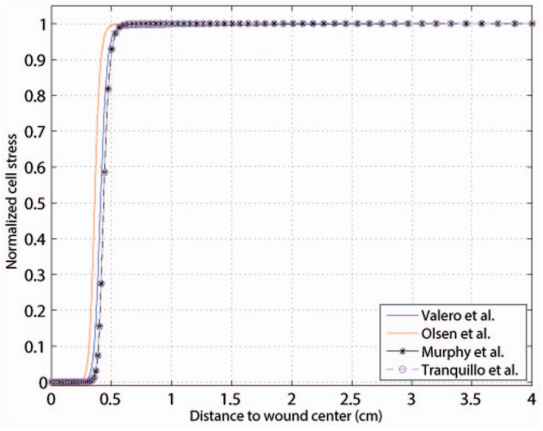

Figure 1. Normalized cell stress (σ_{cell}) distributions created by different laws [21,25,26] **and the proposed model at the beginning of wound contraction.** The wound has a radius of 0.5 cm. Every law produces a similar stress distribution despite dependence on different variables.
doi:10.1371/journal.pone.0092774.g001

Therefore, the first observable consequence of an injury is the distraction of the wound due to fibroblasts distribution (Figure 2). This deformation causes the ECM volumetric strain, θ, to be positive at the wound center and negative (although very close to zero) in the surrounding undamaged tissue (Figure 3), which in turn causes myofibroblasts to appear inside the wound, close to its edge (Figure 4).

As time passes, fibroblasts and myofibroblasts accumulate inside the wound, creating the necessary traction forces to overcome the passive stretch of the wound. From that moment on, the wound contracts, and the sign of ECM volumetric deformation gradually changes from positive to negative from the wound boundary inward (see Figure 3).

Therefore, there are two different behaviors in the wound caused by the non-uniform cell and matrix densities. Cells can deform, contracting the matrix, or cells can be stretched due to the matrix deformation. Therefore, fibroblasts contract the ECM near the wound edge and stretch the wound center. This stretching is also included in the fibroblasts that are inside the wound site, and it regulates their differentiation into myofibroblasts (see Figure 4).

Thus, the proposed differentiation mechanism implies that there is no differentiation from fibroblasts to myofibroblasts in the healthy skin. This outcome is physically coherent, as myofibroblasts appear only inside the wound [31]. The use of volumetric tensile strains to differentiate provides a biophysical explanation for a phenomenon that has been previously simulated in a phenomenological way [21,23,25,26].

Comparative analysis of the predictive ability of the model with in-vivo experiments

The proposed mechano-chemical model makes it possible to study the evolution of the wound from two different perspectives. First, we analyze the deformation of the wound during its contraction. However, the contraction of the wound is accompanied by the synthesis and deposition of new tissue, which fills the wound space. Hence, we also analyze the healing of the wound in terms of collagen density. Collagen does not fill the wound completely until several months or years have passed [1]. Hence, we consider the wound to be healed when its collagen density is at least 75% of the density in healthy skin. It is safe to assume that when this threshold of collagen concentration is reached, the skin has mostly recovered its mechanical properties and functionality.

We have reproduced the wound geometries used by Roy et al. [34] and McGrath and Simon [35] in animal models. Roy et al. [34] considered a circular wound of area of $0.5cm^2$ in pigs, whereas McGrath and Simon [35] considered square wounds with areas of $6.25cm^2$ and $12.54cm^2$ in rats. The area of the tissue initially occupied by the wound is used to determine the contraction pattern of the considered geometries. The temporal evolution of this area (normalized with respect to its initial size) is presented in Figure 6. The release of the skin stresses is a direct consequence of the injury, which causes a fast increase in the wound area. However, as time passes, the wound contracts due to the forces exerted by the cells, finally a size similar to the initial size. Based on the considered geometries, we can conclude that a larger wound size leads to a smoother transition between the distraction-contraction regimes.

The healing pattern for the considered geometries is obtained via the temporal evolution of the wound area (normalized to its initial size). As introduced before, we consider the wound to be all parts of the tissue with less than 75% of the collagen density of the undamaged tissue. This variable is presented in Figures 7 and 8, for the experimental results [34,35]. In both cases, we accurately

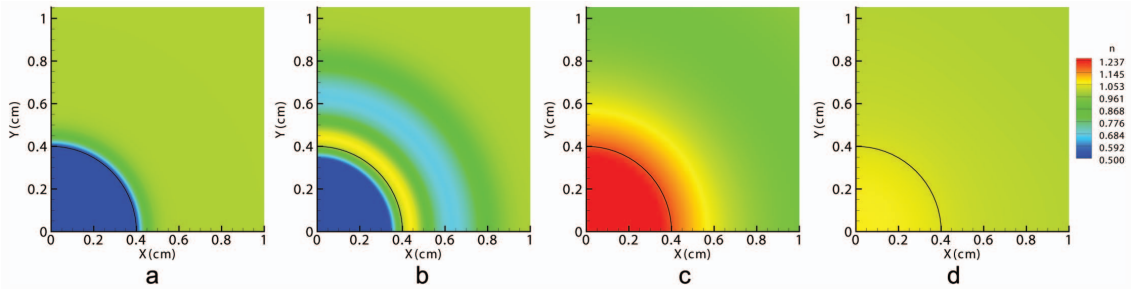

Figure 2. Fibroblast distributions in the tissue at t = 0 (a), at the beginning of the contraction (b), at halfway through the healing time (c) and at healing time (d). The black line denotes the edge between the initial wound and the surrounding skin.
doi:10.1371/journal.pone.0092774.g002

capture the healing kinetics at the early stages of the healing process. Collagen appears rapidly at the early stages of healing and it stabilizes after reaching its maximum value of wound closure (Figure 5).

Roy et al. [34]observed the evolution of an ischemic wound and a non-ischemic wound in a pig. We have used the non-ischemic wound for comparison with our results as we simulate a wound in non-pathological skin. We present wound closure as a function of time. We simulate wound healing in humans, and the experiments were performed on different animal species. When comparing the results, it should be take into consideration that each species has different time parameters due to their different cellular and tissue kinetics [36]. Hence, for each set of experiments (simulations and in vivo) and in order to adjust the differences in time scales, we fix the healing time as the moment when the maximum healing is reached. For the small circular geometry (area of $0.5cm^2$) analyzed by Roy et al. [34] (Figure 7) the numerical simulation closely predicts the closure rate at the latter stages of the healing process. We see that the initial distraction stage lasts for approximately 10% of the healing time and that the healing curves in both cases follow a similar pattern, reaching a similar healing level. In both cases, almost complete healing is obtained.

For the larger geometries, we simulate the experiments of McGrath and Simon [35] (Figure 8), in which square wounds of different areas were considered (sizes of 6.25 cm^2 and 12.54 cm^2). We observe that the numerical simulation underestimates the percentage of wound closure (for the time period considered). As in the experimental work, we found that the larger wounds heal slightly less than smaller wounds. We also found that the elastic modulus of the rat's skin is one order of magnitude smaller than the elastic modulus of the pig's skin.

The results show differences between the two cases based on several reasons. First, the mechanical properties of the two animal species have different orders of magnitude. Moreover, the wound sizes should be considered to be of different orders of magnitude in the two experimental works. Although the wound studied by [34] can be considered small relative to the animal size, the wound studied by [35] has a large size compared with the animal size. This fact greatly influences the healing process. In [35] the wound probably affects the muscular zone with movement, which impairs greater healing.

When studying square wounds, we find that the healing pattern tends to soften the curvature of the wound. This phenomenon has been previously observed in other biological processes, such as bone ingrowth in bone scaffolds. This phenomenon corroborates the idea that wound healing is a mechanically driven process [37].

Discussion

The economic and social impact of the treatment of chronic wounds calls for an integrated and multidisciplinary approach to the problem. Mathematical modeling and computer simulation should be used as additional tools to gain a better understanding of the intricate biochemical and mechanical processes behind wound healing.

In this work, we present a mechano-chemical wound healing model with two main novelties that distinguish it from previous models. We postulate that the main phenomena that occur during wound healing involves cells and are regulated by mechanical

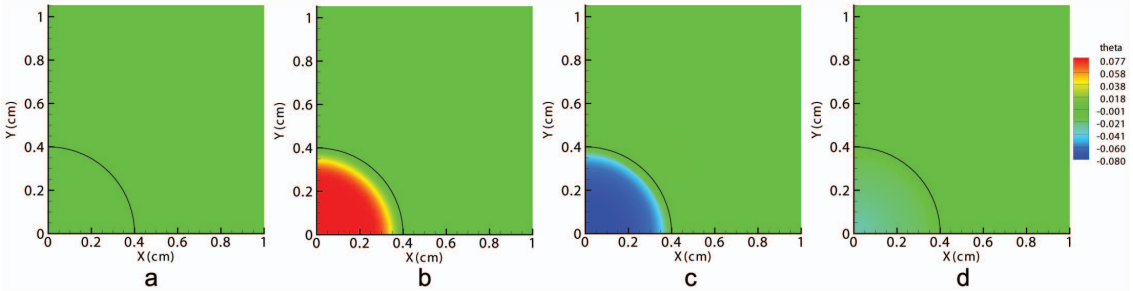

Figure 3. Volumetric deformations in the tissue at t = 0 (a), at the beginning of the contraction (b), at halfway through the healing time (c) and at healing time (d). The black line denotes the edge between the initial wound and the surrounding skin.
doi:10.1371/journal.pone.0092774.g003

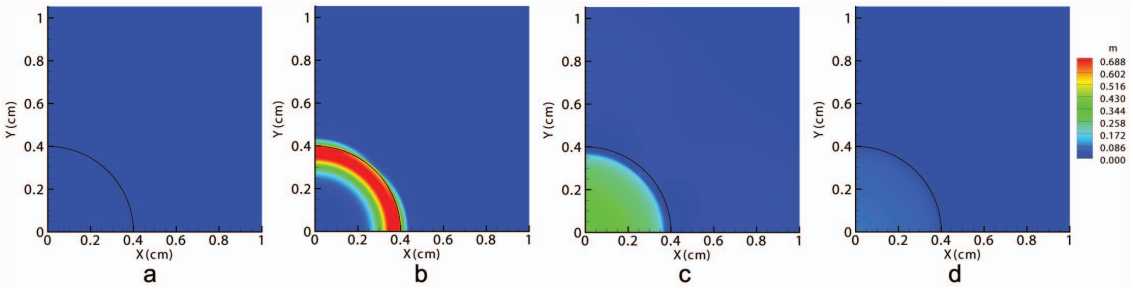

Figure 4. Myofibroblasts distributions in the tissue at t = 0 (a), at the beginning of the contraction (b), at halfway through the healing time (c) and at healing time (d). The black line denotes the edge between the initial wound and the surrounding skin.
doi:10.1371/journal.pone.0092774.g004

stimulation. Thus, we propose to update the phenomenological laws with physical evidence-based laws for fibroblast differentiation and the cell-exerted stresses.

This work provides a mechanical theory of wound contraction that is consistent with the cell function experimental observations [15,16] and with wound healing in animal models [34,35]. The proposed model generalizes from previous models [19,21–23,25] with a cell-regulatory mechanism that handles ECM rigidization and its impact on cell function. Our model provides similar results to those of previous works, but we have proposed a formulation of cell traction generation and fibroblasts differentiation based on a biophysical hypothesis instead of a phenomenological assumption. Taking these modifications into account, the model can help to clarify our knowledge of regenerative phenomena.

The effect of additional phenomena (naturally produced by the organism or externally induced) could be analyzed with the current model definition, either changing the mechanical properties of the affected tissues to the ones measured for each pathology or varying specific model parameters. This is the case of certain pharmacological therapies [38] or genetic mutations involving modifications in the tissue properties, mostly rigidization, that could be studied using the present model. Moreover, it will be possible the study of certain pathologies such as pressure ulcers [39] or fibroproliferative disorders [40], which have a high mechanical component and modify the natural evolution of wound healing. In pressure ulcers, oxygen flow is impaired due to an excessive pressure in the tissue that comprises blood vessels [39]. Moreover, the hydrostatic pressure becomes negative in the skin area subjected to pressure leading to negative volumetric strains. Thus, fibroblasts differentiation into myofibroblasts will be inhibited once the ulcer has begun, and traction forces generated by fibroblasts will not be enough for closing the wound. The opposite cases are fibroproliferative disorders such as keloids and hypertrophic scars, which appear due to an excessive collagen production during healing [40]. It is also known that the appearance of these disorders is promoted by mechanical forces [41,42]. An overexpression of collagen will cause an excessive tension in the tissue that surrounds the wound, which will also produce an excessive fibroblast differentiation. Moreover, it is known that the collagen type created in every process is different, having different stiffness properties, which could be included in the model.

Several assumptions and simplifications were needed to formulate and implement this model. First, although wound healing is a three-dimensional process, we considered a two-dimensional simplification in our work. We considered a plane stress approach, neglecting wound depth and assuming that the deformation on the plane is constant.

Most of the existing models [19,21,25] make great simplifications about wound geometry, considering only one-dimensional axisymmetric wounds. This simplification is useful for analyzing theoretical wounds but cannot be applied to simulate real and more complicated wounds. Thus, we follow [23] and consider a two-dimensional model that could be extended to three dimensions, which would be more appropriate to reproduce the real behavior of wounds in the skin.

Other simplifications in the model are made when defining cell stresses. Although we have assumed that stresses are mainly due to the cell activity, other sources such as patient motion could generate stress. We have also considered the volumetric cell strain

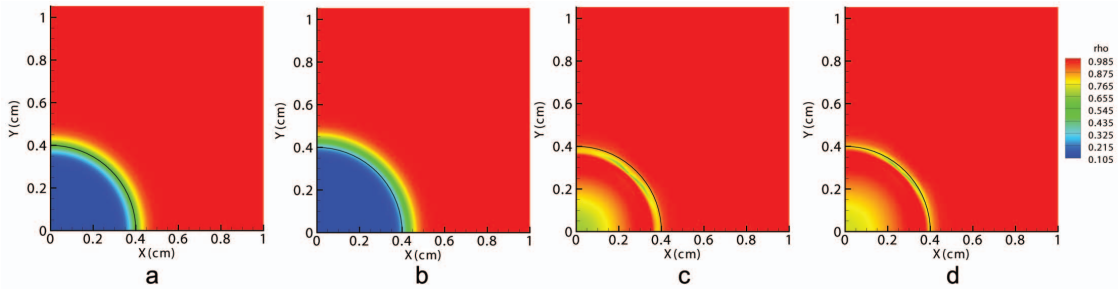

Figure 5. Collagen distributions in the tissue at t = 0 (a), at the beginning of the contraction (b), at halfway through the healing time (c) and at healing time (d). The black line denotes the edge between the initial wound and the surrounding skin.
doi:10.1371/journal.pone.0092774.g005

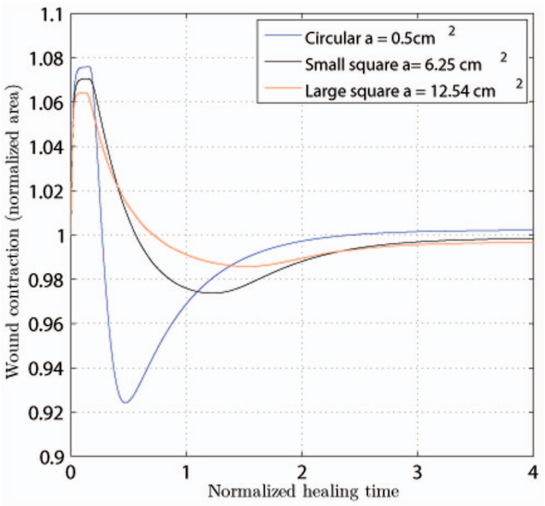

Figure 6. Wound contraction as a function of time for the three studied geometries.
doi:10.1371/journal.pone.0092774.g006

as the mechanical variable that regulates cell biology, however, other mechanical variable such as the deviatoric cell strain or the principal cell strain could have been considered. Moreover, the influences of other factors such as chemical growth factors are indirectly included in the model through the cellular kinetics.

Regarding the numerical results, the wound does not reach complete healing during the studied time. In fact, complete healing is never achieved after a wound occurs [1]; the tissue keeps recovering for months or years. Moreover, a critical size defect (CSD) is known to exist [18]. This CSD is different for each animal species and denotes the wound size above which a wound will not heal during the animal's lifetime.

Although computational simulations reproduce an ideal situation, there are several external and unpredictable factors in animal experiments that should be considered. Moreover, the mechanical properties of the skin vary depending on the location on the body. The skin can displace and contract in different ways depending on how it is oriented relative to tension lines.

Scarring is the step that follows wound contraction, and the model presented here will be of great aid for preliminary qualitative prediction of the scarring level. Moreover, the model makes it possible to study different factors that regulate scarring, such as wound size and shape, the animal species and the mechanical properties of the skin.

Materials and Methods

In this work, we model the temporal evolution of different cellular species (fibroblasts and myofibroblasts), chemicals (a generic growth factor with the combined effects of PDGF and TGF-β on (myo)fibroblasts and the collagen density) and extracellular matrix deformation [30,43]. The cellular and chemical species densities are obtained from a conservation law

$$\frac{\partial Q}{\partial t}+\nabla\cdot\mathbf{J}_Q=f_Q \qquad (5)$$

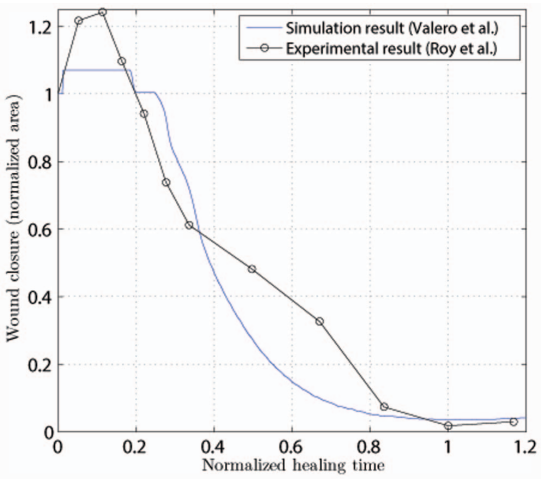

Figure 7. Normalized wound area as a function of the normalized healing time for a circular wound with a radius of 0.4 cm. Comparison with the experimental work of Roy et al.[34].
doi:10.1371/journal.pone.0092774.g007

where Q denotes the cellular/chemical species, $\mathbf{J}_Q$ denotes its net flux over the domain of interest (which may include terms representing random dispersal -migration or diffusion-, directed migration (chemotaxis), and may also include a passive convection term due to ECM deformation), and f_Q denotes net production. The matrix deformation is obtained from the conservation of linear momentum

$$\nabla\cdot(\sigma_{ecm}+\sigma_{cell})=\mathbf{f}_{subs} \qquad (6)$$

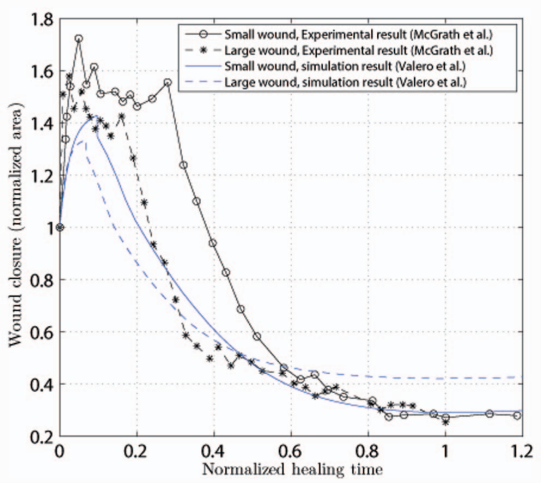

Figure 8. Normalized wound area as a function of the normalized healing time (time/healing time) for two square wounds with areas of 6.25 cm^2 and 12.54 cm^2. Solid lines refer to the small wound, and dashed lines refer to the large wound. Comparison with the experimental work of McGrath and Simon [35].
doi:10.1371/journal.pone.0092774.g008

Table 1. List of model parameters related to fibroblasts and myofibroblasts kinetics.

Parameter	Description	Value	Observations
n_0	fibroblasts density in undamaged dermis	10^4 cells/cm^3	[21]
D_n	fibroblasts diffusion rate	2 10^{-2} cm^2/day	[27]†
a_n	together with b_n determines the maximal chemotaxis rate per unit of GF concentration	$4{\cdot}10^{-10}$ g/cm day	[23]
b_n	GF concentration that produces 25% of the maximal chemotactic response	$2{\cdot}10^{-9}$ g/cm^3	[23]
r_n	fibroblasts proliferation rate	0.832day^{-1}	[27]
$r_{n,max}$	maximal rate of GF induced fibroblasts proliferation	0.3 day^{-1}	[23]
$C_{1/2}$	half-maximal GF enhancement of fibroblasts proliferation	10^{-8} g/cm^3	[21]
K	fibroblasts maximal capacity in dermis	10^7 cells/cm^3	[21]
$k_{1,max}$	maximal rate of fibroblasts differentiation	0.8 day^{-1}	[23]
C_k	half-maximal GF enhancement of fibroblasts differentiation	10^{-8} g/cm^3	[23]
k_2	myofibroblasts desdifferentiation rate	0.693 day^{-1}	[23]
ϵ_r	proportionality factor	0.5	[21]

† Adjusted to fit reported migration rate with a traveling wave model.
doi:10.1371/journal.pone.0092774.t001

where σ_{ecm} denotes the passively resistant ECM stress, σ_{cell} denotes the ECM stress due to the cells-ECM adhesions and $\mathbf{f}_{subs}$ denotes the ECM-substrate anchoring forces that resist ECM deformation.

This work follows the model proposed by Javierre et al. [23], based on the well-established model of Olsen et al. [21]. We consider the presence of two cellular species, fibroblasts (n) and myofibroblasts (m), embedded in a collagen (ρ) matrix and guided by the presence of a chemical growth factor (c). We also consider the matrix displacements ($\mathbf{u}$) as a primary variable in the model (see File S1).

Fibroblasts, connective tissue cells found in the skin, are the main cellular species involved in wound contraction. The main functions of fibroblasts are the synthesis of connective tissue in response to injury and remodeling of the collagen ECM by the exertion of traction forces [44]. Fibroblasts are motile cells that migrate by random dispersal, chemotaxis and passive convection caused by the ECM displacements. Hence, their net flux term can be written as

Table 2. List of model parameters related to collagen and growth factor kinetics.

Parameter	Description	Value	Observations
ρ_0	collagen concentration in undamaged dermis	0.1 g/cm^3	[21]
ρ_{ini}	initial collagen concentration in the wound	10^{-3} g/cm^3	[21]
c_0	GF concentration in the wound	10^{-8} g/cm^3	[21]
r_ρ	collagen production rate	$7.59{\cdot}10^{-10}$ g^3/cm^{6}cell day	$r_\rho = d_\rho \rho_0 (R_\rho^2 + \rho_0^2)$‡
$r_{\rho,max}$	maximal rate of GF induced collagen production	$7.59{\cdot}10^{-9}$ g^3/cm^{6}cell day	[21]
C_ρ	half-maximal GF enhancement of collagen synthesis	10^{-9} g/cm^3	[21]
η	proportionality factor	2	[21]
R_ρ	half-maximal collagen enhancement of ECM deposition	0.3 g/cm^3	[21]
d_ρ	collagen degradation rate per unit of cell density	$7.59{\cdot}10^{-8}$ cm^3/cell day	[21]
D_c	GF diffusion rate	$5{\cdot}10^{-2}$ cm^2/day	[21]
k_c	GF production rate per unit of cell density	$7.5{\cdot}10^{-6}$ cm^3/cell day	[23]§
ζ	proportionality factor	1	[21]
Γ	half-maximal enhancement of net GF production	10^{-8} g/cm^3	[21]
d_c	GF decay rate	0.693 day^{-1}	[23]

‡ Determined collagen degradation kinetics to remain in equilibrium away from the wound.
§ Downestimated to prevent fibro-proliferative disorders [22] with the used GF decay rates.
doi:10.1371/journal.pone.0092774.t002

Table 3. List of model parameters related to the mechanical behavior of cells and ECM.

Parameter	Description	Value	Observations
p_{max}	maximal cellular active stress per unit of ECM	10^{-5} N g/cm^2 cell	[23]
K_{pas}	volumetric stiffness moduli of the passive components of the cell	$2{\cdot}10^{-5}$ N g/cm^2 cell	[28]
K_{act}	volumetric stiffness moduli of the actin filaments of the cell	10^{-4} N g/cm^2 cell	[28]
θ_1	shortening strain of the contractile element	-0.6	[23]
θ_2	lengthening strain of the contractile element	0.5	[28]
τ_d	half-maximal mechanical enhancement of fibroblast differentiation	10^{-5} N g/cm^2 cell	[23]
μ_1	undamaged skin shear viscosity	200 N day/cm^2	[23]
μ_2	undamaged skin bulk viscosity	200 N day/cm^2	[23]
E	undamaged skin Young's modulus	3.34–33.4 N/cm^2	[51]
v	undamaged skin Poisson's ratio	0.3	[51]
ξ	myofibroblasts enhancement of traction per unit of fibroblasts density	10- cm^3/g	[21]
R_τ	traction inhibition collagen density	$5{\cdot}10^{-4}$ g/cm^3	[21]
s	dermis tethering factor	10^{-1} N/cm g	Estimated

doi:10.1371/journal.pone.0092774.t003

$$\boldsymbol{J}_n = -D_n\nabla n + \frac{a_n}{(b_n+c)^2}n\nabla c + n\frac{\partial \boldsymbol{u}}{\partial t}, \tag{7}$$

where D_n denotes the fibroblast diffusion rate, and a_n and b_n are chemotaxis-related parameters. The parameter values can be found in Table 1 and Table 2.

Fibroblasts kinetics is determined by their proliferation, differentiation into myofibroblasts, differentiation back from myofibroblasts and apoptosis. The novelty with respect to Javierre et al.[23] is the signal that triggers fibroblast differentiation. The ability of fibroblasts to sense the strain in the ECM [45] and the regulation of their differentiation to myofibroblasts by mechanical loads [30,31,46] are well known. Hence, we consider whether the differentiation process is driven by the deformation of the tissue where the cells are allocated instead of depending on the mechanical stress of the matrix itself [29]. We also maintain the hypothesis that this differentiation is also enhanced by different growth factors (e.g.,PDGF and TGF-β) [31,47]. Hence, fibroblast differentiation into myofibroblasts can be expressed through the term

$$f_{diff} = -\frac{k_{1,max}c}{C_k+c}\theta^+ n. \tag{8}$$

where $k_{1,max}$ denotes the maximal rate of fibroblast differentiation and C_k regulates the influence of the growth factor during differentiation.

Fibroblasts differentiate into myofibroblasts under the influence of TGF-β and the resulting phenotype is able to exert and maintain higher contractile forces in the tissue [46]. Fibroblast differentiation into myofibroblasts occurs when the ECM has a positive volumetric strain, which is denoted by $\theta^+ = max(\theta,0)$. In this situation, cells are able to exert forces on the tissue, which means that the strain is not mainly caused by the tissue itself. Myofibroblasts are smooth muscle-like cells [31], which means that they are not motile and that their flux is only due to passive convection. Myofibroblast evolution is mainly due to proliferation, differentiation from fibroblasts, inverse differentiation to fibroblasts and apoptosis [48].

Cells in the skin are embedded in the ECM, with the main components being collagen fibers produced by fibroblasts. Hence, we model the ECM density through the collagen density. Collagen fibers are non-motile, and hence their net flux term is expressed in terms of the passive convection of the skin.

Following the model of Olsen et al. [21] we consider the role of fibroblasts and myofibroblasts in collagen synthesis [31,49]. Furthermore, collagen production is enhanced by the presence of growth factors such as TGF-β [50].

The wound-healing process is regulated by several growth factors. Collagen-matrix contraction is regulated by PDGF [30] among other factors, and fibroblast differentiation is driven by TGF-β [31]. In this work, we consider a unique growth factor that regulates these processes for simplicity. The net flux of the growth factor is due to passive convection and also to diffusion through the tissue. Growth factor production is regulated by fibroblasts and myofibroblasts, following [23].

After a wound occurs, there is an instantaneous elastic response of the skin that causes the wound edge to retract, increasing the wound size. During this distraction process, the pre-stress of the skin is relaxed. Hence, the factors determining the change in wound geometry are purely mechanical. The time scale at which stress liberation occurs (on the order of minutes) is much smaller than the time scale at which cellular events such as migration, differentiation, proliferation and matrix production occur (on the order of days). Therefore, we assume that cells do not have time to influence the process, except by the death of cells due to the wounding process.

Once wound distraction has reached equilibrium, we consider the resulting wound geometry. The deformations accumulated until full wound distraction are also felt by the cells and they activate the mechanosensing mechanism controlling wound contraction. The skin is assumed to be a viscoelastic material [23,26].

The second major novelty of this work with respect to earlier works [21,23,25,26] rests on the expression for cell-induced stresses. The ECM deformation is obtained from the conservation of linear momentum (Equation (6)), where $\boldsymbol{\sigma}_{cell}$ denotes the cell-

exerted stresses. If we denote the traction force exerted by one fibroblast as $p_{cell}(\theta)$ [28], we can write the cell-induced stresses as

$$\sigma_{cell} = p_{cell}(\theta)(n + \xi m)I, \quad (9)$$

where the parameter values are included in Table 3.

Finally, we consider the observation that the ECM-substrate anchoring forces resisting ECM deformation are proportional to the tissue displacement and to the ECM density.

Supporting Information

File S1 Description of the Mechano-chemical Model and the Model Implementation.
(PDF)

Author Contributions

Conceived and designed the experiments: CV EJ JMGA MJGB. Performed the experiments: CV. Analyzed the data: CV EJ JMGA MJGB. Contributed reagents/materials/analysis tools: CV EJ JMGA MJGB. Wrote the paper: CV EJ JMGA MJGB.

References

1. Singer A, Clark R (1999) Mechanisms of disease - cutaneous wound healing. New England Journal of Medicine 341: 738–746.
2. Li J, Chen J, Kirsner R (2007) Pathophysiology of acute wound healing. Clinics in dermatology 25: 9–18.
3. Gurtner GC, Werner S, Barrandon Y, Longaker MT (2008)Wound repair and regeneration. Nature 453: 314–321.
4. Vaughan M, Howard E, Tomasek J (2000) Transforming growth factor-beta 1 promotes the morphological and functional differentiation of the myofibroblast. Experimental cell research 257: 180–189.
5. Wells RG (2008) The role of matrix stiffness in regulating cell behavior. Hepatology 47: 1394–1400.
6. Discher D, Janmey P, Wang Y (2005) Tissue cells feel and respond to the stiffness of their substrate. Science 310: 1139–1143.
7. Engler A, Griffin M, Sen S, Bonnetnann C, Sweeney H, et al. (2004) Myotubes differentiate optimally on substrates with tissue-like stiffness: pathological implications for soft or stiff microenvironments. Journal of Cell Biology 166: 877–887.
8. Harland B, Walcott S, Sun SX (2011) Adhesion dynamics and durotaxis in migrating cells. Physical Biology 8: 015011.
9. Lo C, Wang H, Dembo M, Wang Y (2000) Cell movement is guided by the rigidity of the substrate. Biophysical journal 79: 144–152.
10. Saez A, Ghibaudo M, Buguin A, Silberzan P, Ladoux B (2007) Rigidity-driven growth and migration of epithelial cells on microstructured anisotropic substrates. Proceedings of the National Academy of Sciences of the United States of America 104: 8281–8286.
11. Serra-Picamal X, Conte V, Vincent R, Anon E, Tambe DT, et al. (2012) Mechanical waves during tissue expansion. Nature Physics 8: 628–634.
12. Vogel V, Sheetz M (2006) Local force and geometry sensing regulate cell functions. Nature Reviews Molecular Cell Biology 7: 265–275.
13. Borau C, Kim T, Bidone T, Garcia-Aznar JM, Kamm RD (2012) Dynamic mechanisms of cell rigidity sensing: Insights from a computational model of actomyosin networks. Plos One 7: e49174.
14. Jones C, Ehrlich HP (2011) Fibroblast expression of alpha-smooth muscle actin, alpha 2 beta 1 integrin and alpha v beta 3 integrin: Influence of surface rigidity. Experimental and molecular pathology 91: 394–399.
15. Mitrossilis D, Fouchard J, Guiroy A, Desprat N, Rodriguez N, et al. (2009) Single-cell response to stiffness exhibits muscle-like behavior. Proceedings of the National Academy of Sciences of the United States of America 106: 18243–18248.
16. Mitrossilis D, Fouchard J, Pereira D, Postic F, Richert A, et al. (2010) Real-time single-cell response to stiffness. Proceedings of the National Academy of Sciences of the United States of America 107: 16518–16523.
17. Pelham R, Wang Y (1997) Cell locomotion and focal adhesions are regulated by substrate flexibility. Proceedings of the National Academy of Sciences of the United States of America 94: 13661–13665.
18. Adam J (2000) A simplified model of wound healing (with particular reference to the critical size defect) (vol 30, pg 23, 1999). Mathematical and Computer Modelling 31: 237–237.
19. Murray JD, Cook J, Tyson R, Lubkin SR (1998) Spatial pattern formation in biology: I. dermal wound healing. ii. bacterial patterns. Journal of the Franklin Institute-Engineering and Applied Mathematics 335B: 303–332.
20. Sherratt J, Murray J (1991) Mathematical-analysis of a basic model for epidermal wound-healing. Journal of mathematical biology 29: 389–404.
21. Olsen L, Sherratt JA, Maini PK (1995) A mechanochemical model for adult dermal wound contraction and the permanence of the contracted tissue displacement profile. Journal of theoretical biology 177: 113–128.
22. Olsen L, Sherratt JA, Maini PK (1996) A mathematical model for fibro-proliferative wound healing disorders. Bulletin of mathematical biology 58: 787–808.
23. Javierre E, Moreo P, Doblare M, Garcia-Aznar JM (2009) Numerical modeling of a mechanochemical theory for wound contraction analysis. International Journal of Solids and Structures 46: 3597–3606.
24. Murphy KE, Hall CL, McCue SW, McElwain DLS (2011) A two-compartment mechanochemical model of the roles of transforming growth factor beta and tissue tension in dermal wound healing. Journal of theoretical biology 272: 145–159.
25. Murphy KE, Hall CL, Maini PK, McCue SW, McElwain DLS (2012) A fibrocontractive mechanochemical model of dermal wound closure incorporating realistic growth factor kinetics. Bulletin of mathematical biology 74: 1143–1170.
26. Tranquillo R, Murray J (1992) Continuum model of fibroblast-driven wound contraction - inflammation-mediation. Journal of theoretical biology 158: 135.
27. Ghosh K, Pan Z, Guan E, Ge S, Liu Y, et al. (2007) Cell adaptation to a physiologically relevant ecm mimic with different viscoelastic properties. Biomaterials 28: 671–679.
28. Moreo P, Garcia-Aznar JM, Doblare M (2008) Modeling mechanosensing and its effect on the migration and proliferation of adherent cells rid f-8256-2010. Acta Biomaterialia 4: 613–621.
29. Hinz B, Gabbiani G (2003) Mechanisms of force generation and transmission by myofibroblasts. Current opinion in biotechnology 14: 538–546.
30. Grinnell F (2000) Fibroblast-collagen-matrix contraction: growth-factor signalling and mechanical loading. Trends in cell biology 10: 362–365.
31. Tomasek J, Gabbiani G, Hinz B, Chaponnier C, Brown R (2002) Myofibroblasts and mechanoregulation of connective tissue remodelling. Nature Reviews Molecular Cell Biology 3: 349–363.
32. Arora P, Narani N, McCulloch C (1999) The compliance of collagen gels regulates transforming growth factor-beta induction of alpha-smooth muscle actin in fibroblasts. American Journal of Pathology 154: 871–882.
33. Hinz B, Mastrangelo D, Iselin C, Chaponnier C, Gabbiani G (2001) Mechanical tension controls granulation tissue contractile activity and myofibroblast differentiation. American Journal of Pathology 159: 1009–1020.
34. Roy S, Biswas S, Khanna S, Gordillo G, Bergdall V, et al. (2009) Characterization of a preclinical model of chronic ischemic wound. Physiological Genomics 37: 211–224.
35. McGrath M, Simon R (1983) Wound geometry and the kinetics of wound contraction. Plastic and Reconstructive Surgery 72: 66–72.
36. Reina-Romo E, Gomez-Benito MJ, Garcia-Aznar JM, Dominguez J, Doblare M (2010) An interspecies computational study on limb lengthening. Proceedings of the Institution of Mechanical Engineers Part H-Journal of Engineering in Medicine 224: 1245–1256.
37. Bidan CM, Kommareddy KP, Rumpler M, Kollmannsberger P, Brechet YJM, et al. (2012) How linear tension converts to curvature: Geometric control of bone tissue growth. Plos One 7: e36336.
38. Radovanac K, Morgner J, Schulz JN, Blumbach K, Patterson C, et al. (2013) Stabilization of integrin-linked kinase by the hsp90-chip axis impacts cellular force generation, migration and the fibrotic response. Embo Journal 32: 1409–1424.
39. Bluestein D, Javaheri A (2008) Pressure ulcers: Prevention, evaluation, and management. American Family Physician 78: 1186–1194.
40. Gauglitz GG, Korting HC, Pavicic T, Ruzicka T, Jeschke MG (2011) Hypertrophic scarring and keloids: Pathomechanisms and current and emerging treatment strategies. Molecular Medicine 17: 113–125.
41. Aarabi S, Bhatt KA, Shi Y, Paterno J, Chang EI, et al. (2007) Mechanical load initiates hypertrophic scar formation through decreased cellular apoptosis. Faseb Journal 21: 3250–3261.
42. Ogawa R (2011) Mechanobiology of scarring. Wound Repair and Regeneration 19: S2–S9.
43. Guidry C (1992) Extracellular-matrix contraction by fibroblasts - peptide promoters and 2nd messengers. Cancer and metastasis reviews 11: 45–54.
44. Grinnell F (1994) Fibroblasts, myofibroblasts, and wound contraction. Journal of Cell Biology 124: 401–404.
45. Chiquet M, Reneda A, Huber F, Fluck M (2003) How do fibroblasts translate mechanical signals into changes in extracellular matrix production? Matrix Biology 22: 73–80.
46. Grinnell F (2003) Fibroblast biology in three-dimensional collagen matrices. Trends in cell biology 13: 264–269.
47. Grotendorst G, Seppa H, Kleinman H, Martin G (1981) Attachment of smooth-muscle cells to collagen and their migration toward platelet-derived growth-factor. Proceedings of the National Academy of Sciences of the United States of America-Biological Sciences 78: 3669–3672.

48. Desmouliere A, Redard M, Darby I, Gabbiani G (1995) Apoptosis mediates the decrease in cellularity during the transition between granulation-tissue and scar. American Journal of Pathology 146: 56–66.
49. Serini G, Gabbiani G (1999) Mechanisms of myofibroblast activity and phenotypic modulation. Experimental cell research 250: 273–283.
50. Roberts A, Sporn M, Assoian R, Smith J, Roche N, et al. (1986) Transforming growth factor type beta: rapid induction of fibrosis and angiogenesis in vivo and stimulation of collagen formation in vitro. Proceedings of the National Academy of Sciences of the United States of America 83: 4167–4171.
51. Khatyr F, Imberdis C, Vescovo P, Varchon D, Lagarde JM (2004) Model of the viscoelastic behaviour of skin in vivo and study of anisotropy. Skin Research and Technology 10: 96–103.

Supplementary Material

This work follows the model proposed by [1], based on the well established model of [2]. We consider the presence of two cellular species, fibroblasts (n) and its phenotype myofibroblasts (m), embedded in a collagen (ρ) matrix and guided by the presence of a chemical growth factor (c). The density of these species and substances together with the ECM displacements ($\mathbf{u}$) are the model variables.

Mechano-chemical model

The cellular species (fibroblasts and myofibroblasts) and chemical substances (growth factor and collagen) densities are obtained from a conservation law

$$\frac{\partial Q}{\partial t} + \nabla \cdot \mathbf{J}_Q = f_Q \tag{1}$$

where Q denotes the cellular/chemical species, $\mathbf{J}_Q$ denotes its net flux over the domain of interest (that may include terms due to random dispersal -migration or diffusion-, directed migration -chemotaxis-, but contains a passive convection term due to the extracellular matrix (ECM) deformation), and f_Q its net production. The matrix deformation is obtained from the conservation of linear momentum

$$\nabla \cdot \left(\boldsymbol{\sigma}_{ecm} + \boldsymbol{\sigma}_{cell}\right) = \mathbf{f}_{subs} \tag{2}$$

where $\boldsymbol{\sigma}_{ecm}$ denotes the passive resistant ECM stress, $\boldsymbol{\sigma}_{cell}$ the ECM stress due to the cells-ECM adhesions and $\mathbf{f}_{subs}$ the ECM-substrate anchoring forces resisting ECM deformation.

Species concentrations

Fibroblasts are connective tissue cells found in skin and the main cellular species involved in wound contraction. The main functions of fibroblasts are the synthesis of connective tissue in response to injury and the remodeling of the collagen extracellular matrix (ECM) by exerting traction forces on it [3]. Fibroblasts are motile cells whose migration is due to random dispersal, chemotaxis and passive convection caused by the ECM displacements. Hence, its net flux term can be written as

$$\mathbf{J}_n = -D_n \nabla n + \frac{a_n}{(b_n + c)^2} n \nabla c + n \frac{\partial \mathbf{u}}{\partial t}, \tag{3}$$

where all the parameters are listed in Table 1.

Fibroblasts production is due to proliferation, differentiation into myofibroblasts and differentiation back from myofibroblasts. We propose a similar expression to the one presented by [1] but with a different differentiation term. It is well known that fibroblasts sense the strains in the ECM [4], and the differentiation to myofibroblasts is regulated by mechanical loads [5–7]. Hence, we consider that the differentiation process is driven by the deformation of the tissue where the cells are allocated instead of depending on the mechanical stress of the matrix [8]. Moreover, the differentiation process is also enhanced by different growth factors (PDGF,TGF-β) [7, 9]. Hence, the fibroblasts net production is given by the expression

$$f_n = \Big(r_n + \frac{r_{n,max} c}{C_{1/2} + c}\Big) n \big(1 - \frac{n}{K}\big) - \frac{k_{1,max} c}{C_k + c} \theta^+ n + k_2 m. \tag{4}$$

Fibroblasts differentiate into myofibroblasts under the influence of TGF-β and this resulting phenotype is capable of exerting and maintaining higher contraction forces in the tissue [6]. We propose a new differentiation mechanism guided by the cells volumetric strain. We consider that fibroblasts are able to differentiate into myofibroblasts only when their volumetric strain is negative, that is, when fibroblasts

are under compression. In this situation cells are able to exert forces in the tissue. Myofibroblasts are smooth-muscle like cells [7], which means that they are not motile and its flux is uniquely due to passive convection and can be written as,

$$\mathbf{J}_m = m\frac{\partial \mathbf{u}}{\partial t}. \tag{5}$$

Myofibroblasts evolution is mainly due to proliferation, differentiation from fibroblasts and inverse differentiation to fibroblasts and apoptosis [10]. Hence, myofibroblasts net production can be written as follows

$$f_m = \epsilon_r\Big(r_n + \frac{r_{n,max}c}{C_{1/2}+c}\Big)m\big(1-\frac{m}{K}\big) + \frac{k_{1,max}c}{C_k+c}\theta^+ n - k_2 m. \tag{6}$$

Cells in the skin are embedded in the ECM, whose main components are the collagen fibers, which are produced by fibroblasts and myofibroblasts. Hence, we model the ECM density through the collagen density. Collagen fibers are non motile, and hence their net flux is expressed in terms of the passive convection of the skin

$$\mathbf{J}_\rho = \rho\frac{\partial \mathbf{u}}{\partial t}. \tag{7}$$

Following [2] we consider the role of fibroblasts and myofibroblasts on collagen synthesis [7, 11]. Furthermore, collagen production is enhanced by the presence of growth factors like TGF-β [12],

$$f_\rho = \Big(r_\rho + \frac{r_{\rho,max}c}{C_\rho+c}\Big)\frac{n+\eta_b m}{R_\rho^2+\rho^2} - d_\rho\big(n+\eta_d m\big)\rho. \tag{8}$$

The wound healing process is regulated by several growth factors. Collagen-matrix contraction is regulated by PDGF [5] among others and fibroblasts differentiation is driven by TGFβ [7]. In this work, we consider a unique generic growth factor that regulates these processes for simplicity. The net flux of growth factor is due to passive convection and diffusion through the tissue. This can be written as

$$\mathbf{J}_c = -D_c\nabla c + c\frac{\partial \mathbf{u}}{\partial t}. \tag{9}$$

The growth factor production is regulated by fibroblasts and myofibroblasts. Considering a simplification of the expression proposed by [2] and following [1] it can be written as

$$f_c = \frac{k_c(n+\zeta m)c}{\Gamma+c} - d_c c \tag{10}$$

where all the parameter values are included in Table 2.

Mechanosensing and mechanotransduction mechanism

This work proposes a new expression for calculating the stresses exerted by cells during wound healing. The new expression presented in the main manuscript is

$$\sigma_{cell} = p_{cell}(\theta)\,(n+\xi m)\,\mathbf{I} \tag{11}$$

where the traction force per cell, p_{cell}, is a function of the ECM volumetric deformation, θ. In this expression we consider the stiffening effect of the ECM through p_{cell}, that depends on the volumetric strain of the tissue [13]. Traction force per cell was introduced by Moreo et al. [13] and is defined as follows,

$$p_{cell}(\theta) = \frac{K_{act}p_{max}}{K_{act}\theta_1 - p_{max}}(\theta_1 - \theta)\chi_{[\theta_1,\theta^*]}(\theta) + \frac{K_{act}p_{max}}{K_{act}\theta_2 - p_{max}}(\theta_2 - \theta)\chi_{(\theta_1,\theta^*]}(\theta) + K_{pas}\theta \quad (12)$$

where all the parameters and their values are included in Table 3.

In this expression the two mechanisms that a cell uses to generate the stress are considered. The actin mechanism only actuates between some deformation limits, while the passive mechanism is always activated.

Initial distributions of cells and substances

Initial species distributions have been set according to experimental observations. The wound site is occupied by hematoma tissue with low mechanical stiffness and null cell population at the beginning of the analysis. However, we consider that the healthy tissue is saturated with fibroblasts, collagen and growth factor. Nevertheless, the initial density of myofibroblasts in the healthy tissue is zero, as they appear only where there has been damage.

Constitutive relation for the skin material

The skin was assumed as a viscoelastic material [1, 14]. For this kind of materials the passive resistant ECM stress $\boldsymbol{\sigma}_{ecm}$ is defined

$$\boldsymbol{\sigma}_{ecm} = \mu_1\frac{\partial\boldsymbol{\varepsilon}}{\partial t} + \mu_2\frac{\partial\theta}{\partial t}\mathbf{I} + \frac{E}{1+\nu}\Big(\boldsymbol{\varepsilon} + \frac{\nu}{1-2\nu}\theta\mathbf{I}\Big), \quad (13)$$

where the skin's Young's modulus (E) evolves following the expression $E = E_0\frac{\rho}{\rho_0}$, that considers a stiffer ECM as the collagen density increases. All the model parameters are listed in Table 3.

Model implementation

The problem has been solved using the finite element analysis and implemented using an Abaqus User Subroutine ®. Usual shape functions are used to interpolate the values of the primary unknowns (that is, n, m, ρ, c and $\mathbf{u}$) from their nodal values. Time derivatives are approximated using a generalized trapezoidal method.

Weak formulation

Equations (7) and (11) can be written equivalently using Gauss' theorem to obtain the weak formulation of the problem

$$\int_\Omega \frac{\partial Q}{\partial t}\upsilon_Q d\Omega - \int_\Omega \mathbf{J}_Q\cdot\nabla\upsilon_Q d\Omega = \int_\Omega f_Q\upsilon_Q d\Omega - \int_{\partial\Omega}\mathbf{J}_Q\cdot\mathbf{n}_\perp\upsilon_Q d\Gamma \quad (14)$$

$$\int_\Omega \boldsymbol{\sigma} : \frac{1}{2}\Big(\nabla\boldsymbol{\upsilon} + \nabla\boldsymbol{\upsilon}^T\Big)d\Omega = \int_\Omega \mathbf{f}_{subs}\cdot\boldsymbol{\upsilon}d\Omega + \int_{\partial\Omega}\mathbf{t}\cdot\boldsymbol{\upsilon}d\Gamma \quad (15)$$

where $\boldsymbol{\sigma}$ denotes the sum of $\boldsymbol{\sigma}_{ecm}$ and $\boldsymbol{\sigma}_{cell}$. υ_Q and $\boldsymbol{\upsilon}$ represent the weighting functions and $\mathbf{n}_\perp$ denotes the normal vector pointing outwards Ω and $\mathbf{t} := \boldsymbol{\sigma}\mathbf{n}_\perp$ denotes the tension vector. it is possible to obtain the weak formulation.

System of equations nonlinearly coupled

The model primary unknowns can be written as a function of the shape functions and their nodal values

$$Q^h(\mathbf{x},t) = \mathbf{N}_Q(\mathbf{x})\mathbf{Q}(t), \quad \mathbf{u}^h(\mathbf{x},t) = \mathbf{N}_\mathbf{u}(\mathbf{x})\mathbf{U}(t), \tag{16}$$

where the superscript h denotes the finite element solution. The fully discrete and nonlinear algebraic system of equations is found when substituting the above expressions in the weak form (14) and (15). We choose the weighting functions equal to shape functions. Denoting the time-dependent values of the primary variables as $\mathbb{Z}$

$$\mathbb{Z} = \left(\mathbf{n}^T\ \mathbf{m}^T\ \boldsymbol{\rho}^T\ \mathbf{c}^T\ \mathbf{U}^T\right)^T, \tag{17}$$

the system of equations can be expressed as a balance of internal and external forces as follows:

$$\mathbb{F}\big(\mathbb{Z}_{n+1}\big) := \mathbb{F}^{int}\big(\mathbb{Z}_{n+1}\big) - \mathbb{F}^{ext}\big(\mathbb{Z}_{n+1}\big) = \mathbf{0}, \tag{18}$$

where the subscript $n+1$ denotes the time step on which the solution is being computed. Moreover, forces $\mathbb{F}^{int}$ and $\mathbb{F}^{ext}$ can be written in a vectorial form

$$\mathbb{F}^{int} = \Big[(\mathbf{F}_n^{int})^T\ (\mathbf{F}_m^{int})^T\ (\mathbf{F}_\rho^{int})^T\ (\mathbf{F}_c^{int})^T\ (\mathbf{F}_\mathbf{u}^{int})^T\Big]^T \tag{19}$$

$$\mathbb{F}^{ext} = \Big[(\mathbf{F}_n^{ext})^T\ (\mathbf{F}_m^{ext})^T\ (\mathbf{F}_\rho^{ext})^T\ (\mathbf{F}_c^{ext})^T\ (\mathbf{F}_\mathbf{u}^{ext})^T\Big]^T \tag{20}$$

where

$$\mathbf{F}_n^{int} = \int_\Omega \mathbf{N}_n^T \frac{\partial n}{\partial t}\, d\Omega + \int_\Omega \nabla \mathbf{N}_n^T \Big[D_n \nabla n - \frac{a_n}{(b_n+c)^2} n \nabla c - n\frac{\partial \mathbf{u}}{\partial t}\Big]\, d\Omega \tag{21}$$

$$\mathbf{F}_m^{int} = \int_\Omega \mathbf{N}_m^T \frac{\partial m}{\partial t} d\Omega - \int_\Omega \nabla \mathbf{N}_m^T m \frac{\partial \mathbf{u}}{\partial t} d\Omega \tag{22}$$

$$\mathbf{F}_\rho^{int} = \int_\Omega \mathbf{N}_\rho^T \frac{\partial \rho}{\partial t} d\Omega - \int_\Omega \nabla \mathbf{N}_\rho^T \rho \frac{\partial \mathbf{u}}{\partial t} d\Omega \tag{23}$$

$$\mathbf{F}_c^{int} = \int_\Omega \mathbf{N}_c^T \frac{\partial c}{\partial t} d\Omega + \int_\Omega \nabla \mathbf{N}_c^T \Big[D_c \nabla c - c\frac{\partial \mathbf{u}}{\partial t}\Big] d\Omega \tag{24}$$

$$\mathbf{F}_\mathbf{u}^{int} = \int_\Omega \mathbf{B}_\mathbf{u}^T \Big[\mathbf{D}_{elas}\frac{\rho}{\rho_0}\mathbf{B}_\mathbf{u}\mathbf{U} + \mathbf{D}_{visco}\mathbf{B}_\mathbf{u}\dot{\mathbf{U}} + p_{cell}(\theta)(n+\xi m)\mathbf{I}\Big] d\Omega \tag{25}$$

and

$$\begin{aligned}
\mathbf{F}_n^{ext} &= \int_\Omega \mathbf{N}_n^T \Big[\Big(r_n + \frac{r_{n,max}c}{C_{1/2}+c}\Big) n\big(1-\frac{n}{K}\big) - \frac{k_{1,max}c}{C_k+c}\theta^+ n + k_2 m\Big]\, d\Omega \\
\mathbf{F}_m^{ext} &= \int_\Omega \mathbf{N}_m^T \epsilon_r \Big(r_n + \frac{r_{n,max}c}{C_{1/2}+c}\Big) m\big(1-\frac{m}{K}\big) + \int_\Omega \mathbf{N}_m^T \frac{k_{1,max}c}{C_k+c}\theta^+ n d\Omega \\
&\quad - \int_\Omega \mathbf{N}_m^T \Big[k_2 m\Big] d\Omega
\end{aligned} \tag{26}$$

$$\mathbf{F}_\rho^{ext} = \int_\Omega \mathbf{N}_\rho^T \Big[\Big(r_\rho + \frac{r_{\rho,max}c}{C_\rho+c}\Big)\frac{n+\eta_b m}{R_\rho^2+\rho^2} - d_\rho\big(n+\eta_d m\big)\rho\Big] d\Omega \tag{27}$$

$$\mathbf{F}_c^{ext} = \int_\Omega \mathbf{N}_c^T \Big[\frac{k_c(n+\zeta m)c}{\Gamma+c} - d_c c\Big] d\Omega \tag{28}$$

$$\mathbf{F}_\mathbf{u}^{ext} = -\int_\Omega \mathbf{N}_\mathbf{u}^T s\rho\mathbf{u} d\Omega \tag{29}$$

The solution of the nonlinear system of equations is obtained using a standard Newton-Raphson method

References

1. Javierre E, Moreo P, Doblare M, Garcia-Aznar JM (2009) Numerical modeling of a mechano-chemical theory for wound contraction analysis. International Journal of Solids and Structures 46: 3597-3606.

2. Olsen L, Sherratt JA, Maini PK (1995) A mechanochemical model for adult dermal wound contraction and the permanence of the contracted tissue displacement profile. Journal of theoretical biology 177: 113-128.

3. Grinnell F (1994) Fibroblasts, myofibroblasts, and wound contraction. Journal of Cell Biology 124: 401-404.

4. Chiquet M, Reneda A, Huber F, Fluck M (2003) How do fibroblasts translate mechanical signals into changes in extracellular matrix production? Matrix Biology 22: 73-80.

5. Grinnell F (2000) Fibroblast-collagen-matrix contraction: growth-factor signalling and mechanical loading. Trends in cell biology 10: 362-365.

6. Grinnell F (2003) Fibroblast biology in three-dimensional collagen matrices. Trends in cell biology 13: 264-269.

7. Tomasek J, Gabbiani G, Hinz B, Chaponnier C, Brown R (2002) Myofibroblasts and mechano-regulation of connective tissue remodelling. Nature Reviews Molecular Cell Biology 3: 349-363.

8. Hinz B, Mastrangelo D, Iselin C, Chaponnier C, Gabbiani G (2001) Mechanical tension controls granulation tissue contractile activity and myofibroblast differentiation. American Journal of Pathology 159: 1009-1020.

9. Grotendorst G, Seppa H, Kleinman H, Martin G (1981) Attachment of smooth-muscle cells to collagen and their migration toward platelet-derived growth-factor. Proceedings of the National Academy of Sciences of the United States of America-Biological Sciences 78: 3669-3672.

10. Desmouliere A, Redard M, Darby I, Gabbiani G (1995) Apoptosis mediates the decrease in cellularity during the transition between granulation-tissue and scar. American Journal of Pathology 146: 56-66.

11. Serini G, Gabbiani G (1999) Mechanisms of myofibroblast activity and phenotypic modulation. Experimental cell research 250: 273-283.

12. Roberts A, Sporn M, Assoian R, Smith J, Roche N, et al. (1986) Transforming growth factor type beta: rapid induction of fibrosis and angiogenesis in vivo and stimulation of collagen formation in vitro. Proceedings of the National Academy of Sciences of the United States of America 83: 4167-4171.

13. Moreo P, Garcia-Aznar JM, Doblare M (2008) Modeling mechanosensing and its effect on the migration and proliferation of adherent cells rid f-8256-2010. Acta Biomaterialia 4: 613-621.

14. Tranquillo R, Murray J (1992) Continuum model of fibroblast-driven wound contraction - inflammation-mediation. Journal of theoretical biology 158: 135.

Work 5: Modeling anisotropic wound healing: effect of the relative position of wounds with respect to collagen fibers orientation

Journal: *Journal of the Mechanics and Physics of Solids*. Submitted.
Journal Impact factor: 3.406

Contribution of the author of the thesis: the author was in charge of rewriting the formulation for the three-dimensional element, making a review of the existing literature, implementing the new material model, performing all the computational simulations, analyzing the results and determining their implications. Everything was done under the supervision of the other authors. This work was partially performed during a research stay in TU Dortmund (Germany).

Available online at www.sciencedirect.com

ScienceDirect

Journal of the Mechanics and Physics of Solids 00 (2014) 1–12

Modeling anisotropic wound healing: effect of the relative position of wounds with respect to collagen fibers orientation

C. Valero [1a], E. Javierre[b], J.M. García-Aznar[a], M.J. Gómez-Benito[a], A. Menzel[c,d]

[a] *Multiscale in Mechanical and Biological Engineering (M2BE), Aragón Institute of Engineering Research (I3A), University of Zaragoza, Zaragoza, Spain*
[b] *Centro Universitario de la Defensa, Academia General Militar, Zaragoza, Spain*
[c] *Institute of Mechanics, TU Dortmund, Germany*
[d] *Division of Solid Mechanics, Lund University, Sweden*

Abstract

Biological soft tissues exhibit non-linear complex properties that are difficult to quantify. Nevertheless, these properties highly influence different processes that take place in soft tissues and thus its correct identification is crucial to understand them. In both cases, experimental and computational works are needed in order to find the most precise model to replicate the tissues properties. In this work, we present an angiogenesis and wound contraction model in three dimensions that relies on the accurate representation of the mechanical behavior of the skin. Thus, an anisotropic hyperelastic model has been considered to analyze the effect of fiber orientation on the evolution of a healing wound. The implemented model accounts for the contribution of the ground matrix and two families of fibers. Results show that wound volume evolution is hardly influenced by the orientation of the wound with respect to the fibers. However, the strain distributions show pronounced differences depending on the wound relative orientation. Hence, effects such as skin deformation while movement (for instance due to walking) may strongly contribute to enlarge the observed differences. .

Keywords:
Finite Elements, anisotropic hyperelastic, wound healing, angiogenesis, collagen fibers

1. Introduction

Skin covers the entire human body and thus, keeping its integrity is crucial for human living. The two most external layers of the skin are the epidermis and the dermis and they are made of a ground substance and embedded collagen fibers. These collagen fibers are the component that support most of the mechanical loads of the skin. The mechanical properties of the skin decrease when an injury occurs and a wound appears. The regeneration of the skin properties occurs during wound healing, a physiological process that is usually divided into three overlapped stages: inflammation, epithelialization and remodeling.

During the inflammatory stage, inflammatory factors that stimulate cell activity are released and inflammatory cells such as macrophages eliminate strange particles [1]. During this stage the normal oxygen supply is not possible

[1] Corresponding author at: Multiscale in Mechanical and Biological Engineering (M2BE), Aragón Institute of Engineering Research (I3A), University of Zaragoza, Zaragoza, Spain.
E-mail address: claraval@unizar.es (C. Valero).

due to capillaries that were disrupted during injury have not yet been repaired [2]. The formation of new blood vessels from the pre-existing ones is called angiogenesis and it takes place during the epithelialization stage. It allows to re-establish the oxygen supply, necessary for cell activity. This stage is characterized by the contraction of the wound due to the stress generated by cells, mainly fibroblasts and myofibroblasts [3]. These cellular species are the responsible of the new collagen secretion. As long as healing advances, collagen form fibers, initially dispersed, that align with skin stress lines. Protein fibers are embedded on a ground substance, made of proteoglicans and fibronectins [4], which helps cells to move through the fibers. Collagen fibers align in the skin following the stress lines or Langer lines, which are present in the body surface and were discovered by Langer [5]. Langer [5] performed circular cuts in the skin in all the body surface, finding that these cuts turned into ellipses aligned with tension lines when the skin relaxed. The orientation of these cuts defined the natural orientation of collagen fibers, usually parallel to the underlying muscles.

Skin's mechanical properties varies with different factors. This variation really influences healing when a wound occurs. One of the governing factors is collagen density and its organization. Collagen is one of the main proteins that constitutes the skin and it usually forms fibers that aligns with the skin stress lines or Langer lines [5]. Most of the mechanical properties of the skin are due to the fibers, which have an elastic modulus of 150-300 kPa [6], and compose the extracellular matrix (ECM).

There are a number of experimental works focused on the determination of the mechanical properties of the skin. Although it is clear that this behavior is not linear, there are discrepancies about considering the skin a viscoelastic or hyperelastic material. Some experimental works have characterized the skin as a viscoelastic material [7, 8]. Nevertheless, a large number of experimental works have demonstrated that the hyperelastic approach is most suitable to reproduce the skin behavior. Flynn et al. [9] measured in-vivo the force-displacement response in the forearm skin when three-dimensional deformations were applied. Later, they found the material parameters that fit the Ogden hyperelastic model and the Tong and Fung model [10]. Gahagnon et al. [11] studied the anisotropy of forearm skin in-vivo using elastographic tests. They stretched the skin parallel and perpendicularly to Langers lines finding anisotropic behavior.

In-vivo assays to determine the skin properties are difficult to perform and show a high variability between subjects. The wide range of values obtained is due to the different anatomical locations of the skin, the attachment of the dermis to the underlying tissue and patient specific characteristics, which makes difficult to find a unique characterization valid for every skin.

A useful alternative to in-vivo assays is in-vitro experiments. In-vivo studies provide information about the skin in its natural environment, without eliminating natural processes, while in-vitro studies allow to perform more controlled experiments, where different aspects can be isolated and more destructive essays can be performed. Hyperelastic characterization of the skin has been also obtained from in-vitro studies. Annaidh et al. [12] investigated the influence of location and orientation of the skin on its properties, focusing on skin anisotropy. They performed in-vitro tensile tests to human skin samples obtained from different parts of the back, finding a correlation between the orientation of Langer lines and collagen fibers Annaidh et al. [13]. They fit their results with the hyperelastic model developed by Gasser et al. [14]. Groves et al. [15] used tensile test on circular human skin specimens to measure the skin properties. To find skin anisotropy they performed tests along three different load axes. They found that skin has anisotropic hyperelastic behavior and used the model defined by Weiss et al. [16] to characterize it. Moreover, it must be noted that the mechanical properties of the skin vary depending on the anatomical location, orientation and depth but also on the age; skin turn to be less elastic with time and loses its recovery capacity [17].

Having accurate skin properties is highly important for studying processes like wound healing, experimentally and computationally. Wound healing models have been broadly proposed during the last decades. The first wound healing model was developed by Sherratt and Murray [18] and only included the effect of cells guided by a chemical attractant factor. It was later extended by Tranquillo and Murray [19] who included the mechanical behavior of the skin, being the first work to simulate wound contraction. This model has been extended and modified by multiple authors [20, 21, 22, 23, 3]. On the other hand, a number of angiogenesis in wound healing models have been also developed [24, 25, 26, 27, 28, 29, 30, 31, 32]. In this work we extend to three dimensions a model previously developed which considers angiogenesis and wound contraction [32].

It is well established that wound healing is highly influenced by the mechanical properties of the surrounding skin. Although different mechanochemical models have been proposed to simulate wound healing, these have been focused on the interaction between biochemical species and the deformation of a linear elastic extracellular matrix, and little

(or no) attention has been paid to the role that the mechanical properties of the surrounding undamaged skin may have on the outcome of healing. Thus, this work focuses on the coupling of an anisotropic hyperelastic model for the skin with a previously developed mechanobiological model of healing that includes angiogenesis and wound contraction [32]. The model is implemented in three spatial dimensions, which eliminates previously considered simplifications on the wound morphology or the mechanical behavior of the tissues, and it is used to determine the influence of wound orientation with respect to the skin collagen fibers.

2. Materials and methods

In this work we present the evolution of angiogenesis and contraction during wound healing in the skin coupled with a complex constitutive behavior of the healthy skin. Thus, the angiogenesis and contraction model presented in [32] is extended to three spatial dimensions. In this extension, the mechanical constitutive model of the skin is updated to cope with anisotropic effects coming from the orientation of two families of collagen fibers. To this end, we adopt the anisotropic hyperelastic material model presented in [14]. Although this material model was originally proposed to simulate arterial tissue, it can also be used to represent other biological tissues. Thus, Annaidh et al. [12, 13] performed in-vitro experiments with human skin to find the parameters values that fit the constitutive model.

The model can be divided into three major components that are interconnected. On the one hand, there is the coupling of the angiogenesis model, which is mainly driven by the interplay of the oxygen availability, an angiogenic factor and the endothelial cells throughout the tissue, and the healing model, which is driven by the fibroblasts kinetics. On the other hand, we have the traction forces that cells (fibroblasts in this case) exert on the surrounding tissue. Finally, to complete the model we have the constitutive law of the skin material model that controls the contraction of the wound. Each of these modules is described in detail below.

2.1. Biochemical model

The biochemical part of the model reproduces the angiogenesis process and the replacement of the fibrin clot formed during inflammation with a fibroblast-rich extracellular matrix.

Angiogenesis consists on the formation of new blood vessels from the pre-existing ones that were disrupted when the wound occurred. Following [21, 32], we consider that the most relevant factors in this process are the oxygen concentration, the presence of angiogenic factors and the density of endothelial cells. In order to provide a simplified model, we assume that the role of all the involved angiogenic factors can be represented by the macrophage derived growth factor (MDGF), and that the density of endothelial cells can be identified with the density of capillaries through the tissue. Thus, the principal variables of the model are the concentration of oxygen (u_1) and MDGF (u_2), and the density of capillaries (u_3). The time evolution of these species is modeled through reaction-diffusion equations.

Oxygen concentration (u_1) varies because of passive convection (due to the tissue deformation), diffusion and chemical decay. Moreover, oxygen kinetics include the capillaries supply of oxygen. Thus, the oxygen concentration can be formulated as

$$\frac{\partial u_1}{\partial t} + \nabla \cdot \left(u_1 \frac{\partial \mathbf{u}}{\partial t} \right) = D_1 \nabla^2 u_1 + \lambda_{3,1} u_3 - \lambda_{1,1} u_1 \tag{1}$$

where ($\mathbf{u}$) denotes the tissue displacements.

The MDGF concentration (u_2) follows an equivalent equation due to diffusion, chemical decay, passive convection and production,

$$\frac{\partial u_2}{\partial t} + \nabla \cdot \left(u_2 \frac{\partial \mathbf{u}}{\partial t} \right) = D_2 \nabla^2 u_2 + \lambda_{1,2} P(u_1) - \lambda_{2,2} u_2, \tag{2}$$

where the production of MDGF, is formulated through the term $\lambda_{1,2} P(u_1)$. Macrophages appear on locations with low oxygen concentration, and the production of MDGF is inhibited once the oxygen density is restored. Hence, this dependence of MDGF on oxygen availability is modeled through the function $P(u_1)$, defined as,

$$P(u_1) = \begin{cases} 1 - \frac{u_1}{u_1^{\beta_2}} & if \quad u_1 < u_1^{\beta_2}; \\ 0 & otherwise, \end{cases} \tag{3}$$

Parameter	Description	Dimensionless value	Reference
D_1	Oxygen diffusion rate	$4.32{\cdot}10^{-3}$	[26]
$\lambda_{3,1}$	Oxygen production rate caused by the capillary	0.864	[26]
$\lambda_{1,1}$	Oxygen consumption rate	0.864	[26]
D_2	MDGF diffusion rate	0.0864	[26]
$\lambda_{1,2}$	MDGF production rate in hypoxia state	2.592	[32]
$\lambda_{2,2}$	MDGF death rate	0.864	[26]
D_3	Capillary diffusion rate	$4.32{\cdot}10^{-3}$	[32]
$\lambda_{3,2}$	Capillary production rate	1	[32]
$\lambda_{3,3}$	Capillary production rate	1	[32]
u_3^{eq}	Maximal capillary density	1.0	[26]
D_n	Fibroblasts diffusion rate	$2{\cdot}10^{-2}$	[21]
$\lambda_{n,n}$	Fibroblasts death rate	0.7488	[21]
r_n	Maximal rate of fibroblasts proliferation	0.832	[21]
K	Fibroblasts maximal capacity in dermis	10.0	[21]
$u_1^{\beta_2}$	Oxygen concentration below which MDGFs are produced	0.25	[33]

Table 1. List of normalized model parameters related to the biochemical model.

where $u_1^{\beta_2}$ denotes the oxygen concentration below which MDGFs are produced.

The capillaries density (u_3) is modeled as a classical logistic growth equation with passive convection and with a growth rate that is enhanced with the density of MDGF

$$\frac{\partial u_3}{\partial t} + \nabla \cdot \left(u_3 \frac{\partial \mathbf{u}}{\partial t} \right) = D_3 \nabla^2 u_3 + (\lambda_{3,2} u_2 + \lambda_{3,3}) u_3 \left(1 - \frac{u_3}{u_3^{eq}} \right), \tag{4}$$

where u_3^{eq} is the maximal capillary density in the non-damaged skin.

Finally, the healing of the wound can be addressed from the evolution of the fibroblast density *(n)*. Fibroblast evolution is modeled with a logistic growth equation with passive convection, where the fibroblast proliferation rate is dependent on the oxygen concentration

$$\frac{\partial n}{\partial t} + \nabla \cdot \left(n \frac{\partial \mathbf{u}}{\partial t} \right) = D_n \nabla^2 n + r_n u_1 n \left(1 - \frac{n}{K} \right) - \lambda_{n,n} n. \tag{5}$$

Under this hypothesis, healing cannot proceed in absence of oxygen and it is delayed until angiogenesis is (locally) completed.

A complete description of the parameters introduced in the biochemical model is given in Table 1

2.2. Cellular mechanical model

We follow the model of cell induced stresses given in [3] neglecting the contribution of myofibroblasts, since myofibroblasts are not directly included in the angiogenesis model, although their effect is considered by an enhancement of the stress inside the wound. Hence, the fibroblast exerted stresses is given by

$$\sigma_{cell} = p_{cell}(\theta) n \mathbf{I}, \tag{6}$$

where $p_{cell}(\theta)$ depends on the volumetric strain of the ECM. This variable, $p_{cell}(\theta)$, represents the net stress of one fibroblast cell per unit of ECM matrix [34] defined as

$$p_{cell}(\theta) = \begin{cases} K_{pas}, \theta & if \quad \theta < \theta_1 \\ \frac{K_{act} p_{max}}{K_{act}\theta_1 - p_{max}} (\theta_1 - \theta) + K_{pas}\theta, & if \quad \theta_1 \le \theta \le \theta^* \\ \frac{K_{act} p_{max}}{K_{act}\theta_2 - p_{max}} (\theta - \theta_2) + K_{pas}\theta, & if \quad \theta^* < \theta \le \theta_2 \\ K_{pas}\theta, & if \quad \theta > \theta_2, \end{cases} \tag{7}$$

Parameter	Description	Dimensionless value	Reference
p_{max}	maximal cellular active stress per unit of ECM	1	[32]
K_{pas}	volumetric stiffness moduli of the passive components of the cell	$2{\cdot}10^{-1}$	[34]
K_{act}	volumetric stiffness moduli of the actin filaments of the cell	1	[34]
θ_1	shortening strain of the contractile element	-0.6	[21]
θ_2	lengthening strain of the contractile element	0.5	[34]

Table 2. List of normalized model parameters related to the cellular mechanical model.

where θ_1 and θ_2 are the threshold values for the volumetric strain denoting the compression and traction limits within the active part of the cell machinery works. Finally, θ^* is defined as $\theta^* = p_{max}/K_{act}$.

A complete description of the parameters introduced in the cellular mechanical model is given in Table 2.

2.3. Constitutive material model

Skin is modeled as an anisotropic hyperelastic material following [14], which is based on the constitutive law developed by Holzapfel [35], but incorporates the effect of the collagen fibers dispersion κ in the strain energy density function. Furthermore, it has been found that there are two collagen fiber families in the skin [12], whose direction is defined by the mean orientation γ (see Figure 1). With all this in mind, the strain energy density function of the skin $\overline{\mathbf{\Psi}}$ can be decomposed as the sum of the contributions from the ground matrix $\overline{\mathbf{\Psi}}_g$ and the fiber families ($\overline{\mathbf{\Psi}}_{fi}$, i=1,2)

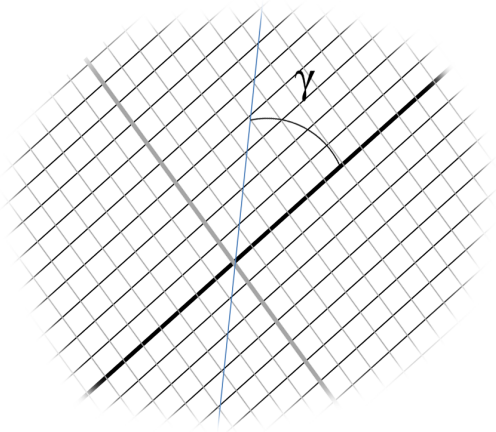

Figure 1. Orientation of the two collagen fibers families.

$$\overline{\mathbf{\Psi}}(\overline{\mathbf{C}}, \mathbf{H}_i) = \overline{\mathbf{\Psi}}_g(\overline{\mathbf{C}}) + \sum_{i=1}^{2} \overline{\mathbf{\Psi}}_{fi}(\overline{\mathbf{C}}, \mathbf{H}_i(\mathbf{a}_{0i}, \kappa)) \tag{8}$$

where $\overline{\mathbf{C}}$ is the symmetric modified right Cauchy-Green tensor [36], $\mathbf{a}_{0i}$ denotes the unit tensor that defines the fiber orientation and $\mathbf{H}_i$ is a symmetric tensor that represents the fiber distribution [35].

The strain energy density function of the ground matrix corresponds to an isotropic neo-Hookean model,

$$\overline{\mathbf{\Psi}}_g = \frac{1}{2} c(\bar{I}_1 - 3) + \frac{1}{D}(J_{el} - 1)^2, \tag{9}$$

Parameter	Description	Value	Reference
c	Material parameter	0.1007 MPa	[12]
D	Compressibility material parameter	0.3766	Estimated
k_1	Material parameter related to the initial stiffening stage	49.06 MPa	[12]
k_2	Material parameter related to the latter stiffening stage	0.1327	[12]
κ	Dispersion factor of the collagen fibers	0.1404	[12]
γ	Mean orientation of the collagen fibers	42º	[12]

Table 3. Parameter values of the hyperelastic material model.

where J_{el} represents the elastic volume ratio, c and D are material constants and $\bar{I}_1$ denotes the first invariant of the isochoric part of the right Cauchy strain tensor of the ground matrix material

$$\bar{I}_1 = tr\overline{\mathbf{C}}. \tag{10}$$

The strain energy of the fiber families $\overline{\mathbf{\Psi}}_{fi}$ (i=1,2) provides the anisotropic component to the material, and is given by

$$\overline{\mathbf{\Psi}}_{fi}(\overline{\mathbf{C}}, \mathbf{H}_i) = \frac{k_1}{2k_2}[exp\{k_2[\kappa\bar{I}_1 + (1-3\kappa)\bar{I}_{4i} - 1]^2\} - 1], \quad i = 1, 2 \tag{11}$$

The parameter κ is used to measure the degree of dispersion or anisotropy of the families, and it varies its value from totally anisotropic ($\kappa = 0$) to isotropic ($\kappa = 1/3$). Moreover, $\bar{I}_{4i}$ is an anisotropic invariant equal to the square of the stretch in the direction of $\mathbf{a}_{0i}$, associated to each family of fibers

$$\bar{I}_{4i} = \mathbf{a}_{0i} \otimes \mathbf{a}_{0i} : \overline{\mathbf{C}}. \tag{12}$$

A complete description of the parameters introduced in the constitutive material model is given in Table 3.

2.4. Implementation

The simulated domain is a three-dimensional cube with two distinct parts: the wound and the surrounding tissue. The material model above-explained is being implemented to reproduce the behavior of the wound and the surrounding healthy tissue. We assume that fibers are not being formed inside the wound in the time frame that we simulate (up to 30 days after wounding). Hence their concentration -inside the wound- remains low and when they begin to appear they are isotropically dispersed. Thus, the wound is considered to be composed only by the ground substance, and the newly created tissue inside the wound is less stiff than the usual healthy tissue. The lower properties of the new tissue drives higher deformations caused by cells force generation than the ones that would appear in healthy tissue.

The studied geometry is a semi-ellipsoidal wound of 8 cm length, 2cm width and 2 cm depth (Figure 2) surrounded by healthy tissue. Due to the wound dimensions, it can not be considered as a planar wound or a deep wound and thus plane stress or plane strain approaches are not suitable. In this case, the whole wound geometry has been simulated. Note, moreover, that skin anisotropy would not be observed if geometric symmetry simplifications were taken.

Regarding the numerical implementation of the complete model, an approach similar to [32] was followed. The Finite Element Method was used to discretize the governing equations, and the time integration of the mechanical and biochemical modules were decoupled in the implementation due to the different timescales to which they respond. The biochemical model was solved at time increments of 0.1 days. When necessary, the cell-induced stresses (σ_{cell}) were computed at the end of the biochemical step and transferred to the mechanical step to obtain the tissue displacements ($\mathbf{u}$) and volumetric deformation (θ). The computational domain was the updated (using a Lagrangian approach) and

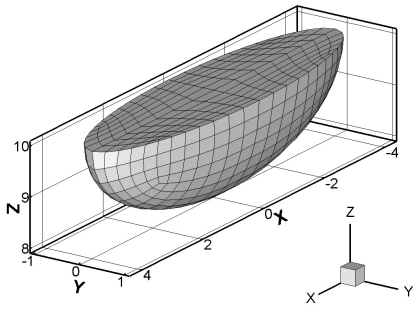

Figure 2. Wound geometry at the initial time.

the control was returned to biochemical step. This procedure was repeated until the final simulation time was reached. The interested reader is referred to [32] to find a more detailed description of the implementation.

In order to study the influence of wound location with respect to collagen fibers, we analyze the wound in two different relative positions. In one of them, the longitudinal axis of the wound is aligned with the middle direction of the fibers, while in the other case the longitudinal axis of the wound is aligned with one family of the fibers (see Figure 3).

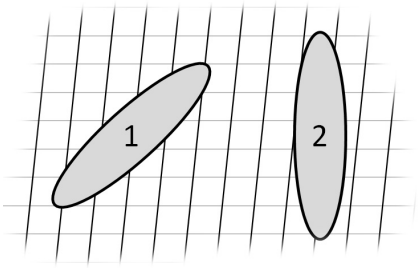

Figure 3. Location of wounds in relation to the collagen fibers, viewed from the top.

3. Results

We evaluate the performance of the proposed model through two sets of results. First we address the temporal and spatial evolution of the biochemical species driving angiogenesis and wound repair for a fixed wound. Subsequently we address the evolution of the wound volume and the spatial distribution of the tissue deformation when the wound orientation (relative to the collagen fibers) is changed. The first set of result allows us to check that the healing kinetics is captured accurately, while the second one allows us to elucidate the role of skin anisotropy on the evolution of the wound. To this end, we follow the semi-ellipsoidal wound described above during a time-frame of 30 days.

The healing kinetics is evaluated first at the *center of the wound*. The center of the wound is defined as the center point of the wound surface. The temporal evolution of the biochemical species on this point is presented in (Figure 4). We find that capillaries, and subsequently oxygen, fill the wound tissue fast, allowing to re-establish the regular oxygen flow around day 10. Moreover, MDGF shows a rapid kinetics, with a maximal concentration around day 2.5 followed by a gradual decay as oxygen flow goes back to normal. MDGF concentration is completely extinguished after day 10. Finally, we observe that fibroblasts fill in the wound slower than oxygen and capillaries because of their necessity of oxygen to function. A steady level on the fibroblasts density is not reached after 30 days.

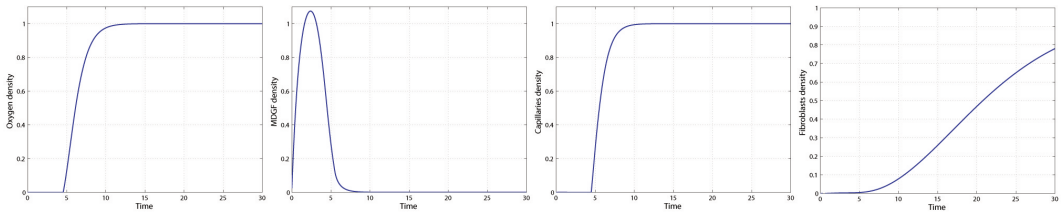

Figure 4. Evolution of the model variables in the wound centre.

In addition to this point-wise characterization of healing, a more general measure of healing is also provided. Figure 5 presents the fibroblast distribution over the wound and also across four different cross-sections at different times (days 0, 10, 20 and 30). These cross-sections are placed at distances 0, 1, 2 and 3 cm from the symmetry transversal plane, as highlighted in Figure 5. Initially there are not fibroblasts inside the wound. This is modeled with a smoothly varying density function, being null at the wound center, gradually increasing towards the wound surface and reaching the density of undamaged skin outside the wound. Density images show how fibroblasts fill the wound as time evolves. This evolution is more clearly seen on the cross-section plots. In all the cases we observe that wound healing is due to fibroblast influx from the wound surface (fibroblast density is always higher on the wound surface than in the wound center). More interestingly, the fibroblast density of undamaged tissue (i.e. the actual healing) is reached earlier in time as the section distance from the middle plane increases. This is due to the decrease on both wound width and depth, and it is certainly related to the density gradients on those directions. Furthermore, the faster healing away from the wound middle section indicates that wound healing of an elongated wound proceeds as *zip fastener*, being initiated on the extremes and progressing towards the center.

Furthermore, the cross-section plots in Figure 5 also give valuable insights into the wound deformation over time. It is clearly seen that the most notable contraction of the wound is due to the retraction of the wound upper surface and not by the contraction of the wound surface in contact with the undamaged tissue.

In order to complete the analysis of the wound healing kinetics, the cell-induced stresses (σ_{cell}) at the chosen times (0, 10, 20 and 30 days post wounding) are presented in Figure 6. Results show that stresses on the undamaged tissue remain unchanged, while stresses inside the wound increase in time (from the wound surface indwards) as fibroblast infiltrate the wound.

Finally, the role of skin anisotropy is discussed. To this end, the wound relative orientation with respect the two families of collagen fibers is changed (see Figure 3). The temporal evolution of the wound volume for the two considered wound locations is presented in Figure 7. Independently of the wound location (relative to fibers orientation), we observe the initial distraction of the wound followed by its gradual contraction over time. This observation agrees with experimental results [37, 38]. In the distraction step, the wound volume increases around 2%, which gives an overall wound contraction of the 10% (relative to its initial volume). We also observe that, for the set of parameters used in the simulation, the overall evolution of the wound is (apparently) hardly affected by its relative position to the collagen fibers.

If we turn into the volumetric deformation of the tissue (Figure 8), we observe different profiles depending on the relative orientation of the wound. Results demonstrate that volumetric deformation follows the fiber directions, i.e. the distraction is higher in the fibers directions. Nevertheless, the local strains are not high enough to make a significant difference in the global contraction of the wound.

4. Discussion

Biological tissues present anisotropic mechanical properties that regulate physiological processes. In this work, the combined effect of angiogenesis and wound contraction has been evaluated on three-dimensional wounds. Although skin has been traditionally assumed to behave as a viscoelastic material in mathematical models [19, 20, 39, 33, 21, 30, 22, 31, 40, 23, 32] the assumption of a hyperelastic material helps in the development of more realistic models. Moreover, characteristics such as anisotropy, that are clearly observed in experimental works give an additional realistic degree. Thus, in this work, an anisotropic hyperelastic material has been chosen to simulate the skin.

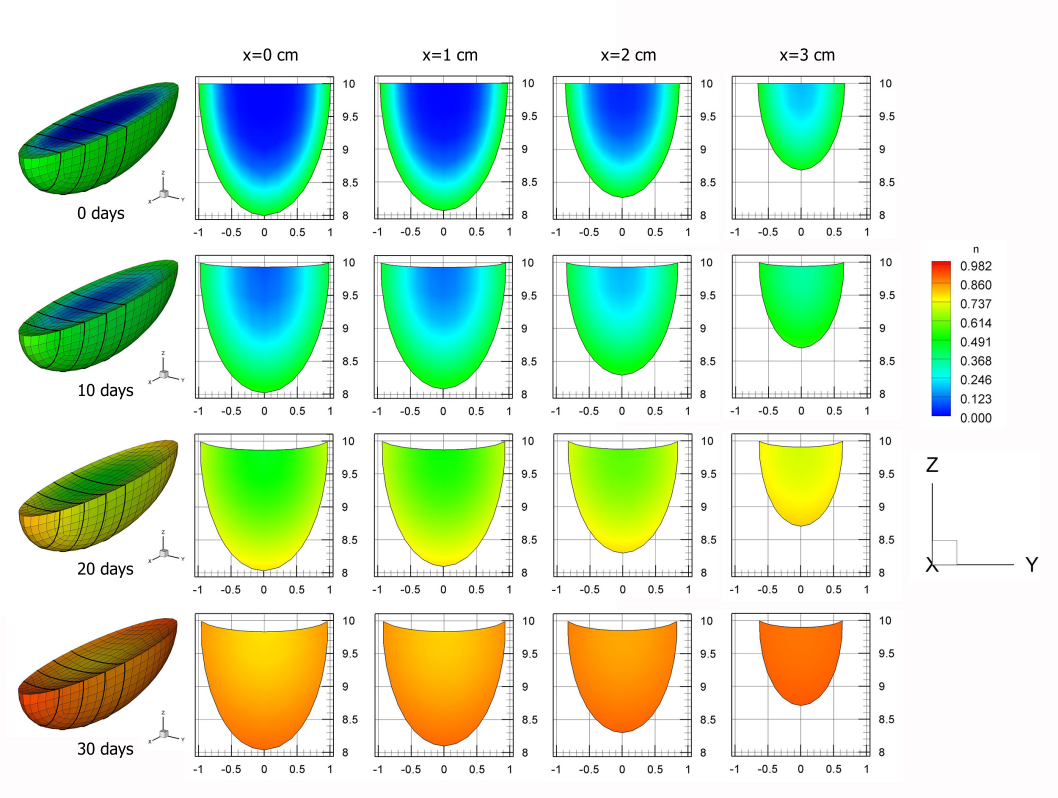

Figure 5. Distribution of fibroblasts in different wound sections along time.

In addition, previous works studied wounds under the assumption of two-dimensional geometries [26, 21, 30, 31, 32] or using one-dimensional simplifications [18, 19, 20, 28, 29, 22, 23]. Therefore, this work provides an important step forward on the modelling and simulation of wound healing. On one hand, the three dimensional approach (which, to our knowledge, has not been previously adopted for this application) allows to simulate any desired geometry. On the other hand, the inclusion of skin anisotropy on the mechanical model of the skin (which, to our knowledge, has neither been tackled for this application) allows to simulate the healing kinetics more accurately. The combination of the two, moreover, opens the discussion of the healing kinetics from aspects that have not been yet considered, and whose impact on the study of both physiological and pathological wounds is extremely high.

In order to demonstrate the model performance, a semi-ellipsoidal wound of fixed dimensions is considered on two different locations (relative to the fibers orientation). Attending to the obtained results, no relevant differences are found on the temporal evolution of the wound volume when the orientation of the wound with respect to the fibers is modified. This observation does not mean that fibers are not acting and some conclusions can be obtained. Fibers give stiffness to the tissue, that other way would be too soft and would not support mechanical loads along its depth.

Firstly, we obtain strains that are relatively small. According to results reported in [12], differences between skin samples with different fiber orientations are not obtained until strains higher than 10% are reached (Figure 10 in Annaidh et al. [12]). Hence, the obtained results agree with quantitative observations for the skin. The strain range obtained in our simulations, not higher than 10%, show that the effect of skin anisotropy is moderate.

Another issue to take into account is the natural stretching of the skin due to the body motion. In this work this deformations is neglected, as it is difficult to quantify and show varying values depending on the body location.

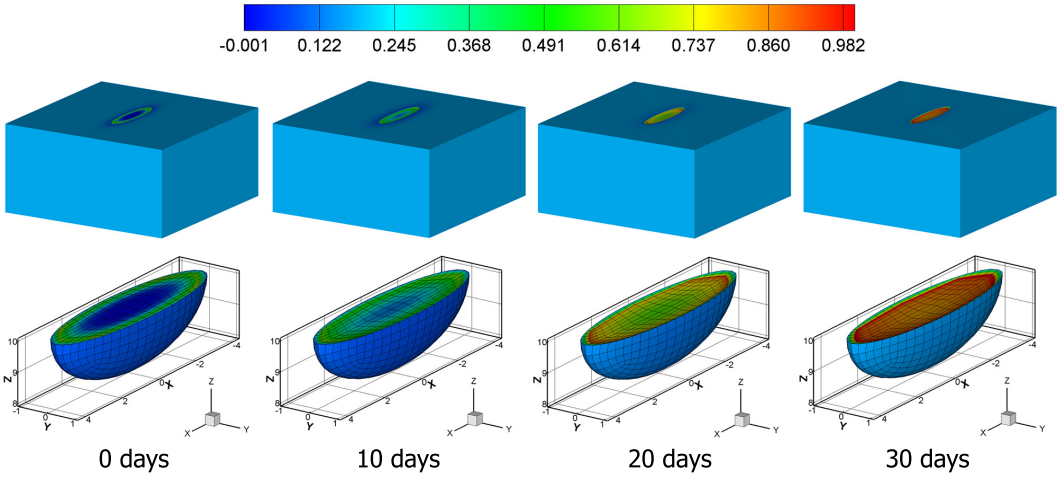

Figure 6. Distribution of the cellular stresses (σ_{cell}) at 0, 10, 20 and 30 days post-wounding. Distribution in the whole geometry (up) and in the wound (down).

For instance, skin in joints is subjected to higher strains than skin in the trunk. Thus, the predictive potential of the model could be enhanced when analyzing cases in which the mechanical component is higher. Moreover, we have not included the stress lines or Langer lines, which are highly influencing the wound healing process. The orientation of the fibers in relation to these lines would probably show higher differences in the contraction process than the fibers alone.

Moreover, skin is transversally isotropic, which means that shows different behavior along its depth, because fibers are displaced in planes parallel to the skin surface.

An important point is that although the material behavior is modeled as anisotropic, the mechanical stimulus considered to regulate the stresses generated by cells is volumetric. This assumption has strong influences because it implies that it is a mean value from the strains that appear in three-dimensional conditions, being better to take into account the directional contributions. Thus, the stresses would be more accurate depending on each direction, which will give to a different stress distribution and probably a different final shape.

In this work we have advanced in designing of a realistic wound healing computational model. The improvements achieved through the implementation of a realistic hyperelastic model in three-dimensional geometries have not been done before and it can be used as a starting point to simulate more complex phenomena in the skin.

Acknowledgments

This research was supported by the European Research Council(ERC) through project ERC-2012-StG 306751 and the Spanish Ministry of Economy and Competitiveness through grant BES2010-037281 and project DPI2012-32888. This project is partly financed by the European Union (through the European Regional Development Fund).

References

[1] A. Singer, R. Clark, Mechanisms of disease - Cutaneous wound healing, New England Journal of Medicine 341 (10) (1999) 738–746.
[2] G. C. Gurtner, S. Werner, Y. Barrandon, M. T. Longaker, Wound repair and regeneration, Nature 453 (7193) (2008) 314–321.
[3] C. Valero, E. Javierre, J. M. Garca-Aznar, M. J. Gmez-Benito, A cell-regulatory mechanism involving feedback between contraction and tissue formation guides wound healing progression, PLoS ONE (2014) n/a–n/a.
[4] H. Gray, P. Williams, L. Bannister, Gray's Anatomy: The Anatomical Basis of Medicine and Surgery, Gray's Anatomy, Churchill Livingstone, ISBN 9780443045608, 1995.

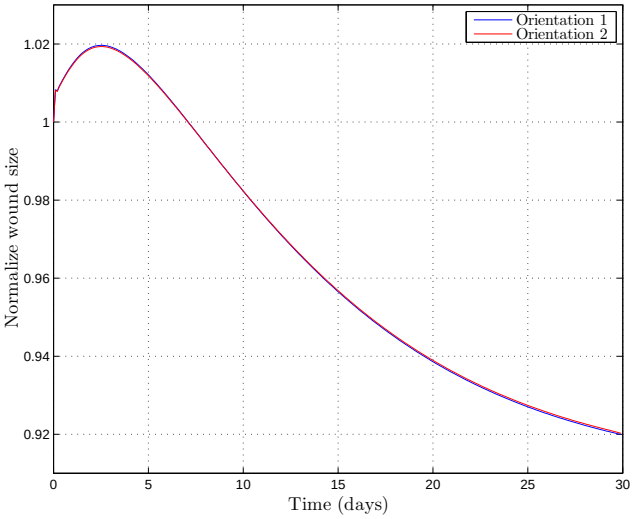

Figure 7. Contraction of wounds with different orientation in relation to the collagen fibers

[5] K. Langer, Zur anatomie und physiologie de haut 1. ueber der spaltbarkeit der cutis., Sitzungsbericht der Akademie der Wissenschaften in Wien 44 (1861) 19.
[6] G. Wilkes, I. Brown, R. Wildnauer, The biomechanical properties of skin, Critical Reviews in Bioengineering (1973) 453–495.
[7] G. Boyer, H. Zahouani, B. A. Le, L. Laquieze, In vivo characterization of viscoelastic properties of human skin using dynamic micro-indentation, 2007 Annual International Conference of the Ieee Engineering in Medicine and Biology Society, Vols 1-16 (2007) 4584–4587.
[8] F. H. Silver, L. M. Siperko, Mechanosensing and mechanochemical transduction: how is mechanical energy sensed and converted into chemical energy in an extracellular matrix?, Critical Reviews in Biomedical Engineering 31 (4) (2003) 255–331.
[9] C. Flynn, A. Taberner, P. Nielsen, Modeling the Mechanical Response of In Vivo Human Skin Under a Rich Set of Deformations, Annals of Biomedical Engineering 39 (7) (2011) 1935–1946.
[10] P. TONG, Y. FUNG, Stress-Strain Relationship for Skin, Journal of Biomechanics 9 (10) (1976) 649–657, pT: J; NR: 8; TC: 120; J9: J BIOMECH; PG: 9; GA: CF452; UT: WOS:A1976CF45200007.
[11] S. Gahagnon, Y. Mofid, G. Josse, F. Ossant, Skin anisotropy in vivo and initial natural stress effect: A quantitative study using high-frequency static elastography, Journal of Biomechanics 45 (16) (2012) 2860–2865.
[12] A. Annaidh, K. Bruyere, M. Destrade, M. D. Gilchrist, C. Maurini, M. Ottenio, G. Saccomandi, Automated Estimation of Collagen Fibre Dispersion in the Dermis and its Contribution to the Anisotropic Behaviour of Skin, Annals of Biomedical Engineering 40 (8) (2012) 1666–1678.
[13] A. N. Annaidh, K. Bruyere, M. Destrade, M. D. Gilchrist, M. Ottenio, Characterization of the anisotropic mechanical properties of excised human skin, Journal of the Mechanical Behavior of Biomedical Materials 5 (1) (2012) 139–148, pT: J; NR: 42; TC: 8; J9: J MECH BEHAV BIOMED; PG: 10; GA: 873QX; UT: WOS:000298899200015.
[14] T. Gasser, R. Ogden, G. Holzapfel, Hyperelastic modelling of arterial layers with distributed collagen fibre orientations, Journal of the Royal Society Interface 3 (6) (2006) 15–35.
[15] R. B. Groves, S. A. Coulman, J. C. Birchall, S. L. Evans, An anisotropic, hyperelastic model for skin: Experimental measurements, finite element modelling and identification of parameters for human and murine skin, Journal of the Mechanical Behavior of Biomedical Materials 18 (2013) 167–180.
[16] J. Weiss, B. Maker, S. Govindjee, Finite element implementation of incompressible, transversely isotropic hyperelasticity, Computer Methods in Applied Mechanics and Engineering 135 (1-2) (1996) 107–128.
[17] C. Escoffier, J. Derigal, A. Rochefort, R. Vasselet, J. Leveque, P. Agache, Age-Related Mechanical-Properties of Human-Skin - an Invivo Study, Journal of Investigative Dermatology 93 (3) (1989) 353–357, pT: J; NR: 16; TC: 141; J9: J Invest Dermatol; PG: 5; GA: AM059; UT: WOS:A1989AM05900009.
[18] J. Sherratt, J. Murray, Models of Epidermal Wound-Healing, Proceedings of the Royal Society B-Biological Sciences 241 (1300) (1990) 29–36.
[19] R. Tranquillo, J. Murray, Continuum Model of Fibroblast-Driven Wound Contraction - Inflammation-Mediation, Journal of theoretical biology 158 (2) (1992) 135.
[20] L. Olsen, J. A. Sherratt, P. K. Maini, A Mechanochemical Model for Adult Dermal Wound Contraction and the Permanence of the Contracted Tissue Displacement Profile, Journal of theoretical biology 177 (2) (1995) 113–128.
[21] E. Javierre, P. Moreo, M. Doblare, J. M. García-Aznar, Numerical modeling of a mechano-chemical theory for wound contraction analysis,

International Journal of Solids and Structures 46 (20) (2009) 3597–3606.
[22] K. E. Murphy, C. L. Hall, S. W. McCue, D. L. S. McElwain, A two-compartment mechanochemical model of the roles of transforming growth factor beta and tissue tension in dermal wound healing, Journal of theoretical biology 272 (1) (2011) 145–159.
[23] K. E. Murphy, C. L. Hall, P. K. Maini, S. W. McCue, D. L. S. McElwain, A Fibrocontractive Mechanochemical Model of Dermal Wound Closure Incorporating Realistic Growth Factor Kinetics, Bulletin of mathematical biology 74 (5) (2012) 1143–1170.
[24] G. Pettet, H. Byrne, D. Mcelwain, J. Norbury, A model of wound-healing angiogenesis in soft tissue, Mathematical biosciences 136 (1) (1996) 35–63.
[25] S. Maggelakis, A mathematical model of tissue replacement during epidermal wound healing, Applied Mathematical Modelling 27 (3) (2003) 189–196.
[26] E. Javierre, F. J. Vermolen, C. Vuik, S. van der Zwaag, Numerical Modelling of Epidermal Wound Healing, Springer-Verlag Berlin, Berlin; Heidelberg Platz 3, D-14197 Berlin, Germany, ISBN 978-3-540-69776-3, 2008.
[27] R. C. Schugart, A. Friedman, R. Zhao, C. K. Sen, Wound angiogenesis as a function of tissue oxygen tension: A mathematical model, Proceedings of the National Academy of Sciences of the United States of America 105 (7) (2008) 2628–2633.
[28] J. A. Flegg, D. L. S. McElwain, H. M. Byrne, I. W. Turner, A Three Species Model to Simulate Application of Hyperbaric Oxygen Therapy to Chronic Wounds, Plos Computational Biology 5 (7) (2009) e1000451.
[29] J. A. Flegg, H. M. Byrne, L. S. McElwain, Mathematical Model of Hyperbaric Oxygen Therapy Applied to Chronic Diabetic Wounds, Bulletin of mathematical biology 72 (7) (2010) 1867–1891.
[30] F. J. Vermolen, E. Javierre, Computer simulations from a finite-element model for wound contraction and closure, Journal of tissue viability 19 (2) (2010) 43–53.
[31] F. J. Vermolen, E. Javierre, A finite-element model for healing of cutaneous wounds combining contraction, angiogenesis and closure, Journal of mathematical biology 65 (5) (2012) 967–996.
[32] C. Valero, E. Javierre, J. M. García-Aznar, M. J. Gomez-Benito, Numerical modelling of the angiogenesis process in wound contraction, Biomechanics and Modeling in Mechanobiology 12 (2) (2013) 349–360.
[33] C. Xue, A. Friedman, C. K. Sen, A mathematical model of ischemic cutaneous wounds, Proceedings of the National Academy of Sciences of the United States of America 106 (39) (2009) 16782–16787.
[34] P. Moreo, J. M. García-Aznar, M. Doblare, Modeling mechanosensing and its effect on the migration and proliferation of adherent cells RID F-8256-2010, Acta Biomaterialia 4 (3) (2008) 613–621.
[35] G. A. Holzapfel, Nonlinear solid mechanics: a continuum approach for engineering, Wiley, Chichester, ISBN 0471823198, 2001.
[36] A. J. M. Spencer, Continuum theory of the mechanics of fibre-reinforced composites, vol. 282 pp. 132 of *CISM Courses and Lectures*, chap. Constitutive theory for strongly anisotropic solids, Springer, Wien, 1984.
[37] M. McGrath, R. Simon, Wound Geometry and the Kinetics of Wound Contraction, Plastic and Reconstructive Surgery 72 (1) (1983) 66–72.
[38] S. Roy, S. Biswas, S. Khanna, G. Gordillo, V. Bergdall, J. Green, C. B. Marsh, L. J. Gould, C. K. Sen, Characterization of a preclinical model of chronic ischemic wound, Physiological Genomics 37 (3) (2009) 211–224.
[39] D. Manoussaki, A mechanochemical model of angiogenesis and vasculogenesis, Esaim-Mathematical Modelling and Numerical Analysis-Modelisation Mathematique Et Analyse Numerique 37 (4) (2003) 581–599.
[40] A. Friedman, C. Xue, A Mathematical Model for Chronic Wounds, Mathematical Biosciences and Engineering 8 (2) (2011) 253–261.

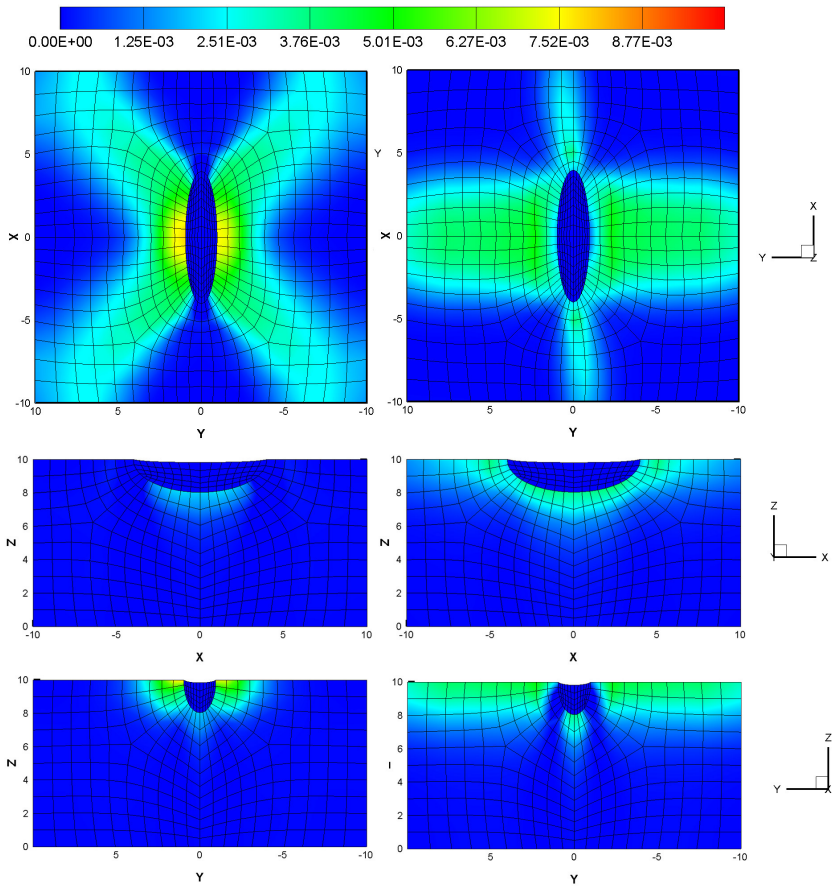

Figure 8. Distribution of the instantaneous volumetric strain (θ) for the two fibers orientation at day 30 post-wounding, viewed along three different planes.

Work 6: A computational study of stress fiber-focal adhesion dynamics governing cell contractility

Journal: *Biophysical Journal*
Impact factor: 3.668

Contribution of the author of the thesis: the author was in charge of performing the computational simulations and analyzing the results. Everything was done under the supervision of the other authors. This work was performed during a research stay in the University of Michigan (USA).

A computational study of stress fiber-focal adhesion dynamics governing cell contractility

M. Maraldi[1], C. Valero[2], K. Garikipati[1,3,*]

[1]Department of Mechanical Engineering, University of Michigan, Ann Arbor, Michigan
[2]M2BE, Aragón Institute of Engineering Research (I3A), University of Zaragoza, Zaragoza, Spain
[3]Department of Mathematics, University of Michigan, Ann Arbor, Michigan

Abstract

We apply a recently developed model of cytoskeletal force generation to study a cell's intrinsic contractility, as well as its response to external loading. The model is based on a non-equilibrium thermodynamic treatment of the mechano-chemistry governing force in the stress fiber-focal adhesion system. Our computational study suggests that the mechanical coupling between the stress fibers and focal adhesions leads to a complex, dynamic, mechano-chemical response. We collect the results in response maps whose regimes are distinguished by the initial geometry of the stress fiber-focal adhesion system, and by the external load on the cell. The results from our model connect qualitatively with recent studies on the force response of smooth muscle cells on arrays of polymeric microposts (Mann et al., *Lab. on a Chip*, **12**, 731-740, 2012).

Received for publication dd/mm/yyyy and in final form dd/mm/yyyy.

Correspondence: krishna@umich.edu

INTRODUCTION

In contractile cells, such as smooth muscle cells and fibroblasts, the generation of traction force is the result of two different actions: myosin-powered cytoskeletal contractility and external mechanical stimuli (applied stretch or force). The cooperation between these two aspects determines the level of the force within the cell and influences the development of cytoskeletal components via the (un)binding of proteins. Important cytoskeletal components that mediate this interplay of mechanics and chemistry are stress fibers and focal adhesions.

Stress fibers are bundles of 10–30 actin filaments held together by the binding protein α-actinin (1); fascin, epsin, filamin and myosin, among other proteins, have also been detected in stress fibers. Cytoskeletal contractility originates from the action of myosin molecules, which attach themselves to the actin filaments and step along them, causing anti-parallel filaments to slide past each other, thus generating a contraction of the stress fiber. The speed at which filament slide past each other decreases with tensile force (2). The myosin stepping rate reaches a stall at some critical value of tensile force, at which contractility ceases.

The binding rates of actin and myosin (and presumably of other proteins, also) into the stress fiber is force-dependent (3); within some regime of tensile force *auto*-generated by stress fiber contractility, the binding rates appear to be boosted, and the fibers grow in thickness (4, 5). Eventually, a sufficiently high force, perhaps externally applied, must cause rapid unbinding of the proteins and cytoskeletal disassembly. The complexity of this mechano-chemical response is enhanced because the stress fibers also demonstrate, besides the aforementioned active response due to myosin action, a passive viscoelastic force-stretch behavior (6).

Focal adhesions are integrin-containing transmembrane structures that anchor the cytoskeletal stress fibers to the extra-cellular matrix (ECM). In addition to integrin they contain scores of other proteins including paxillin, tensin, focal adhesion kinase, talin and vinculin. The latter two proteins connect the integrins to f-actin in the stress fibers, to complete the linkage of the cytoskeleton to the ECM. However, focal adhesions are not merely static anchors. They themselves demonstrate a complex dynamics of growth, disassembly, and even a translational mode in which they appear to slide over the interface between the cell membrane and ECM, strikingly shown by Nicolas and co-workers (42). These regimes of the dynamics are caused by (un)binding of focal adhesion proteins, and notably are force-sensitive; cytoskeletal contractility forces as well as externally applied loads may elicit this mechanosensitive response (7, 8).

It is inevitable that the combination of two such mechano-chemically dependent systems (stress fibers and

0006-3495/08/09/2624/12 $2.00
doi: xx.xxxx/biophysj.xxx.xxxxxx

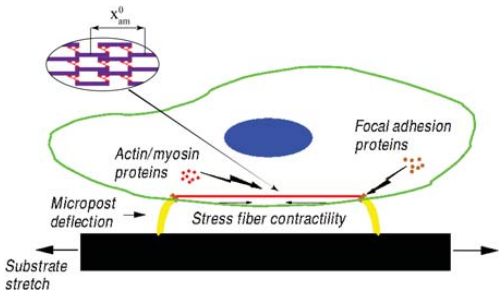

Figure 1: Schematic representation of the model.

focal adhesions) in the cytoskeleton leads to a rich dynamic response, where the force as well as the systems' structures themselves continuously evolve. Some of these aspects have been addressed in the literature, and a variety of models have been proposed which study stress fibers and focal adhesions separately (9–15) or, in some cases, in combination (16–19). They focus on different aspects of the problem, such as cell traction (20), effects of substrate stiffness (21, 22), cell shape (23), cell contractility (24), cytoskeletal orientation under dynamic load (12, 25–27), and stress fiber viscoelasticity (6, 24). Some studies also address the role of the small GTPases, Rho and Rac, in regulating stress fiber formation (28–30).

In this paper, we use a recently developed model for the coupled mechano-chemical response of stress fiber-focal adhesion systems to study the development of contractile force, as well as the behavior of such systems under load. The model is based on non-equilibrium thermodynamics and has been described in detail in a work by Maraldi and Garikipati (31). Our focus here is on the modes of generation and decay of the force in the system, as well as on the growth and disassembly of the stress fibers and focal adhesions. These questions are addressed in the context of both cell contractility in absence of external load and system response to an external stretch. Our motivation comes from studies of force generated by smooth muscle cells plated on micropost arrays (32); nevertheless, our model is capable of much greater detail than is accessible experimentally. The experiments demonstrate variability in the response both between cells and between individual stress fibers in the same cell; accordingly, our aim is to reproduce the broad trends seen in the experiments and provide a key to interpret the response variability observed in the experiments, while examining in greater detail the underlying mechano-chemical dynamics that the model reveals.

THE UNDERLYING MODEL

Calculations were carried out using a modified version of a model proposed by Maraldi and Garikipati (31); the model does not include chemical signaling in order to explicitly highlight the role of mechanical force as a signal, instead. The original layout has been adapted to include the presence of elastic microposts, in order to simulate the behavior of the stress fiber - focal adhesion ensemble under the conditions of the experimental tests performed by Mann et al. (32). Specifically, the model adopted here (Fig. 1) consists of a stress fiber connected to a focal adhesion at each end, with each focal adhesion being attached to the top of a PDMS micropost, and an elastic (PDMS) substrate underlying the microposts; the cytosolic reservoir supplying proteins to the stress fiber and focal adhesions is also included. The substrate can be stretched to introduce an external mechanical loading of the system. The stress fiber and the focal adhesions are mechano-chemical subsystems formed by assembly of representative proteins supplied by the cytosol.

To substantiate the discussion of the results provided in this paper, we briefly report the main concepts behind the model we adopted; further details can be found in the Supporting Material and elsewhere (31, 33). In the model, the stress fiber is considered to span between two focal adhesions and to be always under tension; hence, its reference length, $x^0_{\rm sf}$, is fixed, as it would not be possible to add proteins at its ends without first abrogating the tension. Protein binding/unbinding therefore only affects the thickness of the stress fiber. On the other hand, protein binding/unbinding is allowed to occur anywhere along the focal adhesion; however, to compute the relevant kinematic quantities for this sub-system, only the binding rates at its ends need to be tracked. The force is assumed to be uniformly distributed along the focal adhesion and through the stress fiber's thickness (31).

The number of stress fiber representative proteins and the focal adhesion distal and proximal ends' positions ($N_{\rm sf}$, $x_{\rm d}$ and $x_{\rm p}$, respectively) are the variables tracked with respect to time. The ordinary differential equations constituting the model are (31, 33):

$$\dot{N}_{\rm sf} = \begin{cases} k^{\rm b}_{\rm sf}\left(N^{\rm max}_{\rm sf} - N_{\rm sf}\right)\left(1 - e^{\left(\mu_{\rm sf} - \mu^{\rm sf}_{\rm cyt}\right)/k_BT}\right), & \textit{(b)} \\ k^{\rm u}_{\rm sf}\, e^{\chi_{\rm sf}}\left(e^{-\left(\mu_{\rm sf} - \mu^{\rm sf}_{\rm cyt}\right)/k_BT} - 1\right), & \textit{(u)} \end{cases} \quad (1)$$

$$\dot{x}_{\rm d} = -\lambda^2 \begin{cases} k^{\rm b}_{\rm fa}\left(1 - e^{\left(\mu^{\rm d}_{\rm fa} - \mu^{\rm fa}_{\rm cyt}\right)/k_BT}\right), & \textit{(b)} \\ k^{\rm u}_{\rm fa}\, e^{\chi_{\rm fa}}\left(e^{-\left(\mu^{\rm d}_{\rm fa} - \mu^{\rm fa}_{\rm cyt}\right)/k_BT} - 1\right), & \textit{(u)}, \end{cases} \quad (2)$$

$$\dot{x}_{\rm p} = \lambda^2 \begin{cases} k^{\rm b}_{\rm fa}\left(1 - e^{\left(\mu^{\rm p}_{\rm fa} - \mu^{\rm fa}_{\rm cyt}\right)/k_BT}\right), & \textit{(b)} \\ k^{\rm u}_{\rm fa}\, e^{\chi_{\rm fa}}\left(e^{-\left(\mu^{\rm p}_{\rm fa} - \mu^{\rm fa}_{\rm cyt}\right)/k_BT} - 1\right), & \textit{(u)}, \end{cases} \quad (3)$$

where the label *(b)* indicates the equations used for the case in which $\mu_\alpha - \mu^\alpha_{\rm cyt} \leq 0$ (proteins binding) for sub-system $\alpha = {\rm sf}, {\rm fa}$, whereas *(u)* indicates the equations for the case in which $\mu_\alpha - \mu^\alpha_{\rm cyt} \geq 0$ (proteins unbinding). In Eq. (1), $\mu_{\rm sf}$ is the chemical potential of representative proteins in the stress fiber, $\mu^{\rm sf}_{\rm cyt}$ is the chemical potential of stress fiber proteins

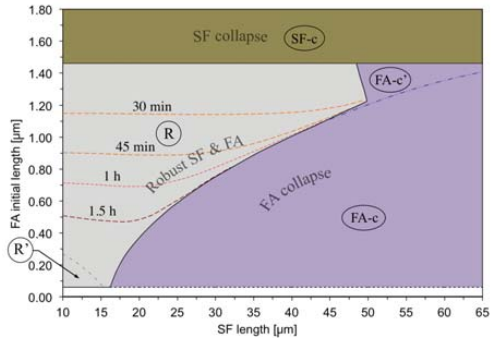

Figure 2: System response map with no applied stretch. *R* is the region in which the stress fiber and the focal adhesion reach full development (*robust stress fiber and focal adhesion* region). The dashed curves are iso-time contours of micropost coverage by the growing focal adhesion. *R′* is the region in which focal adhesion translation causes stress fiber force relaxation to zero. The system collapses in regions *FA-c* and *FA-c′* due to focal adhesion resorption (*focal adhesion collapse* regions), and in *SF-c* due to stress fiber resorption (*stress fiber collapse* region).

in the cytosolic reservoir, and $N_{\rm sf}^{\rm max}$ is the maximum number of stress fiber proteins available to the given stress fiber. In Eq. (2) and Eq. (3), $\mu_{\rm fa}^{\rm d}$ and $\mu_{\rm fa}^{\rm p}$ are the chemical potentials of the proteins in the focal adhesion evaluated at its distal and proximal ends, respectively, $\mu_{\rm cyt}^{\rm fa}$ is their chemical potential in the cytosol and λ is the size of a focal adhesion complex. For the detailed expressions of the chemical potentials see Eqs.(1) in the Supporting Material. Moreover, $k_\alpha^{\rm b}$, $k_\alpha^{\rm u} > 0$ are respectively the binding and unbinding coefficients for sub-system α, k_B is the Boltzmann constant, and $\chi_\alpha = \chi_\alpha(P)$ is a force-dependent exponent regulating the rapid dissociation of molecular bonds (31, 34). We note that the form of Eqs. (1–3) comes from classical non-equilibrium thermodynamics, and incorporates the assumption of local equilibrium (41).

Mechanical equilibrium is assumed to hold; hence, the forces developed within the stress fiber, the focal adhesions and the microposts are equal to one another and identified as the force within the system: $P = P_{\rm sf} = P_{\rm fa} = P_{\rm mp}$. The determination of P is essential for calculating the chemical potentials of the focal adhesion, the stress fiber and the cytosol, which are the driving forces for the chemical processes (31) and appear in the rate equations Eqs.(1–3).

In the Discussion Section, we will observe that the stress fiber's constitutive nature plays a major role in the complex mechanical response of the system. Indeed, the contractile and viscoelastic features of the stress fiber strongly influence the development of the force within the whole system. In particular, the force developed within the stress fiber (and consequently within the whole system, due to mechanical equilibrium) can be expressed as the sum of three different contributions: $P_{\rm sf} = P_{\rm sf}^{\rm e} + P_{\rm sf}^{\rm ve} + P_{\rm sf}^{\rm ac}$, where $P_{\rm sf}^{\rm e}$ is the elastic component, $P_{\rm sf}^{\rm ve}$ accounts for the viscous response and $P_{\rm sf}^{\rm ac}$ is the active contractile force. Fig. 1 also shows the actomyosin contractile units that make up the stress fiber. Each unit consists of one myosin motor and one half-length of each interleaved, anti-parallel actin filament that the motor causes to intercalate. The units also are assumed to have the same length, and the total number of contractile units is therefore proportional to $N_{\rm sf}$. We take each such unit to have the same strain rate in the stress fiber. See Eqs. (2) and the ensuing discussion in the Supporting Material for the complete active contractile force model.

A specific set of parameters was chosen (Tab. 1 in the Supporting Material) and the model was tested for its ability to reproduce the main features of the force response of smooth muscle cells plated on an array of polymeric microposts (32). To access a variety of responses, the initial stress fiber length was varied over a range typically reported for a cell (10–65 μm), while the initial focal adhesion length was varied in the 0–2 μm range. For the tests in which an external load was applied to the system, the extent of the substrate stretch was varied between 0.05 and 0.15, to make connections with Mann et al. (32).

RESULTS

System response map and collapse mechanisms with no applied strain

We first seek to model the contractility of a cell on an array of microposts when the substrate is not subjected to an external strain. The corresponding system responses are collected in the map of Fig. 2.

In region *R*, a robust, fully developed system is obtained, with a stable stress fiber and a growing focal adhesion. Fig. 2 shows that this region may extend down to $\hat{x}_{\rm fa}^0 = \lambda = 58$ nm (black dashed line in Fig. 2), which is the size of a single complex of focal adhesion proteins, and represents the smallest focal adhesion in our model.[1] Notably, even this smallest initial focal adhesion gives rise to a robust system if $x_{\rm sf}^0$ is small. Region *R* spans a wider range of $\hat{x}_{\rm fa}^0$ values than any other region. However, for larger values of $x_{\rm sf}^0$ this range of $\hat{x}_{\rm fa}^0$ becomes increasingly narrow, as other failure mechanisms become dominant (regions *FA-c* and *SF-c*).

Inside region *R* in Fig. 2, the system exhibits different behaviors, some of which are induced by the fact that the focal adhesion is constrained to develop on the surface of the micropost, which has finite area. The dashed curves indicate the times at which the focal adhesion has grown to the size of the micropost diameter. Smaller $\hat{x}_{\rm fa}^0$ translates to greater

[1] The term *focal complex* may be more appropriate in this limit.

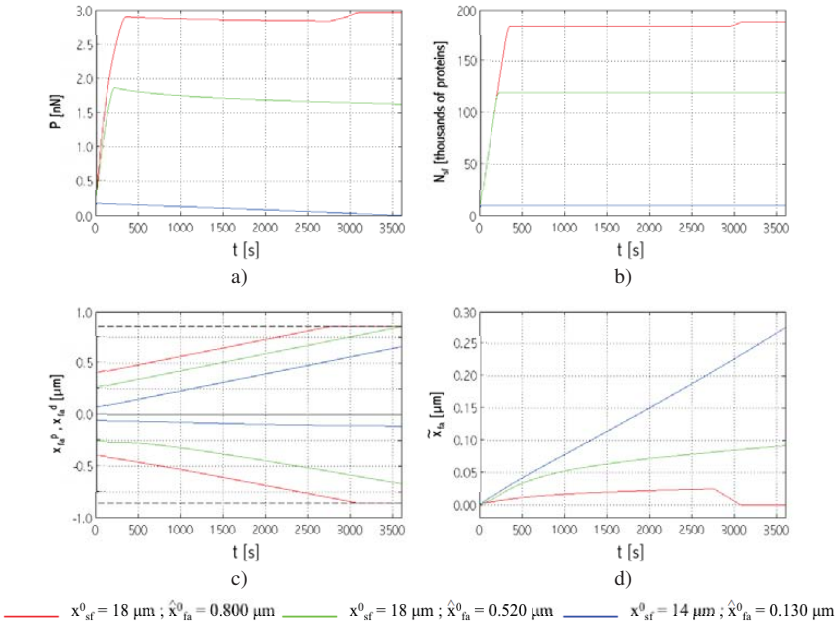

Figure 3: Time evolution of a) force, P; b) number of actin monomers in the stress fiber, $N_{\rm sf}$; c) focal adhesion distal (negative values, $x^{\rm d}_{\rm fa}$) and proximal (positive values, $x^{\rm p}_{\rm fa}$) ends positions; and d) focal adhesion centroid position, $\tilde{x}_{\rm fa}$ for three different system initial configurations belonging to region *R* in Fig. 2. In c) the dashed black lines indicate the position of the micropost edges.

growth times, as would be expected. Further details are provided in the following sub-section. The dash-dot green line in Fig. 2 delimits the sub-region *R′*, characterized by low values of $x^0_{\rm sf}$ and $\hat{x}^0_{\rm fa}$. For these configurations the system does not collapse, but the stress fiber force vanishes at small times. Here, treadmilling of proteins through the cytosol allows the focal adhesion structure to translate in the direction of the force, causing the force in the system to relax to zero (blue curves in Fig. 3).

Outside region *R*, the system collapses due to different failure mechanisms; in region *FA-c*, characterized by low values of the $\hat{x}^0_{\rm fa}/x^0_{\rm sf}$ ratio, the collapse is due to the complete resorption of the focal adhesion. Under these conditions, in fact, the stress fiber is able to generate a high active force, $P^{\rm ac}_{\rm sf}$; as a consequence, the force within the system P is high and exceeds the focal adhesion's ability to sustain mechanical load (see the discussion on the focal adhesion critical load in the Discussion Section), causing its complete resorption by unbinding at its distal end. Similarly, for high values of $x^0_{\rm sf}$ (subregion *FA-c′*) the system experiences focal adhesion collapse due to the finite surface area of the micropost which constrains the growth of the focal adhesion (See Section 2 in the Supporting Material for details).

In region *SF-c* the system collapses due to stress fiber failure. The large focal adhesion increases the system stiffness so that a high force P can be developed under strain control. This ultimately causes stress fiber resorption, and the system collapses even as the large focal adhesion survives.

Time-dependent response of the system with no applied strain

The detailed dynamics of the system in terms of the time evolution of force P, number of proteins in the stress fiber $N_{\rm sf}$, position of the focal adhesion proximal and distal ends ($x^{\rm p}_{\rm fa}$ and $x^{\rm d}_{\rm fa}$, respectively) and centroid position $\tilde{x}_{\rm fa}$ are depicted in Fig. 3 for three typical system configurations belonging to region *R* of the response map in Fig. 2. For configurations in region *FA-c* of the response map, a similar discussion is provided as Supporting Material. The force within the system, P, is often referred to as the *contractile force* in literature; however, we prefer not to use this terminology, as, according to the stress fiber constitutive model used for the present study (31), this force depends not only on contractility, but also on the passive elastic or viscoelastic response of all the sub-systems (see Eqs. (2) in Supporting Material, and the

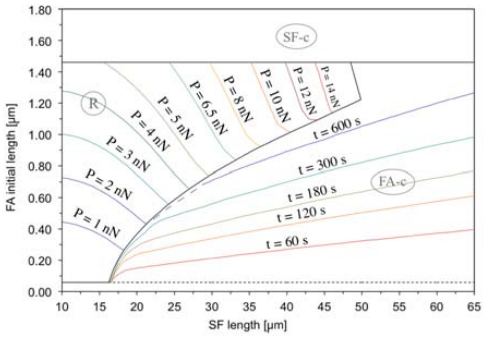

Figure 4: Contour plots of the maximum contractile force P and of the focal adhesion resorption time t for configurations belonging, respectively, to regions *R* and *FA-c* of the map in Fig. 2.

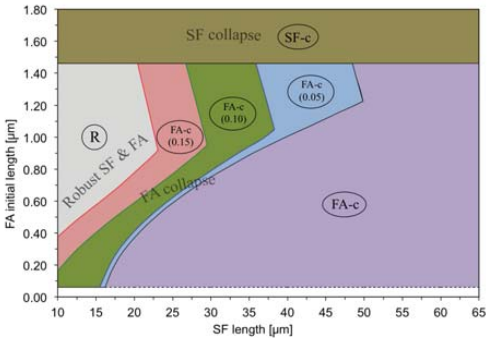

Figure 5: System response map for applied strain. Regions *R* and *FA-c* are modified from Fig. 2. The applied strain appears in parentheses in subregions of *FA-c*.

discussion on stress fiber rheology in the Model Section) and on loads external to the system (see the discussion related to Fig. 6).

Fig. 3a shows the evolution of P; in all cases, the force initially increases and, after a time interval that depends on the initial values $\hat{x}^0_{\rm fa}$ and $x^0_{\rm sf}$, it attains a near-plateau characterized by a negative slope. Accordingly, $N_{\rm sf}$ increases until a critical concentration is reached at which protein recruitment stops (Fig. 3b).

Although the cases in Fig. 3 all fall into region *R*, the detailed dynamics differ notably from one another. The blue curves, for instance, refer to a configuration in region *R′*: while P completely vanishes, neither the stress fiber nor the focal adhesion dissolve, as shown, respectively, in Figs. 3b and 3c. Indeed, the stress fiber grows continuously until the aforementioned critical actin concentration is attained and the focal adhesion also grows, by addition of complexes at both its ends. Interestingly, the relaxation of P corresponds with focal adhesion translation due to protein treadmilling, as seen in the evolving position of the focal adhesion centroid (Fig. 3d). Region *R′* may therefore be regarded as an enhanced translation region.

The red curves in Fig. 3 show the system dynamics when the finite cross-section of the micropost limits focal adhesion growth. A *stiffening* effect is imposed on the system (as seen from the red curve in Fig. 3a, at $t \simeq 3000$ s). As shown in Fig. 3c, the faster-growing proximal end of the focal adhesion is first to reach the corresponding micropost edge (this holds for all system configurations). Consequently, the focal adhesion continues to grow only at the distal end, and its centroid, which is the center of action of the stress fiber force, moves backward (Fig. 3d). The focal adhesion translation away from the direction of the force induces a kinematic stiffening - in the same manner as a translation in the direction of the force induces a kinematic relaxation (see the preceding discussion, as well as the forthcoming one on the competition between stress fiber contractility and focal adhesion translation) - which makes the chemical potential term $(\mu_{\rm sf} - \mu^{\rm sf}_{\rm cyt})$ of Eq. 1 negative and re-establishes a growth regime for the stress fiber. Consequently, more actin and myosin are recruited to the stress fiber and P starts rising again until the slower-growing distal end of the focal adhesion reaches the corresponding micropost edge. The focal adhesion has no more room for growth, $N_{\rm sf}$ reaches a second, higher, critical concentration and the contractile force plateaus out. The stress fiber-focal adhesion system is at equilibrium in this case.

When the system configuration falls outside region *R′* of the response map in Fig. 2 and neither end of the focal adhesion reaches the micropost edge, the dynamics follow the green curves of Fig. 3: the critical value of $N_{\rm sf}$ is reached in the stress fiber, which stops growing, while the focal adhesion continues to grow by recruiting complexes at both ends (Fig. 3c). The observed force relaxation is related to translation as explained above.

The maximum value attained by the force in the system, P, is of interest for robust systems; it depends on $x^0_{\rm sf}$ and $\hat{x}^0_{\rm fa}$, as reported in the contour plot of Fig. 4 for configurations in region *R*. It can be noted that a higher $x^0_{\rm sf}$ results in a higher value of the maximum of P. However, $\hat{x}^0_{\rm fa}$ also has some influence: especially for low $x^0_{\rm sf}$, a high $\hat{x}^0_{\rm fa}$ leads to an increased maximum P. Turning to the stress fiber growth, the maximum, or critical, value of $N_{\rm sf}$ is proportional to the stress fiber radius $r_{\rm sf}$ and to the number of actin filaments $N_{\rm fil}$. From our computations we found that $N_{\rm sf}$ varies as the maximum value of P (data not shown). No equivalent quantities can be identified that are intrinsic to the focal adhesion, as it always remains far from equilibrium and, consequently, its length $\hat{x}_{\rm fa}$, and centroid position $\tilde{x}_{\rm fa}$, are always changing.

The time to failure is a relevant quantity for systems collapsing due to full resorption of the focal adhesion. A

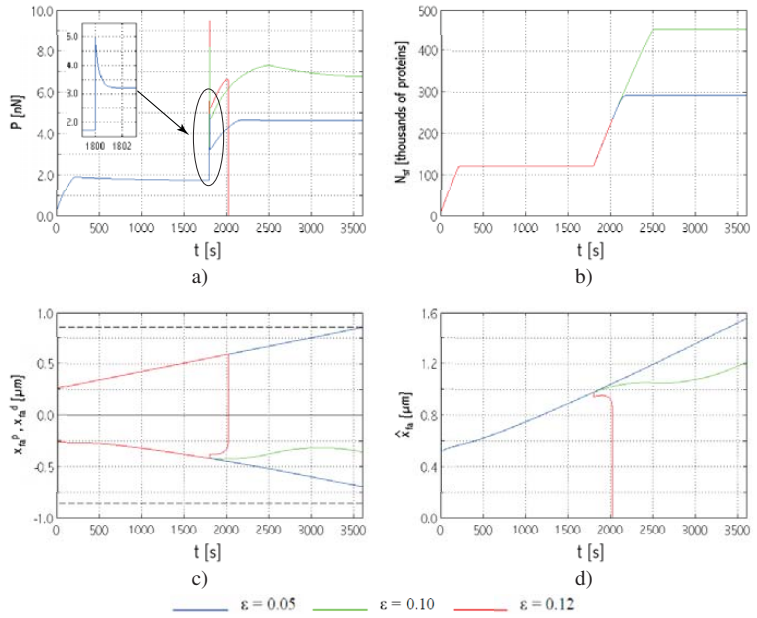

Figure 6: Time evolution of a) force, P; b) number of actin monomers in the stress fiber, $N_{\rm sf}$; c) focal adhesion distal (initially negative values, $x^{\rm d}_{\rm fa}$) and proximal (positive values, $x^{\rm p}_{\rm fa}$) end positions; and d) focal adhesion length ($\hat{x}_{\rm fa}$) for the indicated applied strain. System initial configuration: $x^0_{\rm sf} = 18\mu m$; $\hat{x}^0_{\rm fa} = 0.520\mu m$. In c) the dashed black lines indicate the position of the micropost edges.

contour plot of this parameter is shown in Fig. 4 for configurations in region *FA-c* of the response map. The time to failure rapidly decreases for decreasing $\hat{x}^0_{\rm fa}$, and slowly decreases for increasing $x^0_{\rm sf}$, i.e for configurations far from the boundary between regions *R* and *FA-c*.

For large values of $\hat{x}^0_{\rm fa}$ (region *SF-c* in the response map of Fig. 2) the system always collapses due to complete disassembly of the stress fiber over very short time scales (dynamic data not shown); a large focal adhesion acts as a very stiff support, allowing the force within the system, and hence the strain energy, to increase and drive the stress fiber to a rapid disassembly.

Collapse-mechanisms and system behavior with applied strain

Fig. 5 depicts the system response map under an applied step strain. The numbers in parentheses are the strains for which failure occurs by focal adhesion resorption for that configuration in region *FA-c* (see the discussion on Fig. 6, and Fig.S2). On comparing with the response map under no strain in Fig. 2, it is apparent that region *FA-c* has grown at the expense of *R*; this suggests that, upon stretching, the system is more prone to collapse due to focal adhesion resorption. The region in which the system does survive is restricted to initial configurations with progressively smaller $x^0_{\rm sf}$ and larger $\hat{x}^0_{\rm fa}$.

Our model admits substrate strains that are arbitrary functions of time, but we chose to apply time-discontinuous strains to make connections with the results of Mann et al. (32). The strain was always applied at $t = 1800\ s$, well after the system had attained a near-equilibrium state characterized by $N_{\rm sf}$ and $\hat{x}_{\rm fa}$ being steady, and the contractile force in a near-plateau regime (Fig. 6). As in the unstretched test-cases, $\hat{x}^0_{\rm fa}$ and $x^0_{\rm sf}$ were varied; additionally, time-discontinuous strains of 0.05, 0.10 and 0.15 were applied to the system by varying the stretch of the underlying substrate.

Time-dependent response of the system under different levels of strain

The analysis of the detailed dynamics of the system for different strain amplitudes allows a greater appreciation of the effects of an external strain to the system and enables a more direct comparison with the experiments conducted by Mann et al. (32), in which two different levels of stretch were applied to the cells. The plots in Fig. 6 show the system

dynamics for applied strains of 0.05, 0.10 and 0.12 (the initial geometric configuration being fixed in order to allow a meaningful comparison between the different cases). Upon stretching, P spikes instantaneously (Fig. 6a) because of the elastic response of the system. The force then drops very rapidly due to the passive viscoelastic response of the stress fiber. The inset in Fig. 6a shows these elastic and viscoelastic responses at a finer force-time resolution for the applied strain of 0.05. The externally applied strain also drives the dynamics of the stress fiber (Fig. 6b): more actin monomers are recruited, and the stress fiber grows until a second critical value of $N_{\rm sf}$ is reached. As a consequence, P rises again, driven by $P_{\rm sf}^{\rm ac}$, until it reaches a second maximum (this will be referred to as the global maximum force for that strain) followed by a second near-plateau, with a slightly negative slope. Notably, the global maximum of P and the post-strain critical value of $N_{\rm sf}$ increase if the applied strain increases. An exception, however, occurs if the system experiences focal adhesion collapse: in Fig. 6a, for instance, the global maximum of P for the strain of 0.12 is lower than that for the strain of 0.10.

The focal adhesion has a greater range of responses than the stress fiber (Fig. 6c and 6d). The proximal end always grows upon stretching, while the distal end can either suffer an initial resorption followed by restoration of the growth regime (green curve in Fig. 6c, strain of 0.10) or grow monotonically (blue curve in Fig. 6c, strain of 0.05). Consequently, the focal adhesion can either have a transitory resorption stage or show monotonic growth (Fig. 6d). In contrast to P, the focal adhesion length decreases for increasing strain (Fig. 6d, strain of 0.10 *versus* 0.05). At higher applied strains the focal adhesion begins to shrink irreversibly, causing the system to collapse (red curves in Fig. 6).

DISCUSSION

The key to deciphering the system's complex mechano-chemical coupling lies with the chemical potentials of the stress fiber, focal adhesion and cytosol and with the complex, non-linear mechano-chemical coupling in the model. On this basis, in the following subsections we highlight some aspects of the dynamics of the model that will be relevant to the discussion of the results presented in this paper.

Critical loads for assembly and disassembly

The chemical potentials that drive stress fiber and focal adhesion dynamics are themselves functions of the force, P, developed within the system (Fig. 7). By comparing P with suitable critical values it can be established whether the focal adhesion or stress fiber undergoes growth or disassembly. It is important to recognize, however, that these critical values vary, because they depend upon $N_{\rm sf}$ and $c_{\rm fa}$, which evolve.

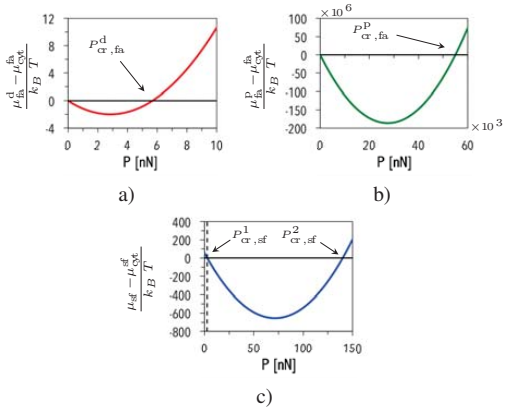

Figure 7: Chemical potentials as functions of the force P at: a) the focal adhesion distal end; b) the focal adhesion proximal end; c) the stress fiber for the set of parameters listed in Tab. 1 in the Supporting Material.

With regard to the focal adhesion sub-system, experiments show that no growth is observed in the absence of force (7, 8); for this reason, all the parameters were chosen such that $\mu_{\rm fa} - \mu_{\rm cyt}^{\rm fa} = 0$ if $P = 0$ (see Fig. 7a and Fig. 7b). As a result, only one critical value of P can be identified for both the distal and the proximal ends of the focal adhesion (namely $P_{\rm cr,fa}^{\rm d}$ and $P_{\rm cr,fa}^{\rm p}$ in Fig. 7); below this force, the chemical potential drives focal adhesion complexes to bind, whereas above it unbinding is experienced at the given focal adhesion end. For $P > P_{\rm cr,fa}^{\rm d}$, it is the growth rate at the focal adhesion proximal end that determines whether the focal adhesion as a whole undergoes growth, translation, or resorption leading to eventual focal adhesion collapse; nevertheless, $P > P_{\rm cr,fa}^{\rm d}$ is a necessary condition for focal adhesion resorption.

Given the parameter values chosen for the present study and system configurations explored, the critical load $P_{\rm cr,fa}^{\rm p}$ – above which $(\mu_{\rm fa}^{\rm p} - \mu_{\rm cyt}^{\rm fa})$ becomes positive leading to protein unbinding at the proximal end – is much greater than the value of P observed in our simulations. Hence, it is not of interest.

On the other hand, for the set of parameters used here, two critical loads can be identified for the stress fiber sub-system (namely $P_{\rm cr,sf}^{1}$ and $P_{\rm cr,sf}^{2}$ in Fig. 7c). The dynamics of the sub-system are therefore dictated by comparing P with such critical forces; in particular, for $P < P_{\rm cr,sf}^{1}$ or $P > P_{\rm cr,sf}^{2}$, the term $(\mu_{\rm sf} - \mu_{\rm cyt}^{\rm sf})$ is positive and the stress fiber undergoes disassembly, whereas for $P_{\rm cr,sf}^{1} < P < P_{\rm cr,sf}^{2}$, the term $(\mu_{\rm sf} - \mu_{\rm cyt}^{\rm sf})$ is negative, and proteins are recruited to the stress fiber.

Our mechano-chemical model highlights the interplay between the mechanics and chemistry in determining the

dynamics of the system. Through the chemical potential, the force in the system affects the protein binding and unbinding rates, which determine the focal adhesion length and the stress fiber thickness. In turn, these system geometric parameters influence the chemical potentials by changing the critical loads. They also control the passive and active contributions to the stress fiber force, and, ultimately, the force in the system, by varying the system stiffness and the number of motor proteins in the stress fiber.

Non-linearities, mechano-chemistry and response maps

The relevant critical loads $P^1_{\rm cr,sf}$, $P^2_{\rm cr,sf}$ and $P^{\rm d}_{\rm cr,fa}$ are non-linear functions of the geometry of the system. The relations between the force P and these critical loads dictate assembly or disassembly of a sub-system. The overall system dynamics that yield the response maps in Fig. 2 and Fig. 5 depend on the rate of change of the critical loads with respect to that of P. In the next few sections we will observe some aspects of the behavior of the system which arise from this mechanism. In summary, in our model the stress fiber can reach a critical concentration only because $P^1_{\rm cr,sf}$ increases faster than P and, after some time, the stress fiber reaches a configuration for which protein binding ceases (see Fig. 8 and the associated discussion). Similarly, but with opposite results, Fig. 9 shows that the focal adhesion collapses because $P^{\rm d}_{\rm cr,fa}$ increases faster than P and, after some time, the focal adhesion is in a configuration for which unbinding starts and proceeds at a increasingly faster rate (see the discussion related to Fig. 9 for further details). The rate at which P and the critical loads change is driven by the model's coupled mechano-chemistry, and by non-linearities in the constitutive relations for chemical potentials, mechanical forces and rate laws. These are critical to the form of the response maps (Figs. 2 and 5).

Stress fiber growth stops when the critical actin concentration is reached

The attainment of a critical value of $N_{\rm sf}$ at which the stress fiber stops recruiting proteins, is explained by the evolution of P relative to $P^1_{\rm cr,sf}$, as shown in Fig. 8a. Initially, $P > P^1_{\rm cr,sf}$ makes $(\mu_{\rm sf} - \mu^{\rm cyt}_{\rm sf}) < 0$, which drives actin and myosin recruitment to the stress fiber (Fig. 8b). Consequently, P increases due to both enhanced acto-myosin contractility and the increased system mechanical stiffness (the stress fiber becomes thicker and the focal adhesions longer). However, $P^1_{\rm cr,sf}$, which is a function of $N_{\rm act}$, also increases. When $P^1_{\rm cr,sf}$ exceeds the stress fiber force, $(\mu_{\rm sf} - \mu^{\rm sf}_{\rm cyt}) > 0$ and actin unbinding should occur. However, $\chi_{\rm sf}$ in Eq. 1 is negative; therefore, actual unbinding rates remain low, and the stress fiber appears stable at its critical concentration (Fig. 8b). Correspondingly, P attains a near-plateau regime in which it slowly decreases under the effect of focal adhesion translation (see the discussion below on competition between stress fiber contractility and focal adhesion translation).

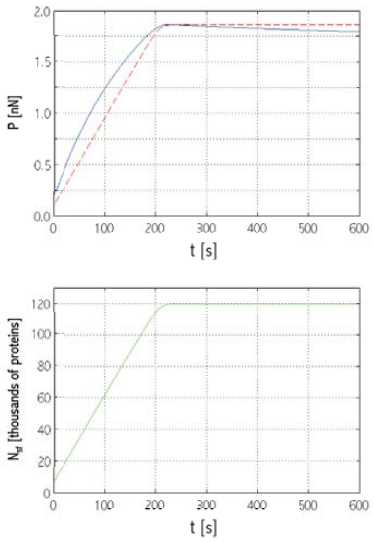

Figure 8: Time evolution of a) stress fiber force P (blue line) and stress fiber critical force $P^1_{\rm cr,sf}$ (dashed red line); b) $N_{\rm sf}$. System initial configuration: $x^0_{\rm sf} = 18\mu$m; $\hat{x}^0_{\rm fa} = 0.520\mu$m (region *R* in Fig. 2).

From this state, if P increases due to *external* perturbations to the system, but $P < P^2_{\rm cr,sf}$ is maintained, a growth regime can be re-established because the condition $(\mu_{\rm sf} - \mu^{\rm sf}_{\rm cyt}) < 0$ is regained. Actin and myosin are then recruited until attainment of a second critical value of $N_{\rm sf}$ for which the stress fiber stops growing. In the present study, the perturbation was applied in the form of a substrate strain (see Fig. 6). A different perturbation induced by the finite cross-section of a micropost has been shown in Fig. 3, also.

Stress fiber activity can trigger different focal adhesion responses

A longer stress fiber contains more myosin proteins and therefore is able to generate a higher active force, $P^{\rm ac}_{\rm sf}$. For this reason, as shown in Fig. 4, the maximum total force is higher for system configurations with longer stress fibers. Secondarily, the passive contribution to the stress fiber force also plays a role in determining its maximum value. As Fig. 4 shows, focal adhesions that are initially large lead to systems developing higher forces, because the mechanical stiffness is higher. Besides having a major effect on the the active force, stress fibers of different geometries also can trigger different focal adhesion responses: for instance, region *R* in Fig.

2 becomes increasingly narrow for longer stress fibers. The reason is that in order to sustain the greater active force generated by a longer stress fiber, the initial focal adhesion needs to be longer. A longer focal adhesion has a higher critical load $P^{\rm d}_{\rm cr,fa}$ and can be subjected to a greater force without collapsing. On the other hand, if the stress fiber is short, the active force generated is lower; hence, even focal adhesions developing from a single focal adhesion complex can sustain the load without failing (see the response map in Fig. 2 and related discussion).

Fig. 9a shows the evolution of both the total force, P, and the focal adhesion critical load, $P^{\rm d}_{\rm cr,fa}$, for a system with initial configuration in region *FA-c* of Fig. 2. Due to the incorporation of more actins and myosins in the stress fiber, P increases and exceeds $P^{\rm d}_{\rm cr,fa}$. Then, the focal adhesion's growth slows down (Fig. 9b) because unbinding occurs at the distal end (as a consequence, the focal adhesion critical load also increases more slowly). However, as $N_{\rm sf}$ is far from its critical value, P continues to increase above $P^{\rm d}_{\rm cr,fa}$, eventually leading to severe resorption at the distal end, and focal adhesion collapse (Fig. 9b). Protein resorption is boosted by the force-dependent term χ_{fa} in Eq. 2, which makes the unbinding rate grow exponentially with the stress fiber force.

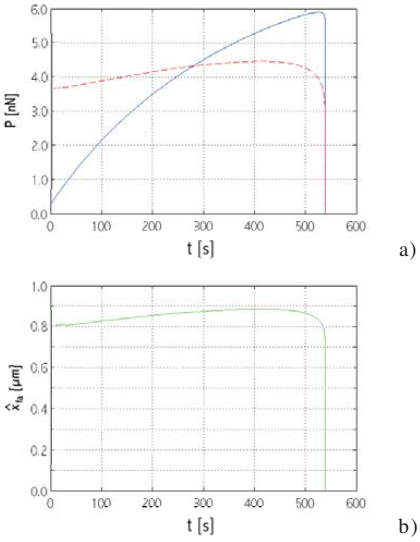

Figure 9: Time evolution of a) P (blue line) and focal adhesion critical force, $P^{\rm d}_{\rm cr,fa}$ (dashed red line); b) $\hat{x}_{\rm fa}$. System initial configuration: $x^0_{\rm sf} = 36\mu$m; $\hat{x}^0_{\rm fa} = 0.800\mu$m (region *FA-c* in Fig. 2).

The focal adhesion size can determine the fate of the stress fiber

For initial configurations in region *SF-c* of Fig. 2, $\hat{x}^0_{\rm fa}$ is large and the stress fiber disassembles within the first few milliseconds of the computation. The reason is that a large $\hat{x}^0_{\rm fa}$ makes the stress fiber-focal adhesion system mechanically very stiff. Therefore, contractility drives P to rapidly exceed $P^2_{\rm cr,sf}$, causing stress fiber disassembly. The disassembly is boosted by the force-dependent term χ_{sf} in Eq. 1, which enhances the actin unbinding rate. The focal adhesion thus can control the fate of the system, by acting as a very stiff support.

Competition between stress fiber contractility and focal adhesion translation determines the force behavior

For the system configurations in region *R* of Fig. 2 (or of Fig. 5 for the applied strain case), the force reaches a plateau after an initial growth stage. The slope of the plateau is regulated by the competition between stress fiber contractility and focal adhesion translation due to protein treadmilling. The action of motor proteins in the stress fiber causes the active component of the stress fiber force $P^{\rm ac}_{\rm sf}$ (and, consequently, the total force P) to increase, whereas when the focal adhesion centroid moves towards the stress fiber, P relaxes. Our computations show that for the overall system dynamics this *kinematic* relaxation mechanism and its interplay with stress fiber contractility is more relevant than the relaxation induced by passive viscoelasticity, because the latter occurs over very short time scales (see the inset in Fig. 6*a*). For instance, for system configurations in region *R′* of Fig. 2, the relaxation induced by focal adhesion translation towards the stress fiber has a major influence and prevails over the stiffening effect provided by the addition of myosin to the stress fiber. Focal adhesion translation is enhanced for small values of $x^0_{\rm sf}$: the low values of the stress fiber force developed within the system lead to a large difference between the chemical potentials at the focal adhesion distal and proximal ends (Fig. 7); thus, the binding rates of the focal adhesion ends prove to be very different. This results in a high rate of focal adhesion translation, which in turn causes the stress fiber force to relax and vanish in a short time (blue curves in Fig. 3).

The influence of substrate loading on the overall system response

As shown in Fig. 6, larger external strains result in system collapse due to complete resorption of the focal adhesion. A high strain leads to a high value of the force in the system, P, which can exceed the focal adhesion critical load, $P^{\rm d}_{cr,sf}$, and induce severe resorption at the focal adhesion distal end (as shown by the red curves in Fig. 6).

On the other hand, if the strain is sufficiently small, the stress fiber force reaches a second plateau; correspondingly,

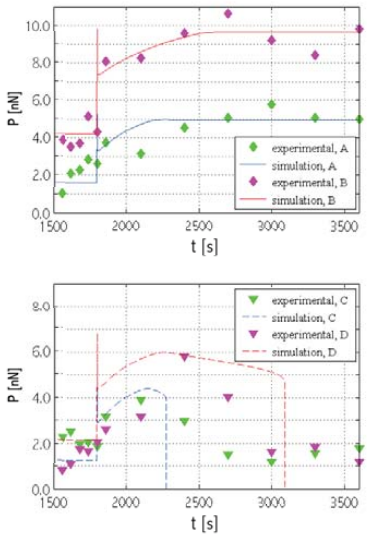

Figure 10: The computed stress fiber force *versus* time compared with force on individual microposts from the work of Mann and co-workers (32). (a) Robust stress fiber-focal adhesion systems (Region R in Fig. 5). (b) Systems that suffer focal adhesion collapse (Region FA-c in Fig. 5). The strain of 0.06 is applied at 1800 s in both cases.

the stress fiber recruits more actins and myosins. The focal adhesion also grows, demonstrating that to some extent an external load can stimulate growth of the stress fiber-focal adhesion system. The strain is externally imposed as a substrate strain in our model, but in living cells may come from the ECM, neighboring cells or other stress fiber-focal adhesion complexes within the same cell.

Connection to recent cell traction force experiments on micropost arrays

Our results can be related to the experiments of Mann et al. on the force response of smooth muscle cells on arrays of polymeric microposts (32). Fig. 10 shows data from their study for the force on individual microposts *versus* time in response to a substrate strain of 0.06. Fig. 10a corresponds to stress fiber-focal adhesion systems that remain robust over the period of the experiments – Region R in Fig. 5. Notably, the computed response has a spike in force at the instant of strain application due to the intrinsic viscoelastic response of the stress fiber, which has a relaxation time $\tau = 10$ s (see the inset in Fig. 6a and the related discussion, and Tab. 1 in the Supporting Material). The 1-minute time resolution of the experiments was too coarse to capture such a spike.

In Fig. 10b stress fiber-focal adhesion systems from Region FA-c (focal adhesion collapse) of Fig. 5 have been compared with experimental curves that show a significant decrease in force. Notably, while the computed curves demonstrate decreases down to zero force, the experiments show a less sharp decreases followed by a plateau. Upon examining the experimental force data we have found that the force trace on each of the two microposts represented in Fig. 10b is not complemented by a force trace that is equal in magnitude and opposite in direction on another micropost. This suggests that while each end of a stress fiber is indeed connected to a focal adhesion on a micropost, different parts of the focal adhesion on these microposts have different stress fibers connected to them. Each stress fiber and the part of the focal adhesions connected to each of its ends would form a system of the type considered in the model, and this system would have well-defined dynamics. However, the force trace on a micropost is the magnitude of the vector resultant of all these different systems, some of which may collapse and all of which have different dynamics. This yields the experimental curves in Fig. 10b characterized by sharply decreasing, but non-vanishing forces. In all cases, matches to the experimental curves were obtained by varying the initial focal adhesion length and the stress fiber unstretched length.

Mann et al. speculate that all the different observed behaviors may be due to the force acting on the focal adhesion before the application of the stretch. Our study shows that the force does affect the system behavior,but is itself determined by the system's initial geometrical configuration – Figs. 2 and 5. This diversity of stress fiber and focal adhesion geometries has not been reported by Mann et al.

Further capabilities of the model

The discussion of Fig. 3 identified an equilibrium state for the system when the focal adhesion grows to cover the micropost cross-section. A non-uniform force distribution over the focal adhesion (33) also allows the attainment of an equilibrium state, but has not been considered here.

The model discussed here can be embedded in a whole cell model, where the effects of location within the cell and history, as well as of cell type, can be considered. Notably, a) both stress fibers and focal adhesions vary in size and length throughout a cell, depending also on cell history, and from one cell type to another; b) the external strain field to which cells are subjected is non-uniform; and c) the kinetic rates of proteins binding/unbinding and the structural and chemical properties of both the stress fibers and the focal adhesions change with the cell type. All these varying conditions, and the different responses they elicit, can be accounted for in the model presented here.

ACKNOWLEDGEMENTS

We thank Prof. Jianping Fu for discussions, and for the use of experimental data.

SUPPORTING CITATIONS

References (35–40) appear in the Supporting Material.

SUPPLEMENTARY MATERIAL

An online supplement to this article can be found by visiting BJ Online at http://www.biophysj.org.

Note for the printed version of the manuscript

For the printed version of the manuscript, the following convention has been used for Figs. 3, 6, 8 and 9: solid red lines have been substituted with solid gray lines; solid green lines with dash-dot black lines; solid blue lines with solid black lines; and dashed red lines with dashed gray lines.

References

1. Pellegrin, S., Mellor, H. 2007. Actin stress fibres. *J. Cell Sci.* 120:3491–3499.
2. Hill, A. 1938. The heat of shortening and the dynamics constants of muscle. *Proc. R. Soc., Series B.* 126:136–195.
3. Pollard, T., Borisy, G. 2003. Cellular motility driven by assembly and disassembly of actin filaments. *Cell.* 112;453–465.
4. Chrzanowska–Wodnicka, M., Burridge, K. 1996. Rho–stimulated contractility drives the formation of stress fibers and focal adhesions. *J. Cell Biol.* 113:1403–1415.
5. Ingber, D. 2003. Tensegrity I. Cell structure and hierarchical systems biology. *J. Cell Sci.* 116:1157–1173.
6. Kumar, S., Maxwell, I., Heisterkamp, A., Polte, T., Lele, T., Salanga, M., et al. 2006. Viscoelastic relaxation of single living stress fibers and its impact on cell shape, cytoskeletal organization, and extracellular matrix mechanics. *Biophys. J.* 90:3762–3773.
7. Riveline, D., Zamir, E., Balaban, N., Schwarz, U., Ishikazi, T., Narumiya, S., et al. 2001. Externally applied local mechanical force induces growth of focal contacts by an mdia1–dependent and rock–independent mechanism. *J. Cell Biol.* 153:1175–1185.
8. Balaban, N., Schwarz, U., Riveline, D., Goichberg, P., Tzur, G., Sabanay, I., et al. 2001. Force and focal adhesion assembly: A close relationship studied using elastic micropatterned substrates. *Nat. Cell Biol.* 3:466–473.
9. Besser, A., Colombelli, J., Stelzer, E., Schwarz, U. 2011. Viscoelastic response of contractile filament bundles. *Phys. Rev. E.* 83:051902–1–051902–12.
10. Besser, A., Schwarz, U. 2007. Coupling biochemistry and mechanics in cell adhesion a model for inhomogeneous stress fiber contraction. *New J. Phys.* 9:425–452.
11. Kaunas, K., Huang, Z., Hahn, J. 2010. A kinematic model coupling stress fiber dynamics with JNK activation in response to matrix stretching. *J. Theor. Biol.* 264:593–603.
12. Kaunas, R. 2008. Modeling cellular adaptation to mechanical stress. In G. Artmann, S. Chien (Ed.), *Bioengineering in Cell and Tissue Research* (pp. 317–348). *New York: Springer.*
13. Kruse, K., Julicher, F. 2000. Actively contracting bundles of polar filaments. *Phys. Rev. Lett.* 85:1778–1781.
14. Stachowiak, M., O'Shaughnessy, B. 2008. Kinetics of stress fibers. *New J. Phys.* 10:025002–1–025002–26.
15. Stachowiak, M., O'Shaughnessy, B. 2009. Recoil after severing reveals stress fiber contraction mechanisms. *Biophys. J.* 97:462–471.
16. Walcott, S., Sun, S. 2010. A mechanical model of actin stress fiber formation and substrate elasticity sensing in adherent cells. *Proc. Natl. Acad. Sci.* 107:7757–7762.
17. Harland, B., Walcott, S., Sun, S. 2011. Adhesion dynamics and durotaxis in migrating cells. *Phys. Biol.* 8:015011–1–015011–10.
18. Deshpande, V., McMeeking, R., Evans, A. 2006. A bio–chemo–mechanical model for cell contractility. *Proc. Natl. Acad. Sci.* 103:14015–14020.
19. Deshpande, V., Mrkisch, M., McMeeking, R., Evans, A. 2008. A bio-chemo--mechanical model for coupling cell contractility with focal adhesion formation. *J. Mech. Phys. Sol.* 56:1484–1510.
20. Tan, J., Tien, J., Pirone, D., Gray, D., Bhadriraju, K., Chen, C. 2003. Cells lying on a bed of microneedles: an approach to isolate mechanical force. *Proc. Natl. Acad. Sci.* 100:1484–1489.
21. Engler, A., Sen, S., Sweeney, H., Discher, D. 2006. Matrix elasticity directs stem cell lineage specification. *Cell.* 126:677–689.
22. Chan, C., Odde, D. 2008. Traction dynamics of filopodia on compliant substrates. *Science.* 322:1687–1691.
23. Chen, C., Alonso, J., Ostuni, E., Whitesides, G., Ingber, D. 2003. Cell shape provides global control of focal adhesion assembly. *Biochem. Biophys. Res. Commun.* 307:355–361.
24. Peterson, L., Rajfur, Z., Maddox, A., Freel, C., Chen, Y., Edlund, M., et al. 2004. Simultaneous stretching and contraction of stress fibers in vivo. *Mol. Biol. Cell.* 15:3497–3508.
25. Franke, R., Grafe, M., Schnittler, H., Seiffge, D., Mittermayer, C., Drenckhahn, D. 1984. Induction of human vascular endothelial stress fibers by fluid shear stress. *Nature.* 307:648–649.
26. Kaunas, R., Nguyen, P., Usami, S., Chien, S. 2005. Cooperative effects of Rho and mechanical stretch on stress fiber organization. *Proc. Natl. Acad. Sci.* 102:15895–15900.
27. Wei, Z., Deshpande, V., McMeeking, R., Evans, A. 2008. Analysis and interpretation of stress fiber organization in cells subject to cyclic stretch. *J. Biomech. Eng.* 130:031009–1–031009–9.
28. Ridley, A., Hall, A. 1992. The small GTP-binding protein Rho regulates the assembly of focal adhesions and actin stress fibers in response to growth factors. *Cell.* 70:389–399.
29. Ridley, A., Paterson, H., Johnston, C., Diekmann, D., Hall, A. 1992. The small GTP-binding protein Rac regulates growth factor-induced membrane ruffling. *Cell.* 70:401–410.
30. Sander, E., ten Klooster, J., van Delft, S., van der Kammenn, R., Collard, J. 1999. Rac downregulates Rho activity: reciprocal activity between both GTPases determines cellular morphology and migratory behavior. *J. Cell Biol.* 147:1009–1022.

31. Maraldi, M., Garikipati, K. 2013. The chemo-mechanics of cytoskeletal force generation. *Submitted.*
32. Mann, J., Lam, R., Weng, S., Sun, Y., Fu, J. 2012. A silicone–based stretchable micropost array membrane for monitoring live–cell subcellular cytoskeletal response. *Lab Chip* 12:731–740.
33. Olberding, J., Thouless, M., Arruda, E., Garikipati, K. 2010. The non–equilibrium thermodynamics and kinetics of focal adhesion dynamics. *PLoS One* 4:e12043.
34. Bell, G. 1978. Models for the specific adhesion of cells to cells. *Science* 200:618–627.
35. Zamir, E., Geiger, B. (2001). Molecular complexity and dynamics of cell-matrix adhesions. J. Cell Sci., 114, 3583-3590.
36. Arnold, M., Cavalcanti-Adam, E.A., Glass, R., Blummel, J., Eck, W., et al. (2004) Activation of integrin function by nanopatterned adhesive interfaces. ChemPhysChem., 5, 383–388.
37. Deguchi, S., Ohashi, T., Sato, M. (2006). Tensile properties of single stress fibers isolated from cultured vascular smooth muscle cells. J. Biomech., 39, 2603–2610.
38. Howard, J., Mechanics of Motor Proteins and the Cytoskeleton. Sinauer Associates, Sunderland Mass. (2001).
39. Wu, J.-Q., Pollard, T. (2005). Counting cytokinesis proteins globally and locally in fission yeast. Science, 310, 310-314.
40. Lord, M., Pollard, T.D. (2004). "UCS protein Rng3p activates actin filament gliding by fission yeast myosin-II" J. Cell Biol., 167 (2), 315–325.
41. de Groot, S.R., Mazur, P., Non-equilibrium thermodynamics. Dover (1984).
42. Nicolas, M., Geiger, B., Safran, S.A., (2004). Cell mechanosensitivity controls the anisotropy of focal adhesions P. Natl. Acad. Sci. USA, 101: 12520-12525.